

See discussions, stats, and author profiles for this publication at: <https://www.researchgate.net/publication/231231153>

# Controlled Synthesis of Isomorphous Coordination Polymers via in Situ Ligand Transformation Reaction: Crystal Structure, Thermal and Magnetic Properties

ARTICLE in CRYSTAL GROWTH & DESIGN · AUGUST 2010

Impact Factor: 4.89 · DOI: 10.1021/cg1007389

CITATIONS

30

READS

36

## 4 AUTHORS:



**Muhammad Nadeem**

Quaid-i-Azam University

22 PUBLICATIONS 126 CITATIONS

SEE PROFILE



**Mohan Bhadbhade**

University of New South Wales

245 PUBLICATIONS 2,625 CITATIONS

SEE PROFILE



**Roland Bircher**

Sherwin-Williams Company

32 PUBLICATIONS 821 CITATIONS

SEE PROFILE



**John A Stride**

University of New South Wales

128 PUBLICATIONS 1,697 CITATIONS

SEE PROFILE



**UNSW**  
THE UNIVERSITY OF NEW SOUTH WALES  
SYDNEY • AUSTRALIA

**Metal-Organic Frameworks:  
Functional Materials by Form and Design**

A Thesis Submitted in Partial Fulfilment of the  
Requirements for the Degree  
of  
Doctor of Philosophy  
in  
Chemistry  
By

***Muhammad Arif Nadeem***

School of Chemistry  
The University of New South Wales  
Sydney, Australia

## Title: Metal-Organic Frameworks: Functional Materials by Form and Design

A range of metal-organic framework (MOF) materials, consisting of extended structures of coordination polymers incorporating paramagnetic metal ions ( $\text{Mn}^{\text{II}}$ ,  $\text{Fe}^{\text{II}}$ ,  $\text{Co}^{\text{II}}$ ,  $\text{Ni}^{\text{II}}$  and  $\text{Cu}^{\text{II}}$ ), have been synthesized using bridging ligands such as carboxylate-decorated and/or nitrogen containing aromatics. The *in situ* ligand transformation of 1,2,3-benzene tricarboxylic acid into isophthalate to form four isomorphous coordination polymers was found to be highly dependent upon the reaction temperature, only occurring at higher temperatures such as 220°C. The structural and magnetic properties of all of the compounds have been studied in detail, with many showing bulk magnetic ordering and magnetic phase transitions. In  $[\text{Co}(\text{bim})(\text{acetate})]_n$ , benzimidazole complexation led to antiferromagnetic superexchange interactions between the cobalt(II) ions, however at very low temperatures the magnetic behaviour changed from antiferromagnetic to weak ferromagnetic ordering as a result of spin canting. Similarly, another 3D MOF  $[\text{Ni}^{\text{II}}_2(\text{pda})(\text{OH})_2(\text{H}_2\text{O})]_n$  based on linear 1D  $\text{Ni}^{\text{II}}$  chains connected via  $\text{Ni}_4\text{O}_4$ -cubanes, has been synthesized, offering a rare example of a magnetic material in which the magnetic phase transitions (MPTs) are potentially coupled to slow relaxation phenomena. This particular material showed an antiferromagnetic ordering at 21 K, with a magnetic phase transition from AF to CAF at 2.8 K. We were also able to design a topology in which the bulk magnetic ordering to higher temperatures were found to be shifted to considerably higher temperatures. For example, two 3D isostructural MOFs based on  $\mu_3\text{-O}$  centered metal clusters  $\{[\text{M}^{\text{III}}_3(\text{pydc})_3(\mu_3\text{-O})]_n\text{Cl}$ ,  $\text{M} = \text{Mn}, \text{Co}\}$ , have been synthesized, displaying bulk magnetic ordering at around 45 K; whilst only the cobalt based MOF displayed any spin canting behavior, and then only below 10 K. Other aspects of this thesis involved the introduction of flexible ligand systems such as 1,4-phenylene diacetic acid (pda) and di-(4-pyridyl)-ethane (dpe) in the synthesis of MOFs. Four novel isostructural MOFs  $\{[\text{M}(\text{pda})(\text{dpe})]_n$ , where  $\text{M} = \text{Mn}^{\text{II}}$ ,  $\text{Co}^{\text{II}}$ ,  $\text{Ni}^{\text{II}}$  and  $\text{Cu}^{\text{II}}$  were synthesised using pda and dpe, and were found to show bulk magnetic ordering. We also have reported a microporous framework,  $[\text{Cu}_5(\text{ipO})_2(\text{pyz})_2]_n$ , which exhibits a remarkable preferential adsorption for  $\text{H}_2$  over  $\text{N}_2$ , having a ratio of  $\text{H}_2$  selectivity in excess of 5 at sub-ambient pressures.

I also authorise University Microfilms to use the 350 word abstract of my thesis in Dissertation Abstracts International (this is applicable to doctoral theses only).

.....  
 ..... Signature ..... Witness ..... Date .....

The University recognises that there may be exceptional circumstances requiring restrictions on copying or conditions on use. Requests for restriction for a period of up to 2 years must be made in writing. Requests for a longer period of restriction may be considered in exceptional circumstances and require the approval of the Dean of Graduate Research.

**FOR OFFICE USE ONLY**

---

Date of completion of requirements for Award:

## *Certificate of Originality*

I hereby declare that this submission is my own work and to the best of my knowledge it contains no materials previously published or written by another person, nor material which to a substantial extent has been accepted for the award of any other degree or diploma at UNSW or any other educational institution, except where due acknowledgment is made in the thesis. Any contribution made to the research by others, with whom I have worked at UNSW or elsewhere, is explicitly acknowledged in the thesis.

I also declare that the intellectual content of this thesis is the product of my own work, except to the extent that assistance from others in the project's design and conception or in style, presentation and linguistic expression is acknowledged.

.....

Muhammad Arif Nadeem

April 2010

# *Acknowledgements*

I would have never been able to complete this thesis without the assistance by a multitude of individuals throughout all stages, many of whom through lack of space I will be unable to name. It is my pleasure to acknowledge their efforts, support, love, and guidance throughout the course of my PhD thesis.

First and foremost, I am thankful to Allah for His blessings and love as the eternal guardian for me to give me enough power and perseverance to go through the tough times of the research. All powers and glory goes to Him, now and forever.

I would like to gratefully acknowledge the supervision of *A/Prof. John Arron Stride* many insightful conversations during the development of the ideas in this thesis, for helpful comments, for his dedication, guidance, and for having presented me with the numerous opportunities to broaden my academic and social horizon. I would like to thank heartedly *Dr. Roland Bircher*, for his kind assistance and guidance in the interpretation of magnetic data, discussions, comments and impressive way of conveying thoughts. I am also thankful to *Dr. Mohan Bhadbhade* who trained me in crystallography.

I wish to express my gratitude to my colleagues, *Mohammed, Tom, Trung, Maggie, Fehmida* and *Fatemeh* for their useful advice, discussions and support. I am thankful to my research partner *Maggie Ng* for her cooperation and bringing new exciting ideas during my research work. My special thanks go to my friends in Sydney, *Shahzad, Haris, Zafar, Omer, Shoaib, Usman, Wissam*, and *Sufian* for providing me humorous moments and constant source of entertainment during the boring times throughout this journey. I would always remember them in my experience of choosing restaurants for dinners, late night suppers and chilling out. Financially, I would like to thank University New South Wales *UNSW* for funding my scholarships.

I am extremely grateful to my parents: Muhammad Rafiq Chaudhary and Hameeda Bano, for their love, care, perseverance and determination for encouraging me always to accept challenges and pursue the journey of PhD. I dedicate this work to them. I am greatly thankful to my brother and sisters: *Tarif Azeem, Shazia, Nazia* and *Arifa* for their encouragement and good wishes.

So Many Pedestrians - So Little Time. Nevertheless, let me say also thanks to my wife *Tahira Jabeen* always offering support and love and my kids *Hassan* and *Maheen* whose voice always reminding me to finish the work quickly.

Muhammad Arif Nadeem

7<sup>th</sup> April 2011

# *Abstract*

A range of metal-organic framework (MOF) materials, consisting of extended structures of coordination polymers incorporating paramagnetic metal ions ( $\text{Mn}^{\text{II,III}}$ ,  $\text{Fe}^{\text{II}}$ ,  $\text{Co}^{\text{II,III}}$ ,  $\text{Ni}^{\text{II}}$  and  $\text{Cu}^{\text{II}}$ ), have been synthesized using bridging ligands such as carboxylate-decorated and/or nitrogen containing aromatics. The *in situ* ligand transformation of 1,2,3-benzene tricarboxylic acid into isophthalate to form four isomorphous coordination polymers was found to be highly dependent upon the reaction temperature, only occurring at higher temperatures such as 220°C. The structural and magnetic properties of all of the compounds have been studied in detail, with many showing bulk magnetic ordering and magnetic phase transitions. In  $[\text{Co}(\text{bIM})(\text{acetate})]_n$ , benzimidazole complexation led to antiferromagnetic superexchange interactions between the cobalt(II) ions, however at very low temperatures the magnetic behaviour changed from antiferromagnetic to weak ferromagnetic ordering as a result of spin canting. Similarly, another 3D MOF  $[\text{Ni}^{\text{II}}_2(\text{pda})(\text{OH})_2(\text{H}_2\text{O})]_n$  based on linear 1D  $\text{Ni}^{\text{II}}$  chains connected via  $\text{Ni}_4\text{O}_4$ -cubanes, has been synthesized, offering a rare example of a magnetic material in which the magnetic phase transitions (MPTs) are potentially coupled to slow relaxation phenomena. This particular material showed an antiferromagnetic ordering at 21 K, with a magnetic phase transition from AF to CAF at 2.8 K. We were also able to design a topology in which the bulk magnetic ordering to higher temperatures were found to be shifted to considerably higher temperatures. For example, two 3D isostructural MOFs based on  $\mu_3\text{-O}$  centered metal clusters  $\{[\text{M}^{\text{III}}_3(\text{pydc})_3(\mu_3\text{-O})]_n\cdot\text{Cl}$ ,  $\text{M} = \text{Mn}, \text{Co}\}$ , have been synthesized, displaying bulk magnetic ordering at around 45 K; whilst only the cobalt based MOF displayed any spin canting behavior, and then only below 10 K. Other aspects of this thesis involved the introduction of flexible ligand systems such as 1,4-phenylene diacetic acid (pda) and di-(4-pyridyl)-ethane (dpe) in the synthesis of MOFs. Four novel isostructural MOFs  $\{[\text{M}(\text{pda})(\text{dpe})]_n$ , where  $\text{M} = \text{Mn}^{\text{II}}, \text{Co}^{\text{II}}, \text{Ni}^{\text{II}}$  and  $\text{Cu}^{\text{II}}\}$  were synthesised using pda and dpe, and were found to show bulk magnetic ordering. We also have reported a microporous framework,  $[\text{Cu}_3(\text{ipO})_2(\text{pyz})_2]_n$ , which exhibits a remarkable preferential adsorption for  $\text{H}_2$  over  $\text{N}_2$ , having a ratio of  $\text{H}_2$  selectivity in excess of 5 at sub-ambient pressures.

## *List of Publications*

This thesis is submitted as a series of original publications with each publication as a separate chapter apart from the first chapter which is introductory chapter and a final summary chapter. Following publications are included in this thesis.

### **Peer reviewed journal publications:**

- 1) Muhammad A. Nadeem, M. Bhadbhade, R. Bircher and John A. Stride, Three isolated structural motifs in one crystal: Penetration of two 1D chains through large cavities within 2D polymeric sheets, *CrystEngCommun.*, 2010, 12, 1391-1393
- 2) Muhammad A. Nadeem, M. Bhadbhade, R. Bircher and John A. Stride, Controlled synthesis of isomorphous coordination polymers via *in situ* ligand transformation reaction: crystal structure, thermal and magnetic properties, *Cryst. Growth Des.* 2010, 10, 4060-4067
- 3) Muhammad A. Nadeem, D. Craig, R. Bircher and John A. Stride, Magneto-structural correlation of a three-dimensional Mn based metal-organic framework, *Dalt. Trans.*, 2010, 39, 4358-3374
- 4) Muhammad A. Nadeem, M. Bhadbhade and John A. Stride, Four new coordination polymers constructed from benzene tricarboxylic acid: synthesis, crystal structure, thermal and magnetic properties, *Dalt. Trans.*, 2010, 39, 9860-9865
- 5) Leo Arai, Muhammad A. Nadeem, M. Bhadbhade and John A. Stride, A 2D Cobalt based coordination polymer constructed from benzimidazole and acetate ion exhibiting spin-canted antiferromagnetism, *Dalt. Trans.*, 2010, 39, 3372-3374
- 6) Muhammad A. Nadeem, M. Bhadbhade, Roland Bircher and John A. Stride, Two isostructural metal-organic frameworks having long-range magnetic ordering at 45 K, *Chem. Eur. J.*, 2011, manuscript submitted.
- 7) Maggie Ng, Muhammad A. Nadeem, M. Bhadbhade and John A. Stride, A series of isostructural metal organic frameworks constructed from flexible ligand system, synthesis, crystal structure and magnetic properties, *Inorg. Chem.*, 2011, manuscript submitted.
- 8) Muhammad A. Nadeem, M. Ng and John A. Stride, Magnetic phase transition in an unprecedented Ni<sub>4</sub>O<sub>4</sub>-cubane based 3D metal-organic framework, *Angew. Chem. Int. Ed.*, 2011, manuscript submitted
- 9) Muhammad A. Nadeem, Matthew R. Hill, Arron W. Thornton and John A. Stride, A copper based microporous metal-organic framework displaying selective adsorption of



hydrogen over nitrogen via flexible, hysteretic adsorption, *Dalt. Trans.*, 2010, 40, 3398-3401

**Conference presentations:**

- The International Conference on Nanoscience and Nanotechnology, ICONN 2010, 22-26<sup>th</sup> Feb 2010, Sydney, Australia (Oral Presentation).
- The International Conference on Molecular materials, MOLMAT 2010, 5-8<sup>th</sup> July 2010, Montpellier, France (Poster Presentation).
- The 39<sup>th</sup> International Conference on Coordination Chemistry, ICCC 2010, 25-30<sup>th</sup> July 2010, Adelaide, Australia (Poster Presentation).
- Australian Synchrotron User meeting 2010, 22-24<sup>th</sup> Nov, 2010. Melbourne, Australia (Poster Presentation).

# *Table of Contents*

Chapter No.	Title	Page
	Acknowledgments	iv
	Abstract	vi
	List of Publications	vii
	List of figures	xiv
	List of tables	xxi
	Abbreviations	xxii
<b>Chapter-1</b>	<b><i>Introduction</i></b>	<b>1</b>
	1.1 Metal-organic frameworks (MOFs)	2
	1.2. Historical background	3
	1.3 Synthesis	4
	1.3.1. <i>In situ.</i> ligand synthesis	5
	1.4. Characterization	6
	1.5. Applications	7
	1.5.1 Gas Adsorption	7
	1.5.2. Gas separation	11
	1.5.3. Catalytic applications	14
	1.6. Magnetism in MOFs	16
	1.7. Aims of the project	21
	References	22
<b>Chapter-2</b>	<b><i>Three isolated structural motifs in one crystal: penetration of two 1D chains through large cavities within 2D polymeric sheets</i></b>	<b>26</b>
	Acknowledgments	29
	Notes and references	29
	Supporting information	30
<b>Chapter-3</b>	<b><i>Controlled synthesis of isomorphous coordination polymers via in situ. ligand transformation reaction: crystal structure, thermal and magnetic properties</i></b>	<b>32</b>
	Abstract	33

	Introduction	33
	Experimental section	33
	Materials and physical techniques	33
	Magnetometry	33
	Synthesis of $[\text{Ni}_2(\text{ip})_2(\text{bpy})_2]\text{n}$ (1)	34
	Synthesis of $[\text{Co}_2(\text{ip})_2(\text{bpy})_2]\text{n}$ (2)	34
	Synthesis of $[\text{Ni}_2(\text{ip})_2(\text{pyz})_2]\text{n}$ (3)	34
	Synthesis of $[\text{Co}_2(\text{ip})_2(\text{pyz})_2]\text{n}$ (4)	34
	Crystallographic analysis	34
	Results and Discussion	34
	Synthesis	34
	Crystal structure	35
	Thermogravimetric analysis	36
	Magnetic properties	36
	$\text{Ni}_2(\text{ip})_2(\text{bpy})_2$	36
	$\text{Ni}_2(\text{ip})_2(\text{pyz})_2$	38
	$\text{Co}_2(\text{ip})_2(\text{bpy})_2$	38
	$\text{Co}_2(\text{ip})_2(\text{pyz})_2$	39
	Conclusion	39
	Acknowledgment	39
	References	39
	Supporting information	41
<b>Chapter-4</b>	<b><i>Magneto-structural correlations of a three-dimensional Mn based metal-organic framework</i></b>	<b>44</b>
	Introduction	45
	Experimental	45
	Synthesis	45
	Crystallographic analysis	46
	Magnetic measurements	46
	Results and discussion	46
	Description of the structure	46
	Magnetic properties	47
	Conclusion	48

	Notes and references	48
	Supporting information	50
<b>Chapter-5</b>	<b><i>Four new coordination polymers constructed from benzene tricarboxylic acid: synthesis, crystal structure, thermal and magnetic properties</i></b>	<b>51</b>
	Introduction	52
	Experimental	52
	Materials and physical techniques	52
	Magnetometry	53
	Synthesis of $[\text{Mn}_2(\text{btc})(\text{F})]_n$ (1)	53
	Synthesis of $[\text{Co}_2(\text{btc})(\text{F})]_n$ (2) and $[\text{Co}_3(\text{btc})(\text{Hbtc})(\text{OH})(\text{H}_2\text{O})_{11}]_n$ (4)	53
	Synthesis of $[\text{Fe}_3(\text{btc})(\text{Hbtc})(\text{OH})(\text{H}_2\text{O})_{11}]_n$ (3)	53
	Crystallographic analyses	53
	Results and discussion	53
	Crystal structure	53
	Thermogravimetric analysis	55
	Magnetic properties	55
	Conclusion	57
	Acknowledgements	57
	Notes and references	57
	Supporting Information	58
<b>Chapter-6</b>	<b><i>A 2D cobalt based coordination polymer constructed from benzimidazole and acetate ion exhibiting spin-canted antiferromagnetism</i></b>	<b>61</b>
	Notes and references	64
	Supporting information	65
<b>Chapter-7</b>	<b><i>Two iso-structural metal-organic frameworks having long-range magnetic ordering at 45 K</i></b>	<b>69</b>
	Abstract	70
	Introduction	70
	Results and Discussion	71
	Crystal structure	71

	Thermogravimetric analysis	71
	Magnetic properties	72
	Conclusion	73
	Experimental Section	73
	Materials and physical techniques	73
	Magnetometry	73
	Synthesis of $[\text{Mn}_3(\text{pydc})_3(\mu_3\text{-O})]\cdot\text{Cl}$ (1) and $[\text{Co}_3(\text{pydc})_3(\mu_3\text{-O})]\cdot\text{Cl}$	73
	Crystallographic Analyses	73
	Acknowledgements	73
	Supporting information	76
<b>Chapter-8</b>	<b><i>A series of novel isostructural metal-organic frameworks constructed from mixed flexible ligands: Synthesis, crystal structure and physical properties</i></b>	<b>84</b>
	Introduction	86
	Experimental Section	87
	Materials and physical techniques	87
	Magnetometry	87
	Synthesis of $[\text{Mn}(\text{pda})(\text{dpe})]_n$ (1), $[\text{Co}(\text{pda})(\text{dpe})]_n$ (2), $[\text{Ni}(\text{pda})(\text{dpe})]_n$ (3) and $[\text{Cu}(\text{pda})(\text{dpe})]_n$ (4)	88
	Crystallographic analyses	89
	Crystal structure	89
	Thermogravimetric analysis	90
	Magnetic Properties	90
	Conclusions	93
	Acknowledgements	93
	References	101
	Supporting Information	103
<b>Chapter-9</b>	<b><i>Magnetic phase transition in an unprecedented <math>\text{Ni}_4\text{O}_4</math>-cubane based 3D metal-organic framework</i></b>	<b>110</b>
	Experimental Section	113
	Synthesis of 1	113
	Supporting information	116

<b>Chapter-10</b>	<b><i>A flexible copper based microporous metal-organic framework displaying selective adsorption of hydrogen over nitrogen</i></b>	<b>121</b>
	Notes and references	124
	Supporting information	126
<b>Chapter-11</b>	<b><i>Summary</i></b>	<b>130</b>
	<b><i>Appendix</i></b>	<b>136</b>

# *List of Figures*

Figure	Title	Page
<b>Chapter-1</b>		
Figure 1	Schematic representation of MOFs built from metal ion as nodes and organic ligand as spacers	2
Figure 2	A Mn-paddle wheel based porous MOF synthesized in John Stride lab, UNSW	3
Figure 3	Examples of inorganic SBUs. (a) Triangle, (b) square planar, (c) tetrahedron, (d) octahedron, and (e) trigonal prism	5
Figure 4	Schematic representation of selected applications of MOFs	7
Figure 5	Crystal structures of MOF-210 (a), MOF-205 (b) MOF-200 (c)	9
Figure 6	(A) Low-pressure N <sub>2</sub> isotherms of MOF-5, -177, -200, -205, and -210 at 77 K. Simulated isotherms of MOF-200 and -210 were overlaid. P/P <sub>0</sub> , relative pressure. High-pressure H <sub>2</sub> isotherms were measured at 77 K (B), and (C) CH <sub>4</sub> and (D) CO <sub>2</sub> isotherms were measured at 298 K of the same MOFs.	10
Figure 7	High-pressure methane sorption isotherms at various temperatures (a), 3D framework of PCN-14 (b)	10
Figure 8	Schematic illustration of selective gas adsorption in rigid MOFs	12
Figure 9	Schematic illustration of selective gas adsorption in a flexible MOF	12
Figure 10	Schematic illustration of catalytic process in porous MOFs	15
Figure 11	Schematic representation of different spin orientations of unpaired electrons	16
Figure 12	Diagrammatic representation of Curie-Weiss law	17
Figure 13	The number of published articles containing key words “coordination polymers” (blue), “magnetic coordination polymers” (red),	18
Figure 14	First example of nanoporous material showing magnetic ordering phenomena at low temperature	21
<b>Chapter-2</b>		
Figure 1	Illustration for the three coordination polymers exhibited in the	27

	crystal structure of 1: (a) Cu-dimer and Cu-chain building block (A) and (b and c) linear chain of B and C polymer respectively	
Figure 2	(a) Coordination geometry of Cu(II) centre in complex 1 in stick representation (left) and polygon representation (right); (b) packing of neighbouring chain and dimer subunits of polymer A, forming meshed grid type layers	28
Figure 3	A view showing the insertion of polymer B (blue), C (green) and lattice water molecules (red) into the voids created by packing of layers in polymer A (purple)	28
Figure S1	Detail of hydrogen-bonding between the 2D layers, generating the pseudo-3D structure	30
Figure S2	Thermogravimetric analysis of $\text{Cu}_3(\text{Hbtc})(\text{btc})(\text{bpy})_2$	31
<b>Chapter-3</b>		
Figure 1	The reaction route of 1,2,3-btcH3 at two different reaction temperatures in the presence of Ni(II) and Co(II) ions	35
Figure 2	(a) View of coordination environment in complex 1; (b) view of coordination environment in complex 3	36
Figure 3	A view of two-dimensional layer of complex 1 in the ac-plane.	36
Figure 4	(a) A view of two-dimensional layer of complex 3 in the ac-plane; (b) view along the c-axis showing the packing of the layers in $\pi$ - $\pi$ stacking mode	36
Figure 5	$\chi T$ vs. $T$ per dimer of 1 (red circles), 2 (blue circles), 3 (brown diamonds), and 4 (light blue diamonds) measured at 1000 Oe. Inset: $\chi T$ vs. $T$ per dimer, shown on a logarithmic temperature scale to emphasize the line shape at low temperatures	37
Figure 6	$\chi^{-1}$ vs. $T$ per dimer of 1 (red circles), 2 (blue circles), 3 (brown diamonds), and 4 (light blue diamonds) measured at 1000 Oe	37
Figure 7	$\chi T$ vs $T$ per dimer of 1 (red circles) and 3 (brown diamonds)	37
Figure 8	$M$ vs. $H$ per dimer of 1 (red circles), 2 (blue circles), 3 (brown diamonds), and 4 (light blue diamonds) measured at 2 K.	38
Figure 9	Field cooled (triangles) and zero-field cooled (circles) susceptibility per dimer of 3 shown as $\chi$ vs $T$ (dark and light blue) and $\chi T$ vs. $T$ (red and brown), measured at 1000 Oe.	38



Figure S1	Thermogravimetric analysis of 1-4	42
Figure S2	$\chi$ vs. $T$ per dimer of 1 (red circles), 2 (blue circles), 3 (brown diamonds) and 4 (light blue diamonds) measured at 1000 Oe. <i>Inset: <math>\chi T</math> vs. <math>T</math> per dimer, shown on a logarithmic temperature scale to emphasize the line shape at low temperatures</i>	43
<b>Chapter-4</b>		
Chart 1	Binding modes of carboxylate ligands	45
Figure 1	Basic structural unit of compound 1 (hydrogen atoms are not shown for clarity)	46
Figure 2	Coordination modes of btc (left) and Hbtc (right) in complex	46
Figure 3	View along $a$ axis, the adjacent chains are separated by btc ligands to form two dimensional sheet on $bc$ plane	47
Figure 4	Temperature dependent magnetic susceptibility of 1 shown as $\chi_M$ vs. $T$ (circles) $\chi_M T$ vs. $T$ (triangles). The insert shows a close-up of the low-temperature region. Dotted and solid lines correspond to the best fits obtained using eqn (2) and 4, respectively, with the parameters given in the text	47
Figure S1	Schematic of the exchange interactions in $[\text{Na}\{\text{Mn}_3(\text{Hbtc})_2(\text{btc})\}.5\text{H}_2\text{O}\}_n]$ : Models 1 and 2 use $J_1 = J_2$ : Model 3 has $J_1 \neq J_2$	50
<b>Chapter-5</b>		
Figure 1	(a) Packing diagram of 1 along $c$ -axis showing the each infinite 1D chain is surrounded by six neighbouring chains. (b) A view of infinite 1D chain constructed from fluoride bridged $\text{Mn}^{\text{II}}$ ions	54
Figure 2	Basic structural unit of compound 3	54
Figure 3	A view of hydrogen bonding network connecting neighbouring 1D chains in 3. Hydrogen atoms are omitted for clarity	54
Figure 4	(a) A Packing diagram of 3 along $c$ -axis showing the 3D supramolecular architecture build by the overlapping of infinite 1D zigzag chains of $[\text{Fe}_3(\text{btc})(\text{Hbtc})(\text{OH})(\text{H}_2\text{O})_{11}]$ via strong hydrogen bonding	55
Figure 5	Thermogravimetric analysis of 1-4	55
Figure 6	Powder XRD of hydrated and dehydrated samples of 3-4	55
Figure 7	Graph of field cooled magnetic susceptibility data of 1 at 0.1 T.	56

	Inset shows the plot of $\chi_M^{-1}$ vs. $T$ (K)	
Figure 8	Graph of field cooled magnetic susceptibility data of 2 at 0.1 T	56
Figure 9	The curve of $\chi_M$ vs. $T$ of 4 at 0.1 T (1 kOe) field. Inset showing the field dependent magnetization curve	56
Figure S1	A graph of field dependent magnetization of 1 and 2	58
<b>Chapter-6</b>		
Figure 1	Basic structural unit of 1	62
Figure 2	A packing diagram of 1 along the $a$ -axis highlighting the 2D sheets of bIM ligands showing nature of magnetic exchange coupling in a canted antiferromagnetic behaviour. Benzene ring is omitted for clarity	63
Figure 3	(a) Field cooled (FC) and zero-field (ZFC) plot of $\chi_M$ vs. $T$ at $H = 1000$ Oe, (b) Plot of $\chi_M T$ vs. $T$ ( $H = 1000$ Oe) (FC). Inset shows the $\chi_M^{-1}$ vs. $T$ plot, (c) $\chi_M T$ vs. $T$ at various fields, (d) Magnetic hysteresis loops at 2 and 5 K.	63
Figure S1	Calculated and experimental powder XRD pattern of 1	65
Figure S2	$\chi_M$ vs. $T$ plot at various fields	66
Figure S3	$M$ vs. $H$ plot at $T = 2$ K	67
Figure S4	TGA curve of 1	68
<b>Chapter-7</b>		
Figure 1	Basic structural unit of 1	71
Figure 2	(a) The two trimer units are alternately stacked along the $c$ -axis (b) alternative packing of trimers with choride ions between them viewed perpendicular to the $c$ -axis (c) View of 3-D framework on $ab$ -plane	72
Figure 3	(a) Field cooled (FC) and zero-field (ZFC) plot of $\chi_M$ vs. $T$ at $H = 1000$ Oe, (b) Plot of $\chi_M T$ vs. $T$ ( $H = 1000$ Oe) (FC). (c) Plot of $\chi_M^{-1}$ vs. $T$ ( $H = 1000$ Oe) (d) $\chi_M$ vs. $T$ at various fields	72
Figure 4	(a) Field cooled (FC) and zero-field (ZFC) plot of $\chi_M$ vs. $T$ at $H = 1000$ Oe, (b) Plot of $\chi_M T$ vs. $T$ ( $H = 1000$ Oe) (FC). (c) Plot of $\chi_M^{-1}$ vs. $T$ ( $H = 1000$ Oe) (d) $\chi_M T$ vs. $T$ at various fields	72
Figure S1	A view showing the microporous nature of the materials	76
Figure S2	Moment vs. Field plot of Complex 1, inset showing the hysteresis	77

	loop	
Figure S3	$\chi_M$ vs. $T$ plot of complex 2 at various fields	78
Figure S4	Moment vs. Field plot of Complex 2, inset showing the hysteresis loop	79
Figure S5	Comparison of calculated and experimental powder XRD pattern of complex 1	80
Figure S6	Comparison of calculated and experimental powder XRD pattern of complex 2	81
Figure S7	Thermogravimetric analysis of complex 1-2	82
<b>Chapter-8</b>		
Figure 1	The basic structural unit of 3 showing flexibility of two pda and dpe ligands	95
Figure 2	(a) A packing diagram of complex 3 in the $ac$ -plane	96
Figure 3	A packing diagram of complex 3 in the $ab$ -plane, showing different binding modes of two arms of pda ligand to form the 3D architecture	97
Figure 4	Magnetic data of 1, (a) Field cooled (FC) and zero-field (ZFC) plot of $\chi_M$ vs. $T$ at $H = 1000$ Oe, (b) Plot of $\chi_M T$ vs. $T$ ( $H = 1000$ Oe) (FC), (c) Magnetic hysteresis loops at 5K5 K, (d) Plot of $\chi_M T$ vs. $T$ at different applied fields	98
Figure 5	Magnetic data of 2, (a) Field cooled (FC) and zero-field (ZFC) plot of $\chi_M$ vs. $T$ at $H = 1000$ Oe, (b) Plot of $\chi_M T$ vs. $T$ ( $H = 1000$ Oe) (FC), (c) Magnetic hysteresis loops at 2.5K5 K (black) and 5 K (blue). (d) Plot of $\chi_M T$ vs. $T$ at different applied fields	99
Figure 6	Magnetic data of 3, a plot of $\chi_M$ and $\chi_M T$ vs. $T$ ( $H = 1000$ Oe)	100
Figure S1	Thermogravimetric curves of 1-3	106
Figure S2	A comparison of calculated powder XRD pattern of 2 with simulated form single crystal data	107
Figure S3	A comparison of calculated powder XRD pattern of 3 with simulated form single crystal data	108
Figure S4	A graph of moment vs field for 1-2 showing that saturation magnetisation at 9 T	109

<b>Chapter-9</b>		
Figure 1	(a) A view showing pdaa ligand linked the two neighbouring 1D chains running perpendicular to each other ( $\text{Ni}_4\text{O}_4$ cubane is omitted for clarity) , (b) two 1D chains are also bridged via $\text{Ni}_4\text{O}_4$ cubane	111
Figure 2	A packing diagram of 1 showing 1D chains are separated via $\text{Ni}_4\text{O}_4$ cubane, running perpendicular to each along the direction of the $a$ and $b$ axes direction (pdaa ligand is partially omitted for clarity)	112
Figure 3	(a) Field cooled (FC) and zero-field (ZFC) plot of $\chi_M$ vs. $T$ at $H = 1000$ Oe, (b) Plot of $\chi_M T$ vs. $T$ ( $H = 1000$ Oe) (FC), inset shows plot of $\chi_M^{-1}$ vs. $T$ (c) $\chi_M T$ vs. $T$ at various fields (d) Magnetic hysteresis loops at 2.5K (blue) and 5 K (black)	112
Figure 4	Temperature and frequency dependence of the real ( $\chi_M'$ ) and imaginary ( $\chi_M''$ ) parts of the ac susceptibility for 1. The solid lines are guide for the eyes	112
Figure 5	Magnetic dc susceptibility data showing the various magnetic phase changes at low temperature for 1	113
Figure S1	Temperature and frequency dependence of $\chi_M' T$ parts of the ac susceptibility for 1	117
Figure S2	A graph of field dependent magnetization of 1	118
Figure S3	Comparison of powder XRD of calculated (red) with experimental (black) pattern of 1	119
Figure S4	Thermogravimetric analytical curve of 1	120
<b>Chapter-10</b>		
Figure 1	A view of the microporous framework 1 showing pores along the $c$ -axis	123
Figure 2	Plot of $\text{N}_2$ and $\text{H}_2$ adsorption/desorption isotherms at 77 K	123
Figure 3	$\text{H}_2/\text{N}_2$ selectivity as a function of pressure	123
Figure 4	Perspective view down the $a$ -axis of microporous framework 1	123
Figure 5	Calculated cavity diameter distribution within the microporous framework 1 using RASPA 1.0	124
Figure S1	Powder diffraction of microporous framework 1 indicating a phase	126

	pure material	
Figure S2	Perspective view down the <i>c</i> -axis of microporous framework 1	127
Figure S3	Thermogravimetric analysis of microporous framework 1	128

# *List of Tables*

<b>Table</b>	<b>Title</b>	<b>Page</b>
<b>Chapter-3</b>		
Table 1	Crystallographic data	34
Table 2	Selected bond lengths (Å) and bond angles (°)	35
Table 3	Magnetic properties of compounds 1-4	37
<b>Chapter-4</b>		
Table 1	Crystallographic data for 1	46
Table 2	Selected bond lengths (Å) and bond angles (°) for compound 1	47
Table 3	Fit parameters for the linear chain models	48
<b>Chapter-5</b>		
Table 1	Crystallographic data and structure refinement results for 1–4	54
Table S1	Selected bond lengths (Å) and bond angles (°) of 1 and 2	59
Table S2	Selected bond lengths (Å) and bond angles (°) of 3 and 4	60
<b>Chapter-7</b>		
Table 1	Crystallographic data of 1-2	71
Table S1	Selected bond lengths (Å) and bond angles (°) of 1 and 2	83
<b>Chapter-8</b>		
Table 1	Crystallographic data and structure refinement results for 1-4	94
Table S1	Selected bond lengths (Å) and bond angles (°) of 1 and 2	104
Table S2	Selected bond lengths (Å) and bond angles (°) of 3 and 4	105
<b>Chapter-10</b>		
Table S1	Gas Adsorption/Desorption data	129

## *Abbreviations*

---

MOF	metal organic framework
ip	isophthalate
bpy	dipyridyl
btcH3	benzenetricarboxylic acid
pyz	Pyrazine
pzdc	pyrazine dicarboxylic acid
pydc	pyridine dicarboxylic acid
H <sub>2</sub> pda	1,4-phenylene diacetic acid
dpe	di-(4-pyridyl)-ethane
ppms	physical property measurement system
AF	antiferromagnetism
CAF	canted antiferromagnetism
MPT	magnetic phase transition
ZFC	zero field cooled
FC	field cooled
TGA	thermogravimetric analysis
bIM	benzimidazole
$\chi^M$	Molar magnetic susceptibility

---

# **Introduction**



## 1.1 Metal-organic frameworks (MOFs)

It is well-known that zeolites, porous crystalline aluminosilicates, form three-dimensional microporous structures and feature tetrahedral inorganic oxyanions such as  $\text{SiO}_4$ ,  $\text{AlO}_4$  and  $\text{PO}_4$ . The microporosity of these structures contributes to the adsorption and catalytic activities of such materials. The 4, 6, 8, 10, 12, 14, 16, 18 and 20 membered rings of these oxyanions form unique one-, two- and three-dimensional channel structures. Metallosilicates, metalloaluminophosphates etc. have also been synthesized by substituting Si and/or Al cations of the tetrahedral oxyanions with various transition metal cations; the physical properties and relevance of these materials to specific applications have been widely studied. In addition, it has been discovered that multidentate organic ligands can bridge metal centers through coordination bonds to form one, two- or three-dimensional frameworks which may or may not have nanoporosity and as such can be thought of as being analogous to zeolites. Such compounds are now widely known as “*metal-organic frameworks (MOFs)*”, or “*coordination polymers*”. Thus, MOFs comprise a group of materials that have channels or pores analogous to those found in zeolites and are typically synthesized by the assembly of organic “*spacers*” linking metal ion “*nodes*” (figure 1).

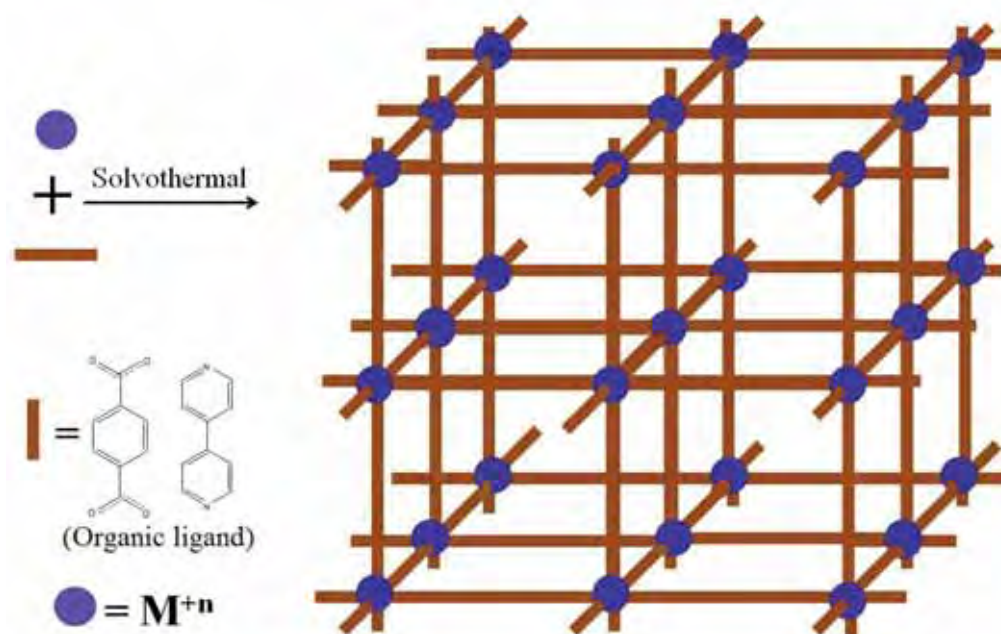


**Figure 1.** Schematic representation of MOFs built from metal ion as nodes and organic ligand as spacers.

The considerable attention garnered by MOFs is attributed to their porosity (figure 2), tunability, high internal surface areas and high thermal stability.<sup>1</sup> Although high surface areas are already known for both activated carbons and zeolites, it is the absence of any dead volume in MOFs which principally gives them, on a weight-specific basis, the highest porosities and world record specific surface areas. It is reported, for example, that in the case of the specific material MOF-177, the surface area reaches  $5640 \text{ m}^2\text{g}^{-1}$ ,<sup>2</sup> for MIL-101 up to  $5900 \text{ m}^2\text{g}^{-1}$ ,<sup>3</sup> and more recently, MOF-210 has been reported to have a record Brunauer-Emmett-Teller and Langmuir surface areas of 6240 and  $10,400 \text{ m}^2\text{g}^{-1}$ , respectively.<sup>4</sup> Moreover, unlike traditional porous zeolite materials whose pores are confined by tetrahedral oxide skeletons and thus are difficult to tune, the pores within MOFs can be systematically adjusted by the judicious choice of bridging organic linkers. Thus, the combination of very high degrees of porosity, surface area, pore size and wide chemical inorganic-organic composition has recently brought these materials to the attention of many researchers both in academia and industry.

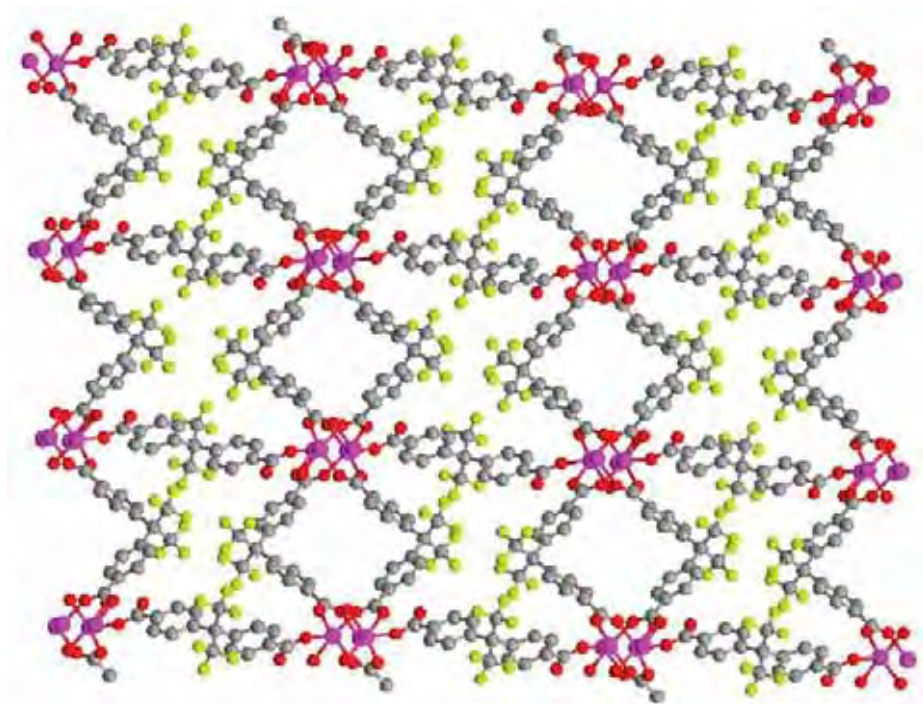


**Figure 2.** A Mn-paddle wheel based porous MOF synthesized in John Stride lab, UNSW.

## 1.2. Historical background

Three decades before the commonly assumed '*discovery*' of MOFs, Tomic made reference to materials which would nowadays be called MOFs in 1965.<sup>5</sup> Also, in 1965, Biondi *et al.* reported that Cu(II) tricyanomethanide to be a crystalline, polymeric

compound<sup>6</sup>, and some interesting features of MOFs, such as high thermal stability and high metal content were already noted. In 1990, Hoskins and Robson reported on the design of scaffold-like materials using Cu(I) centres and tetracyanotetraphenylmethane.<sup>7</sup> Interest in the field was again kindled by the group of O. M. Yaghi, who published the structure of MOF-5 in late 1999,<sup>8</sup> and the concept of reticular design, with totally different carboxylate linkers, in 2002.<sup>9</sup> Structures, properties and possible applications of MOFs were studied and now several hundred different MOFs have been identified to date.

### 1.3 Synthesis

Hydro(solvo)thermal reactions, well established for the synthesis of zeolites and MOFs, are typically carried out in sealed teflon-lined autoclaves, or "*bombs*", in the temperature range 120-220 °C under autogenous pressure (generally 10-30 atm.) and exploit the self-assembly of the product from soluble precursors. The reduced viscosity of solvents under these conditions enhances the diffusion processes so that crystal growth from solution is favoured. Under such non-equilibrium crystallization conditions, metastable kinetic phases, rather than the thermodynamically-favoured phases, are more likely to be isolated. In the majority of cases, crystals form at the reaction temperature and not upon cooling to room temperature. Small changes in one or more of the reaction variables of the hydrothermal parameter space, such as time, temperature, pH, stoichiometry and duration can have a profound influence on the reaction outcome.<sup>10</sup> Usually, the synthesis of MOFs is straightforward, using soluble salts as the source for the metal component, e.g. metal nitrates, chlorides or acetates. The organic ingredients, which are mostly mono-, di-, tri- and tetracarboxylic acids, are supplied in a polar organic solvent, typically an amine (triethylamine), amide (diethylformamide, dimethylformamide) or basic water. After combination of these inorganic and organic components under stirring, the metal-organic structures are formed by self-assembly at temperatures starting at room temperature and up to solvothermal conditions at 220°C within a few hours.

It is difficult to predict the network structures produced from the solvothermal reactions of a given simple metal ion and organic linker(s), because free metal ions contain too many binding sites for the organic linkers and have little directional information. Yaghi *et al.* defined the secondary building unit (SBU) as the '*geometry of the unit defined by the point of extension*' and illustrated possible inorganic SBUs (figure 3).<sup>11</sup> The design

and synthesis of metallosupramolecular networks based on SBUs facilitate network design and synthesis.

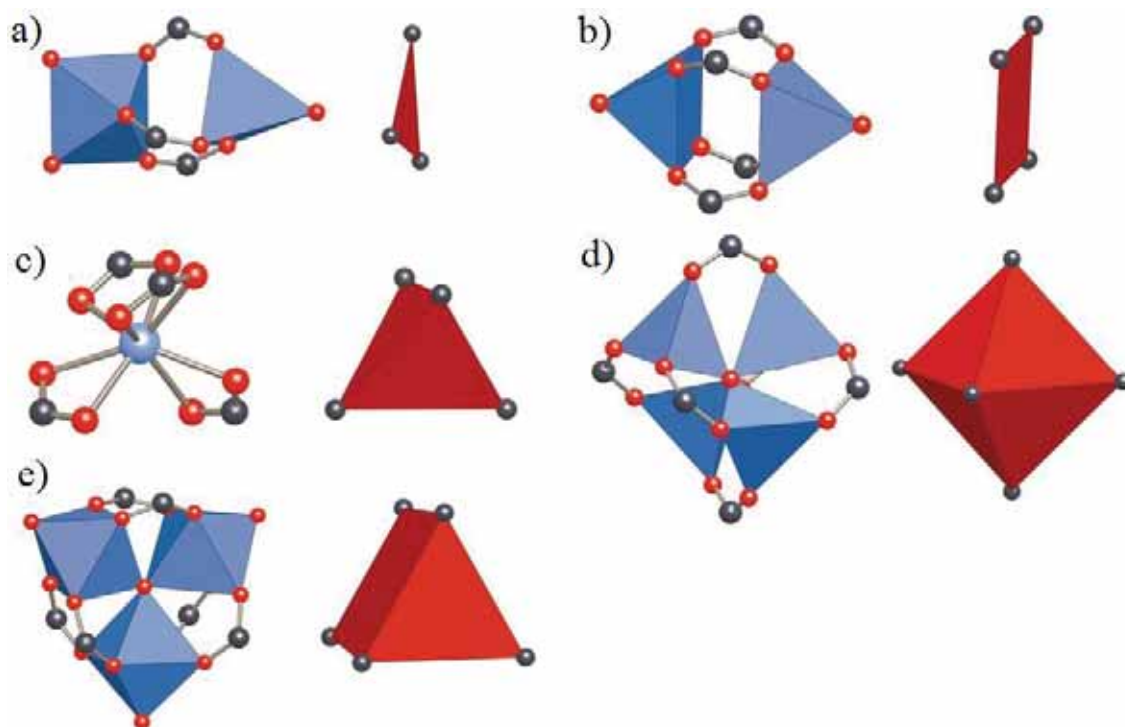


**Figure 3.** Examples of inorganic SBUs. (a) Triangle, (b) square planar, (c) tetrahedron, (d) octahedron, and (e) trigonal prism. (Reproduced from Ref.4)

### 1.3.1. *In situ*. ligand synthesis

Traditionally, coordination complexes are obtained by reactions of pre-synthesized or commercially available ligands with metal ions. Recently, *in situ*. ligand synthesis has been developed as a new approach to the crystal engineering of complexes in which ligand precursors are used in place of ligands to react with metals directly to produce single crystals of the desired complexes. *In situ*. ligand synthesis is of great interest in coordination chemistry and organic chemistry for the preparation of crystalline coordination complexes, and for the discovery of new organic reactions and understanding their mechanisms<sup>12</sup>. Its application as a new approach in crystal engineering of coordination complexes was first proposed by Champness and Schröder in 1997, when they unexpectedly observed *in situ*. cyclisation of 1,2-*trans*-(4-pyridyl)-ethene to yield ligand 1,2,3,4-tetrakis(4-pyridyl) cyclobutane.<sup>13</sup> Following Champness and Schröder's success, a variety of novel coordination complexes involving *in situ*. synthesis of ligands have been documented, most of which were prepared by hydro(solvo)thermal methods. The *in situ*. ligand synthesis, as an approach in the crystal

engineering of complexes, has the following benefits: (1) *in situ*. synthesis of ligands from an organic precursor removes the need to synthesize ligands that simplify the synthesis steps; (2) *in situ*. slow formation of ligands will ensure the growth of single crystals sufficiently large to allow X-ray single-crystal structural determination; (3) it is an environmental friendly synthesis procedure. Until now, more than 10 types of hydro(solvo)thermal *in situ*. ligand syntheses have been found, which include carbon carbon bond formation<sup>14</sup>, hydroxylation<sup>15</sup>, tetrazole formation by formal cycloaddition of cyano and azide<sup>16</sup>, triazole formation by [2+2+1] cycloaddition of cyano and amine, replacement of carboxyl with sulfonic group<sup>17</sup>, alkylation<sup>18</sup>, ether bond formation via dehydration coupling<sup>19</sup>, hydrolysis<sup>20</sup>, oxidation-hydrolysis<sup>21</sup>, acylation<sup>22</sup> and decarboxylation<sup>23</sup>.

Compared with traditional synthetic methods, hydro(solvo)thermal reactions generate more capacity for *in situ*. ligand synthesis due to the relatively critical reaction conditions. Indeed, hydro(solvo)thermal method has demonstrated increasing success in providing alternative pathways to crystalline complexes with *in situ*. synthesized ligands which are difficult to obtain by routine synthetic methods. For instance, the novel ligands 6-hydroxyl-2,2'-bipyridine (Hobpy) and 2-hydroxyl-1,10-phenanthroline (Hopphen), which are quite difficult to obtain by routine synthetic methods, are easily formed under hydrothermal conditions.<sup>7</sup> Rigid tetradentate ligands 2,2'-biphenanthroline (2,2'-biphen) and 2,2';6,2'';6'',2'''-quaterpyridine (quaterpy), which are not easy to obtain from 1,10-phenanthroline (phen) and 2,2'-bipyridine (2,2'-bpy), are *in situ*. formed via dehydrogenative coupling of bipyridine-like ligands under hydrothermal conditions.<sup>24</sup>

#### 1.4. Characterization

As MOFs are both crystalline and highly porous materials, most frequently X-ray diffraction (XRD) is used to characterize the crystallinity and phase purity, adsorption measurements can be performed to determine the porosity, and more elaborate studies making use of neutron scattering to determine sorption sites and the complete picture of any long-range magnetic ordering. As the metal content reaches values between 20-40 wt%, it is also desirable to check the local metal cluster arrangements and environments using more elaborate methodologies such as extended X-ray adsorption fine structure (EXAFS), X-ray adsorption near-edge structure (XANES) or X-ray photon spectroscopy (XPS). The adsorbates in the pores of MOFs can be investigated by UV-VIS, IR, Raman and inelastic neutron scattering spectroscopies.<sup>25</sup>



## 1.5. Applications

MOFs have been regarded as promising materials with many applications including gas storage, gas separation, catalysis, magnetic and optical properties, photoluminescence, drug delivery (figure 2) etc.; only a few of these are briefly discussed here.



**Figure 4.** Schematic representation of selected applications of MOFs.

### 1.5.1 Gas Adsorption

Due to the unique structure of MOFs and especially due to the absence of dead volume, it becomes possible to increase the volumetric specific gas storage above previously known levels. This effect can be very pronounced and depends on the type, temperature and pressure of the gas, as well as on the specific MOF material being used. The mechanism by which increased storage is achieved in MOF-filled gas cylinders over empty gas bottles is easy to understand, once the underlying principles are considered. The filling of a conventional gas cylinder is achieved simply by applying physical effects dependent upon the pVT-characteristics of the gas in question. Considering MOF-filled gas cylinders, the above mentioned effect is overlaid by an additional adsorption effect inside the MOF. As these frameworks are almost completely free of dead-volume, there is almost no notable loss of storage capacity due to space blocking by non-accessible volume. Summarizing, pVT-filling plus adsorption contributes to an

enhanced volumetric storage capacity. The structures, properties and possible applications of MOFs suitable as storage media have been studied in detail.<sup>26</sup> Comparisons with oxides, molecular sieves, porous carbon and heteropolyanion salts have been made by Barton and co-authors.<sup>27</sup>

The rapid consumption of petroleum deposits and the escalating air pollution problems caused by burning fossil fuels have driven the global research community to look for cleaner and renewable energy resources.<sup>28</sup> Albeit not a primary energy source, hydrogen is an ideal energy carrier. It almost triples the gravimetric heat of combustion of gasoline ( $120 \text{ MJ kg}^{-1}$  vs.  $44.5 \text{ MJ kg}^{-1}$ ). More importantly, the energy-releasing procedure of hydrogen oxidation, in either an internal combustion engine or a fuel-cell stack, produces only water as a by-product. In order to facilitate the research and application of hydrogen as an energy carrier, the US Department of Energy (DOE) has set the targets for on-board hydrogen storage systems: 6.0 wt% and  $45 \text{ g L}^{-1}$  by the year 2010, and 9.0 wt% and  $81 \text{ g L}^{-1}$  by 2015.<sup>29</sup> These targets should be reached at near-ambient temperature (from  $-40$  to  $85 \text{ }^{\circ}\text{C}$ ) and reasonable pressures (less than 100 atm.). Note that these are the goals for the system including container and any necessary accessories, the hydrogen storage capacity of the material itself should be even higher. In solid-state storage systems, a hydrogen atom/molecule either forms a strong chemical bond to a solid support (chemisorption) or interacts weakly with a sorbent (physisorption). The most frequently-studied sorbents are activated carbons, carbon nanostructures, zeolites, porous polymers, and MOFs. Because of the weak sorbent-sorbate interaction, physisorption-based hydrogen storage systems show fast kinetics with charging times of minutes. However, the same weak interaction results in gravimetric hydrogen uptake of a sorbent at ambient temperature and applicable pressure of typically less than 2 wt%.

In 2003, Rosi *et al.* reported the first MOF-based hydrogen storage result.<sup>30</sup> Since then, the hydrogen storage capacities of more than around 150 MOFs have been reported. A lot of factors i.e surface area and pore volume pore size and geometry, catenation, ligand structure and functionalization, unsaturated metal sites, chemical doping and spill over and sample preparation influence the hydrogen uptake capacity of MOFs. Among MOFs, MOF-210 currently ranks highest for gravimetric hydrogen uptake, with a value of  $86 \text{ mg g}^{-1}$  at 77 K and 70 bar (figure 5 & 6).<sup>4</sup> MOF-177 showed an uptake of 7.6 wt% at 77 K and 70 bar.<sup>31</sup> In the case of MIL-101 [ $\text{Cr}_3\text{F}(\text{H}_2\text{O})_2\text{O}(\text{bdc})_3$ ] bdc=benzene dicarboxylic acid, the high pressure hydrogen uptake at 77 K is not the

highest.<sup>32</sup> However, according to the author, the sample has not been fully activated due to the small opening within the cage structure. Moreover, in order to meet the DOE requirements, researchers are now trying to enhance the volumetric capacity of the materials for hydrogen uptakes. A recent report, for example, highlights the idea in which MOF-177 [Zn<sub>4</sub>O(btb)<sub>2</sub>] btb= benzene tribenzoic acid, was mechanically compressed to prepare monoliths with bulk densities more than three times its crystallographic density which is attributed to their decreasing micropore volume, which gave 78% increase in the total volumetric hydrogen storage capacity.<sup>33</sup>

MOFs are also emerging as promising materials for adsorbing CO<sub>2</sub> and CH<sub>4</sub> gas. In general, most research efforts in this area have focused on either (1) increasing the MOF pore volume and surface area to increase gas capacity or (2) modifying the pore chemistry by incorporating functional moieties having high affinities for these gases.<sup>34</sup> In 2007, Ma, *et al.*, reported an anthracene derivative based MOF PCN-14 [Cu<sub>2</sub>(H<sub>2</sub>O)<sub>2</sub>(adip).2DMF] adip= 9,10-anthracenediyl di-isophthalate, with a pore volume of 0.87 cm<sup>3</sup>g<sup>-1</sup>, which exhibited an absolute methane-adsorption capacity of 230 v/v, 28% higher than the DOE target (180 v/v) for methane storage (figure 7).<sup>35</sup> In 2010, Yaghi *et al.*, calculated total uptakes (446, 394, and 476 mg g<sup>-1</sup> for MOF-200,-205, and -210, respectively) which were more than 50% greater than those of PCN-14,<sup>4</sup> although the excess methane uptake in MOF-200, -205, and -210 (234, 258, and 264 mg g<sup>-1</sup> at 80 bar, respectively) were smaller than that in PCN-14 (253 mg g<sup>-1</sup> at 290 K and 35 bar, respectively), however all isotherms were not saturated.

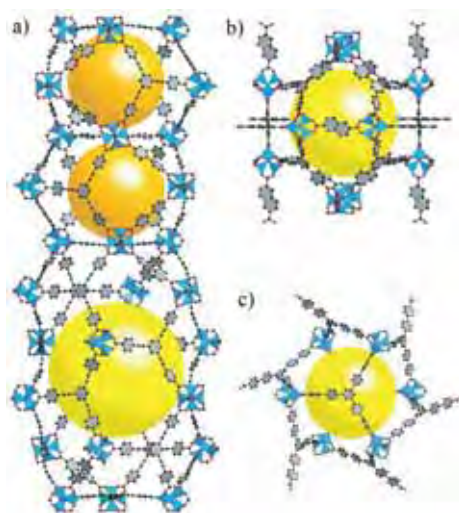


**Figure 5.** Crystal structures of MOF-210 (a), MOF-205 (b) MOF-200 (c). [Reproduced from ref. 4]



Similarly, CO<sub>2</sub> uptake value of 2400 mg g<sup>-1</sup> in both MOF-200 and -210 (figure 6) exceeds those of any other porous material, such as MOF-177 and MIL-101c(Cr) (1470 and 1760 mg g<sup>-1</sup>, respectively).

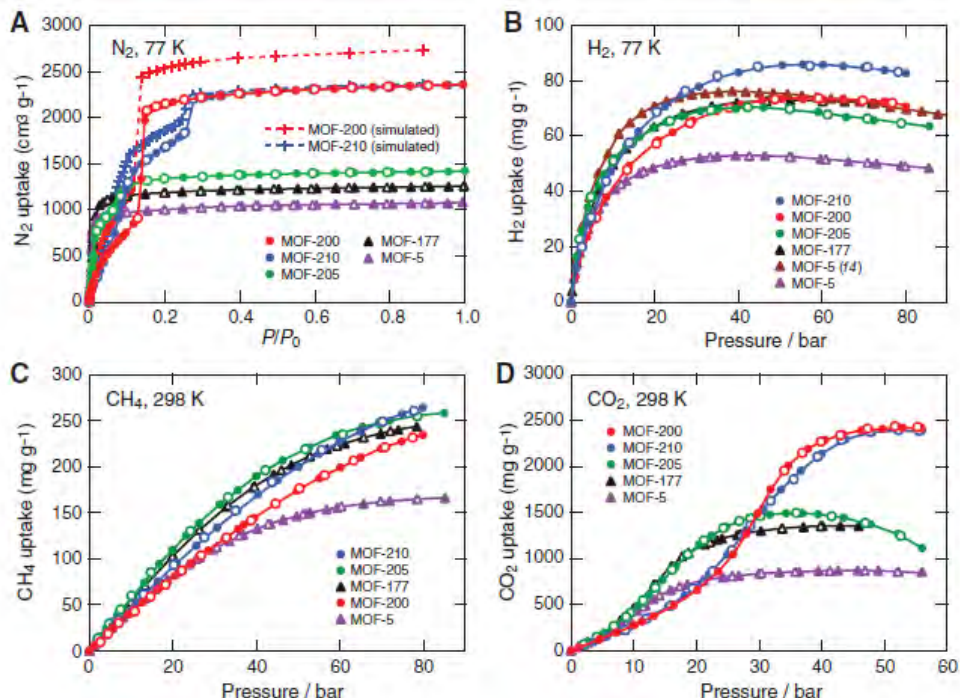


**Figure 6.** (A) Low-pressure N<sub>2</sub> isotherms of MOF-5, -177, -200, -205, and -210 at 77 K. Simulated isotherms of MOF-200 and -210 were overlaid. P/P<sub>0</sub>, relative pressure. High-pressure H<sub>2</sub> isotherms were measured at 77 K (B), and (C) CH<sub>4</sub> and (D) CO<sub>2</sub> isotherms were measured at 298 K of the same MOFs. [Reproduced from ref. 4]

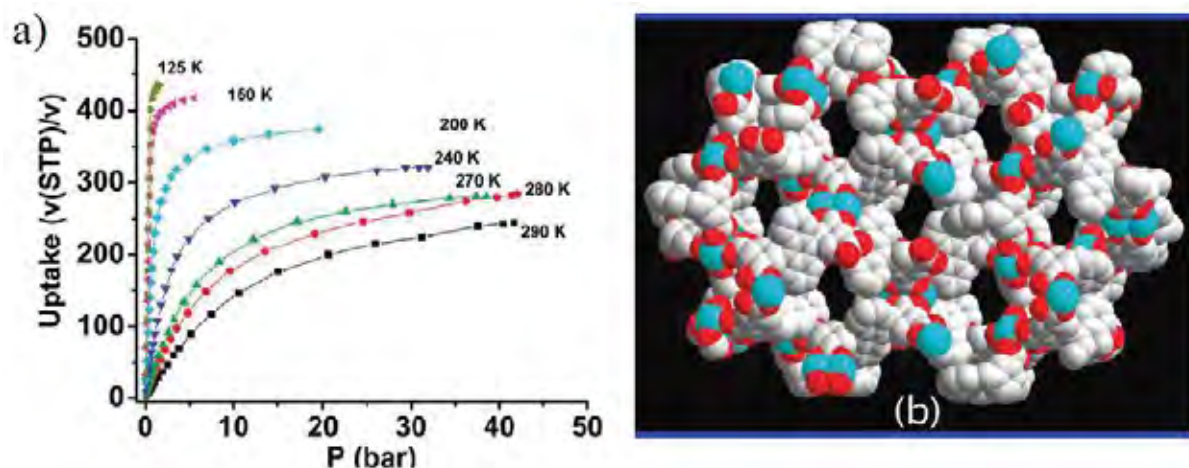


**Figure 7.** High-pressure methane sorption isotherms at various temperatures (a), 3D framework of PCN-14 (b) [Reproduced from ref. 35]

### 1.5.2. Gas separation

Selective adsorption occurs when different affinities for different substances on the surface of an adsorbent emerge at given conditions. Separation is a process that divides a mixture into its components. Separation can be achieved based on selective adsorption. As the opposite process of mixing, which is favored by the second law of thermodynamics, separation is normally not a spontaneous procedure. Consequently, it often requires major energy consumption, which stimulates many research interests in separation science and technology.<sup>36</sup> Gas separation techniques include cryogenic distillation, membrane-based, and adsorption-based technologies. Since the invention of synthetic-zeolites in the 1940s, with the emergence of various adsorbents and the development of adsorption-based separation processes, adsorption has become a key gas separation tool in industry.<sup>37</sup> With the synthesis of more and more new sorbent materials with tailor-made porosity and surface properties and the urgent demand for green separation procedures, adsorptive separation will become increasingly more important. Thus, adsorptive separation will likely play a key role in future energy and environmental technologies. Notable examples are H<sub>2</sub> and CH<sub>4</sub> purifications, CO<sub>2</sub> capture, CO removal for fuel cell technology, desulfurization of transportation fuels, and other technologies for meeting higher environmental standards. Many porous materials, such as aluminosilicate zeolites, carbon and metal-oxide molecular-sieves, aluminophosphates, activated carbon, activated alumina, carbon nanotubes, silica gel, pillared clays, inorganic and polymeric resins, porous organic materials, and porous metal-organic composites have been explored as adsorbents, some of which have now found their uses in industry. Gas adsorptive separation by a porous material is usually achieved by one or several of the following mechanisms:<sup>38</sup> (1) due to size and/or shape exclusion, certain components of a gas mixture are prevented from entering the pores of an adsorbent while other components are allowed to enter the pores where they are subsequently adsorbed, known as the molecular sieving effect; (2) due to different adsorbate surface and/or adsorbate packing interactions, preferential adsorption of certain components over others occurs on the surface of an adsorbent, known as the thermodynamic equilibrium effect; (3) due to different diffusion rates, certain components enter the pores and become adsorbed faster than other components, known as the kinetic effect; (4) due to the quantum effects, some light molecules have different diffusion rates in narrow micropores, which allows such molecules to be separated, also known as the quantum sieving effect.

MOFs are ideal adsorbents for gas storage and separation due to their large surface areas, adjustable pore sizes, and controllable surface properties. As potential adsorbents in gas separation and purification, MOFs offer unique advantages for specific applications based on their structural characteristics. Currently, the investigation of MOFs as adsorbents in gas separation is in its early stage. Arbitrarily, MOFs can be categorized into rigid and flexible/ dynamic classes.<sup>39</sup>



**Figure 8.** Schematic illustration of selective gas adsorption in rigid MOFs [Reproduced from ref. 40]

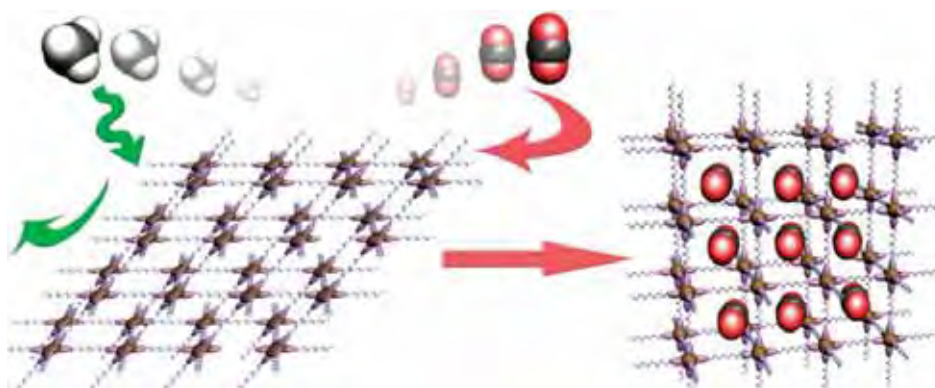


**Figure 9.** Schematic illustration of selective gas adsorption in a flexible MOF, [Reproduced from ref. 40].

Rigid MOFs have comparatively stable and robust porous frameworks with permanent porosity, similar to zeolites and other inorganic porous materials, whereas flexible

MOFs possess dynamic, “*soft*” frameworks that respond to external stimuli, such as pressure, temperature, and guest molecules.<sup>40</sup>

Selective adsorption based mainly on the molecular sieving effect has been confirmed in several MOFs. Only few examples are described here. Structural analysis revealed that manganese formate has a robust 3D framework structure with 1D channels.<sup>41</sup> These channels contain larger cages, which are connected to each other via a small window. Gas sorption experiments indicated that at 78 K this material can selectively adsorb H<sub>2</sub> over N<sub>2</sub> and Ar, and at 195 K CO<sub>2</sub> over CH<sub>4</sub>. In both cases, the adsorption capacities of the excluded gases N<sub>2</sub>, Ar, and CH<sub>4</sub> were almost zero. Thus, the selectivity was attributed to the small aperture of the channels. The selective adsorption of H<sub>2</sub> but not N<sub>2</sub> due to size exclusion has also been observed in Mg<sub>3</sub>(ndc)<sub>3</sub> ndc=narhthalene dicarboxylic acid,<sup>42</sup> PCN-13,<sup>43</sup> Sm<sub>4</sub>Co<sub>3</sub>(pyta)<sub>6</sub>(H<sub>2</sub>O)<sub>x</sub> pyta= 2,4,6-pyridine tricarboxylate,<sup>44</sup> Cu(F-pymo)<sub>2</sub> pymo= 5-fluoro-pyrimidin-2-olate,<sup>45</sup> and Zn<sub>2</sub>(cnc)<sub>2</sub>-(dpt). Guest, cnc= 4-carboxycinnamic acid, dpt= 3,6-di-4-pyridyl-1,2,4,5-tetrazine.<sup>46</sup> at 77 K. A coordinatively linked interpenetrated MOF, PCN-17,<sup>47</sup> was reported recently, which has a porous structure containing large cages linked by relatively small apertures and which retains its porosity at temperatures as high as 480°C. The interpenetration and sulfate bridging in PCN-17 reduces its pore (window) size to approximately 3.5 Å leading to selective adsorption of H<sub>2</sub> and O<sub>2</sub> over N<sub>2</sub> and CO. This material may thus have applications for the separation of N<sub>2</sub> and O<sub>2</sub>, the separation of H<sub>2</sub> from CO in fuel-cell applications, as well as the H<sub>2</sub> enrichment of the N<sub>2</sub>/H<sub>2</sub> exhaust. MIL-96<sup>48</sup> and Zn<sub>2</sub>(cnc)<sub>2</sub>(dpt)<sup>49</sup> were also found to selectively adsorb CO<sub>2</sub> over CH<sub>4</sub> based on size/shape exclusion. These materials may be useful in the separation of CO<sub>2</sub> and CH<sub>4</sub>, which is an essential industrial process for natural-gas purification and landfill-gas separation. It should be pointed out that in some systems the activation temperature of the sample has important effects on the pore sizes and its guest-free counterpart. The former has the ability to selectively adsorb H<sub>2</sub> over N<sub>2</sub> whereas the latter adsorbs CO<sub>2</sub> over CH<sub>4</sub>. In two additional examples, Cd<sub>3</sub>(OH)<sub>2</sub>(apt)<sub>4</sub>·(H<sub>2</sub>O)<sub>2</sub><sup>50</sup> and CUK-1 [Co<sub>3</sub>(2,4-pdc)<sub>2</sub>(OH)<sub>2</sub>].9H<sub>2</sub>O pdc= pyridine dicarboxylic acid,<sup>51</sup> channels inside the MOFs are larger than all of the adsorbed gas molecules. The former selectively adsorbed H<sub>2</sub> and CO<sub>2</sub> but not N<sub>2</sub>, and the latter adsorbed O<sub>2</sub> and H<sub>2</sub> over N<sub>2</sub> and Ar at low temperatures. In addition, it should also be noted that for the same MOF, the adsorption properties may be distinct at different temperatures. One such example is Mn(HCOO)<sub>2</sub>.<sup>52</sup> As



discussed above, at low temperatures, this MOF exhibited selective adsorption of H<sub>2</sub> over N<sub>2</sub>, whereas at room temperature, no selectivity was found for the two gases.

As demonstrated above, MOFs have great potential in applications around gas separations because both their pore size, shape and surface properties, can be easily tuned by the selection of metal or metal clusters, ligand design and functionalization, as well as by post-synthetic modification. For molecular sieving to occur, it is essential to use restricted small pores.

### 1.5.3. Catalytic applications

Heterogeneous catalysis was one of the earliest proposed applications for crystalline MOF materials, as well as one of the earliest demonstrated applications. A defining characteristic of functional MOF materials is porosity, and early-on the analogy between MOFs and another class of catalytic porous materials, aluminosilicate zeolites, was noted. Zeolites, of course, are among the most commercially important classes of catalyst. As purely inorganic materials, they are extraordinarily robust and, therefore well suited to catalysis under extreme conditions, whilst their porosity yields internal surface areas that are relatively large, thereby facilitating their catalytic reactivity. Although crystalline MOFs share some of the catalytically relevant features of zeolites (large internal surface areas and uniform pore and cavity sizes), they also differ in some quite important ways. Firstly, because they also contain organic components, MOFs can be synthesized in a much greater array of chemical varieties than zeolites. Secondly, whilst many MOFs show good thermal stability (400-500 °C), none approach the stability of zeolites. Thirdly, whilst many MOFs exhibit zeolite-like permanent microporosity, others collapse upon the removal of entrapped solvent molecules. The persistence of microporosity after solvent evacuation is essential for gas-phase catalysis. For catalysis of condensed-phase reactions, however, it may not be essential. The uniformity of the pores and controllability in channel sizes of MOFs accounts for much of their catalytic selectivity (figure 10).<sup>53</sup> Indeed, one of the earliest reported examples of catalytic behaviour in MOFs (i.e., cyanosilylation of various aldehydes) was based on a material (a 2D polymer of 4,4'-bipyridine and cadmium nitrate) that likely would not have survived solvent removal.<sup>54</sup> Only a few dozen reports of chemical catalysis by crystalline, microporous MOFs have appeared to date; a few of these are briefly described here as examples. Alaerts *et al.* investigated the behaviour of the anhydrous version of HKUST-1 [Cu<sub>3</sub>(btc)<sub>2</sub>(H<sub>2</sub>O)<sub>3</sub>] as an acid catalyst.<sup>55</sup> Recognizing the potential for opportunistic catalysis at defect sites (such as exposed carboxylic acids), they

examined three reactions: isomerisation of  $\alpha$ -pinene oxide, cyclization of citronellal, and the rearrangement of  $\alpha$ -bromoacetals, whose product selectivity patterns differ significantly for Brønsted vs. Lewis acid-catalyzed pathways. Based on experimental data, these researchers concluded that  $[\text{Cu}_3(\text{btc})_2]$  indeed functions primarily as a Lewis acid catalyst. Kaskel and co-workers evaluated the behavior of MIL-101, a large-cavity MOF having the formula  $[\text{Cr}_3\text{F}(\text{H}_2\text{O})_2\text{O}(\text{bdc})_3]$ ,<sup>56</sup> as a cyanosilylation catalyst. The coordinated water molecules in MIL-101 are easily removed to expose Cr(III) sites. As one might expect, given the greater Lewis acidity of Cr(III) vs. Cu(II), MIL-101 is much more active than HKUST-1 as a catalyst for the cyanosilylation of aldehydes. Additionally, the Kaskel group observed that the catalytic sites of MIL-101, in contrast to those of HKUST-1, are immune to unwanted reduction by benzaldehyde. Lu *et al.* examined the oxidative catalytic behavior of a porous three-dimensional MOF having the formula  $[\text{Co}(\text{bpb})]\cdot 3\text{DMF}$ , (bpb = 1,4-bis(4'-pyrazolyl)-benzene).<sup>57</sup> Exposure to tert-butyl hydroperoxide is believed to convert Co(II) to Co(III). Addition of cyclohexene results in the formation of tert-butyl-2-cyclohexenyl peroxide in 83% yield, albeit with some degradation of the MOF after a few dozen turnovers.

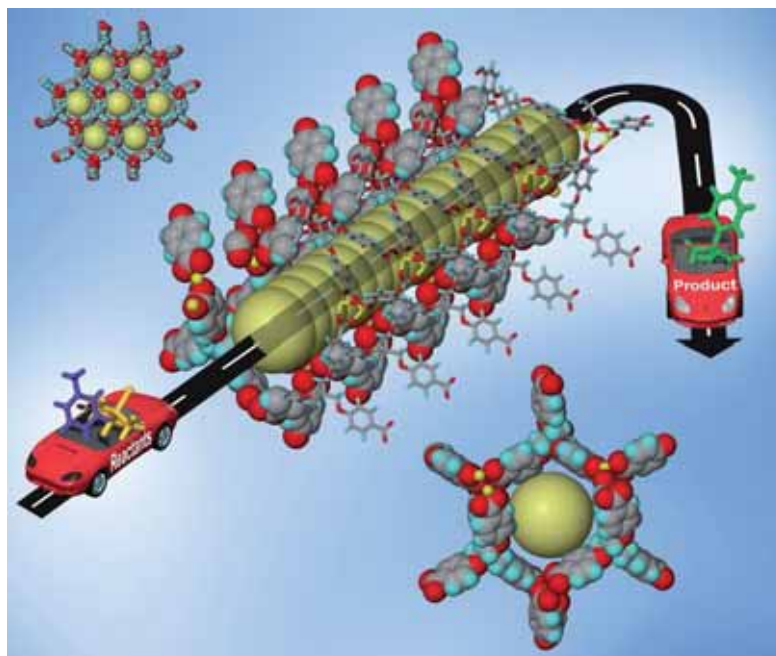


**Figure 10.** Schematic illustration of catalytic process in porous MOFs, [Reproduced from ref.53].

The future of the field clearly lies in demonstrating advantageous catalytic behaviour that is unique to MOFs. As noted above, a small number of examples of unique catalyst structures and product distributions have begun to appear. Many more remain to be discovered.

### 1.6. Magnetism in MOFs

The origin of magnetism lies in the orbital and spin motions of electrons and how the electrons interact with one another. In some materials there is no collective interaction of atomic magnetic moments, whereas in other materials there is a very strong interaction. On the basis of spin alignment of unpaired electrons, the magnetic behavior of materials can be classified into various major groups (1) diamagnetism, (2) paramagnetism, (3) ferromagnetism, (4) antiferromagnetism, (5) ferrimagnetism, (6) canted antiferromagnetism etc. Materials in the first two groups are those that exhibit no collective magnetic interactions and are not magnetically ordered. Materials in the last four groups exhibit long-range magnetic order below a certain critical temperature.

Probably the most interesting aspect of magnetochemistry concerns the interactions of magnetic ions. For example, if two ions interact through an intervening ligand; a so-called superexchange mechanism, which is generally accepted as the most important source of metal-metal interactions or magnetic exchange in coordination compounds. In three dimensional crystalline systems, if the spins on a given lattice are all aligned spontaneously in the same direction, then the ordered state is ferromagnetic, and if the spins align antiparallel then the phenomena is known as antiferromagnetism (figure 11).

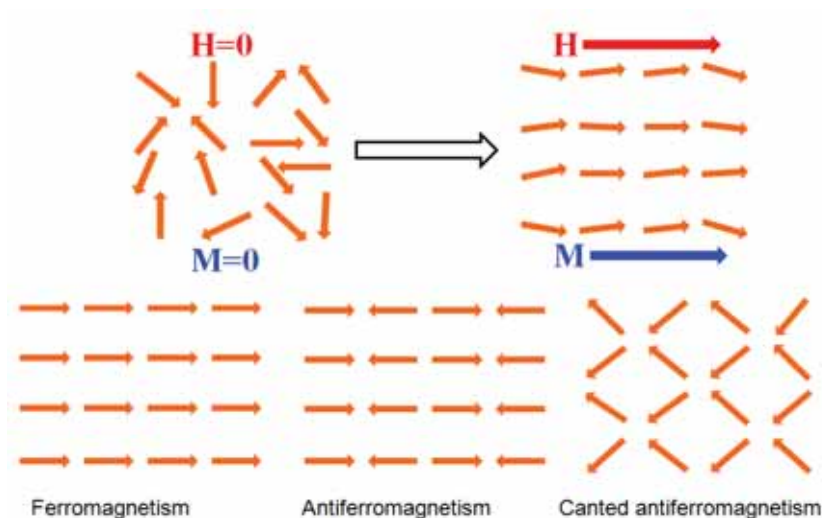


**Figure 11.** Schematic representation of different spin orientations of unpaired electrons

The spontaneous ordering of spins persists below a certain critical temperature, usually called Curie temperature ( $T_C$ ) for ferromagnetic materials and the Néel temperature ( $T_N$ ) for antiferromagnetic materials. The magnetic susceptibility obeys the Curie-Weiss law at temperatures well above critical temperatures, where the spins act as a paramagnetic system (figure 12). Classical or molecular field theory (MFT) assumes that there is some sort of internal magnetic field which orients the spin, while the course thermal agitation opposes this effect; the temperature  $T_C$  is that temperature at which the spontaneous magnetization loses the battle. The most convenient way to establish experimentally that a compound obeys the Curie-Weiss law is to obtain a horizontal straight line for the  $\chi T$  vs.  $T$  plot. A plot of  $\chi^{-1}$  vs.  $T$  for a system obeying the Curie-Weiss law gives a straight line of which the slope is  $C^{-1}$  ( $C$  = Curie constant). The intercept with the  $T$  axis yields both the sign and the value of  $\theta$  ( $\theta$  = Weiss constant). In the framework of this model, a positive  $\theta$  indicates the ferromagnetic interactions and a negative  $\theta$  indicates antiferromagnetic interactions. If the magnetic data are represented in the form of  $\chi T$  vs.  $T$  plot, a positive  $\theta$  leads to an increase and negative  $\theta$  value leads to a decrease of  $\chi T$  on cooling, the lower the temperature more pronounced this effect (figure 12).

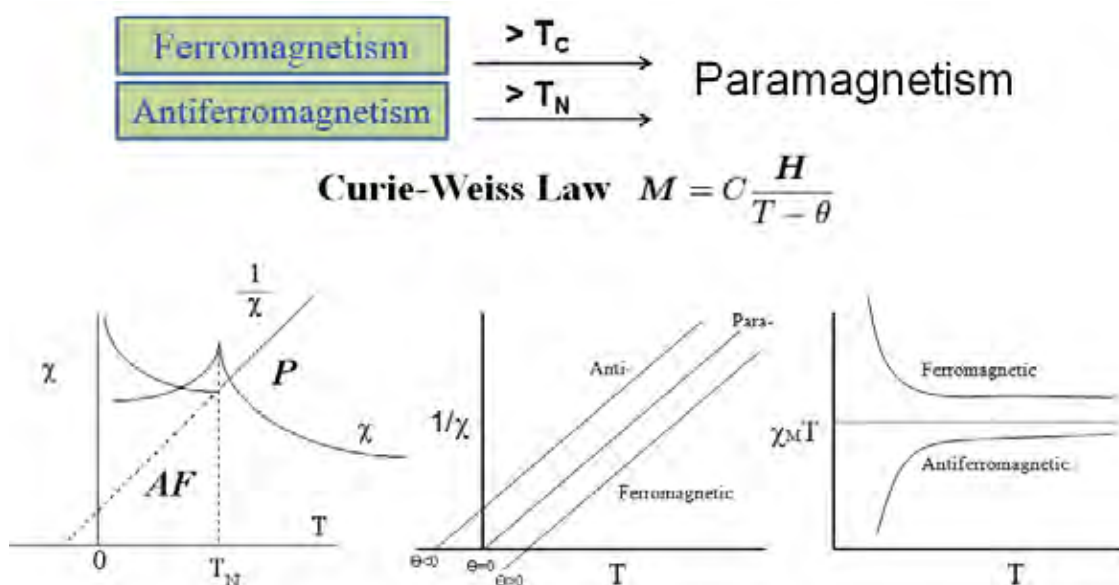


**Figure 12.** Diagrammatic representation of Curie-Weiss law

The magnetic properties of hybrid inorganic-organic compounds, in which extended inorganic networks or local paramagnetic centers (mostly of transition metal and



lanthanide ions) are linked by diamagnetic linkers that can efficiently mediate magnetic exchange, have evoked considerable interest. The mode of linkage and the dimensionality of the inorganic sub network, along with the size, geometry, chemical functionality and various coordinating modes of the linkers, provide excellent means of controlling and modulating the magnetic properties in these solids. The connection between moment carriers at distances that lie within a range of interaction is required, and is often fulfilled in MOFs. Magnetism can also be introduced via magnetic guests within a non-magnetic framework. So far the majority of magnetic frameworks are those containing paramagnetic metal centres and in particular, the first row transition metals (V, Cr, Mn, Fe, Co, Ni and Cu). These metals, which may exist in different oxidation states, allow variation of the two important parameters, spin quantum number and magnetic anisotropy. Despite the fact that the magnetic properties of MOFs have generally been explored and many different magnetic MOFs have been synthesized and shown to have bulk magnetic ordering phenomena, a lot of work is still required in this field in order to deliver truly multi-functional porous magnetic materials.

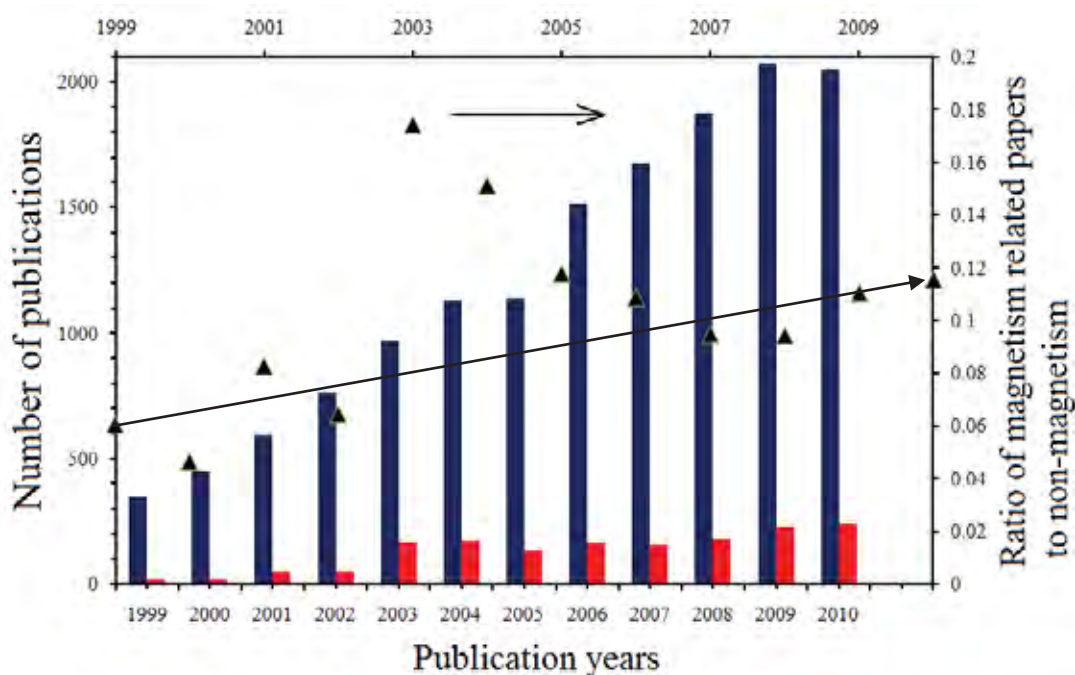


**Figure 13.** The number of published articles containing key words “coordination polymers” (blue), “magnetic coordination polymers” (red), survey by Scifinder until 2010

It is clear from figure 13 that of 18,486 articles published in the field of MOFs (until Dec., 2010), only 1517 articles were identified as studying the magnetic properties of MOFs. The ratio of magnetism related papers of MOFs to non-magnetic articles

abruptly increased in 2003 and gradually decreases until 2009 before continuing on its long-term increase, indicating that work in this field requires and continues to receive more attention.

As the guideline for the rational design of new materials, magneto-structural correlations are an essential element in the research of molecule-based magnets. Magnets with controllable structures and properties are a very important topic and crystal engineering design plays an important role in this methodology. In MOFs, magnetic interactions between nearest neighbour metal centers are mediated by organic ligands. The ligands used in the development of MOFs are usually those having oxygen (water, hydroxide, alkoxide, alcohol and carboxylate) or nitrogen (amine, pyridine, azide and azole) coordinating atoms and in a few cases, sulfur (thiolate). Water or alcohol can contribute one (terminal) or two (one-atom bridge) bonds between metals; whilst hydroxide or alkoxide groups can contribute from one (terminal) to up to three (one-atom bridging) bonds.<sup>39</sup> In contrast, carboxylate can contribute from one to up to four bonds to the metals, adopting combinations of syn and anti configurations that have consequences on the magnetic exchange between nearest neighbours. Ancillary ligands containing nitrogen can contribute one bond per pyridine nitrogen atom and one or two per azide nitrogen atom to the metals. As a result, several structural modes i.e. metallic dimers, trimers, tetramers, chains and ladders connected via organic moieties in 3D architectures ultimately govern the overall magnetic properties. Despite the great progress in the construction of magnetic molecular materials, it still remains a challenge to obtain extended networks with spontaneous magnetizations and predictable magnetic properties. So far the ultimate goal of scientists is to develop materials with strong interactions between magnetic centers and those which show long range magnetic ordering. Another goal is to cross-fertilize the magnetism with the porosity. The synergism of both magnetic properties and the exceptional characteristics of microporous materials can open a new route to the development of low-density magnetic materials, magnetic sensors and multifunctional materials. Compounds with FM interactions are of greatest interest, but good examples of hybrid compounds with strong FM interactions are still yet to be discovered. Such compounds, especially if they are microporous, would be valuable since they might be able to separate nitrogen and oxygen, making use of the paramagnetism of molecular oxygen. Since the critical temperature has been observed only at low temperatures, scientists are now also focussing to target a

geometry which can give magnetic ordering phenomena at higher  $T_C$ 's. Few examples of already reported exciting magnetic MOFs are briefly discussed here.

A cobalt 1,4-cyclohexane dicarboxylate,  $[\text{Co}_5(\text{OH})_8(\text{CHDC})\cdot 4\text{H}_2\text{O}]$ , has a  $T_C$  of 60 K, a temperature that is among the highest observed in this class of compounds.<sup>58</sup> Its structure is based on metal–hydroxide octahedral–tetrahedral layers pillared by dicarboxylate ions ( $\text{I}^2\text{O}^1$  type). A 3D framework is formed that contains channels filled with water. The dehydration–rehydration process is reversible, thereby conferring to this hybrid some porous properties. Removal of the water molecules leads to a shift of the layers combined with a tilt and a rotation of the organic moieties and a shortening of the interlayer space of about 1 Å. The first example of a metal–radical open-framework material  $[\text{Cu}_3(\text{ptmtc})_2(\text{py})_6(\text{EtOH})_2(\text{H}_2\text{O})]_n$  (ptmtc, polychlorinated triphenylmethyl tricarboxylic acid radical), (MOROF-1) that combines very large pores with magnetic ordering at low temperatures (figure 14).<sup>59</sup> An interesting 3D cobalt terephthalate complex,  $[\text{Co}_2(\text{OH})_2(1,4\text{-bdc})]$ , is built up from inorganic layers where two types of parallel tilted chains of edge-sharing octahedra are linked by OH bridges.<sup>60</sup> The layers are then connected together through terephthalate linkers into a 3D architecture. Magnetic studies show that the intralayer exchange interaction between Co(II) ions is ferromagnetic, but the whole system orders antiferromagnetically at 48 K with a metamagnetic transition above a threshold field of 0.2 T. The existence of conjugated  $\pi$  electrons in the terephthalate bridges explains the antiferromagnetic interactions between the layers. Below 45 K, the compound exhibits canted antiferromagnetism associated with a noncollinear orientation of the moments between the layers. The magnetization loop shows a large coercive field of 5.9 T at 4.2 K, which must be related to extremely large single-ion anisotropy on the Co sites. The copper analogue of the above cobalt terephthalate, however, exhibits ferromagnetic coupling through the terephthalate bridge between the ferromagnetic sheets. The nickel fumarate structure  $[\text{Ni}_3(\text{OH})_2(\text{H}_2\text{O})_4(\text{C}_4\text{H}_2\text{O}_4)_2\cdot 2\text{H}_2\text{O}]$ , consists of a metal oxide chain built from trimers consisting of two edge-sharing octahedra linked by a  $\mu_3\text{-OH}$  to a vertex of a third one. The chains are connected by fumarate ions to form a 3D framework.<sup>61</sup> This compound behaves as a ferrimagnet at  $T < 20$  K, with a spontaneous bulk magnetization below 6 K.

It is clear that metal–organic framework systems offer wide range of structures which can ultimately give rise to wide range of new exciting magnetic materials.

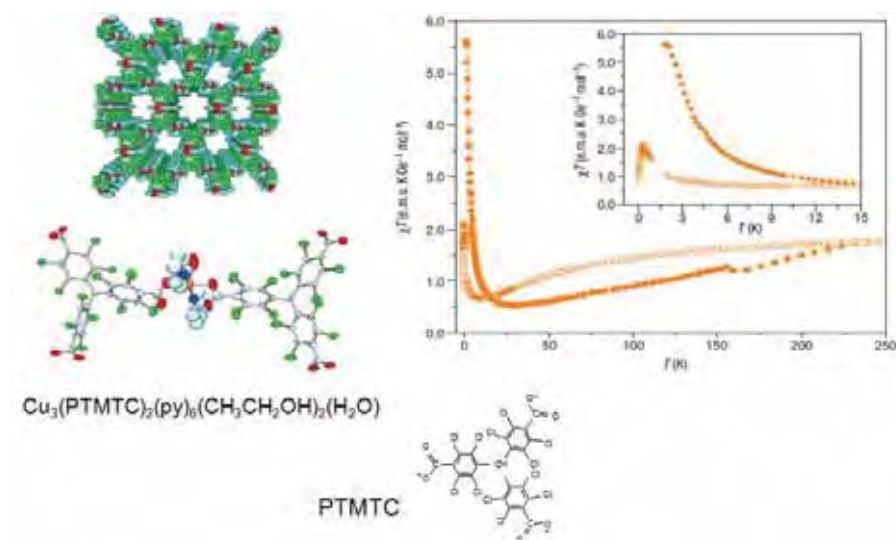


**Figure 14.** First example of microporous material showing magnetic ordering phenomena at low temperature [Reproduced from ref. 59]

To summarize, while some of the physical properties of MOFs have been examined, as described in this chapter, there is need for greater in-depth studies. Certain potential combinations of properties may be unique to these materials, for example, it would be exciting if we could make a high  $T_c$  magnet with channels into which molecules could be adsorbed. In addition, there are many properties that are yet to be discovered in hybrid systems, such as thermoelectricity, superconductivity, lasing and metal-insulator transitions etc.

### 1.7. Aims of the project

We have set ourselves a task:

- The synthesis of new metal-organic network materials possessing targeted functionality
- To fully characterize the new materials using a range of techniques, including powder XRD, single crystal analysis, UV-Vis & IR-spectroscopy, elemental analysis etc.
- To examine the affect of various reaction parameters on *in situ*. ligand synthesis
- To characterize the adsorption/desorption cycling of the materials, targeted at their application to gas separation
- To study the nature of magnetic exchange interactions

## References

- <sup>1</sup> (a) R. Evans and W. B. Lin, *Acc. Chem. Res.*, 2002, **35**, 511; (b) B. Kesanli and W. B. Lin, *Coord. Chem. Rev.*, 2003, **246**, 305; (c) S. Kitagawa, R. Kitaura and S. Noro, *Angew. Chem. Int. Ed.*, 2004, **116**, 2388; (d) C. N. R. Rao, S. Natarajan and R. Vaidhyanathan, *Angew. Chem. Int. Ed.*, 2004, **116**, 1490; (e) J. L. C. Rowsell and O. M. Yaghi, *Micropor. Mesopor. Mat.*, 2004, **73**, 3; (f) G. Férey, C. Mellot-Draznieks, C. Serre and F. Millange, *Acc. Chem. Res.*, 2005, **38**, 217; (g) D. Bradshaw, J. B. Claridge, E. J. Cussen, T. J. Prior and M. J. Rosseinsky, *Acc. Chem. Res.*, 2005, **38**, 273; (h) Y. Robin and K. M. Fromm, *Coord. Chem. Rev.*, 2006, **250**, 2127; (i) M. A. Nadeem, M. Bhadbhade, R. Bircher and J. A. Stride, *CrysEngComm.*, 2010, **12**, 1391.
- <sup>2</sup> A. G. Wong-Foy, A. J. Matzger and O. M. Yaghi, *J. Am. Chem. Soc.*, 2006, **128**, 3494.
- <sup>3</sup> G. Férey, C. Mellot-Draznieks, C. Serre, F. Millange, J. Dutour, S. Surblé and I. Margiolaki, *Science*, 2005, **309**, 2040.
- <sup>4</sup> H. Furukawa, N. Ko, Y. B. Go, N. Aratani, S. B. Choi, E. Choi, A. O. Yazaydin, R. Q. Snurr, M. O'Keeffe, J. Kim and O. M. Yaghi, *Science*, 2010, **239**, 424.
- <sup>5</sup> E. A. Tomic, *J. Appl. Polym. Sci.*, 1965, **9**, 3745.
- <sup>6</sup> C. Biondi, M. Bonamico, L. Torelli and A. Vaciago, *Chem. Commun.*, 1965, 191.
- <sup>7</sup> B. F. Hoskins and R. Robson, *J. Am. Chem. Soc.*, 1990, **112**, 1546.
- <sup>8</sup> H. Li, M. Eddaoudi, M. O'Keeffe and O. M. Yaghi, *Nature*, 1999, **402**, 276.
- <sup>9</sup> (a) M. Eddaoudi, J. Kim, N. Rosi, D. Vodak, J. Wachter, M. O'Keeffe and O. M. Yaghi, *Science*, 2002, **295**, 469; (b) O. M. Yaghi, M. Eddaoudi, H. Li, J. Kim and N. Rosi, Patent, WO 2002/088148, 2002.
- <sup>10</sup> P. J. Hagrman, D. Hagrman and J. Zubietta, *Angew. Chem. Int. Ed.*, 1999, **38**, 2638.
- <sup>11</sup> O. M. Yaghi, M. O'Keeffe, N. W. Ockwig, H. K. Chae, M. Eddaoudi and J. Kim, *Nature*, 2003, **423**, 705.
- <sup>12</sup> (a) E. C. Constable, *Metals and Ligand Reactivity*, VCH, Weinheim, 1996; (b) R. A. Michelin, M. Mozzon and R. Bertani, *Coord. Chem. Rev.*, 1996, **147**, 299.
- <sup>13</sup> J. Blake, N. R. Champness, S. S. M. Chung, W.-S. Li and M. Schröder, *Chem. Commun.*, 1997, 1675.
- <sup>14</sup> R. K. Feller, P. M. Forster, F. Wudl and A. K. Cheetham, *Inorg. Chem.*, 2007, **46**, 8717.
- <sup>15</sup> (a) X.-M. Zhang, M.-L. Tong and X.-M. Chen, *Angew. Chem. Int. Ed.*, 2002, **41**, 1029; (b) X.-M. Zhang, M.-L. Tong, M.-L. Gong, H.-K. Lee, L. Luo, K.-F. Li, Y.-X.

- Tong and X.-M. Chen, *Chem. Eur. J.*, 2002, **8**, 3187; (c) X. He and C.-Z. Lu, *Z. Anorg. Allg. Chem.*, 2003, **630**, 1756; (d) D.-R. Xiao, Y. Hou, E.-B. Wang, S.-T. Wang, Y.-G. Li, G.-J. De, L. Xu and C.-W. Hu, *J. Mol. Struct.*, 2003, **659**, 13; (e) J. Tao, Y. Zhang, M.-L. Tong, X.-M. Chen, T. Yuen, C. L. Lin, X.-Y. Huang and J. Li, *Chem. Commun.*, 2002, 1342.
- <sup>16</sup> (a) R.-G. Xiong, X. Xue, H. Zhao, X.-Z. You, B. F. Abrahams and Z.-L. Xue, *Angew. Chem. Int. Ed.*, 2002, **41**, 3800; (b) X. Xue, X.-S. Wang, L.-Z. Wang, R.-G. Xiong, B. F. Abrahams, X.-Z. You, Z.-L. Xue and C.-M. Che, *Inorg. Chem.*, 2002, **41**, 6544.
- <sup>17</sup> R.-G. Xiong, J. Zhang, Z.-F. Chen, X.-Z. You, C.-M. Che and H.-K. Fun, *J. Chem. Soc. Dalton Trans.*, 2001, 780.
- <sup>18</sup> J.-K. Cheng, Y.-G. Yao, J. Zhang, Z.-J. Li, Z.-W. Cai, X.-Y. Zhang, Z.-N. Chen, Y.-B. Chen, Y. Kang, Y.-Y. Qin and Y.-H. Wen, *J. Am. Chem. Soc.*, 2004, **126**, 7796.
- <sup>19</sup> X.-M. Zhang, J.-J. Hou and H.-S. Wu, *Dalton Trans.*, 2004, 3437.
- <sup>20</sup> (a) X.-M. Zhang, *Eur. J. Inorg. Chem.*, 2004, 544; (b) O. R. Evans and W. Lin, *Chem. Mater.*, 2001, **13**, 3009; (c) M.-L. Tong, L.-J. Li, K. Mochizuki, H.-C. Chang, X.-M. Chen, Y. Li and S. Kitagawa, *Chem. Commun.*, 2003, 428.
- <sup>21</sup> (a) X.-M. Zhang, H.-S. Wu and X.-M. Chen, *Eur. J. Inorg. Chem.*, 2003, 2959; (b) X. Li, R. Cao, D. Sun, Q. Shi, W. Bi and M. Hong, *Inorg. Chem. Commun.*, 2003, **6**, 815.
- <sup>22</sup> (a) X.-X. Hu, J.-Q. Xu, P. Cheng, X.-Y. Chen, X.-B. Cui, J.-F. Song, G.-D. Yang and T.-G. Wang, *Inorg. Chem.*, 2004, **43**, 2261; (b) X.-X. Hu, C.-L. Pan, J.-Q. Xu, X.-B. Cui, G.-D. Yang and T.-G. Wang, *Eur. J. Inorg. Chem.*, 2004, 1566.
- <sup>23</sup> (a) Y. Yan, C.-D. Wu and C.-Z. Lu, *Z. Anorg. Allg. Chem.*, 2003, **629**, 1991; (b) X.-M. Zhang and R.-Q. Fang, *Inorg. Chem.*, 2005, **44**, 3955; (c) Y. Yan, C.-D. Wu and C.-Z. Lu, *Z. Anorg. Allg. Chem.*, 2003, **629**, 1991.
- <sup>24</sup> C. M. Liu, S. Gao and H.-Z. Kou, *Chem. Commun.*, 2001, 1670.
- <sup>25</sup> H. K. Chae, D. Y. Siberio-Pérez, J. Kim, Y. B. Go, M. Eddaoudi, A. J. Matzger, M. O'Keeffe and O. M. Yaghi, *Nature*, 2004, **427**, 523.
- <sup>26</sup> (a) J. L. C. Rowsell and O. M. Yaghi, *Microporous Mesoporous Mater.*, 2004, **73**, 3; (b) G. Férey, *Chem. Soc. Rev.*, 2008, **37**, 191.
- <sup>27</sup> T. J. Barton, L. M. Bull, W. G. Klemperer, D. A. Loy, B. McEnaney, M. Misono, P. A. Monson, G. Pez, G. W. Scherer, J. C. Vartuli and O. M. Yaghi, *Chem. Mater.*, 1999, **11**, 2633.
- <sup>28</sup> A. W. C. Van den Berg and C. O. Area'n, *Chem. Commun.*, 2008, **6**, 668.



- 
- <sup>29</sup> DOE Office of Energy Efficiency and Renewable Energy Hydrogen, Fuel Cells & Infrastructure Technologies Program Multi-Year Research, Development and Demonstration Plan, available at: <http://www.eere.energy.gov/hydrogenandfuelcells/mypp>.
- <sup>30</sup> N. L. Rosi, J. Eckert, M. Eddaoudi, D. T. Vodak, J. Kim, M. O’Keeffe and O. M. Yaghi, *Science*, 2003, **300**, 1127.
- <sup>31</sup> H. Furukawa, M. A. Miller and O. M. Yaghi, *J. Mater. Chem.*, 2007, **17**, 3197.
- <sup>32</sup> M. Latroche, S. Surblé, C. Serre, C. Mellot-Draznieks, P. L. Llewellyn, J. H. Lee, J. S. Chang, S. H. Jhung and G. Férey, *Angew. Chem., Int. Ed.*, 2006, **45**, 8227.
- <sup>33</sup> R. Zacharia, D. Cossement, L. Lafi and R. Chahine, *J. Mater. Chem.*, 2010, **20**, 2145.
- <sup>34</sup> J. An and N. L. Rosi, *J. Am. Chem. Soc.*, 2010, **132**, 5578.
- <sup>35</sup> S. Ma, D. Sun, J. M. Simmons, C. D. Collier, D. Yuan and H.-C. Zhou, *J. Am. Chem. Soc.*, 2008, **130**, 1012.
- <sup>36</sup> R. T. Yang, *Adsorbents: Fundamentals and Applications*, John Wiley & Sons, Hoboken, 2003.
- <sup>37</sup> (a) R. Xu, W. Pang, J. Yu, Q. Huo and J. Chen, *Chemistry of Zeolites and Related Porous Materials: Synthesis and Structure*, John Wiley & Sons (Asia) Pvt Ltd., Singapore, 2007; (b) R. T. Yang, *Gas Separation by Adsorption Progress*, Butterworth, Boston, 1987.
- <sup>38</sup> J. U. Keller and R. Staudt, *Gas Adsorption Equilibria, Experimental Methods and Adsorptive Isotherms*, Springer Science and Business Media, Inc., Boston, 2005.
- <sup>39</sup> J.-R. Li, R. J. Kuppler and H.-C. Zhou, *Chem. Soc. Rev.*, 2009, **38**, 1477.
- <sup>40</sup> (a) S. Kitagawa and M. Kondo, *Bull. Chem. Soc. Jpn.*, 1998, **71**, 1739; (b) S. Kitagawa and K. Uemura, *Chem. Soc. Rev.*, 2005, **34**, 109; (c) A. J. Fletcher, K. M. Thomas and M. J. Rosseinsky, *J. Solid State Chem.*, 2005, **178**, 2491.
- <sup>41</sup> D. N. Dybtsev, H. Chun, S. H. Yoon, D. Kim and K. Kim, *J. Am. Chem. Soc.*, 2004, **126**, 32.
- <sup>42</sup> M. Dincă and J. R. Long, *J. Am. Chem. Soc.*, 2005, **127**, 9376.
- <sup>43</sup> S. Q. Ma, X. S. Wang, C. D. Collier, E. S. Manis and H.-C. Zhou, *Inorg. Chem.*, 2007, **46**, 8499.
- <sup>44</sup> J. Y. Lee, D. H. Olson, L. Pan, T. J. Emge and J. Li, *Adv. Funct. Mater.*, 2007, **17**, 1255.

- 
- <sup>45</sup> J. A. R. Navarro, E. Barea, A. Rodríguez-Diéguez, J. M. Salas, C. O. Ania, J. B. Parra, N. Masciocchi, S. Galli and A. Sironi, *J. Am. Chem. Soc.*, 2008, **130**, 3978.
- <sup>46</sup> M. Xue, S. Q. Ma, Z. Jin, R. M. Schaffino, G. S. Zhu, E. B. Lobkovsky, S. L. Qiu and B. L. Chen, *Inorg. Chem.*, 2008, **47**, 6825.
- <sup>47</sup> S. Q. Ma, X. S. Wang, D. Q. Yuan and H.-C. Zhou, *Angew. Chem., Int. Ed.*, 2008, **47**, 4130.
- <sup>48</sup> T. Loiseau, L. Lecroq, C. Volkringer, J. Marrot, G. Férey, M. Haouas, F. Taulelle, S. Bourrelly, P. L. Llewellyn and M. Latroche, *J. Am. Chem. Soc.*, 2006, **128**, 10223.
- <sup>49</sup> M. Xue, S. Q. Ma, Z. Jin, R. M. Schaffino, G. S. Zhu, E. B. Lobkovsky, S. L. Qiu and B. L. Chen, *Inorg. Chem.*, 2008, **47**, 6825.
- <sup>50</sup> Y. Zou, S. Hong, M. Park, H. Chun and M. S. Lah, *Chem. Commun.*, 2007, 5182.
- <sup>51</sup> S. M. Humphrey, J.-S. Chang, S. H. Jung, J. W. Yoon and P. T. Wood, *Angew. Chem., Int. Ed.*, 2007, **46**, 272.
- <sup>52</sup> (a) D. N. Dybtsev, H. Chun, S. H. Yoon, D. Kim and K. Kim, *J. Am. Chem. Soc.*, 2004, **126**, 32; (b) D. G. Samsonenko, H. Kim, Y. Sun, G.-H. Kim, H.-S. Lee and K. Kim, *Chem.-Asian J.*, 2007, **2**, 484.
- <sup>53</sup> P. K. Thallapally, C. A. Fernandez, R. K. Motkuri, S. K. Nune, J. Liu and C. H. F. Peden, *Dalton Trans.*, 2010, **39**, 1692.
- <sup>54</sup> M. Fujita, Y. J. Kwon, S. Washizu and K. Ogura, *J. Am. Chem. Soc.*, 1994, **116**, 1151.
- <sup>55</sup> L. Alaerts, E. Séguin, H. Poelman, F. Thibault-Starzyk, P. A. Jacobs and D. E. D. Vos, *Chem.-Eur. J.*, 2006, **12**, 7353.
- <sup>56</sup> A. Henschel, K. Gedrich, R. Kraehnert and S. Kaskel, *Chem. Commun.*, 2008, 4192.
- <sup>57</sup> Y. Lu, M. Tonigold, B. Bredenkotter, D. Volkmer, J. Hitzbleck and G. Langstein, *Z. Anorg. Allg. Chem.*, 2008, **634**, 2411.
- <sup>58</sup> M. Kurmoo, H. Kumagai, S. M. Hughes and C. J. Kepert, *Inorg. Chem.*, 2003, **42**, 6709.
- <sup>59</sup> D. Maspoch, D. Ruiz-Molina, K. Wurst, N. Domingo, M. Cavallini, F. Biscarini, J. Tejada, C. Rovira and J. Veciana, *Nature Mater.*, 2003, **2**, 190.
- <sup>60</sup> Z.-L. Huang, M. Drillon, N. Masciocchi, A. Sironi, J.-T. Zhao, P. Rabu and P. Panissod, *Chem. Mater.*, 2000, **12**, 2805.
- <sup>61</sup> S. Konar, P. S. Mukherjee, E. Zangrando, F. Lloret and N. R. Chaudhuri, *Angew. Chem. Int. Edn.*, 2002, **41**, 1561.



**Three isolated structural motifs in one crystal:  
penetration of two 1D chains through large cavities  
within 2D polymeric sheets**

*Muhammad A. Nadeem, Mohan Bhadbhade, Roland Bircher and John A. Stride*

**ACKNOWLEDGMENT OF CONTRIBUTION TO AUTHORSHIP**

The article is published in journal “*CrystEngCommun*”. J.A.S. conceived and managed the research project, M.A.N. synthesised the samples and collected all data. M.A.N. and M.B. solved the crystal structure. R.B. provided consultation on the structure. All authors discussed the results and commented on this manuscript.

# Three isolated structural motifs in one crystal: penetration of two 1D chains through large cavities within 2D polymeric sheets†

Muhammad Arif Nadeem,<sup>a</sup> Mohan Bhadbhade,<sup>b</sup> Roland Bircher<sup>c</sup> and John Arron Stride<sup>\*ac</sup>

Received 29th October 2009, Accepted 25th November 2009

First published as an Advance Article on the web 17th December 2009

DOI: 10.1039/b922698m

**An unprecedented architecture comprising of three isolated coordination polymers within the same crystalline structure has been obtained, in which two independent infinite one dimensional polymer chains, Cu(bpy)(H<sub>2</sub>O), fill the voids generated by a third, two dimensional, host framework, Cu<sub>3</sub>(Hbtc)(btc)(bpy)<sub>2</sub>.**

The wide-spread interest in polymeric coordination networks focuses not only on their potential as functional materials possessing host–guest behaviours in fields such as catalysis and for magnetic and electronic devices, but also for the intriguing variety of architectures and topologies that they display.<sup>1</sup> It is well known that structural geometries can be moderated by both judicious selection of the ligand coordination about the metal ions and the chemical nature of the terminal and bridging ligands. However, it is quite rare to observe distinct coordination polymers within a single crystal structure, especially polymers having different structural motifs.<sup>2</sup> In cases in which more than one polymeric structure has been observed within a single structure, the polymers usually align in an interpenetrating fashion.<sup>3,1c</sup> Biradha and Fujita have reported a structure in which three Cd based coordination polymers co-exist in one crystal, with an orthogonal interpenetration of two equivalent 1D polymers into a third, 2D, polymer.<sup>4</sup> In addition, Shin *et al.* observed the interpenetration of Co based topological isomers,<sup>5</sup> whilst Du *et al.* have reported an unusual mixed ligand Cu based coordination polymer having two interpenetrating, structurally different motifs in a single crystal structure.<sup>3a</sup> However, among these materials, polymeric architectures having voids filled with 1D metal–organic chains as guests within the same structure are extremely rare. Yang *et al.* have reported a metal–organic framework containing two independent 3D Cu based polymers incorporating helical structures, interwoven into a 3D network that then hosted a 1D linear polymer.<sup>6</sup> Recently, Xiong *et al.* reported an unusual framework in which parallel 1D infinite chains reside in the cavities of *p*-sulfonatocalix[4]arene-trisilver blocks.<sup>7</sup> Here we report an unusual 2D coordination polymer, the voids of which are filled by not one, but two structurally identical 1D guest metal–organic polymer chains. We also note the presence of

a Cu(II) atom in an unusual hepta-coordinated geometry. Examples of hepta-coordinated Cu(II) are extremely rare, however, recently, Potapov *et al.* reported a Cu(II) ion coordinated with five oxygen and two nitrogen atoms, in that case resulting in a hepta-coordinated triangular prism.<sup>8</sup>

In our attempts to produce higher dimensional pillared-layer architectures through molecular recognition, we recently chose a combination of a linear bridging ligand, 4,4'-bipyridyl (bpy), and an aromatic ligand, benzene 1,2,3-tricarboxylic acid (H<sub>3</sub>btc), to fabricate mixed network structures incorporating different metal ions. We have isolated an unusual topological framework (**1**) that contains an intriguing unit cell having five geometrically distinct metal ions. Complex **1** consists of three types of polymers: a 2D polymer consisting of Cu-dimer and Cu-chain building blocks [Cu<sub>3</sub>(Hbtc)(btc)(bpy)<sub>2</sub>] (**A**), and two structurally identical but crystallographically different 1D linear chains, **B** and **C**, comprising [Cu(bpy)(H<sub>2</sub>O)] units (Fig. 1).

In total, complex **1** can be formulated as [(**A**)(**B**)(**C**)·2H<sub>2</sub>O·OH] and was synthesised in a hydrothermal approach.† Polymer **A** consists of three crystallographically distinct Cu atoms which can be

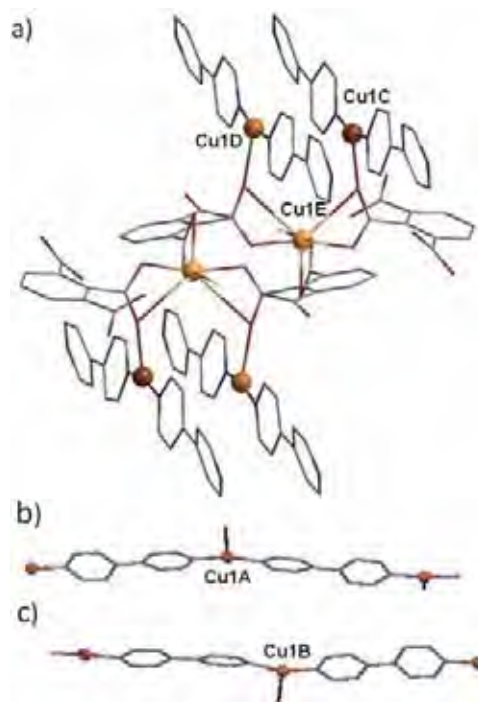


**Fig. 1** Illustration for the three coordination polymers exhibited in the crystal structure of **1**: (a) Cu-dimer and Cu-chain building block (**A**) and (b and c) linear chain of **B** and **C** polymer respectively.

<sup>a</sup>School of Chemistry, University of New South Wales, Sydney, NSW, 2052, Australia. E-mail: j.stride@unsw.edu.au; Fax: +61 02 9385 6141; Tel: +61 02 9385 4675

<sup>b</sup>Analytical Centre, University of New South Wales, Sydney, NSW, 2052, Australia

<sup>c</sup>Bragg Institute, Australian Nuclear Science and Technology Organisation, PMB 1, Menai, NSW, 2234, Australia

† Electronic supplementary information (ESI) available: Colour-coded detailed figure of hydrogen-bonding between the 2D layers of **A**, with **B** and **C** highlighted. CCDC reference number 738786. For ESI and crystallographic data in CIF or other electronic format see DOI: 10.1039/b922698m

assigned to the three polymeric building blocks, namely isolated dimers (Cu1E) and two Cu rods (Cu1C, Cu1D). Oxidation states of +2 and +1 for the Cu ions in dimers and rods, respectively, were assigned by BVS calculations.<sup>9</sup> An unusual structural feature of polymer **A** is the hepta-coordinated geometry of the Cu1E ion, with an O<sub>7</sub> donor set. The equatorial plane is determined by three oxygen atoms (O4F, O6F, O4E) from carboxylate groups of two symmetry related btc ligands and an Hbtc ligand, as well as a coordinated water molecule (O1WE), forming a distorted square planar environment. The three remaining coordination sites are occupied at axial positions by oxygen atoms (O3F, O5F, O3E) from carboxylate groups of btc and Hbtc ligands. It should be noted that in the CuO<sub>7</sub> coordination sphere, the Cu–O bonding distances vary significantly, with equatorial bond lengths of 1.92–1.94 Å, much shorter than typical literature values,<sup>10,11</sup> indicating strong Cu–O contacts, whilst the axial bond lengths range between 2.85 and 2.97 Å. The whole coordination environment of the Cu(II) ion thus forms an augmented triangular prism (Fig. 2a). To the best of our knowledge, the only other example of a hepta-coordinated Cu(II) involving a CuO<sub>7</sub> group is a high pressure phase (II) of CuGeO<sub>3</sub>, obtained at pressures in excess of 6.4 GPa,<sup>12</sup> making **A** the only example of such a centre under ambient conditions. The two coordinating btc ligands in **A** are symmetry related and bridge two Cu1E *via* neighbouring carboxylate groups, forming dimers having a Cu–Cu distance of 6.110 Å. The Cu1C and Cu1D ions are linked by bpy to form parallel pairs of rods in the [101] direction. The bpy moieties of neighbouring chains are stacked due to  $\pi$ – $\pi$  and C–H... $\pi$  interactions.<sup>13</sup> The distorted planar trigonal

coordination sphere of Cu1C and Cu1D is completed by O atoms from Hbtc and btc, respectively, to link Cu1E dimers and rods covalently through *syn-anti* carboxylate bridges (Fig. 1a). The observed bond lengths in the linear chains (Cu–N 1.88(2)–1.91(2), Cu–O 2.21(16)–2.32(16) Å) are comparable to those reported in literature for the Cu(I) oxidation state.<sup>14</sup> Alternate layers of dimers and rods are stacked in the *b*-direction. Each dimer is covalently bound to two pairs of parallel Cu1D and Cu1C rods, forming a wave-like pattern along the *b*-axis and extending to meshed grid type layers along the rods (Fig. 2b). Neighbouring layers are offset and linked to a 2D structure by a strong hydrogen bonding network *via* lattice water molecules within the dimer layers, leaving channels of approximate dimensions 18 × 14 Å.

The voids in polymer **A** are filled by the two polymers **B** and **C** (Fig. 3). These consist of linear rods, which also run parallel to the chains observed in **A**. The Cu ions have three-fold coordination in each of the rod-like polymers and sit in a coordinating position between two nitrogen atoms (N1 and N2) of bpy and one oxygen atom (O1) of a coordinated water molecule, resulting in a distorted T-shaped junction between each bpy unit (Fig. 1b and c). As for the chain subunits of **A**, an oxidation state of +1 was assigned to the Cu ions in **B** and **C** by BVS calculations. The two polymers **B** and **C** are very similar in overall geometry, but have slightly different bond angles about the Cu(I) centre.

The N1–Cu–N2 bond angles of the [Cu(bpy)(H<sub>2</sub>O)] T-shaped unit are 161.93(9) and 158.34(9)° in polymers **B** and **C** respectively. Similarly, the N1–Cu1–O1W bond angles range from 96.32(9) to 101.71(9)° and 97.73(8) to 103.89(8)° in polymers **B** and **C**, respectively. The perpendicular distance between the two rods is *ca.* 3.5 Å, filling the voids in polymer **A** with pairs of parallel rod-like polymer chains (**B** and **C**) composed of [Cu(bpy)(H<sub>2</sub>O)] units (Fig. 3). The coordination geometry of the Cu ions in **B** and **C** is very similar to the chain subunits of polymer **A**, with a coordinated water replacing the *syn-anti* carboxylate bridge. The water ligands are part of a complex hydrogen bonding network involving lattice water, hydroxide ions and carboxylate groups of btc and Hbtc (Fig. S1, ESI†). These act to stabilise and regulate the positions of **B** and **C** in the channels of **A**. The rods are further held in position by interactions with the bpy ligands of neighbouring chain subunits of **A**. The bpy bridging ligands display a range of geometries in the three polymers **A**, **B** and **C**. In particular, the dihedral angle between the planes of the two aromatic rings of each bpy are 10.86 and 17.50°, in **B** and **C** respectively, whilst in **A** the dihedral rotation in each of the two bpy

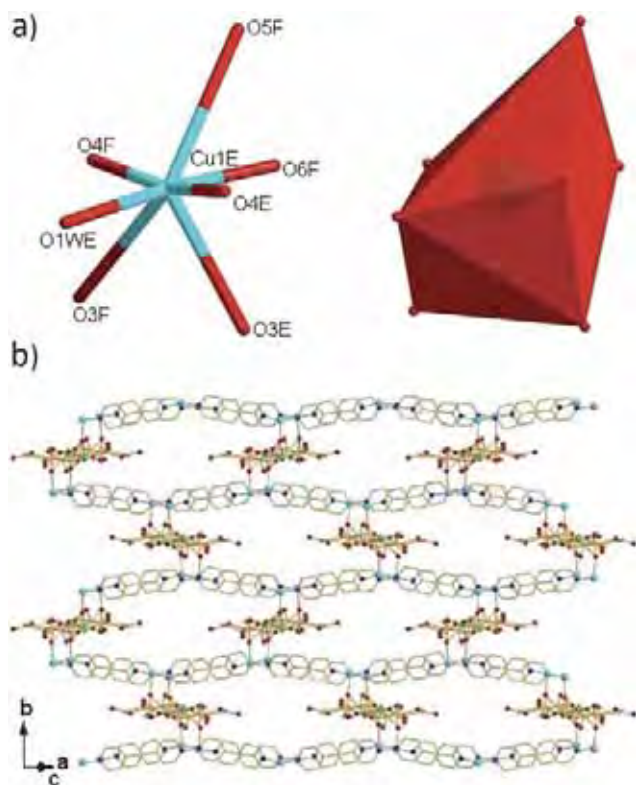


**Fig. 2** (a) Coordination geometry of Cu(II) centre in complex **1** in stick representation (left) and polygon representation (right); (b) packing of neighbouring chain and dimer subunits of polymer **A**, forming meshed grid type layers.

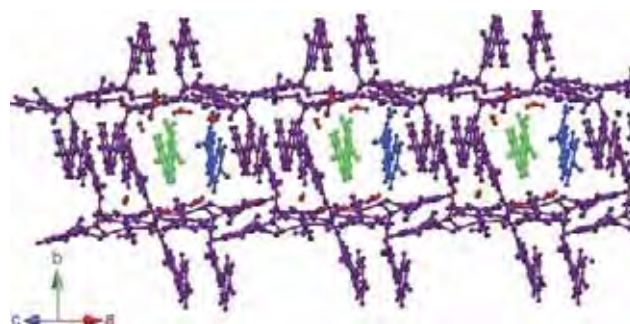


**Fig. 3** A view showing the insertion of polymer **B** (blue), **C** (green) and lattice water molecules (red) into the voids created by packing of layers in polymer **A** (purple).

molecules is 20.02 and 18.36°. The geometric flexibility about the central bond of the bpy ligands is crucial to the overall structural integrity of the 3D supramolecular structure, with more rigid ligands unable to adopt the varied coordination geometries. In addition to the importance of the bpy ligands, lattice water molecules play an important role in the formation of the title compound by providing stability between adjacent meshed grid layers of polymer **A**, as well as the introduced guest polymers **B** and **C**, and in the case of the OH<sup>−</sup> ions, charge balance.

In conclusion, we present an unprecedented supramolecular architecture: a polymer of meshed grid layers consisting of two structurally different building blocks, linked by hydrogen bonds into a 2D structure, the voids of which are filled by the incorporation of two 1D guest metal–organic polymers. This result highlights the remarkable potential for complex hierarchical structures achievable simply *via* the intermolecular interaction of lattice water molecules coupled to guest–host interactions of metal–organic networks and polymers.

## Acknowledgements

This research was supported by an ARC grant (DP0880199) and a UNSW UIPA scholarship to M.A.N. Author contributions: J.A.S. conceived and managed the research project, M.A.N. synthesised the samples and collected all data. M.A.N. and M.B. solved the crystal structure. R.B. provided consultation on the structure. All authors discussed the results and commented on this manuscript.

## Notes and references

‡ *Synthesis*: to a stirred solution of mixed ligands, H<sub>3</sub>btc (0.5 mmol) and bpy (0.5 mmol) in water (6 ml), an aqueous solution of Cu(NO<sub>3</sub>)<sub>2</sub>·2.5H<sub>2</sub>O (0.5 mmol in 4 ml of water) was added. The mixture was stirred for 15 min, resulting in a blue slurry which was then transferred to, and sealed within, a 23 ml Teflon-lined autoclave. The reactor vessel was heated at 150 °C for three days, before allowing to cool to room temperature. Green prismatic crystals were obtained in *ca.* 7% yield (based on copper). Anal. Calcd for C<sub>58</sub>H<sub>49</sub>Cu<sub>5</sub>N<sub>8</sub>O<sub>18</sub> (*M*<sub>r</sub> = 1463.75): C, 47.59% N, 7.68% Cu, 21.70%. Found: C, 46.83% N, 8.23% Cu, 21.10%. *Crystal data*: C<sub>58</sub>H<sub>49</sub>Cu<sub>5</sub>N<sub>8</sub>O<sub>18</sub>, *M*<sub>r</sub> = 1463.75, monoclinic, space group *P*2(1)/*n* (no. 14), *a* = 15.9264(5), *b* = 18.2649(6), *c* = 19.6173(6) Å, α = 90.00, β = 106.10(10), γ = 90.00°, *V* = 5482.7(3) Å<sup>3</sup>, *T* = 150(2) K, *Z* = 4, ρ<sub>calcd</sub> = 1.773 g cm<sup>−3</sup>, λ = 0.7107 Å, 42 445 reflections collected, 9626 unique (*R*<sub>int</sub> = 0.0496), *R*(*F*) = 0.0304 and *wR*<sub>2</sub> = 0.0985 using 8315 reflections with *I* > 2σ(*I*). Data were collected on a Bruker kappa APEXII

CCD Area Detector instrument and the structure was solved by direct methods (SHELXS-97). All non-hydrogen atoms were refined with anisotropic thermal parameters. IR data (*ν*<sub>max</sub>/cm<sup>−1</sup>): 3395sbr (−OH), 3099w, 1603s (C=O), 1564m (C=C), (C=N)<sub>bpy</sub>, 1487w, 1446w, 1370m, 816m, 696w, 479m. *Thermogravimetric analysis*: the sample undergoes dehydration between 150 and 220 °C, the loss of the organic groups of the 1D polymers **B** and **C** at 261 °C and ultimately sample degradation above 390 °C (Fig. S2†).

- (a) R. Kitaura, K. Seki, G. Akiyama and S. Kitagawa, *Angew. Chem., Int. Ed.*, 2003, **42**, 428–431; (b) O. S. Jung, Y. J. Kim, K. M. Kim and Y. A. Lee, *J. Am. Chem. Soc.*, 2002, **124**, 7906–7907; (c) D. P. Martin, R. M. Supkowski and R. L. LaDuca, *Inorg. Chem.*, 2007, **46**, 7917–7922; (d) L. Carlucci, G. Ciani, M. Moret, D. M. Proserpio and S. Rizzato, *Angew. Chem., Int. Ed.*, 2000, **39**, 1506–1510; (e) X. L. Wang, C. Qin, E. B. Wang, L. Xu, Z. M. Su and C. W. Hu, *Angew. Chem., Int. Ed.*, 2004, **43**, 5036–5040; (f) M. B. Zaman, K. Udachin, J. A. Ripmeester, M. D. Smith and H. C. Zur Loye, *Inorg. Chem.*, 2005, **44**, 5047–5059.
- (a) G. O. Lloyd, J. L. Atwood and L. J. Barbour, *Chem. Commun.*, 2005, 1845–1847; (b) B. Li, Y. Peng, B. Li and Y. Zhang, *Chem. Commun.*, 2005, 2333–2335; (c) D. B. Cordes, A. S. Bailey, P. L. Caradoc-Davies, D. H. Gregory, L. R. Hanton, K. Lee and M. D. Spicer, *Inorg. Chem.*, 2005, **44**, 2544–2552.
- (a) M. Du, X.-J. Jiang and X.-J. Zhao, *Chem. Commun.*, 2005, 5521–5523; (b) Q.-X. Yao, Z.-F. Ju, X.-H. Jin and J. Zhang, *Inorg. Chem.*, 2009, **48**, 1266–1268; (c) X. He, C.-Z. Lu, C.-D. Wu and L.-J. Chen, *Eur. J. Inorg. Chem.*, 2006, 2492–2503; (d) M. B. Zaman, M. D. Smith and H.-C. Zur Loye, *Chem. Commun.*, 2001, 2256–2257.
- K. Biradha and M. Fujita, *Chem. Commun.*, 2002, 1866–1867.
- D. M. Shin, I. S. Lee, Y. K. Chung and M. S. Lah, *Chem. Commun.*, 2003, 1036–1037.
- E. Yang, J. Zhang, Z.-J. Li, S. Gao, Y. Kang, Y.-B. Chen, Y.-H. Wen and Y.-G. Yao, *Inorg. Chem.*, 2004, **43**, 6525–6527.
- K. Xiong, M. Wu, Q. Zhang, W. Wei, M. Yang, F. Jiang and M. Hong, *Chem. Commun.*, 2009, 1840–1842.
- A. S. Potapov, E. A. Nudnova, G. A. Domina, L. N. Kirpotina, M. T. Quinn, A. I. Khlebnikov and I. A. Schepetkin, *Dalton Trans.*, 2009, 4488–4498.
- N. E. Brese and M. O'Keeffe, *Acta Crystallogr., Sect. B: Struct. Sci.*, 1991, **47**, 192–197.
- X. Gao, J. Dou, D. Li, F. Dong and D. Wang, *J. Coord. Chem.*, 2005, **58**, 1127–1132.
- J.-J. Zhang, S.-M. Hu, S.-C. Xiang, T. Sheng, X.-T. Wu and Y.-M. Li, *Inorg. Chem.*, 2006, **45**, 7173–7181.
- A. Yoshiasa, G. Yagyu, T. Ito, T. Yamanaka and T. Nagai, *Z. Anorg. Allg. Chem.*, 2000, **626**, 36–41.
- C. Janiak, *J. Chem. Soc., Dalton Trans.*, 2000, 3885–3896.
- (a) X.-C. Huang, J.-P. Zhang, Y.-Y. Lin, X. L. Yu and X.-M. Chen, *Chem. Commun.*, 2004, 1100–1101; (b) J. Tao, Y. Zhang, M.-L. Tong, T. Yuen, C. L. Lin, X. Huang and J. Li, *Chem. Commun.*, 2002, 1342–1343; (c) L.-M. Zheng, P. Yin and X.-Q. Xin, *Inorg. Chem.*, 2002, **41**, 4084–4086.



## Supporting information:

### Three isolated structural motifs in one crystal: Penetration of two 1D chains through large cavities within 2D polymeric sheets

Muhammad Arif Nadeem,<sup>a</sup> Mohan Bhadbhade,<sup>b</sup> Roland Bircher<sup>c</sup> and John Arron Stride\*<sup>a,c</sup>

<sup>a</sup> School of Chemistry, University of New South Wales, Sydney, NSW 2052, Australia. Fax: +61 (02) 9385 6141; Tel: +61 (0)2 9385 4672; E-mail: j.stride@unsw.edu.au

<sup>b</sup> Analytical Centre, University of New South Wales, Sydney, NSW 2052, Australia.

<sup>c</sup> Bragg Institute, Australian Nuclear Science and Technology Organisation, PMB 1, Menai, NSW 2234, Australia.

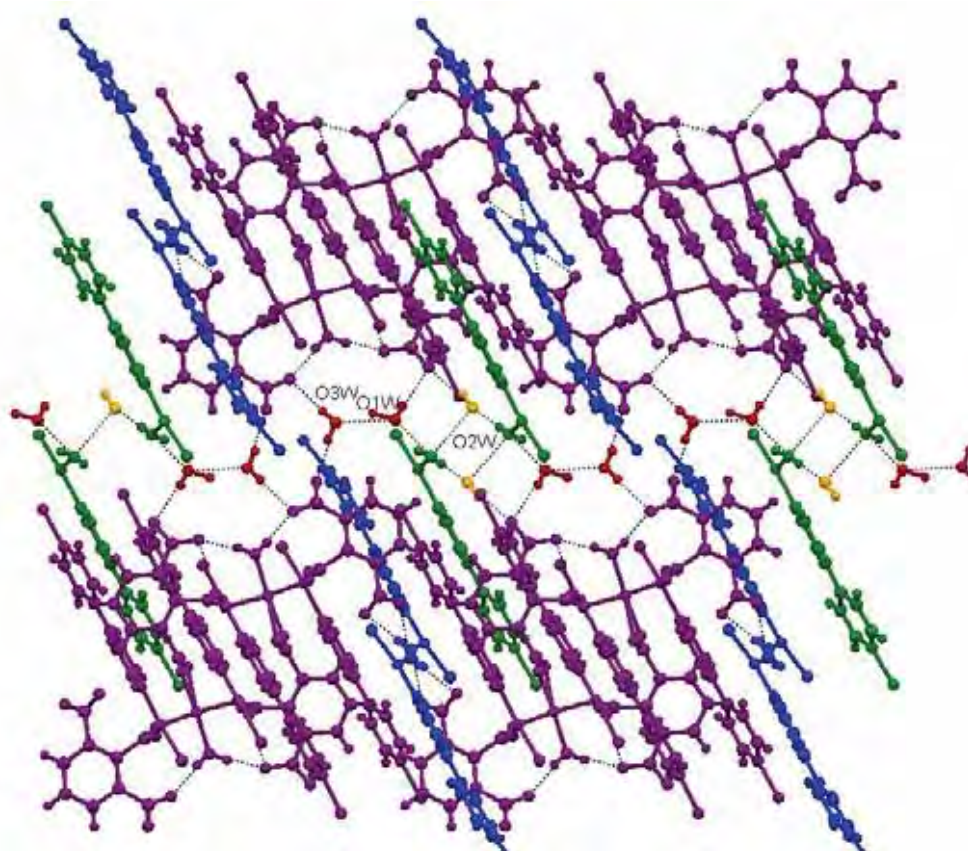


Figure S1: Detail of hydrogen-bonding between the 2D layers, generating the pseudo-3D structure. Polymer **A** (2D) shown in purple and the two 1D polymers, **B** and **C**, in green and blue respectively. Lattice water molecules are shown in red, whilst hydroxide ions ( $\text{OH}^-$ ) in yellow.

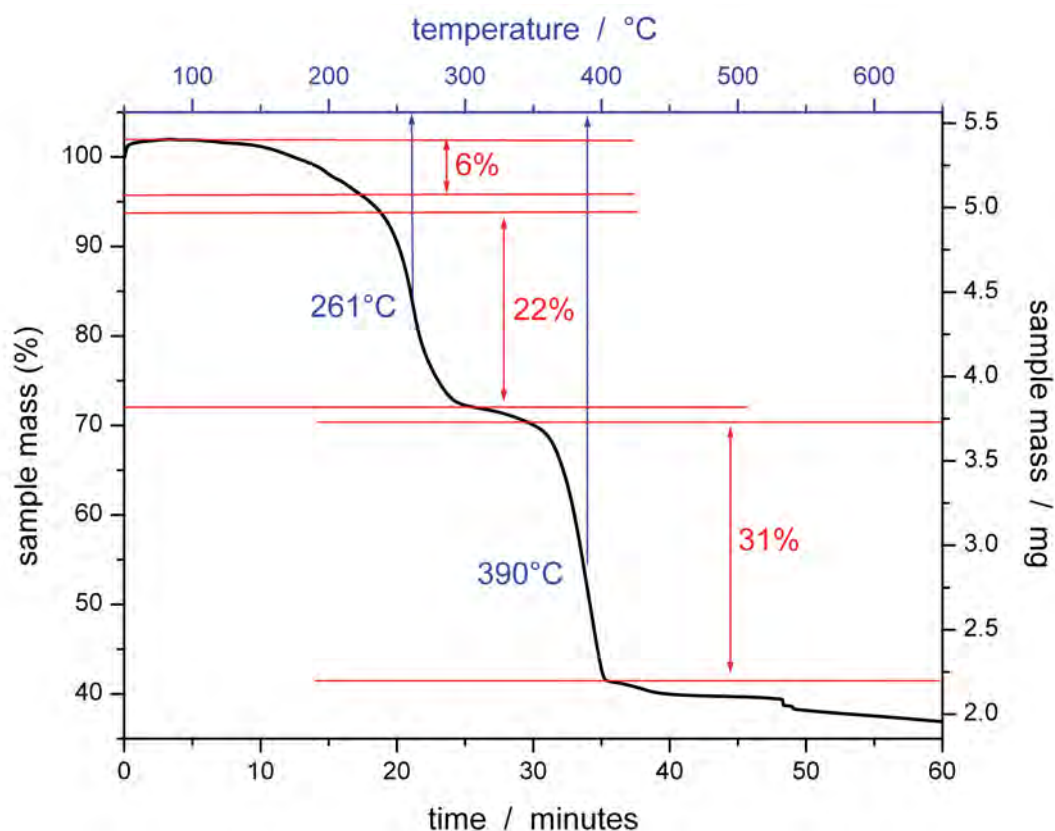


Figure S2: Thermogravimetric analysis of  $\text{Cu}_3(\text{Hbtc})(\text{btc})(\text{bpy})_2$ . Three distinct regions of mass loss were observed: (i) 6% over the temperature range of 150 - 220°C corresponding to the loss of water molecules (both coordinated and non-coordinated), *theoretical*: 9.8%; (ii) 22% around 261°C corresponding to the loss of the organic components of the 1D polymers **B** and **C**, *theoretical*: 21.3%; and (iii) 31% at 390°C corresponding to sample degradation. There is an additional small mass loss around 530°C. All samples were run under a flow of nitrogen at a heating rate of 10°C/min.

**Controlled synthesis of isomorphous coordination polymers via *in situ*. ligand transformation reaction: Crystal structure, thermal and magnetic properties**

*Muhammad A. Nadeem, Mohan Bhadbhade, Roland Bircher and John A. Stride*

**ACKNOWLEDGMENT OF CONTRIBUTION TO AUTHORSHIP**

The article is published in journal “*Crystal Growth & Design*”. J.A.S. conceived and managed the research project, M.A.N. synthesised the samples and collected all data. M.A.N. and M.B. solved the crystal structure. R.B. provided consultation on the interpretation of magnetic data and helped in writing manuscript. All authors discussed the results and commented on this manuscript.

# Controlled Synthesis of Isomorphous Coordination Polymers via in Situ Ligand Transformation Reaction: Crystal Structure, Thermal and Magnetic Properties

Muhammad A. Nadeem,<sup>†</sup> Mohan Bhadbhade,<sup>§</sup> Roland Bircher,<sup>‡</sup> and John A. Stride<sup>\*,†,‡</sup>

<sup>†</sup>*School of Chemistry, University of New South Wales, Sydney, NSW 2052, Australia,* <sup>§</sup>*Analytical Centre, University of New South Wales, Sydney, NSW 2052, Australia, and* <sup>‡</sup>*Bragg Institute, Australian Nuclear Science and Technology Organisation, PMB 1, Menai, NSW 2234, Australia*

Received June 2, 2010

**ABSTRACT:** A series of isomorphous  $[M_2(ip)_2(L)_2]_n$  ( $M = Co, Ni$ ;  $ip =$  isophthalate;  $L = 4,4'$ -dipyridyl and pyrazine) coordination polymers was synthesized via in situ ligand transformation reactions, in which 1,2,3-benzene tricarboxylic acid ( $1,2,3-btcH_3$ ) undergoes decarboxylation to isophthalate ( $ip$ ), which was found to be highly dependent on the reaction temperature. The polymers crystallize in the same crystal triclinic system  $P\bar{1}$ . The magnetic properties were investigated by a Quantum Design physical property measurement system (PPMS); all four compounds feature almost isostructural  $M(II)$  dimers having ferromagnetic (FM) interactions. The interdimer interactions mediated by two different carboxylate groups of  $ip$  are weak, while there is no significant magnetic exchange via the  $4,4'$ -dipyridyl ligands along the chain direction. However, substitution with pyrazine leads to antiferromagnetic exchange of nearest neighbor dimers.

## Introduction

Metal–organic hybrid materials, consisting of paramagnetic metal ions incorporated into coordination polymers to form extended structures, are currently of great interest in the field of molecular magnetism and materials chemistry due to their fascinating structural diversities and potential applications as functional materials.<sup>1</sup> Bridging ligands have been shown to transmit magnetic interactions via superexchange interactions in addition to the simple binding of metal centers into specific coordination geometries. In this respect, phenyldicarboxylates are frequently used as efficient linkers in the design of polymeric complexes.<sup>2,3</sup> Recently, isophthalic acid has been used to construct one- and two-dimensional (1D and 2D) polymeric Mn complexes in which the isophthalate ion functions as a mediator for transmitting the exchange interactions between the paramagnetic metal centers.<sup>4</sup>

A variety of metal coordination frameworks, some having aesthetically beautiful topologies as well as interesting physical properties, have been synthesized. However, the rational control of the construction of polymeric networks remains a great challenge in the field of crystal engineering. In the development of new strategies for the crystal engineering of coordination networks and supramolecular architectures, pillared-layer assemblies have been shown to be precursors in an efficient route for the construction of porous frameworks having controllable channel sizes and chemical functionalities.<sup>5</sup> In particular, the pillared-layer networks based on coordination bonds are more attractive than those based on the hydrogen-bonded assemblies, owing to their high structural and thermal stabilities.<sup>6</sup>

Additionally, in recent years, interest in hydro- and solvothermal reactions with in situ ligand synthesis has grown. According to Sun,<sup>7</sup> there are more than 10 types of in situ ligand syntheses reported to date using hydro(solvo)thermal

reactions since it was first proposed by Champness and Schröder in 1997;<sup>8</sup> for example carbon–carbon coupling,<sup>9</sup> hydroxylation of carboxylate esters and organic nitriles,<sup>10</sup> cleavage and formation of disulfide bonds,<sup>11</sup> and decarboxylation of aromatic groups<sup>12</sup> have been reported.

In the light of above-mentioned facts, we present herein a systematic study of the hydrothermal reactions of 1,2,3-benzene tricarboxylic acid ( $1,2,3-btcH_3$ ) and linear bridging ligands  $4,4'$ -dipyridyl ( $bpy$ ) and pyrazine ( $pyz$ ) with metal ( $Co, Ni, Cu$ ) salts, under different reaction conditions. The aim is to both directly study the affect of temperature on in situ ligand transformation, in this case decarboxylation of  $1,2,3-btcH_3$  into isophthalic acid ( $ip = 1,3$  benzene dicarboxylic acid), and to arrive at pillared-layer structures with a view to studying their magnetic properties.

## Experimental Section

**Materials and Physical Techniques.** All reagents and solvents employed in the syntheses were commercially available and used as received and without further purification. The syntheses of **1–4** were carried out in 23 mL Teflon-lined autoclaves under autogenous pressure. Elemental analyses were performed on a Carlo Erba Elemental Analyser EA 1108. The Fourier transform infrared (FT-IR) spectra were measured with an AVATAR 320 spectrometer in KBr disks. Thermal analyses were carried out using Mettler Toledo TGA/DSC 1 equipment with a heating rate of  $10\text{ }^\circ\text{C min}^{-1}$ .

**Magnetometry.** Variable temperature magnetic susceptibility and magnetization measurements were performed with a Quantum Design PPMS EverCool system equipped with a vibrating sample magnetometer and a 9 T magnet. Data were collected on polycrystalline samples. The magnetic susceptibility measurements were performed for field-cooled and zero-field-cooled samples in magnetic fields of 0.1 T. Pascal's constants were used to estimate the diamagnetic corrections.<sup>13</sup> Magnetization data were collected in fields up to 9 T and in the temperature range between 2.0 and 10.0 K. A hysteresis loop measurement was performed at 2.0 K with maximum fields of  $+7.0\text{ T}$  and  $-7.0\text{ T}$ .

**Synthesis of  $[Ni_2(ip)_2(bpy)_2]_n$  (**1**).** A mixture of 0.5 mmol of  $1,2,3-btcH_3$  (0.123 g), 0.5 mmol of  $bpy$  (0.079 g), and 2 mmol of KOH

\*To whom correspondence should be addressed. Fax: +61 (02) 9385 6141. Tel: +61 (0)2 9385 4675. E-mail: j.stride@unsw.edu.au.



Table 1. Crystallographic Data

	compound 1	compound 2	compound 3	compound 4
empirical formula	C <sub>18</sub> H <sub>12</sub> N <sub>2</sub> NiO <sub>4</sub>	C <sub>18</sub> H <sub>12</sub> CoN <sub>2</sub> O <sub>4</sub>	C <sub>12</sub> H <sub>8</sub> N <sub>2</sub> NiO <sub>4</sub>	C <sub>12</sub> H <sub>8</sub> N <sub>2</sub> CoO <sub>4</sub>
formula weight	379.01	379.23	302.91	303.13
temperature (K)	150(2)	150(2)	150(2)	150(2)
wavelength (Å)	0.71073	0.71073	0.71073	0.71073
crystal system	triclinic	triclinic	triclinic	triclinic
space group	<i>P</i> $\bar{1}$	<i>P</i> $\bar{1}$	<i>P</i> $\bar{1}$	<i>P</i> $\bar{1}$
<i>a</i> / Å	9.1738(3)	8.9237(3)	6.9721(3)	7.0878(5)
<i>b</i> / Å	9.9099(3)	10.0609(3)	8.3039(4)	8.2937(7)
<i>c</i> / Å	10.0623(4)	10.0893(4)	10.0576(5)	10.0615(8)
$\alpha$	79.141(2)°	77.9170(10)°	102.586(2)°	101.988(3)°
$\beta$	71.968(2)°	79.698(2)°	93.856(2)°	93.525(4)°
$\gamma$	72.471(2)°	73.5840(10)°	107.143(2)°	107.925(3)°
volume/Å <sup>3</sup>	824.88(5)	842.70(5)	537.63(4)	545.45(7)
<i>Z</i>	2	2	2	2
$\rho$ / Mg m <sup>-3</sup>	1.526	1.495	1.871	1.846
limiting indices	$-10 \leq h \leq 10$ $-11 \leq k \leq 11$ $-11 \leq l \leq 11$	$-10 \leq h \leq 10$ $-11 \leq k \leq 11$ $-11 \leq l \leq 11$	$-8 \leq h \leq 8$ $-9 \leq k \leq 9$ $-11 \leq l \leq 11$	$-8 \leq h \leq 8$ $-9 \leq k \leq 9$ $-11 \leq l \leq 11$
reflections number	2899	2953	1879	1906
<i>R</i> <sub>int</sub>	0.040	0.036	0.046	0.040
$\sigma$ <sub>max</sub>	25.0°	25.0°	25.0°	25.0°
<i>S</i>	0.62	0.91	0.69	0.67
<i>F</i> (000)	388	386	308	306
<i>wR</i> ( <i>F</i> <sup>2</sup> )	0.082	0.101	0.086	0.089

(0.112 g) in 6 mL of distilled water was stirred for 30 min followed by addition of a solution of NiCl<sub>2</sub>·6H<sub>2</sub>O (0.237 g, 1 mmol) in 4 mL of H<sub>2</sub>O. The resulting green solution was stirred for about 30 min at room temperature, then sealed in a 23 mL Teflon-lined stainless steel autoclave and heated at 220 °C for three days under auto-genous pressure. The reaction system was then cooled to room temperature over 4 h. Green platelike crystals of **1** suitable for single crystal X-ray diffraction analysis were collected from the final reaction system by filtration and dried in air at ambient temperature (42.28% yield based on nickel). Anal. calcd.: C, 56.99% H, 3.16 N, 7.38%. Found: C, 56.64% H, 3.33%, N, 7.37%. IR data ( $\nu_{\text{max}}$ /cm<sup>-1</sup>): 3451sbr, 1625sd, 1543 m, 1481w, 1425 m, 1411s, 1396s, 1220w, 1093w, 814 m, 751 m, 742 m, 636 m, 536w.

**Synthesis of [Co<sub>2</sub>(ip)<sub>2</sub>(bpy)<sub>2</sub>]<sub>n</sub> (**2**).** An identical procedure as that for **1** was followed to prepare **2**, except that NiCl<sub>2</sub>·6H<sub>2</sub>O was replaced by CoCl<sub>2</sub>·6H<sub>2</sub>O (0.237 g, 1 mmol). For **2**, yield: 62.67% based on Co. Anal. calcd.: C, 56.95% H, 3.16 N, 7.38%. Found: C, 56.04% H, 3.25%, N, 7.28%. IR data ( $\nu_{\text{max}}$ /cm<sup>-1</sup>): 3457sbr, 1606sd, 1578 m, 1481w, 1453 m, 1411s, 1225w, 1086w, 813 m, 739 m, 721 m, 631w.

**Synthesis of [Ni<sub>2</sub>(ip)<sub>2</sub>(pyz)<sub>2</sub>]<sub>n</sub> (**3**).** An identical procedure as that for **1** was followed to prepare **3**, except that bpy was replaced by pyz (0.040 g, 0.5 mmol). For **3**, yield: 26.21% based on Ni. Anal. calcd.: C, 47.53% H, 2.64 N, 9.24%. Found: C, 45.31% H, 2.69%, N, 8.75%. IR data ( $\nu_{\text{max}}$ /cm<sup>-1</sup>): 3111 m, 3063 m, 1619s, 1580 m, 1529s, 1451 m, 1395s, 1166 m, 1122 m, 1062s, 976w, 833 m, 817s, 722s, 524w, 482 m, 431 m.

**Synthesis of [Co<sub>2</sub>(ip)<sub>2</sub>(pyz)<sub>2</sub>]<sub>n</sub> (**4**).** An identical procedure as that for **3** was followed to prepare **4**, except that NiCl<sub>2</sub>·6H<sub>2</sub>O was replaced by CoCl<sub>2</sub>·6H<sub>2</sub>O (0.040 g, 0.5 mmol). For **4**, yield: 32.77% based on Co. Anal. calcd.: C, 47.50% H, 2.63 N, 9.23%. Found: C, 47.34% H, 2.67%, N, 8.88%. IR data ( $\nu_{\text{max}}$ /cm<sup>-1</sup>): 3105 m, 3058 m, 1631s, 1573 m, 1537s, 1483 m, 1453 m, 1164 m, 1122 m, 1055s, 974 m, 918 m, 834 m, 815s, 722s, 520w, 471s, 434 m.

**Crystallographic Analysis.** Crystallographic data of **1–4** were collected at 150 K on a Bruker kappa APEXII-CCD Area Detector instrument with Mo K $\alpha$  monochromated radiation ( $\lambda$  = 0.71073 Å) using the  $\omega$ - $\phi$  scan technique. An empirical absorption correction was applied. The structures were solved by direct methods and refined by full-matrix least-squares against *F*<sup>2</sup> using the SHELXS-97 and SHELXL-97 programs.<sup>14</sup> Anisotropic thermal parameters were assigned to all non-hydrogen atoms and the hydrogen atoms were set in calculated positions and refined as riding atoms with a common fixed isotropic thermal parameter. Analytical expressions of neutral atom scattering factors were employed, and anomalous dispersion corrections were incorporated. The crystallographic data and selected bond lengths and bond angles for **1–4** are listed in

Tables 1 and 2. CCDC 752724–752727 contains the supplementary crystallographic data for this paper. These data can be obtained free of charge from The Cambridge Crystallographic Data Centre via [www.ccdc.cam.ac.uk/data\\_request/cif](http://www.ccdc.cam.ac.uk/data_request/cif).

## Results and Discussion

**Synthesis.** The crystals of **1–4** were successfully synthesized by reacting the ligands with the corresponding metal salts at 220 °C for 3 days under hydrothermal conditions. The IR spectra of **1–2** and **3–4** are fully consistent with them being isostructural pairs of compounds. When the hydrothermal reaction of NiCl<sub>2</sub>·6H<sub>2</sub>O, 4,4'-bpy, 1,2,3-btcH<sub>3</sub>, and KOH was carried out at 220 °C, the complex [Ni<sub>2</sub>(ip)<sub>2</sub>(bpy)<sub>2</sub>] (**1**) was obtained. Surprisingly, the results of single crystal analysis indicated that the Ni(II) atom in complex (**1**) is coordinated by isophthalate (ip), rather than deprotonated species of 1,2,3-btcH<sub>3</sub>, demonstrating that during the reaction the central carboxylic group is cleaved from the ring in the reaction medium, as there is no other source of ip. A second experiment was carried out substituting CoCl<sub>2</sub>·6H<sub>2</sub>O for NiCl<sub>2</sub>·6H<sub>2</sub>O, with 1,2,3-btcH<sub>3</sub> and 4,4'-bpy under the same conditions. Complex [Co<sub>2</sub>(ip)<sub>2</sub>(bpy)<sub>2</sub>] (**2**), also incorporating ip rather than 1,2,3-btc, was isolated. In 2004, Zheng et al., observed a similar phenomenon when reacting Cu(II) salts with 1,2,3-btcH<sub>3</sub> and 4,4'-bpy. They isolated three different products involving decarboxylation and hydroxylation of the benzene ring, which was highly dependent on pH.<sup>15</sup> When we tried these reactions under different conditions of pH, no product was obtained. Moreover, the change of base from KOH to NaOH was not found to affect the reaction outcome. However, when we tried these reactions at a lower temperature (150 °C), no decarboxylation of 1,2,3-btc was observed and complexes [Co<sub>3</sub>(1,2,3-btc)<sub>2</sub>(4,4'-bpy)<sub>2</sub>] and [Ni(1,2,3-btcH)<sub>2</sub>(4,4'-bpy)(H<sub>2</sub>O)]·H<sub>2</sub>O were obtained, which have been reported recently.<sup>16</sup> We conclude that decarboxylation of 1,2,3-btcH<sub>3</sub> is highly dependent on the reaction temperature. To further confirm this hypothesis and to also generate variable void volumes within the material, we carried out more experiments using pyz as the linear “pillar” ligand instead of 4,4'-bpy, under the same conditions. As a result of these reactions, the complexes

Table 2. Selected Bond Lengths (Å) and Bond Angles (°)

Compound 1			
Ni(1)–O(4)	2.0281(12)	O(3)–Ni(1)–N(2)	90.89(5)
Ni(1)–O(3)	2.0315(12)	N(1)–Ni(1)–N(2)	176.17(5)
Ni(1)–N(1)	2.1024(15)	O(4)–Ni(1)–O(1)	157.32(5)
Ni(1)–N(2)	2.1036(15)	O(3)–Ni(1)–O(1)	97.43(5)
Ni(1)–O(1)	2.1180(12)	N(1)–Ni(1)–O(1)	88.47(5)
Ni(1)–O(2)	2.1408(12)	N(2)–Ni(1)–O(1)	90.67(5)
O(4)–Ni(1)–O(3)	104.56(5)	O(4)–Ni(1)–O(2)	95.60(5)
O(4)–Ni(1)–N(1)	87.79(5)	O(3)–Ni(1)–O(2)	159.22(5)
O(3)–Ni(1)–N(1)	85.52(5)	N(1)–Ni(1)–O(2)	90.37(5)
O(4)–Ni(1)–N(2)	94.42(5)	N(2)–Ni(1)–O(2)	92.53(5)
O(1)–Ni(1)–O(2)	62.06(5)		
Compound 2			
Co(1)–O(1)	2.0159(15)	O(4)–Co(1)–N(2)	90.67(7)
Co(1)–O(2)	2.0459(15)	O(1)–Co(1)–N(1)	86.76(7)
Co(1)–O(4)	2.1248(16)	O(2)–Co(1)–N(1)	87.65(7)
Co(1)–N(2)	2.146(2)	O(4)–Co(1)–N(1)	89.90(7)
Co(1)–N(1)	2.153(2)	N(2)–Co(1)–N(1)	176.65(6)
Co(1)–O(3)	2.2294(16)	O(1)–Co(1)–O(3)	152.08(6)
O(1)–Co(1)–O(2)	115.09(7)	O(2)–Co(1)–O(3)	91.92(6)
O(1)–Co(1)–O(4)	92.47(6)	O(4)–Co(1)–O(3)	60.22(6)
O(2)–Co(1)–O(4)	152.12(7)	N(20)–Co(1)–O(3)	95.70(7)
O(1)–Co(1)–N(2)	89.92(7)	N(1)–Co(1)–O(3)	87.45(7)
O(2)–Co(1)–N(2)	93.38(7)		
Compound 3			
Ni(1)–O(1)	2.0154(15)	O(1)–Ni(1)–O(2)	108.84(6)
Ni(1)–O(2)	2.0323(15)	O(1)–Ni(1)–N(2)	92.24(7)
Ni(1)–N(2)	2.088(2)	O(2)–Ni(1)–N(2)	92.95(7)
Ni(1)–O(4)	2.0911(15)	O(1)–Ni(1)–O(4)	158.61(7)
Ni(1)–N(1)	2.097(2)	O(2)–Ni(1)–O(4)	92.27(6)
Ni(1)–O(3)	2.1466(16)	N(2)–Ni(1)–O(4)	89.96(7)
O(1)–Ni(1)–N(1)	88.02(7)	O(2)–Ni(1)–O(3)	154.12(6)
O(2)–Ni(1)–N(1)	85.85(7)	N(2)–Ni(1)–O(3)	91.62(7)
N(2)–Ni(1)–N(1)	178.79(7)	O(4)–Ni(1)–O(3)	62.26(6)
O(4)–Ni(1)–N(1)	90.23(7)	N(1)–Ni(1)–O(3)	89.52(7)
O(1)–Ni(1)–O(3)	96.40(6)		
Compound 4			
Co(1)–O(2)	2.0056(19)	O(3)–Co(1)–N(2)	89.26(8)
Co(1)–O(1)	2.0348(18)	O(2)–Co(1)–N(1)	86.52(8)
Co(1)–O(3)	2.1227(19)	O(1)–Co(1)–N(1)	87.95(8)
Co(1)–N(2)	2.148(2)	O(3)–Co(1)–N(1)	91.32(8)
Co(1)–N(1)	2.156(2)	N(2)–Co(1)–N(1)	178.76(8)
Co(1)–O(4)	2.196(2)	O(2)–Co(1)–O(4)	151.38(8)
O(2)–Co(1)–O(1)	115.03(8)	O(1)–Co(1)–O(4)	92.85(7)
O(2)–Co(1)–O(3)	91.39(8)	O(3)–Co(1)–O(4)	60.61(7)
O(1)–Co(1)–O(3)	153.46(8)	N(2)–Co(1)–O(4)	92.99(8)
O(2)–Co(1)–N(2)	92.37(8)	N(1)–Co(1)–O(4)	88.24(8)
O(1)–Co(1)–N(2)	92.02(8)		

[Ni<sub>2</sub>(ip)<sub>2</sub>(pyz)<sub>2</sub>] (**3**) and [Co<sub>2</sub>(ip)<sub>2</sub>(pyz)<sub>2</sub>] (**4**), also incorporating ip, were isolated from reactions at 220 °C. We also performed the same reactions with ip as precursor under same conditions but we did not able to get any product, which shows that the decarboxylation of btcH<sub>3</sub> is important for the synthesis of **1–4** as use of ip as precursor gave no product under similar conditions.

Furthermore, when we performed the same reactions with Cu(NO<sub>3</sub>)<sub>2</sub>·2.5H<sub>2</sub>O, a mixed valence Cu<sup>I</sup>–Cu<sup>II</sup> complex [Cu<sub>2</sub>(ipO)(bpy)] (ipO = 2-hydroxyisophthalate) was obtained in which central carboxylic group of 1,2,3-btcH<sub>3</sub> had changed into a hydroxyl group. This complex was reported in 2002 by Tao et al., who observed the transformation of isophthalate (ip) into ipO in an in situ redox reaction.<sup>17</sup> This leads us to conclude that when Co(II) and Ni(II) salts are used as precursors, decarboxylation of 1,2,3-btcH<sub>3</sub> occurs only at higher temperatures (around 220 °C) (Figure 1). However, when Cu(II) salts are used as precursors, the mechanism may involve rapid

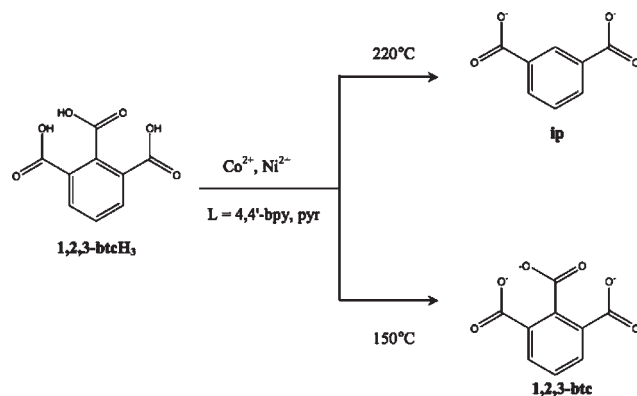
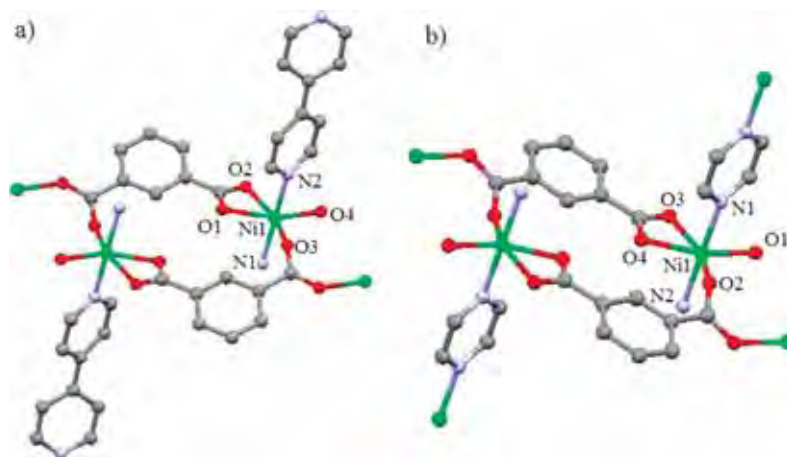


Figure 1. The reaction route of 1,2,3-btcH<sub>3</sub> at two different reaction temperatures in the presence of Ni(II) and Co(II) ions.

decarboxylation at the 2-position of 1,2,3-btcH<sub>3</sub>, then hydroxylation on this site due to a metal/ligand redox reaction.<sup>13</sup>

**Crystal Structure.** The X-ray structure analysis reveals that **1** and **2** are isomorphous; here, complex **1** is taken as an example to depict the structure in detail. The basic structural motif for these polymers is similar to that previously reported for Cd(II), Zn(II), and Ni(II) containing polymers, but we observe slight differences in the structural parameters.<sup>18,19</sup> Two equivalent Ni(II) atoms are separated by 4.53 Å and are bridged by *syn-anti* carboxylate groups of ip ligands. Each Ni(II) atom is in a distorted octahedral geometry, coordinated by four oxygen atoms in the equatorial plane, two from bridging carboxylate ions [*d*(Ni1–O3) = 2.031(12) and *d*(Ni1–O4) = 2.028(12) Å] and two from the chelating carboxylate end of an ip ligand [*d*(Ni1–O1) = 2.114(12) and *d*(Ni1–O2) = 2.141(12) Å], and two trans-related  $\mu$ -4,4'-bpy ligands [*d*(Ni1–N1) = 2.102(15) and *d*(Ni1–N2) = 2.103(15) Å] at the axial positions (Figure 2). The two equivalent Ni(II) atoms are linked by ip ligands to form a [Ni<sub>2</sub>O<sub>4</sub>C<sub>2</sub>] eight-membered ring. The dinuclear metal units are bridged by ip to form infinite 1D chains along the crystallographic *c*-axis, while the 4,4'-bpy molecules act as pillars to link the adjacent chains via N atoms, resulting in infinite 2D layers between the crystallographic *ab*-axis. The  $\pi$ – $\pi$  stacking interactions between the ip at a distance of 9.910 Å and 4,4'-bpy aromatic rings at a distance of 9.910 Å of adjacent layers extend the 2D network into a 3D supermolecular framework having large rectangular cavities of ca. 9 × 10 Å (Figure 3). A comparison of the crystal structures of **1** and **2** suggests that although the two structures belong to same crystal system and space group, the values of the crystallographic cell parameters ( $\alpha$ ,  $\beta$ ,  $\gamma$ ) differ, probably due to the change in metal size or the difference in the dihedral twisting of the aromatic rings of the 4,4'-bpy in **1** and **2**, Table 1; the dihedral angle between the planes of the two aromatic rings of 4,4'-bpy is 26.77 and 13.43°, in **1** and **2**, respectively. The interplanar distance between the ip aromatic rings of adjacent layers is 3.957 and 3.799 Å, in **1** and **2**, respectively.

Compounds **3** and **4** were also found to be isomorphous. The local coordination environment around the metal atom is similar to those found in **1** and **2** (Figure 2). The topology of the structure is also similar to that of **1** and **2**, except for the fact that pyz acts as the pillar ligand instead of 4,4'-bpy, linking adjacent 1D chains consisting of ip ligands and metal centers running along the *c*-axis, Figure 4. The pyz molecules link the adjacent 1D chains into 2D sheets parallel to the *ac*-plane. In complex **3**, the Ni–O distances range from



**Figure 2.** (a) View of coordination environment in complex **1**; (b) view of coordination environment in complex **3**.

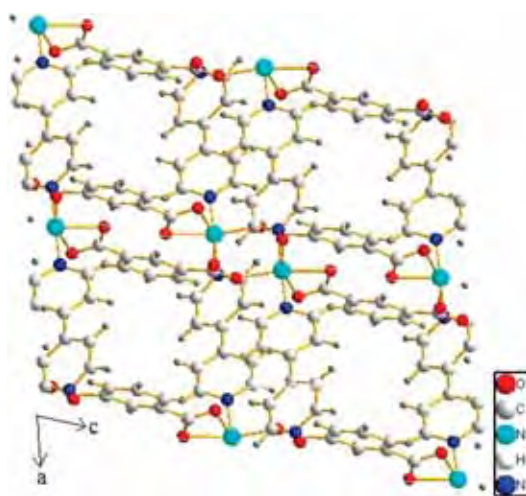


**Figure 3.** A view of two-dimensional layer of complex **1** in the *ac*-plane.

2.0154(15) to 2.1466(16) Å, and the Ni–N distances are 2.088(2) and 2.097(1) Å. The bond angles around the octahedral Ni(II) center range from 62.26(6) to 178.79(7)°. In complex **4**, the Co–O distances range between 2.0056(19) and 2.196(2) Å and the Co–N distances are 2.148(2) and 2.156(2) Å. The bond angles around the octahedral Co(II) center range from 60.61(7) to 178.76(8)°.

**Thermogravimetric Analysis.** Complexes **1–4** are stable at ambient conditions, and thermogravimetric analyses were performed to explore their thermal stabilities. As depicted in Figure S1 of Supporting Information, all the complexes are thermally very stable up to 450 °C. As there are no solvent molecules in the frameworks, there is a plateau region ranging from 50 to 450 °C followed by sudden decrease in the weight, suggesting the onset of decomposition temperature of the complexes with a total weight loss of ca. 78, 80, 76, and 76% for complexes **1–4**, respectively, indicating the total loss of the organic fragments in each, resulting in the simple oxides NiO and CoO.

**Magnetic Properties.** The analysis of **1–4** revealed considerable changes in the magnetic properties for the different metal ion and bridging ligand combinations. The results of our analyses are listed in Table 3. We first focus on the analyses of the Ni compounds **1** and **3** and consequently apply our findings to the Co materials **2** and **4**.

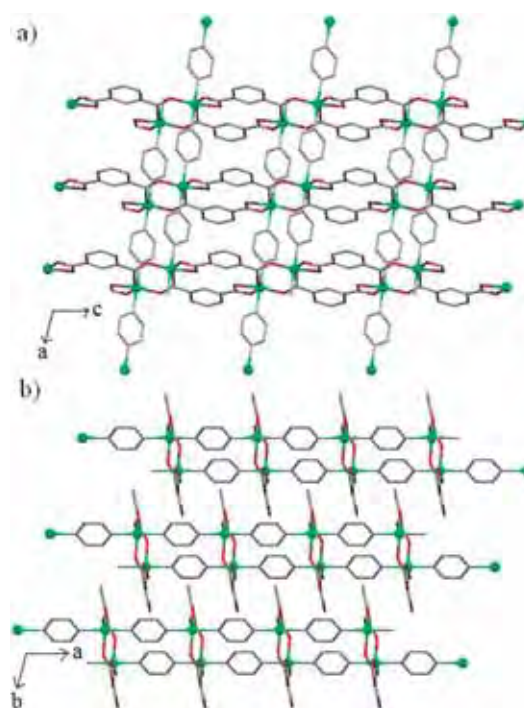


**Figure 4.** (a) A view of two-dimensional layer of complex **3** in the *ac*-plane; (b) view along the *c*-axis showing the packing of the layers in  $\pi$ – $\pi$  stacking mode.

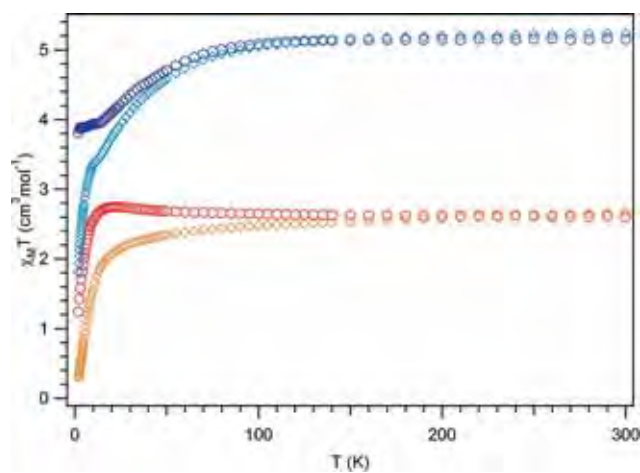
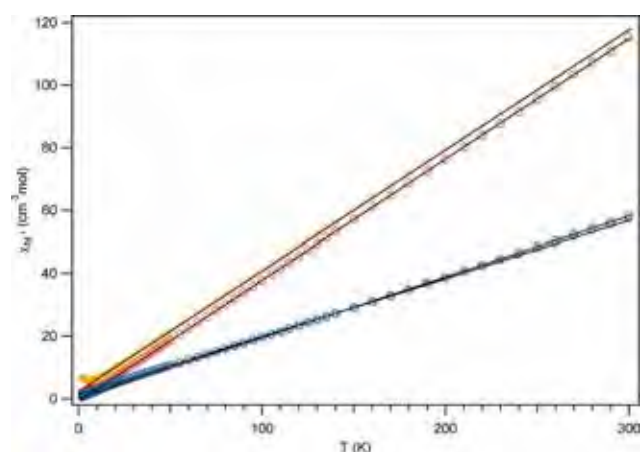
The temperature-dependent magnetic susceptibility per dimeric unit of **1–4** in a magnetic field of 1000 Oe is shown as  $\chi T$  vs  $T$  in Figure 5 (for  $\chi$  vs  $T$  see Supporting Information, Figure S2).

**Ni<sub>2</sub>(ip)<sub>2</sub>(bpy)<sub>2</sub>.** The temperature-dependent susceptibility of **1** plotted as  $\chi T$  vs  $T$  stays almost constant upon cooling from a value of 2.60 cm<sup>3</sup> K mol<sup>−1</sup> at 300 K to reach a broad maximum of 2.75 cm<sup>3</sup> K mol<sup>−1</sup> at 20 K. It then sharply drops to a value of 1.24 cm<sup>3</sup> K mol<sup>−1</sup> at 2 K (Figure 5). The data obeys the Curie–Weiss law ( $\chi = C/(T - \theta)$ ) in the temperature range 20–300 K with a Curie constant  $C = 1.30$  cm<sup>3</sup> K mol<sup>−1</sup> per Ni(II) and a Weiss constant  $\theta = 1.9$  K (Figure 6). The Landé factor  $g = 2.28$  extracted from  $C$  is in good agreement with other known Ni(II) compounds,<sup>20</sup> whereas the small positive value of the Weiss constant implies weak ferromagnetic (FM) exchange.

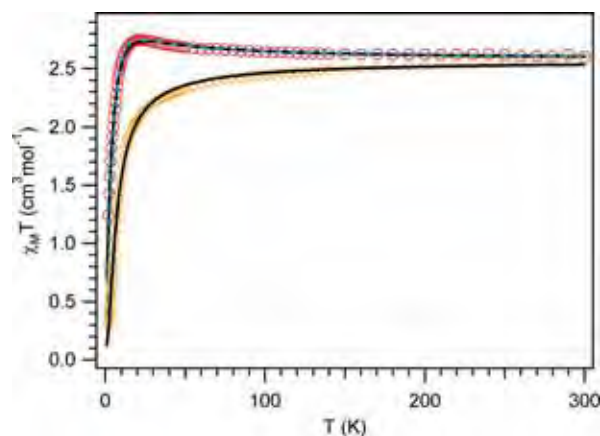


**Table 3. Magnetic Properties of Compounds 1–4**

property	Ni <sub>2</sub> (ip) <sub>2</sub> -(bpy) <sub>2</sub> ( <b>1</b> )	Ni <sub>2</sub> (ip) <sub>2</sub> -(pyz) <sub>2</sub> ( <b>3</b> )	Co <sub>2</sub> (ip) <sub>2</sub> -(bpy) <sub>2</sub> ( <b>2</b> )	Co <sub>2</sub> (ip) <sub>2</sub> -(pyz) <sub>2</sub> ( <b>4</b> )
$C$ [cm <sup>3</sup> K mol <sup>−1</sup> ]	1.30	1.30	2.59	2.71
$\theta$ [K]	1.9	−6.2	−1.6	−7.9
$\chi T$ (300 K)	2.60	2.58	5.15	5.24
$J_{\text{dimer}}$ [cm <sup>−1</sup> ]	6.6			
$J_{\text{chain}}$ [cm <sup>−1</sup> ]		−6.1		
$zJ$ [cm <sup>−1</sup> ]	−1.6	1.2		
$g$	2.27	2.27		
$g$ (spin only, from $C$ )	2.28	2.28	2.35	2.40
$g$ (spin only, from $\chi T^{\text{max}}$ )	2.28	2.27	2.34	2.36
$\chi T^{\text{max}}$ [cm <sup>3</sup> K mol <sup>−1</sup> ]	2.75			
$\chi T^{\text{plateau 1}}$ [cm <sup>3</sup> K mol <sup>−1</sup> ]			3.94	3.39
$\chi T^{\text{plateau 2}}$ [cm <sup>3</sup> K mol <sup>−1</sup> ]			3.89	
$T(\chi^{\text{max}})$ [K]		6		
$M$ (9 T) [ $\mu\text{B}$ ]	3.79	2.81	4.61	4.69
$T_{\text{N}}$ [K]		14		
$H_{\text{c}}$ [Oe]		205		
$M_{\text{f}}$ [ $\mu\text{B}$ ]		0.0026		
$\alpha$ [°]		0.076		

**Figure 5.**  $\chi T$  vs  $T$  per dimer of **1** (red circles), **2** (blue circles), **3** (brown diamonds), and **4** (light blue diamonds) measured at 1000 Oe. Inset:  $\chi T$  vs  $T$  per dimer, shown on a logarithmic temperature scale to emphasize the line shape at low temperatures.**Figure 6.**  $\chi^{-1}$  vs  $T$  per dimer of **1** (red circles), **2** (blue circles), **3** (brown diamonds), and **4** (light blue diamonds) measured at 1000 Oe. The solid lines are fits of the data to the Curie–Weiss law with parameters described in the text.

The crystal structure of **1** defines three possible pathways for magnetic exchange between the Ni ions. The strongest

**Figure 7.**  $\chi T$  vs  $T$  per dimer of **1** (red circles) and **3** (brown diamonds). Inset:  $\chi$  vs  $T$  per dimer of **1** and **3**. The solid and dotted lines modeling **1** are fits to a model of an exchange coupled Ni(II) dimer including a molecular field term and single-ion anisotropy, respectively, using the parameters given in the text. The solid line modeling the data of **3** is the best fit to a AF chain model incorporating a molecular field term, as given in the text.

interactions are expected within dimers of Ni ions bridged by two bidentate *syn-syn* carboxylate groups of ip. The other two pathways via two chelating carboxylate groups of a single ip ligand and via bpy involve a considerable number of chemical bonds and are therefore thought to be small. We have used the Hamiltonian in eq 1 to describe our system.

$$\hat{H} = -J\hat{S}_1\hat{S}_2 + \mu_B g + \sum \hat{S}_i H + \delta_i \sum D_i [\hat{S}_{i,z}^2 - 1/3S(S+1)] \quad (1)$$

The first term describes the intradimer exchange interaction with coupling constant  $J$ , the second term is the Zeeman-interaction ( $\mu_B$  and  $g$  have their usual meaning), and the third term stands for the single-ion anisotropy ( $\delta_i$  is 1 or 0 depending on whether anisotropy is included in the analysis or not). The weaker exchange pathways were treated using the molecular-field approximation (eq 2)

$$\chi = \frac{\chi_{\text{dimer}}}{1 - (2zJ/Ng^2\mu_B^2)\chi_{\text{dimer}}} \quad (2)$$

The best fit was obtained with  $g = 2.27$ ,  $J = 6.6 \text{ cm}^{-1}$ , and  $zJ = -1.6 \text{ cm}^{-1}$  ( $R = \Sigma(\chi_{\text{calc}} - \chi_{\text{obs}})^2 / \Sigma(\chi_{\text{obs}})^2 = 0.018$  over the whole temperature range). A fit of similar quality could be obtained by inclusion of an axial anisotropy term in the Hamiltonian in eq 1 ( $\delta_i$  set to 1), with  $g = 2.28$ ,  $J = 2.6 \text{ cm}^{-1}$  and  $D_{\text{Ni}} = 12.9 \text{ cm}^{-1}$  ( $R = 0.021$ ), (Figure 7). Both parameter sets indicate weak FM intradimer exchange. The decrease of  $\chi T$  at lower temperatures is explained by the two models by weak antiferromagnetic (AF) interdimer interactions via ip and bpy ligands or axial single-ion anisotropy, respectively. We have refrained from using a model incorporating both a molecular field term and axial anisotropy in order to avoid overparametrization.

We have measured isothermal magnetization curves for **1** to confirm the above findings, Figure 8. The magnetization at 2 K rises almost linearly between zero and 1 T; at higher fields the slope of the curve decreases continuously, but it does not reach saturation, with a value of  $3.79 N\mu_B$  at 9 T. The curve is considerably flatter than expected for an isotropic Ni-dimer with FM coupling of a few  $\text{cm}^{-1}$ , whereas simulations using the best fit parameters of the anisotropic dimer model underestimate

the experimental data. We conclude that both axial anisotropy and weak AF interdimer interactions are present in **1**. The former is a well-known characteristic of Ni(II) compounds,<sup>20a,b,21</sup> whereas the latter is in agreement with the exchange pathways present in the crystal structure.

**Ni<sub>2</sub>(ip)<sub>2</sub>(pyz)<sub>2</sub>.** The magnetic susceptibility of **3** shown as  $\chi T$  vs  $T$  in Figure 5 gradually decreases from a room temperature value of  $2.58 \text{ cm}^3 \text{ K mol}^{-1}$  to  $0.30 \text{ cm}^3 \text{ K mol}^{-1}$  at 2 K. Fits of the data to the Curie–Weiss law affect best fit parameters  $C = 1.30 \text{ cm}^3 \text{ K mol}^{-1}$  per Ni(II) and  $\theta = -6.2 \text{ K}$ , Figure 6, indicating weak AF interactions in the system.

The exchange pathways via carboxylate groups of the ip ligand in **3** are almost identical to **1**. However, pyz is known to promote stronger exchange interactions than bpy. An isolated dimer model is therefore not an appropriate description for the magnetic system anymore. Furthermore,  $\chi$  vs  $T$  shows a broad maximum at 6 K, Figure S2 of Supporting Information, a key feature of AF chains. Accordingly, we have used an AF chain model proposed by Hiller,<sup>22</sup> eq 3, to describe the chains formed by Ni(II) and pyz.

$$\chi_{\text{chain}} = \frac{Ng^2\mu_B^2}{kT} \times \frac{(2.0 + 0.0194x^2 + 0.777x^3)}{(3.0 + 4.346x + 3.232x^2 + 5.834x^3)} \quad (3)$$

with  $x = |J_{\text{chain}}|/(2kT)$

Similar to **1** we have introduced a molecular-field term in our model, which in this case describes the interactions between the Ni-pyz chains ( $\chi_{\text{dimer}}$  was replaced by  $\chi_{\text{chain}}$  in eq 2). The best fit was obtained with  $g = 2.27$ ,  $J_{\text{chain}} = -6.10 \text{ cm}^{-1}$  and  $zJ = 1.18 \text{ cm}^{-1}$  and  $R = 0.023$ , Figure 7. This indicates AF coupled chains along pyz with weak FM interactions between the chains. The value of  $zJ$  is smaller than the intradimer interactions observed for **1** because it also includes weak AF interdimer interactions via the third exchange pathway mediated by ip. Neglecting the latter, this parameter set describes a spin ladder with AF exchange along the ladder and weak FM intradimer exchange on the rungs. Magnetization measurements of **3** at 2 K start almost linearly up to 1.5 T before rising more steeply. The curve passes an inclination point at 5 T, finally reaching a value of  $2.81 N\mu_B$  at 9 T (Figure 8). The curve shape and the value at 9 T which is much lower than the saturation value of two Ni(II) ( $4.0 N\mu_B$  with  $S = 1$ ,  $g = 2.0$ ) suggest an AF ground state for **3**, in agreement with the spin ladder picture developed above.

The presence of both inter and intrachain interactions as well as the measured magnetization curves have prompted us to look for indications of three-dimensional (3D) magnetic ordering. We have measured the magnetic susceptibility in field-cooled (FC) and zero-field-cooled (ZFC) mode, Figure 9. The FC curve deviates from the ZFC curve with a bifurcation temperature of 14 K, following the same general curve shape to the lowest measured temperature. The steep discontinuity often visible in the magnetic susceptibility of weak ferromagnets is likely suppressed by the applied magnetic field.<sup>23</sup> However, the existence of a very weak spontaneous magnetization is confirmed by magnetic hysteresis measurements at 2 K with a coercive field of  $H_C = 200 \text{ Oe}$  and a very weak remanent magnetization of  $M_R = 0.0051 N\mu_B$ . Using the formula  $\sin(\alpha) = M_R/M_S$  we determine a canting angle  $\alpha = 0.076^\circ$  for **3**. Compound **3** can be classified as a very soft weak ferromagnet.

**Co<sub>2</sub>(ip)<sub>2</sub>(bpy)<sub>2</sub>.** The magnetic susceptibility of **2** shown as  $\chi T$  vs  $T$  is almost constant between 300 and 150 K at the room temperature value of  $5.15 \text{ cm}^3 \text{ K mol}^{-1}$ . Upon further

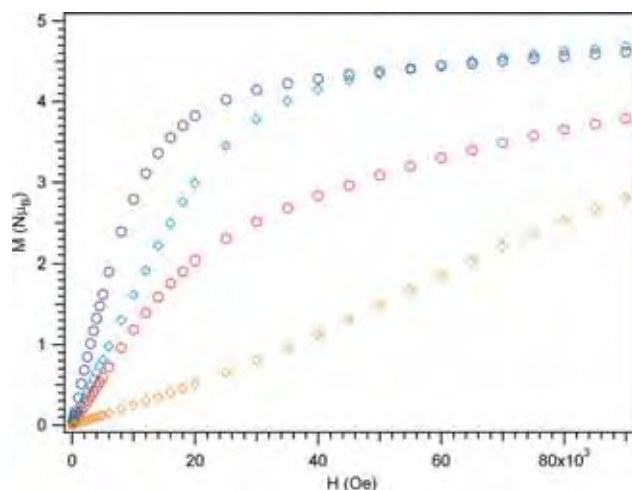


**Figure 8.**  $M$  vs  $H$  per dimer of **1** (red circles), **2** (blue circles), **3** (brown diamonds), and **4** (light blue diamonds) measured at 2 K.

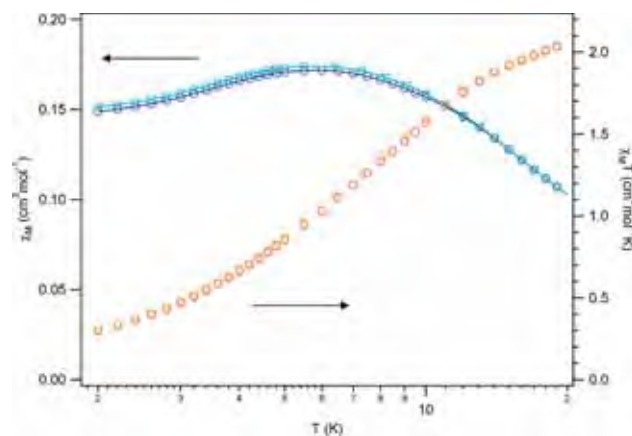


**Figure 9.** Field cooled (triangles) and zero-field cooled (circles) susceptibility per dimer of **3** shown as  $\chi$  vs  $T$  (dark and light blue) and  $\chi T$  vs  $T$  (red and brown), measured at 1000 Oe.

cooling it decreases gradually until reaching a plateau of  $3.94 \text{ cm}^3 \text{ K mol}^{-1}$  at 13 K. Below 10 K the curve drops to a second plateau at  $3.89 \text{ cm}^3 \text{ K mol}^{-1}$  before the onset of a steep decrease becomes visible at the lowest measured temperatures. The room temperature value is much larger than the spin-only value of  $3.75 \text{ cm}^3 \text{ K mol}^{-1}$  calculated for 2 Co(II) ions ( $S = 3/2$ ,  $g = 2$ ), indicating the presence of unquenched spin–orbit coupling found in high-symmetry ligand environments in the  $^4T_{1g}$  ground state of Co(II). This usually makes it difficult to quantitatively analyze the magnetic data of Co(II) compounds. The spin–orbit coupling in **2** is quenched to a certain extent as evidenced by a room temperature value lower than  $6.78 \text{ cm}^3 \text{ K mol}^{-1}$  calculated for two Co(II) ions in perfect octahedral coordination (weak field limit, no admixture of excited multiplets). This is likely due to a deviation from octahedral symmetry, in good agreement with the crystal structure.

Curie–Weiss fits in the range 20–300 K yield Curie and Weiss constants of  $2.59 \text{ cm}^3 \text{ K mol}^{-1}$  and  $-1.6 \text{ K}$ , respectively, in good agreement with other Co(II) compounds.<sup>24</sup> The negative Weiss constant is often observed in Co(II) compounds and is often a sign for unquenched spin–orbit coupling rather than AF exchange.<sup>25</sup> However, the fact that the susceptibility of **2** reaches a plateau at low temperature

rather than decreasing gradually toward zero indicates the presence of FM coupling in the system. We can expect the FM coupling to happen within the Co(II) dimers in **2**, analogous to the isostructural compound **1**. The sharp decrease at the lowest temperatures can be attributed to zero-field splitting effects and/or AF interdimer interactions, as found in **1**.

The FM dimer picture is further confirmed by isothermal magnetization measurements. At 2 K the magnetization rises linearly to  $2.79 N\mu_B$  at 1 T and gradually reaches a linear dependence again at higher fields without complete saturation ( $4.61 N\mu_B$  at 9 T). The value at 9 T can be quantified by a pair of FM coupled Co(II) ions with  $S_{\text{eff}} = 1/2$  and  $g_{\text{eff}} = 4.6$ . Effective  $g$ -values of this magnitude are very common for Co(II) compounds. As a rule of thumb, the three orthogonal values of the  $g$ -tensor add up to 13, leading to  $g_{\text{eff}} = 4\ 1/3$  in strictly octahedral symmetry. The magnetization curve increases less sharply than a Brillouin function with  $S_{\text{eff}} = 1$  and  $g_{\text{eff}} = 4\ 1/3$ . Again, this can be explained by the presence of weak AF interdimer interactions as well as ZFS effects.

**Co<sub>2</sub>(ip)<sub>2</sub>(pyz)<sub>2</sub>.** The magnetic susceptibility of **4** (Figure 5) behaves almost identical to **2** in the high temperature region, decreasing slowly from  $5.24\text{ cm}^3\text{ K mol}^{-1}$  at 300 K. Below 150 K, it then decreases gradually in a similar fashion to **2**, but more steeply. At 12 K the onset of a plateau is visible, but the susceptibility sharply decreases further with decreasing temperature. The room temperature value is consistent with two Co(II) ions in distorted octahedral ligand field. The value is almost equal to **2**, which was to be expected with regard to the almost isostructural Co(II) dimers in the two compounds. The magnetic susceptibility between 20 and 300 K obeys the Curie–Weiss law with  $C = 2.71$  and  $\theta = -7.9$  K. Since the Co(II) ions in the structures of **2** and **4** are in almost identical coordination environments we can attribute the larger negative Weiss constant to AF interactions mediated by pyz, consistent with our analysis of **1** and **3**. The stronger AF interactions are further accentuated by the decrease of  $\chi T$  at low  $T$  in **4** as opposed to the constant plateau in **2**.

The magnetization of **4** at 2 K rises linearly between 0 and 1 T with a smaller slope than observed for **2**. In the field range 5–9 T, the magnetization curve of the two compounds is basically identical. This finding again supports the stronger AF interactions in **4** due to the stronger magnetic coupling promoted by pyz as compared to bpy.

We have changed two parameters in the series of the four compounds **1–4**, namely, the diamine bridging ligand and the metal ion. Both parameters have a distinct effect on the resulting magnetic properties. The four compounds feature almost isostructural M(II) dimers with FM interactions. The interdimer interactions mediated by two different carboxylate groups of ip are weak. Moreover, there seems to be almost no magnetic exchange via bpy (**1** and **2**). The substitution with pyz however leads to antiferromagnetic exchange. The derived magnetic exchange constants within the Ni-dimers and along the chain mediated by pyz are of the same magnitude as for similar compounds.

Likewise, the magnetic interactions between nickel ions are stronger than for cobalt. This is visible for the onset of FM interactions in **1** as compared to **2** and, to a larger extent, for the AF interdimer interactions with both types of amine ligands, as accentuated by the magnetization curves. Furthermore, **3** is the only compound showing magnetic ordering in the

measured temperature range, which is obviously due to stronger magnetic interactions than in the other three compounds.

## Conclusion

Four new isomorphous coordination polymers were synthesized via in situ ligand transformation reaction by varying the metal ion and linear bridging ligand. The study reveals that ligand transformation reaction is highly dependent on temperature of the reaction and only occur at high temperature (220 °C). Magnetic studies reveals that ferromagnetic interactions exist within the M(II) dimers while interdimer interactions are weak in all the compounds. No magnetic ordering has been observed except compound **3** in the measured temperature range. This study illustrates the importance of various factors that affect the outcome of the final product.

**Acknowledgment.** This work was supported by the Australian Research Council Discovery Project Grant DP0880199. The authors acknowledge Rene Maquart at the University of Sydney for his assistance with collecting magnetic data.

**Supporting Information Available:** Thermogravimetric curves (S1) and  $\chi$  vs  $T$  plots per dimer of **1–4** (S2). This material is available free of charge via the Internet at <http://pubs.acs.org>.

## References

- (a) Dinca, M.; Yu, A. F.; Long, J. R. *J. Am. Chem. Soc.* **2006**, *128*, 8904–8913. (b) Cheetham, A. K.; Rao, C. N. R. *Science* **2007**, *318*, 58–59. (c) Yang, J.; Yue, Q.; Li, G.-D.; Cao, J.-J.; Li, G.-H.; Chen, J.-S. *Inorg. Chem.* **2006**, *45*, 2857–2865. (d) Li, Z.-G.; Wang, G.-H.; Jia, H.-Q.; Hu, N.-H.; Xu, J.-W. *CrystEngComm* **2008**, *10*, 173–176. (e) Matsuda, R.; Kitaura, R.; Kitagawa, S.; Kubota, Y.; Belosludov, R. V.; Kobayashi, T. C.; Sakamoto, H.; Chiba, T.; Takata, M.; Kawazoe, Y.; Mita, Y. *Nature* **2005**, *436*, 238–241. (f) Li, J.-R.; Yu, Q.; Tao, Y.; Bu, X.-H.; Ribas, J.; Batten, S. R. *Chem. Commun.* **2007**, 2290–2292. (g) Férey, G.; Millange, F.; Morcrette, M.; Serre, C.; Doublet, M.-L.; Greneche, J.-M.; Tarascon, J.-M. *Angew. Chem., Int. Ed.* **2007**, *46*, 3259–3263.
- (a) Shen, W.-Z.; Chen, X.-Y.; Cheng, P.; Yan, S.-P.; Zhai, B.; Liao, D.-Z.; Jiang, Z.-H. *Eur. J. Inorg. Chem.* **2005**, 2297–2305.
- (a) Mahata, P.; Sen, D.; Natarajan, S. *Chem. Commun.* **2008**, 1278–1280.
- (a) Ma, C.; Chen, C.; Liu, Q.; Liao, D.; Li, L.; Sun, L. *New J. Chem.* **2003**, *27*, 890–894. (b) Manna, S. C.; Zangrando, E.; Ribas, J.; Chaudhuri, N. R. *Eur. J. Inorg. Chem.* **2008**, 1400–1405. (c) Ma, C.-B.; Chen, C.-N.; Liu, Q.-T.; Liao, D.-Z.; Li, L.-C. *Eur. J. Inorg. Chem.* **2008**, 1865–1870. (d) Lin, J.-G.; Zang, S.-Q.; Tian, Z.-F.; Li, Y.-Z.; Xu, Y.-Y.; Zhu, H.-Z.; Meng, Q.-J. *CrystEngComm* **2007**, *9*, 915–921.
- (a) Ding, B.-B.; Weng, Y.-Q.; Mao, Z.-W.; Lam, C.-K.; Chen, X.-M.; Ye, B.-H. *Inorg. Chem.* **2005**, *44*, 8836–8845. (b) Ma, B.-Q.; Coppens, P. *Chem. Commun.* **2003**, 412–413.
- (a) Wang, X.-L.; Qin, C.; Wang, E.-B.; Li, Y.-G.; Hu, C.-W.; Xu, L. *Chem. Commun.* **2004**, 378–379. (b) Chun, H.; Dybtsev, D. N.; Kim, H.; Kim, K. *Chem.—Eur. J.* **2005**, *11*, 3521–3529.
- Bai, Z.-S.; Xu, J.; Su, Z.; Sun, W.-Y. *Inorg. Chem. Commun.* **2008**, *11*, 1227–1230.
- Blake, J.; Champness, N. R.; Chung, S. S. M.; Li, W.-S.; Schröder, M. *Chem. Commun.* **1997**, 1675–1676.
- (a) Feller, R. K.; Forster, P. M.; Wudl, F.; Cheetham, A. K. *Inorg. Chem.* **2007**, *46*, 8717–8721. (b) Liu, C.-M.; Gao, S.; Kou, H.-Z. *Chem. Commun.* **2001**, 1670–1671.
- (a) Evens, O. R.; Lin, W. B. *Acc. Chem. Res.* **2002**, *35*, 511–522. (b) Wu, C.-D.; Ayyappan, P.; Evens, O. R.; Lin, W. B. *Cryst. Growth Des.* **2007**, *7*, 1690–1694.
- (a) Wang, J.; Zhang, Y.-H.; Li, H.-X.; Lin, Z.-J.; Tong, M.-L. *Cryst. Growth Des.* **2007**, *7*, 2352–2360. (b) Han, L.; Bu, X.; Zhang, Q.; Feng, P. *Inorg. Chem.* **2006**, *45*, 5736–5738. (c) Humphrey, S. M.;



- Mole, R. A.; Rawson, J. M.; Wood, P. T. *Dalton Trans.* **2004**, 1670–1678.
- (12) (a) Zhang, X.-M.; Fang, R.-Q. *Inorg. Chem.* **2005**, *44*, 3955–3959. (b) Yan, Y.; Wu, C.-D.; Lu, C.-Z. *Z. Anorg. Allg. Chem.* **2003**, *629*, 1991–1995.
- (13) Kahn, O. *Molecular Magnetism*; VCH: Weinheim, Germany, 1993.
- (14) Sheldrick, G. M. *SHELXS 97, Program for the Solution of Crystal Structures*; University of Göttingen: Germany, 1997.
- (15) Zheng, Y. Z.; Tong, M. L.; Chen, X. M. *New J. Chem.* **2004**, *28*, 1412–1415.
- (16) Zheng, Y.-Z.; Zhang, Y.-B.; Tong, M.-L.; Xue, W.; Chen, X.-M. *Dalton Trans.* **2009**, 1396–1406.
- (17) Tao, J.; Zhang, Y.; Tong, M. L.; Chen, X. M.; Yuen, T.; Lin, C. L.; Huang, X.; Li, J. *Chem. Commun.* **2002**, 1342–1343.
- (18) Tian, G.; Zhu, G.; Fang, Q.; Guo, X.; Xue, M.; Sun, J.; Qui, S. *J. Mol. Str.* **2006**, *787*, 45–49.
- (19) Tao, J.; Chen, X.-M.; Huang, R.-B.; Zheng, L.-S. *J. Sol. State Chem.* **2003**, *170*, 130–134.
- (20) (a) Sieber, A.; Boskovic, C.; Bircher, R.; Waldmann, O.; Ochsenein, S. T.; Chaboussant, G.; Güdel, H. U.; Kirchner, N.; Slageren, J. V.; Wernsdorfer, W.; Neels, A.; Stoeckli-Evans, H.; Janssen, S.; Juranyi, F.; Mutka, H. *Inorg. Chem.* **2005**, *44*, 4315–4325. (b) Herchel, R.; Boca, R.; Krzystek, J.; Ozarowski, A.; Durán, M.; Slageren, J. V. *J. Am. Chem. Soc.* **2007**, *129*, 10306–10307. (c) Rogez, G.; Rebilly, J.-N.; Barra, A.-L.; Sorace, L.; Blondin, G.; Kirchner, N.; Duran, M.; Van Slageren, J.; Parsons, S.; Ricard, L.; Marvilliers, A.; Mallah, T. *Angew Chem., Int. Ed.* **2005**, *44*, 1876–1879. (d) Ferguson, A.; Lawrence, J.; Parkin, A.; Sanchez-Benitez, J.; Kamenev, K. V.; Brechin, E. K.; Wernsdorfer, W.; Hill, S.; Murrie, M. *Dalton Trans.* **2008**, 6409–6414.
- (21) Wilson, A.; Lawrence, J.; Yang, E.-C.; Nakano, M.; Hendrickson, D. N.; Hill, S. *Phys. Rev. B* **2006**, *74*, 140403.
- (22) Hiller, W.; Sträehle, J.; Datz, A.; Hanack, M.; Hatfield, W. E.; Ter Haar, L. W.; Güetlich, P. *J. Am. Chem. Soc.* **1984**, *106*, 329–335.
- (23) Hu, K.-L.; Kurmoo, M.; Wang, Z.; Gao, S. *Chem.—Eur. J.* **2009**, *15*, 12050–12064.
- (24) (a) Alley, K. G.; Bircher, R.; Abrahams, B. F.; Moubaraki, B.; Waldmann, O.; Ochsenein, S. T.; Fernandez-Alonso, F.; Murray, K. S.; Güdel, H. U.; Boskovic, C. *Inorg. Chem.* **2007**, *45*, 8950–8957. (b) Marshall, S. R.; Incarvito, C. D.; Manson, J. L.; Rheingold, A. L.; Miller, J. S. *Inorg. Chem.* **2000**, *39*, 1969–1973.
- (25) Mabbs, F. E.; Machin, J. E. *Magnetism and Transition Metal Complexes*; Chapman and Hall: London, 1973.

## Supporting Information

### **Controlled synthesis of isomorphous coordination polymers via *in situ* ligand transformation reaction: crystal structure, thermal and magnetic properties**

*Muhammad A. Nadeem,<sup>†</sup> Mohan Bhadbhade,<sup>§</sup> Roland Bircher<sup>‡</sup> and John A. Stride\**

<sup>†,‡</sup>

<sup>†</sup> *School of Chemistry, University of New South Wales, Sydney, NSW 2052, Australia.*

*Fax: +61 (02) 9385 6141; Tel: +61 (0)2 9385 4675; E-mail: j.stride@unsw.edu.au*

<sup>§</sup> *Analytical Centre, University of New South Wales, Sydney, NSW 2052, Australia.*

<sup>‡</sup> *Bragg Institute, Australian Nuclear Science and Technology Organisation, PMB 1,  
Menai, NSW 2234, Australia.*



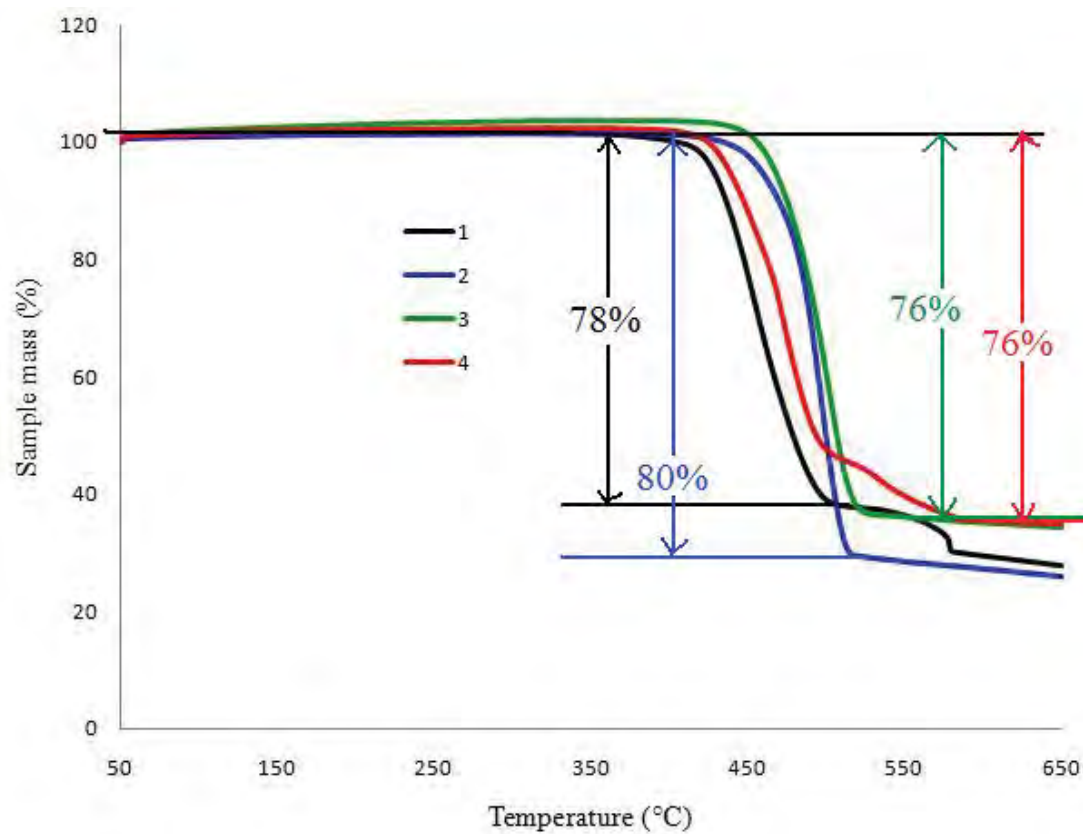


**Figure S1:** Thermogravimetric analysis of **1-4**

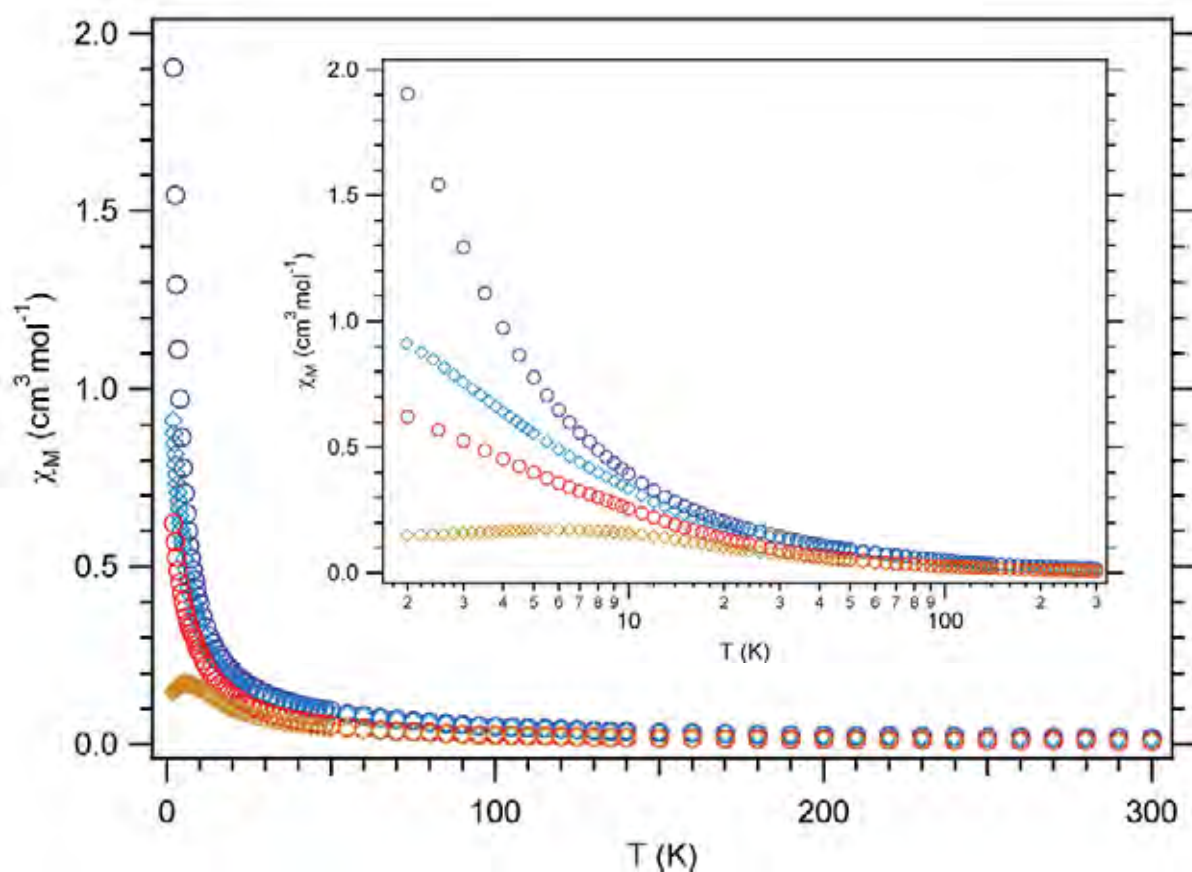


**Figure S2:**  $\chi$  vs.  $T$  per dimer of **1** (red circles), **2** (blue circles), **3** (brown diamonds) and **4** (light blue diamonds) measured at 1000 Oe. *Inset:*  $\chi T$  vs.  $T$  per dimer, shown on a logarithmic temperature scale to emphasize the line shape at low temperatures.

## **Magneto-structural correlations of a three-dimensional Mn based metal–organic framework**

*Muhammad Arif Nadeem, Donald J. Craig, Roland Bircher and John A. Stride*

### **ACKNOWLEDGMENT OF CONTRIBUTION TO AUTHORSHIP**

The article is published in journal “*Dalton Transactions*”. J.A.S. conceived and managed the research project, M.A.N. synthesised the samples and collected all data. D.J.C. solved the crystal structure. R.B. provided consultation on the interpretation of magnetic data and helped in writing manuscript. All authors discussed the results and commented on this manuscript.

# Magneto-structural correlations of a three-dimensional Mn based metal–organic framework†‡

Muhammad Arif Nadeem,<sup>a</sup> Donald J. Craig,<sup>b</sup> Roland Bircher<sup>c</sup> and John A. Stride<sup>\*a,c</sup>

Received 30th October 2009, Accepted 3rd March 2010

First published as an Advance Article on the web 29th March 2010

DOI: 10.1039/b922750d

A 3D metal–organic framework,  $[\text{Na}\{\text{Mn}_3(\text{Hbtc})_2(\text{btc})\}\cdot 5\text{H}_2\text{O}]_n$  (**1**) ( $\text{H}_3\text{btc}$  = 1,3,5-benzene tricarboxylic acid), was synthesized under hydrothermal conditions. The structure of **1** was established by single crystal X-ray diffraction analysis; **1** crystallizes in the monoclinic space group  $P2_1/c$ ,  $a = 9.753(3)$  Å,  $b = 12.751(2)$  Å,  $c = 14.174(4)$  Å,  $\beta = 109.41(1)^\circ$ . The complex **1** is isostructural to previously reported MIL-45 and consists of one dimensional wave like chains of carboxylate bridged hexa-coordinated Mn(II) ions. Variable temperature magnetic susceptibility measurements revealed dominant antiferromagnetic exchange interactions and the intra-chain exchange constants  $J_1 = -2.4$  cm<sup>-1</sup> and  $J_2 = -0.6$  cm<sup>-1</sup> compare well with literature values for similar materials. Inter-chain interactions are expected to be very small in this compound and there is no indication of magnetic ordering phenomena in the temperature range from 300–2 K.

## Introduction

Metal–organic frameworks (MOFs) are crystalline hybrid inorganic–organic solids with structures composed of metal clusters with multidimensional nets or frameworks by organic linkers.<sup>1</sup> The crystal engineering of coordination frameworks has attracted great interest from chemists, not only due to the unusual topologies and interesting properties such as high surface area and porosity, but also to their potential applications in gas adsorption, ion-exchange, and catalysis technologies.<sup>2,3</sup> In particular, carboxylate containing ligands have drawn much attention in recent years owing to the diversity of the binding modes of carboxylate groups to metal atoms (Chart 1).

The studies reported to date suggest that the formation of coordination frameworks is influenced by many factors, including the nature of the ligands, the coordination geometry of the metal ions, the ratio between the metal salt and ligand, and the reaction conditions.<sup>4</sup>

In our effort to prepare new multifunctional MOFs we have focused on the ligand  $\text{H}_3\text{btc}$ . The three carboxylate groups of this ligand can adopt multiple coordination modes, which can affect the topology and magnetic properties of final product.<sup>5,6</sup> 1,3,5-benzene tricarboxylic acid ( $\text{H}_3\text{btc}$ ) has been used successfully by other groups to prepare a broad variety of MOFs with intriguing magnetic and gas adsorption properties.<sup>7</sup> In this paper we describe the synthesis, structural and magnetic properties

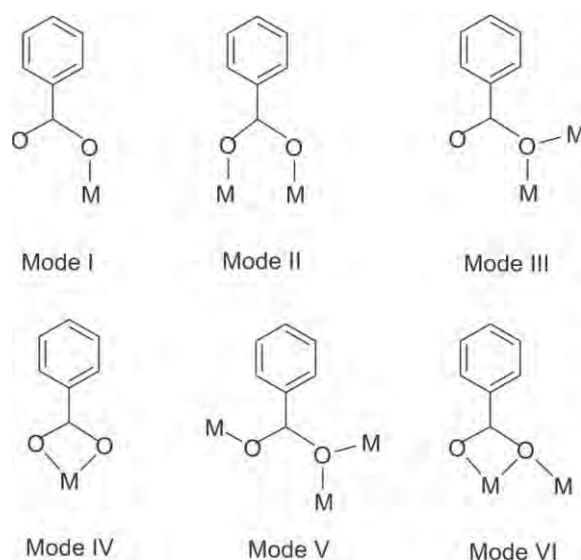


Chart 1 Binding modes of carboxylate ligands.

of the new 3D compound  $[\text{Na}\{\text{Mn}_3(\text{Hbtc})_2(\text{btc})\}\cdot 5\text{H}_2\text{O}]_n$  (**1**). The previously reported MIL-45,  $\text{K}[\text{M}_3(\text{BTC})_3]\cdot 5\text{H}_2\text{O}$  ( $\text{M} = \text{Co}$  and  $\text{Fe}$ ) is isostructural to **1** which showed the ferromagnetic open framework<sup>8</sup> while we aim to study the antiferromagnetic framework of complex **1**.

## Experimental

### Synthesis

A mixture of  $\text{H}_3\text{btc}$  (0.84 g, 4 mmol) and  $\text{NaOH}$  (0.48 g, 12 mmol) in 10 ml distilled water was stirred for 1 h, followed by addition of a solution of  $\text{MnCl}_2\cdot 4\text{H}_2\text{O}$ , (1.26 mmol) in 5 ml  $\text{H}_2\text{O}$ . The resulting solution was stirred for about 1 h at room temperature, then sealed in a 23 ml, teflon-lined, stainless steel autoclave and heated at 220 °C for three days under autogenous pressure. The

<sup>a</sup>School of Chemistry, University of New South Wales, Sydney, NSW 2052, Australia. E-mail: j.stride@unsw.edu.au; Fax: +61 (02) 9385 6141; Tel: +61 (0)2 9385 4675

<sup>b</sup>Analytical Centre, University of New South Wales, Sydney, NSW 2052, Australia

<sup>c</sup>Bragg Institute, Australian Nuclear Science and Technology Organisation, PMB 1, Menai, NSW 2234, Australia

† Dedicated to Dr Donald Craig.

‡ Electronic supplementary information (ESI) available: Fig. S1. CCDC reference number 752721. For ESI and crystallographic data in CIF or other electronic format see DOI: 10.1039/b922750d

**Table 1** Crystallographic data for **1**

Empirical formula	C <sub>27</sub> H <sub>21</sub> Mn <sub>3</sub> NaO <sub>23</sub>
Formula weight	901.3
Temperature/K	294
Wavelength/Å	0.71073
Crystal system	Monoclinic
Space group	<i>P2<sub>1</sub>/c</i>
<i>a</i> /Å	9.753(3)
<i>b</i> /Å	12.751(2)
<i>c</i> /Å	14.174(4)
β/°	109.41(1)
Volume/Å <sup>3</sup>	1662.5(7)
<i>Z</i>	2
ρ/g cm <sup>-3</sup>	1.80
Completeness to ≤ 25°	100.00%
Limiting indices	0 ≤ <i>h</i> ≤ 11 0 ≤ <i>k</i> ≤ 15 -16 ≤ <i>l</i> ≤ 16
Reflections number	3097
<i>R</i> <sub>int</sub>	0.013
<i>F</i> <sub>000</sub>	906.0
<i>S</i>	1.91
<i>R</i> [ <i>F</i> <sup>2</sup> > 2σ( <i>F</i> <sup>2</sup> )]	0.038
<i>wR</i> ( <i>F</i> <sup>2</sup> )	0.059

reaction mixture was then cooled to room temperature over a period of 4 h. Pink crystals of **1** suitable for single crystal X-ray diffraction analysis were collected from the final reaction mixture by filtration and dried in air at ambient temperature (52.8% yield based on manganese), Anal. calcd. C<sub>27</sub>H<sub>21</sub>Mn<sub>3</sub>NaO<sub>23</sub>: C 35.98%, Mn 18.28%. Found, C 37.15%, Mn 19.36%. FT-IR (KBr, cm<sup>-1</sup>): 3409 brs, 2997 w, 1720 s, 1622 s, 1559 s, 1447 s, 1378 s, 1266 m, 1193 s, 1103 s, 1023 w, 938 w, 755 s, 715 s, 525 s, 461 s. The broad band at 3409 cm<sup>-1</sup> is characteristic of the ν<sub>OH</sub> of a protonated carboxylic group of Hbtc.<sup>9</sup> The TGA data of **1** showed an initial weight loss between 85 and 200 °C corresponding to the loss of coordinated water molecules, (exp% = 10, calc% = 9.9). The second weight loss at 350 °C is attributed to the loss of all btc ligands to yield Mn<sub>3</sub>O<sub>4</sub> as residue.

### Crystallographic analysis

A crystal of **1** was mounted on a glass fibre, and data was collected at 294 K on a Bruker kappa APEXII CCD area detector instrument. The diffractometer employs graphite monochromated Mo-Kα (0.7107 Å) radiation. The structure was solved by direct methods and all non-hydrogen atoms were refined by the full-matrix least-squares method. Hydrogen atoms on water molecules are shown in calculated positions. Details of crystal parameters, data collection and refinement are summarized in Table 1. The crystallographic data have been deposited in the CCDC and can be obtained free of charge from The Cambridge Crystallographic Data Centre via [www.ccdc.cam.ac.uk/data\\_request/cif](http://www.ccdc.cam.ac.uk/data_request/cif) quoting: CCDC-752721.‡

### Magnetic measurements

Variable temperature magnetic susceptibility and magnetization measurements were performed with a Quantum Design PPMS EverCool system equipped with a vibrating sample magnetometer and a 9 T magnet. Data was collected on powdered crystals. The magnetic susceptibility measurements were performed for field-cooled and zero-field-cooled samples in magnetic fields of

0.1 T. Pascal's constants were used to estimate the diamagnetic corrections of **1**.<sup>10</sup> Magnetization data were collected in fields of up to 9 T, at three temperatures in the range between 2.0 and 10.0 K. A hysteresis loop measurement was performed at 2.0 K with saturation fields of ±7.0 T.

## Results and discussion

### Description of the structure

Compound **1** crystallizes in the monoclinic space group *P2<sub>1</sub>/c*. Analysis of the single crystal X-ray diffraction data indicates two crystallographically distinct Mn(II) ions. The oxidation state was confirmed by bond valence sum calculations.<sup>11</sup> Both Mn(II) ions have an octahedral coordination environment, Fig. 1.

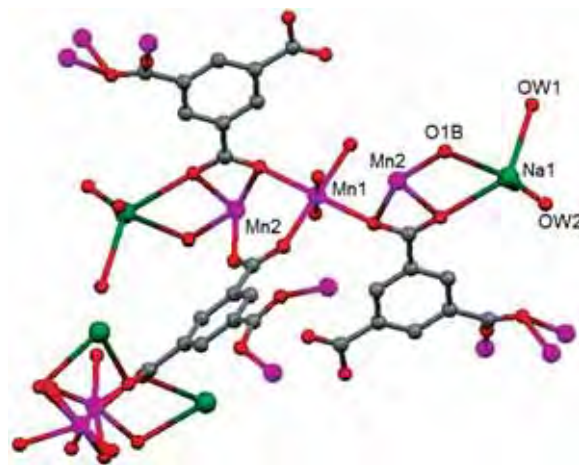


**Fig. 1** Basic structural unit of compound **1** (hydrogen atoms are not shown for clarity).

Mn1 is located on an inversion centre and is coordinated with three pairs of oxygen atoms (Mn–O between 2.078(3) Å and 2.213(2) Å) belonging to four different Hbtc ligands and two different btc ligands. Mn2 is coordinated by 6 oxygen atoms (Mn–O between 2.105(3) Å and 2.410(3) Å) belonging to two different btc ligands and three Hbtc ligands. One of the latter acts in a bidentate chelating mode, whereas a second Hbtc ligand provides an additional loose bond with a Mn–O distance of 2.612(3) Å (Fig. 1 & 2). Selected bond distances and angles are listed in Table 2.

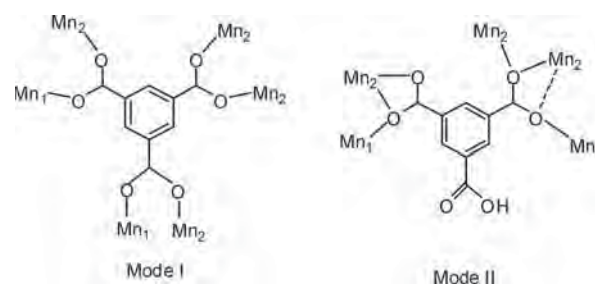


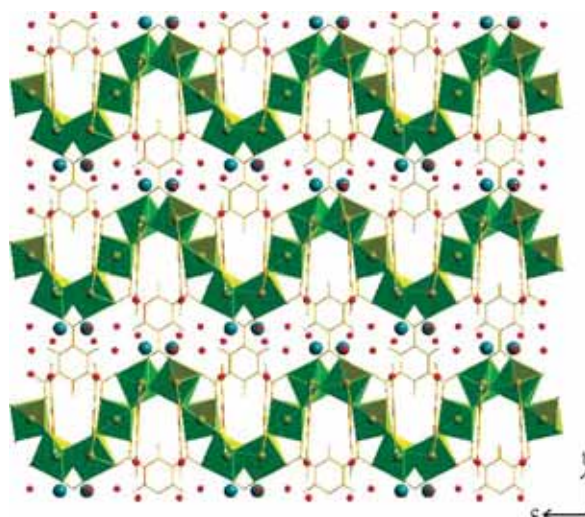
**Fig. 2** Coordination modes of btc (left) and Hbtc (right) in complex.

Two Mn2 and a Mn1 ions are connected to form linear Mn<sub>3</sub> subunits with Mn1–Mn2 distances of 3.48 Å. Each Mn1–Mn2 pair is bridged by two *syn-syn* η<sup>1</sup>:η<sup>1</sup>:μ<sub>2</sub> carboxylate groups of Hbtc and



**Table 2** Selected bond lengths (Å) and bond angles (°) for compound **1**

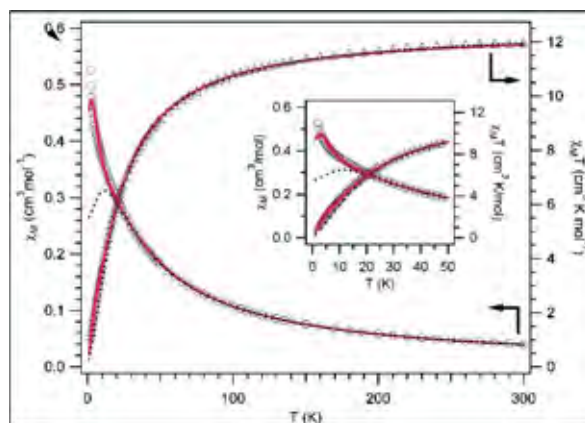
Mn(1)–O(1A)	2.213(2)
Mn(1)–O(1A)	2.156(3)
Mn(1)–O(4A)	2.156(3)
Mn(1)–O(4A)	2.078(3)
Mn(1)–O(4B)	2.213(2)
Mn(2)–O(1A)	2.219(2)
Mn(2)–O(3A)	2.263(3)
Mn(2)–O(3A)	2.272(3)
Mn(2)–O(1B)	2.105(3)
Mn(2)–O(3B)	2.121(3)
O(1A)–Mn(2)	2.219(2)
O(3A)–Mn(2)	2.263(3)
O(3A)–Mn(2)	2.272(3)
O(4A)–Mn(1)	2.156(3)
O(3B)–Mn(2)	2.121(3)
O(1A)–Mn(1)–O(1A)	180.0(2)
O(1A)–Mn(1)–O(4A)	78.7(1)
O(1A)–Mn(1)–O(4A)	101.3(1)
O(1A)–Mn(1)–O(4B)	88.3(1)
O(1A)–Mn(1)–O(4B)	91.7(1)
O(1A)–Mn(1)–O(4A)	78.7(1)
O(1A)–Mn(1)–O(4B)	91.7(1)
O(1A)–Mn(1)–O(4B)	88.3(1)
O(4A)–Mn(1)–O(4A)	180.0(2)
O(4A)–Mn(1)–O(4B)	91.5(1)
O(4A)–Mn(1)–O(4B)	88.5(1)
O(4A)–Mn(1)–O(4B)	88.5(1)
O(4A)–Mn(1)–O(4B)	91.5(1)
O(4B)–Mn(1)–O(4B)	180.0(3)
O(1A)–Mn(2)–O(3A)	90.61(9)
O(1A)–Mn(2)–O(3A)	116.4(1)
O(1A)–Mn(2)–O(1B)	152.3(1)
O(1A)–Mn(2)–O(3B)	95.1(1)
O(3A)–Mn(2)–O(3A)	78.8(1)
O(3A)–Mn(2)–O(1B)	85.9(1)
O(3A)–Mn(2)–O(3B)	170.0(1)
O(3A)–Mn(2)–O(1B)	89.8(1)
O(3A)–Mn(2)–O(3B)	105.8(1)
O(1B)–Mn(2)–O(3B)	85.2(1)
Mn(1)–O(1A)–Mn(2)	103.7(1)
Mn(2)–O(3A)–Mn(2)	97.4(1)

**Fig. 3** View along *a* axis, the adjacent chains are separated by btc ligands to form two dimensional sheet on *bc* plane.

different 2D sheets are 8.08 Å and 8.15 Å, respectively. Moreover, each chain is surrounded by eight neighbouring chains running parallel to the *c*-axis.

### Magnetic properties

Variable temperature magnetic susceptibility data of **1** collected at 0.1 T is plotted in Fig. 4.  $\chi_m T$  decreases gradually from 11.92 cm<sup>3</sup> K mol<sup>−1</sup> at 300 K to 1.05 cm<sup>3</sup> K mol<sup>−1</sup> at 2.0 K; the room temperature value is slightly lower than the spin-only value of 13.13 cm<sup>3</sup> K mol<sup>−1</sup> for three non-interacting Mn(II) centres with *g* = 2.0. This behaviour is consistent with dominant antiferromagnetic (AFM) interactions. The temperature dependent susceptibility obeys the Curie–Weiss law in the temperature range 25–300 K with parameters  $\theta$  = −20.1 K and *C* = 4.27 cm<sup>3</sup> K mol<sup>−1</sup> per Mn(II).<sup>9</sup> This is further support for the predominantly AFM nature of the exchange interactions.

**Fig. 4** Temperature dependent magnetic susceptibility of **1** shown as  $\chi_m$  vs. *T* (circles)  $\chi_m T$  vs. *T* (triangles). The insert shows a close-up of the low-temperature region. Dotted and solid lines correspond to the best fits obtained using eqn (2) and 4, respectively, with the parameters given in the text.

btc ligands and a bridging-chelating  $\eta^1:\eta^2:\mu_2$  carboxylate group of a second Hbtc ligand. This bridging geometry is very common in linear trinuclear Mn<sub>3</sub> clusters and Mn chains.<sup>9,12</sup> One of the bridging Hbtc carboxylate groups is coordinated to a Na ion, whereas the second carboxylate group of the Hbtc ligand joins two Mn<sub>3</sub> subunits *via* a monoatomic carboxylate bridge between neighbouring Mn2 ions. Additional links are provided by a second monoatomic carboxylate bridge from a Hbtc ligand and a *syn-syn*  $\eta^1:\eta^1:\mu_2$  carboxylate bridge from btc. The linked Mn<sub>3</sub> subunits form wave like chains that lie along the crystallographic *c*-axis. Despite the large number of Mn carboxylate compounds in the literature, there are only very few reports of a bridging geometry with two monoatomic and only one *syn-syn* carboxylate, as present between the Mn<sub>3</sub> units in **1**.

The benzene rings of the btc ligands are stacked along the *a*-axis; two carboxylate groups provide bridges between Mn1 and Mn2 in the same chain, whereas the third carboxylate group bridges two Mn2 ions of neighbouring chains, linking them into 2D sheets parallel to the *bc*-plane (Fig. 3). The benzene rings of the Hbtc ligands are stacked in the *c*-direction. The two deprotonated carboxylate groups form a link between two neighbouring chains along *a*, thereby linking the 2D sheets into a three-dimensional structure. The closest Mn–Mn distances within and between

**Table 3** Fit parameters for the linear chain models

Equation	$g$	$J$ (Mn1-Mn2)/cm <sup>-1</sup>	$J$ (Mn2-Mn2)/cm <sup>-1</sup>
(2)	1.96	-1.9	-1.9
(3)	1.97	-1.7	-1.7
(4)	1.95	-2.4	-0.6

The crystal structure of **1** suggests that the intra-chain interactions dominate the magnetic behaviour at elevated temperatures with inter-chain interactions expected to be much weaker due to the nature of the magnetic exchange path. In order to quantify the intra-chain exchange interactions, we have analysed the temperature dependent susceptibility data with various 1D chain models for isotropic Heisenberg chains. The determined parameters for all models correspond to an exchange Hamiltonian of the form

$$\mathbf{H}_{\text{ex}} = \sum -J_{ij} \mathbf{S}_i \mathbf{S}_j \quad (1)$$

The magnetic susceptibility of an infinite chain of classical spins can be described by the analytical expression<sup>9</sup>

$$\chi_m = \frac{Ng^2\mu_B^2 S(S+1)}{3kT} \times \frac{(1+u)}{(1-u)} \quad (2)$$

where  $u = \coth[J S(S+1)/kT] - [kT/(J S(S+1))]$ .

An alternative description of magnetic susceptibility is given by a parametric expression based on numerical results of Weng *et al.*<sup>13</sup> and coefficients determined by Hiller *et al.*<sup>14</sup>

$$\chi_m = \frac{Ng^2\mu_B^2}{kT} \times \frac{(A + Bx^2)}{(1 + Cx + Dx^3)} \quad (3)$$

where  $x = |J|/(2kT)$ ,  $A = 2.9167$ ,  $B = 208.04$ ,  $C = 15.543$  and  $D = 2707.2$ .

The magnetic susceptibility data of **1** was fit using both models. Similar sets of parameters  $J$  and  $g$  were obtained (Table 3), with the first model giving a slightly better agreement to the data. However, both models were found to underestimate the data in the temperature range below 25 K. This deviation can be attributed to the fact that the experimental data does not show the maximum in  $\chi_m$  typical for AFM chains as described by the two models. A further effort with a third model was therefore undertaken to better reproduce the experimental data. The Mn(II) chains in **1** comprise of two crystallographically distinct exchange interactions, forming an infinite exchange pattern  $[J_1 J_1 J_2]_{\infty}$ .  $J_1$  and  $J_2$  define the strength of the exchange interactions Mn1-Mn2 and Mn2-Mn2, respectively. A schematic of the exchange interactions upon the crystal structure for each of the models is shown in Figure S1 (Supporting Information†). The magnetic susceptibility can be described as<sup>15</sup>

$$\chi_m = \frac{Ng^2\mu_B^2}{3kT} \times \frac{3(1-u_1^4 u_2^2) + 4u_1(1-u_1^2 u_2^2) + 2u_2(1-u_1^2)^2(1+u_1)^2 + 2u_1^2(1-u_2^2)}{(1-u_1^2 u_2^2)^2} \quad (4)$$

where  $u_i = \coth[J_i S_i(S_i+1)/kT] - [kT/(J_i S_i(S_i+1))]$

The shape of the  $\chi_m T$  vs.  $T$  curve of **1** clearly indicates that the dominant interactions are AFM in nature. The absence of

a distinct minimum in the measured temperature range, further suggests that the second exchange constant is either only weakly ferromagnetic or is also antiferromagnetic in nature. A least-squares fit of the experimental data to eqn (4) indeed results in the parameter set  $g = 1.95$ ,  $J_1 = -2.4$  cm<sup>-1</sup> and  $J_2 = -0.6$  cm<sup>-1</sup>. This model provides a good fit of  $\chi_m T$  vs.  $T$ , that is significantly better below 25 K than that obtained with the previous models. Nevertheless there are still deviations at the lowest temperatures. The signs and strengths of the exchange interactions obtained with this model all lie in the same order of magnitude as values previously reported for carboxylate bridged Mn(II) chains and trimers.<sup>7b,16,17,18</sup> Only a few examples are available in literature on the exchange interactions between Mn(II) ions with two 1,1- $\mu_2$  and one *syn-syn* 1,3- $\mu_2$  carboxylate bridges.<sup>19</sup>

The determined parameters lead to a resulting spin of  $S = 5/2$  per AFM coupled Mn<sub>3</sub> unit, which in turn is AFM coupled to the neighbouring Mn<sub>3</sub> units, to yield a spin ground state of  $S = 0$ . This is in good agreement with the slow and almost linear increase of the magnetization with increasing applied magnetic field (Fig. 4). At 2 K no magnetic hysteresis can be observed and no difference can be found between the zero-field cooled (ZFC) and field cooled (FC) susceptibility curves measured at 0.1 T. The absence of signs of magnetic order suggests that the inter-chain interactions are much smaller than the intra-chain interactions. The onset of inter-chain interactions is possibly responsible for the deviations observed between the models and the experimental data at the lowest temperatures.

## Conclusion

A 3D coordination polymer  $[\text{Na}\{\text{Mn}_3(\text{Hbtc})_2(\text{btc})\} \cdot 5\text{H}_2\text{O}]_n$  (**1**) has been synthesized under hydrothermal conditions. Infinite zig-zag  $[\text{Mn2-Mn1-Mn2}]_n$  chains are linked by btc to form 2D layers, whereby each Hbtc bridges the 2D sheets to a three-dimensional structure. Compound **1** exhibits dominant antiferromagnetic interactions within the chain, while inter-chain interactions are expected to be very small, supported by the absence of such in the magnetization data. Finally compound **1** is stable up to 350 °C in air.

## Notes and references

- (a) S. L. James, *Chem. Soc. Rev.*, 2003, **32**, 276; (b) J. L. C. Rowsell and O. M. Yaghi, *Microporous Mesoporous Mater.*, 2004, **73**, 3; (c) N. W. Ockwig, O. Delgado-Friedrichs, M. O'Keeffe and O. M. Yaghi, *Acc. Chem. Res.*, 2005, **38**, 176.
- (a) P. J. Hagrman, D. Hagrman and J. Zubieta, *Angew. Chem., Int. Ed.*, 1999, **38**, 2638; (b) R. Kitaura, K. Fujimoto, S.-I. Noro, M. Kondo and S. Kitagawa, *Angew. Chem., Int. Ed.*, 2002, **41**, 133; (c) S.-I. Noro, R. Kitaura, M. Kondo, S. Kitagawa, T. Ishii, H. Matsuzaka and M. Yamashita, *J. Am. Chem. Soc.*, 2002, **124**, 2568.
- (a) S. R. Batten and R. Robson, *Angew. Chem., Int. Ed.*, 1998, **37**, 1460; (b) F. A. A. Paz and J. Klinowski, *Chem. Commun.*, 2003, 1484; (c) Y. Zhang, J. Li, J. Chen, Q. Su, W. Deng, M. Nishiura, T. Imamoto, X. Wu and Q. Wang, *Inorg. Chem.*, 2000, **39**, 2330.
- (a) J. Fan, H.-F. Zhu, T.-a. Okamura, W.-Y. Sun, W.-X. Tang and N. Ueyama, *Chem.-Eur. J.*, 2003, **9**, 4724; (b) J. Fan, W.-Y. Sun, T.-a. Okamura, W.-X. Tang and N. Ueyama, *Inorg. Chem.*, 2003, **42**, 3168; (c) W. Y. Sun, J. Fan, T. a. Okamura, J. Xie, K.-B. Yu and N. Ueyama, *Chem.-Eur. J.*, 2001, **7**, 2557.
- (a) W. Zhang, S. Bruda, C. P. Landee, J. L. Parent and M. M. Turnbull, *Inorg. Chim. Acta*, 2003, **342**, 193; (b) M.-H. Zeng, M.-C. Wu, H. Liang, Y.-L. Zhou, X.-M. Chen and S.-W. Ng, *Inorg. Chem.*, 2007, **46**, 7241.

- 6 (a) E. Colacio, J. M. Dominguez-Vera, M. Ghazi, R. Kivekas, M. Klinga and J. M. Moreno, *Eur. J. Inorg. Chem.*, 1999, 441; (b) P. King, R. Clerac, C. E. Anson, C. Coulon and A. K. Powell, *Inorg. Chem.*, 2003, **42**, 3492; (c) D. Schulz, T. Weyhermüller, K. Wieghardt, C. Butzlaff and A. X. Trautwein, *Inorg. Chim. Acta*, 1996, **246**, 387.
- 7 (a) O. M. Yaghi, G. Li and H. Li, *Nature*, 1995, **378**, 703; (b) S. O. H. Gutschke, M. Molinier, A. K. Powell, R. E. P. Winpenny and P. T. Wood, *Chem. Commun.*, 1996, 823.
- 8 M. R-Cavellec, C. Albinet, C. Livage, N. Guillou, M. Nogues, J. M. Greneche and G. Ferey, *Solid State Sci.*, 2002, **4**, 267.
- 9 R. M. Silverstein and F. X. Webster, *Spectrometric Identification of Organic Compounds*, 6th edition, John Wiley & Sons, 1998.
- 10 O. Kahn, *Molecular Magnetism*. VCH Publishers Inc., New York, 1993.
- 11 N. E. Brese and M. O'Keeffe, *Acta. Cryst.*, 1991, **B47**, 192–197.
- 12 S. G. Baca, I. L. Malaestean, T. D. Keene, H. Adams, M. D. Ward, J. Hauser, A. Neels and S. Decurtins, *Inorg. Chem.*, 2008, **47**, 11108.
- 13 C. H. Weng, *Ph.D. Dissertation*, Carnegie-Mellon University, Pittsburgh, PA, 1968.
- 14 W. Hiller, J. Strähle, A. Datz, M. Hanack, W. E. Hatfield, L. W. Ter Haar and P. Guetlich, *J. Am. Chem. Soc.*, 1984, **106**, 329.
- 15 M. A. M. Abu-Youssef, M. Drillon, A. Escuer, M. A. S. Goher, F. A. Mautner and R. Vicente, *Inorg. Chem.*, 2000, **39**, 5022.
- 16 D. P. Kessissoglou, *Coord. Chem. Rev.*, 1999, **185–186**, 837.
- 17 M. J. Plater, M. R. St J. Foreman, R. A. Howie, J. M. S. Shackle, E. Coronado, C. J. Gomez-Garcia, T. Gelbrich and M. B. Hursthouse, *Inorg. Chim. Acta*, 2001, **319**, 159.
- 18 M. Xue, G. Zhu, Q. Fang, X. Guo and S. Qiu, *J. Mol. Struct.*, 2006, **796**, 165.
- 19 Z. J. Zhong and X.-Z. You, *Polyhedron*, 1994, **13**, 2157.



## SUPPORTING INFORMATION:

### Magneto-structural correlations of a three-dimensional Mn based metal-organic framework

Muhammad Arif Nadeem,<sup>a</sup> Donald J. Craig,<sup>b</sup> Roland Bircher<sup>c</sup> and John A. Stride<sup>\*a,c</sup>

<sup>a</sup> School of Chemistry, University of New South Wales, Sydney, NSW 2052, Australia. Fax: +61 (02) 9385 6141; Tel: +61 (0)2 9385 4675; E-mail: j.stride@unsw.edu.au

<sup>b</sup> Analytical Centre, University of New South Wales, Sydney, NSW 2052, Australia.

<sup>c</sup> Bragg Institute, Australian Nuclear Science and Technology Organisation, PMB 1, Menai, NSW 2234, Australia.

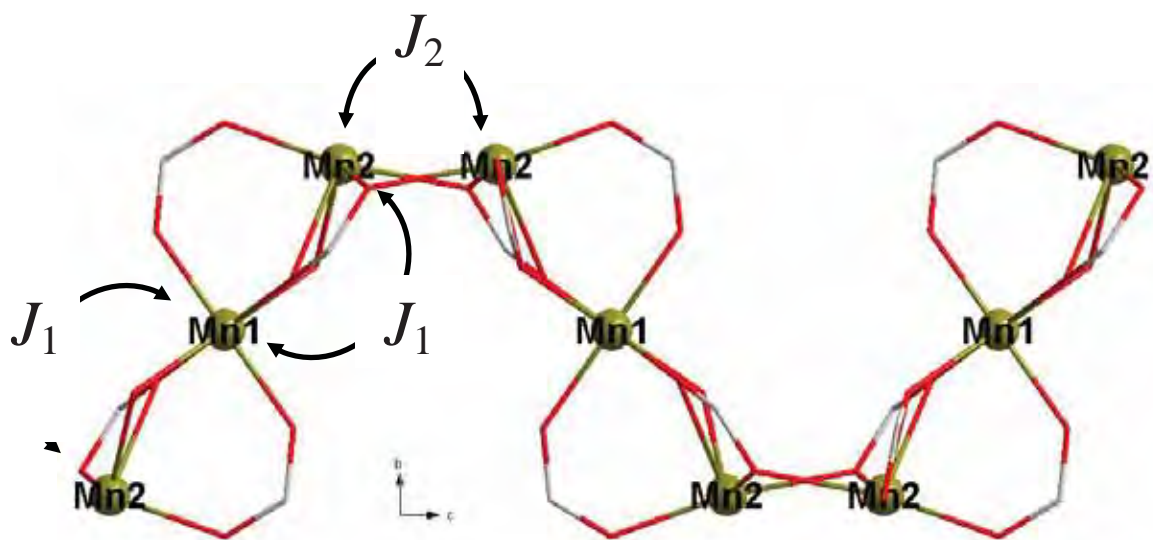


**Figure S1:** Schematic of the exchange interactions in  $[\text{Na}\{\text{Mn}_3(\text{Hbtc})_2(\text{btc})\} \cdot 5\text{H}_2\text{O}]_n$ : Models 1 and 2 use  $J_1 = J_2$ ; Model 3 has  $J_1 \neq J_2$ .

**Four new coordination polymers constructed from  
benzene tricarboxylic acid: synthesis, crystal structure,  
thermal and magnetic properties**

*Muhammad Arif Nadeem, Mohan Bhadbhade and John Arron Stride*

**ACKNOWLEDGMENT OF CONTRIBUTION TO AUTHORSHIP**

The article is published in journal “*Dalton Transactions*”. J.A.S. conceived and managed the research project, M.A.N. synthesised the samples and collected all data. M.A.N. and M.B. solved the crystal structure. All authors discussed the results and commented on this manuscript.

# Four new coordination polymers constructed from benzene tricarboxylic acid: synthesis, crystal structure, thermal and magnetic properties†

Muhammad Arif Nadeem,<sup>a</sup> Mohan Bhadbhade<sup>b</sup> and John Arron Stride<sup>\*a,c</sup>

Received 4th June 2010, Accepted 11th August 2010

DOI: 10.1039/c0dt00600a

The use of 1,3,5-benzene tricarboxylic acid (H<sub>3</sub>btc) as an organic linker has allowed us to achieve the rational design of two pairs of isostructural coordination polymers having molecular formulae [M<sub>2</sub>(btc)(F)]<sub>n</sub> (M(II) = Mn (**1**), Co (**2**)) and [M<sub>3</sub>(btc)(Hbtc)(OH)(H<sub>2</sub>O)<sub>11</sub>]<sub>n</sub> (M(II) = Fe (**3**), Co (**4**)) where btc and Hbtc represent the fully and doubly de-protonated tricarboxylates respectively. These compounds were synthesized using hydrothermal methods and characterized by thermal analysis and variable temperature magnetic measurements. The X-ray analysis reveals that compounds **1** and **2** crystallize in the monoclinic space group *C2/c* while compounds **3** and **4** crystallize in the monoclinic space group *C2*. Compounds **1** and **2** feature fluoride bridged 1D metal chains linked together *via* carboxylate groups of btc, whilst compounds **3** and **4** consist of 1D zigzag chains having strong hydrogen bonds with neighbouring chains. Variable temperature magnetic measurements show an overall antiferromagnetic behaviour for compounds **1**, **2** and **4**, with no indication of magnetic ordering phenomena in the temperature range from 300–2 K. As **3** and **4** are isostructural, we assume that the magnetic properties are similar.

## Introduction

Metal–organic frameworks (MOFs) have been regarded as promising materials with many applications including gas storage, catalysis, microelectronics, sensors and in molecular recognition.<sup>1</sup> The assembly of these materials from inorganic units reticulated with rigid organic linkers is currently a topic of intense research. Carboxylate containing ligands have drawn much attention owing to the wide diversity in binding modes of the carboxylate groups to metal atoms. In particular, 1,3,5-benzene tricarboxylic acid (H<sub>3</sub>btc) is a rigid ligand that has proved versatile in the construction of coordination polymers.<sup>2</sup> H<sub>3</sub>btc offers a huge number of possible structures of coordination polymers with a wide range of properties. There is also current interest in MOFs containing paramagnetic metal ions, driven by potential applications as molecule-based magnetic materials.<sup>3</sup> The carboxyl groups of H<sub>3</sub>btc can not only bridge two or more metal centres to produce polymers with versatile structural motifs, but can also adopt various types of bridging modes, which affect the magnetic properties.<sup>4</sup> Hydrogen bonding can also play a vital role in the construction of a variety of architectures because extended metal carboxylates can form characteristic hydrogen bonds *via* the oxygen atoms of carboxylate ligands, and both coordinated and uncoordinated water molecules. For example,

the coordination polymer [Cu<sub>2</sub>(pzdc)<sub>2</sub>(pyz)]<sub>n</sub> (pzdc = pyrazine-2,3-dicarboxylate, pyz = pyrazine), retains the uncoordinated oxygen atoms at the carboxylate groups of the pzdc-ligand and each uncoordinated oxygen atom interacts with guest molecules *via* hydrogen bonding interactions.<sup>5</sup> Similarly, another coordination polymer constructed from H<sub>3</sub>btc, [Ni<sub>6</sub>(μ-OH)<sub>4</sub>(1,3,5-btc)<sub>4</sub>(H<sub>2</sub>O)<sub>12</sub>]<sub>n</sub>, shows strong intracluster hydrogen bonding interactions of the free oxygens of carboxylate groups in H<sub>3</sub>btc with μ-OH.<sup>6</sup> In the present study, we carried out the hydrothermal synthesis of four coordination polymers [Mn<sub>2</sub>(btc)(F)]<sub>n</sub> **1**, [Co<sub>2</sub>(btc)(F)]<sub>n</sub> **2**, [Fe<sub>3</sub>(btc)(Hbtc)(OH)(H<sub>2</sub>O)<sub>11</sub>]<sub>n</sub> **3**, [Co<sub>3</sub>(btc)(Hbtc)(OH)(H<sub>2</sub>O)<sub>11</sub>]<sub>n</sub> **4**. The polymers **1** and **2** are isostructural and feature a 3D network constructed from fluoride bridged metal chains. Fluoride bridged metal complexes are well known to have interesting magnetic properties, for example Behera *et al.* reported a fluoride ion-bridged cobalt-based complex [Co<sub>3</sub>F<sub>6</sub>(SO<sub>4</sub>)<sub>2</sub>] having a kagome lattice, which showed bulk magnetic ordering at low temperature.<sup>7</sup> To the best of our knowledge, no coordination polymer has been reported constructed from fluoride bridged metal chains. The polymers **3** and **4** are also isostructural and feature 1D chains, which show strong interchain hydrogen bonding between the coordinated water molecules and carboxylate oxygen atoms of the btc, resulting in the complex 3D supra-architecture.

## Experimental

### Materials and physical techniques

All reagents and solvents employed were commercially available and used as received without further purification. The syntheses of **1–4** were carried out in 23 mL Teflon-lined autoclaves under autogenous pressure. Elemental analyses were performed on a Carlo Erba Elemental Analyser EA 1108. The FT-IR spectra were measured with an AVATAR 320 spectrometer as KBr disks.

<sup>a</sup>School of Chemistry, University of New South Wales, Sydney, NSW, 2052, Australia. E-mail: j.stride@unsw.edu.au; Fax: +61 (02) 9385 6141; Tel: +61 (0)2 9385 4675

<sup>b</sup>Analytical Centre, University of New South Wales, Sydney, NSW, 2052, Australia

<sup>c</sup>Bragg Institute, Australian Nuclear Science and Technology Organisation, PMB 1, Menai, NSW, 2234, Australia

† Electronic supplementary information (ESI) available: Fig. S1, Tables S1 and S2. CCDC reference numbers 779475–779478. For ESI and crystallographic data in CIF or other electronic format see DOI: 10.1039/c0dt00600a

Thermal analyses were carried out under nitrogen using a Mettler-Toledo TGA/DSC, with the heating rate of 10 °C min<sup>-1</sup>.

### Magnetometry

Variable temperature magnetic susceptibility and magnetization measurements were performed with a Quantum Design PPMS EverCool system equipped with a vibrating sample magnetometer and a 9 T magnet. Data were collected on powder samples obtained by crushing single crystals in a mortar and pestle. The magnetic susceptibility measurements were performed for field-cooled and zero-field-cooled samples in magnetic fields of 0.1 T. Pascal's constants were used to estimate the diamagnetic corrections.<sup>8</sup> Magnetization data were collected in fields up to 9 T and in the temperature range between 2.0 and 300.0 K. Hysteresis loops were measured at 2.0 K with maximum fields of  $\pm 9.0$  T.

### Synthesis of [Mn<sub>2</sub>(btc)(F)]<sub>n</sub> (1)

1 mmol of 1,3,5-H<sub>3</sub>btc (0.210 g) was stirred in a 6 mL solution of LiOH (4 mmol, 0.095 g) for 15 min, followed by addition of a solution of MnCl<sub>2</sub>·4H<sub>2</sub>O (0.297 g, 1.5 mmol) in 4 mL H<sub>2</sub>O, then 1 mmol (0.0259 g) of LiF was added to a stirring solution. The resulting solution was stirred for about 15 min at room temperature, sealed in a 23-mL Teflon-lined stainless steel autoclave and heated at 220 °C for three days under autogenous pressure. The reaction system was subsequently cooled to room temperature over 4 h. Light pink plate like crystals of **1** suitable for single crystal X-ray diffraction analysis were collected from the final reaction mixture by filtration and dried in air at ambient temperature (17.06% yield based on Mn). *Anal.* calcd.: C, 32.17% H, 0.89% Found: C, 32.70% H, 1.07%. IR data ( $\nu_{\max}$ /cm<sup>-1</sup>): 3450sbr, 1612s, 1587m, 1454s, 1362m, 1302w, 1207w, 767s, 710s, 648w, 612w, 564m, 466m.

### Synthesis of [Co<sub>2</sub>(btc)(F)]<sub>n</sub> (2) and [Co<sub>3</sub>(btc)(Hbtc)(OH)(H<sub>2</sub>O)]<sub>n</sub> (4)

An identical procedure as that for **1** was followed to prepare **2**, except that MnCl<sub>2</sub>·4H<sub>2</sub>O was replaced by CoCl<sub>2</sub>·6H<sub>2</sub>O (0.355 g, 1.5 mmol). A mixture of dark pink (**2**) and light pink (**4**) crystals were obtained. The crystals were separated manually. For **2**, yield: 6.78% based on Co. *Anal.* calcd.: C, 31.42% H, 0.87 Found: C, 32.21% H, 0.99%. IR data ( $\nu_{\max}$ /cm<sup>-1</sup>): 3445sbr, 1612 s, 1558w, 1514 m, 1435 s, 1372 m, 1210w, 1128w, 716 s, 624w, 564 s, 479 m, 444m. For **4**, yield: 21.31% based on Co. *Anal.* calcd.: C, 26.96% H, 3.51%. Found: C, 25.70% H, 3.79%. IR data ( $\nu_{\max}$ /cm<sup>-1</sup>): 3429sbr, 1613s, 1554w, 1430s, 1368s, 750m, 721m.

### Synthesis of [Fe<sub>3</sub>(btc)(Hbtc)(OH)(H<sub>2</sub>O)]<sub>n</sub> (3)

An identical procedure as that for **1** was followed to prepare **3**, except that MnCl<sub>2</sub>·4H<sub>2</sub>O was replaced by anhydrous FeCl<sub>2</sub> (0.189 g, 1.5 mmol). Light yellow crystals were obtained. For **3** yield: 25.25% based on Fe. *Anal.* calcd.: C, 27.29% H, 3.56%. Found: C, 28.45% H, 3.05%. IR data ( $\nu_{\max}$ /cm<sup>-1</sup>): 3450sbr, 1667w, 1615s, 1569w, 1435s, 1349m, 763m, 721s, 553m.

### Crystallographic analyses

Crystallographic data of **1–4** were collected at 150 K on a Bruker kappa APEXII-CCD area detector instrument with Mo-

K $\alpha$  monochromated radiation ( $\lambda = 0.71073$  Å) using the  $\omega$ - $\phi$  scan technique. An empirical absorption correction was applied. The structures were solved by direct methods and refined by full-matrix least squares against  $F^2$  using the SHELXS-97 and SHELXL-97 programs.<sup>9</sup> Anisotropic thermal parameters were assigned to all non-hydrogen atoms. The hydrogen atoms were set in calculated positions and refined as riding atoms with a common fixed isotropic thermal parameter. Analytical expressions of neutral atom scattering factors were employed, and anomalous dispersion corrections were incorporated. The crystallographic data for **1–4** are listed in Table 1 and selected bond lengths and bond angles are listed in tables S1 and S2 of ESI. The crystallographic data have been deposited in the CCDC and can be obtained free of charge from The Cambridge Crystallographic Data Centre via [www.ccdc.cam.ac.uk/data\\_request/cif](http://www.ccdc.cam.ac.uk/data_request/cif) quoting: CCDC numbers 779475–779478.†

## Results and discussion

### Crystal structure

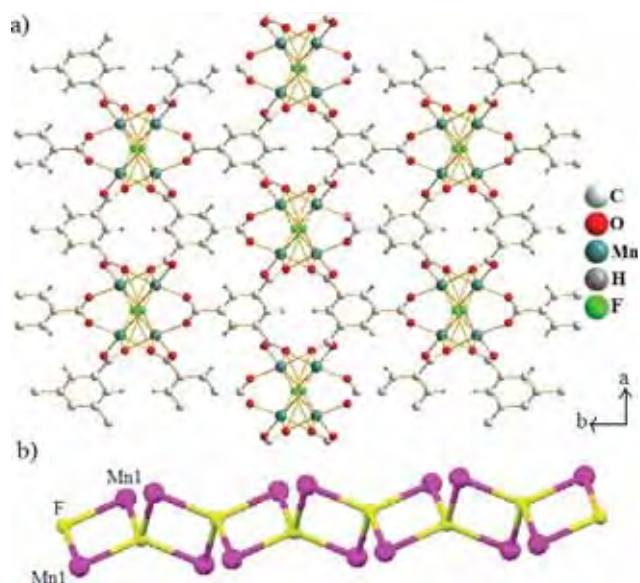
The X-ray structure analysis reveals that **1** and **2** are isostructural, crystallising in a monoclinic system in the  $C2/c$  space group; complex **1** is taken as an example to depict the structure in detail. Analysis of the single crystal X-ray diffraction data identifies only one crystallographically unique Mn(II) ion lying in a distorted octahedral geometry. The equatorial plane is determined by three oxygen atoms of three different btc ligands (Mn–O between 2.0454(15) Å and 2.1932(14) Å) and a fluorine atom (Mn–F 2.1490(7) Å). The two remaining coordination sites are occupied at axial positions by one oxygen atom (O2) of a fourth btc ligand (Mn–O2 2.1519(14) Å) and a fluorine atom (Mn–F 2.3398(10) Å). The characteristic feature of complex **1** is a fluoride bridged 1D chain of Mn(II) atoms, Fig. 1b. The crystallographically unique fluoride ion is in a tetrahedral geometry coordinated with two Mn(II) ions at a distance of 2.1490(7) Å and two Mn(II) ions at a distance of 2.3398(10) Å along the  $b$ -axis. Each Mn(II) ion bridges the two fluoride ions on either side, forming a rectangle; this forms the basic subunit of a 1D Mn(II) chain running along the  $c$ -axis.

Crystallographically there is only one type of btc ligand in the crystal structure, which bridges two Mn(II) ions on either side of the ring, forming a 2D sheet in the  $ac$ -plane. Another carboxylate group also bridges the two Mn(II) ions within the 1D chain in a  $\text{syn-syn } \eta^1:\eta^1:\mu_2$  chelating mode to form a three dimensional network. Each fluoride bridged 1D chain is surrounded by six other neighbouring chains, with Mn–Mn distances ranging from 3.357 to 3.984 Å within the chain, whilst the minimum inter-chain Mn–Mn distance is 7.493 and 8.293 Å along the  $a$  and  $b$ -axes respectively. All of the aromatic rings of btc are  $\pi$ - $\pi$  stacked along the  $c$ -axis with an interfacial distance of 5.212 Å, Fig. 1a. The Co-analogue contains contracted metal–ligand bond distances and a smaller unit cell volume in accord with the smaller size of Co(II) with respect to Mn(II). Compounds **3** and **4** are also isostructural and the same structure has been reported by other authors using different metal ions, metal precursors and conditions of the reaction.<sup>10</sup> Only structure **3** is discussed here: Single crystal X-ray analysis showed that **3** adopts a 1D zig zag chain with a basic structural unit of [Fe<sub>3</sub>(btc)(Hbtc)(OH)(H<sub>2</sub>O)]<sub>n</sub> as an inorganic building unit. **3** consists of two crystallographically

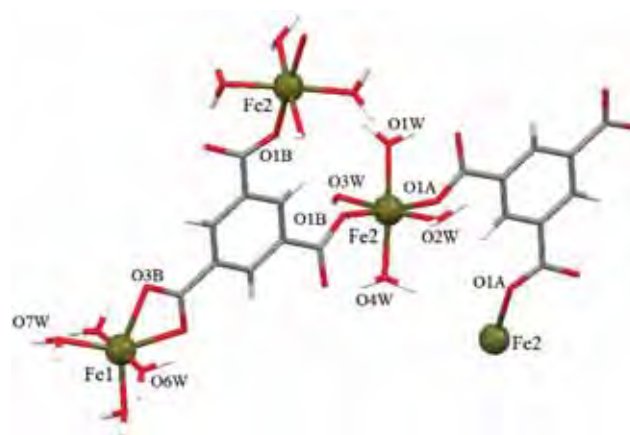


**Table 1** Crystallographic data and structure refinement results for 1–4

	1	2	3	4
Empirical formula	C <sub>9</sub> H <sub>3</sub> FMn <sub>2</sub> O <sub>6</sub>	C <sub>9</sub> H <sub>3</sub> Co <sub>2</sub> FO <sub>6</sub>	C <sub>9</sub> H <sub>12</sub> Fe <sub>1.50</sub> O <sub>12</sub>	C <sub>9</sub> H <sub>14</sub> Co <sub>1.50</sub> O <sub>12</sub>
Formula weight	335.99	343.97	395.96	400.58
Temperature/K	150(2)	150(2)	150(2)	150(2)
Crystal system	Monoclinic	Monoclinic	Monoclinic	Monoclinic
Space group	C2/c	C2/c	C2	C2
<i>a</i> /Å	10.7409(7)	10.7409(6)	17.488(2)	17.4095(19)
<i>b</i> /Å	19.2474(12)	18.8422(12)	12.9304(17)	12.946(1)
<i>c</i> /Å	5.2120(3)	5.0778(3)	6.5221(8)	6.5020(5)
$\alpha$ /°	90	90	90	90
$\beta$ /°	115.581(2)	115.932(2)	111.523(5)	111.889(3)
$\gamma$ /°	90	90	90	90
Volume/Å <sup>3</sup>	971.88(10)	924.18(10)	1372.0(3)	1359.8(2)
<i>Z</i>	4	4	4	4
$\rho$ /Mg m <sup>-3</sup>	2.296	2.472	1.917	2.059
<i>S</i>	0.64	0.68	0.79	0.78
<i>F</i> (000)	656	672	804	854
Limiting indices	$-10 \leq h \leq 12$ $-22 \leq k \leq 22$ $-6 \leq l \leq 5$	$-12 \leq h \leq 12$ $-18 \leq k \leq 22$ $-5 \leq l \leq 6$	$-20 \leq h \leq 20$ $-15 \leq k \leq 15$ $-7 \leq l \leq 6$	$-20 \leq h \leq 18$ $-15 \leq k \leq 14$ $-7 \leq l \leq 7$
Reflections number	3531	3275	4874	4416
<i>R</i> <sub>int</sub>	0.030	0.039	0.058	0.060
$\theta$ <sub>max</sub> /°	25.0	25.0	25.0	25.0
<i>wR</i> ( <i>F</i> <sup>2</sup> )	0.072	0.078	0.119	0.110

**Fig. 1** (a) Packing diagram of 1 along *c*-axis showing the each infinite 1D chain is surrounded by six neighbouring chains. (b) A view of infinite 1D chain constructed from fluoride bridged Mn<sup>II</sup> ions.

independent iron ions (Fe1 and Fe2) and two different btc (btc and Hbtc) ligands (Fig. 2). Each Fe1 is coordinated to four water molecules and two oxygen atoms (O3B) of btc, which give rise to a distorted octahedral coordination environment (the Fe1–O bond length is in the range 2.034–2.203 Å and O–Fe1–O angle is in the range 59.5–106.93°). Each Fe1 is then bridged with two Fe2 ions *via* the remaining two carboxylates of btc, each of which bind with the Fe2 in a monodentate fashion on either side of the ring. Each Fe2 is in an octahedral geometry and coordinated with three water molecules, one hydroxyl ion and two oxygen atoms (O1A and O1B) from two different organic linkers (Hbtc and btc respectively), the Fe2–O bond length is in the range 2.076–

**Fig. 2** Basic structural unit of compound 3.

2.207 Å and the O–Fe1–O angles are in the range of 86.64–92.91°. The two Fe2 ions are separated by two carboxylate groups of the Hbtc linker at a distance of 7.848 Å, to form a 1D zigzag chain in the *ac*-plane. 1D layers assemble into a 3D network *via* complex hydrogen bonding interactions, Fig. 3. Between these 1D layers, the shortest C...C distance is 3.290 Å, indicating that

**Fig. 3** A view of hydrogen bonding network connecting neighbouring 1D chains in 3. Hydrogen atoms are omitted for clarity.

both  $\pi$ - $\pi$  and hydrogen bonding interactions are present. All of the terminal water molecules are involved in hydrogen bonding interactions. Two symmetry related water molecules (O6W and O7W) attached to Fe1 form a strong hydrogen bond with the Hbtc carboxylate groups of neighbouring chains at a distance of 2.787 and 2.841 Å. Likewise, all of the water molecules attached to Fe2 take part in complex hydrogen bonding interactions; for example, O3W (bonded to Fe2) is connected to two neighbouring chains *via* strong hydrogen bonds with two oxygen atoms (O2A and O3B) at a distance of 2.665 and 2.895 Å respectively, resulting in a 3D supra-architecture constructed from the interpenetration of 1D zigzag chains, Fig. 4.

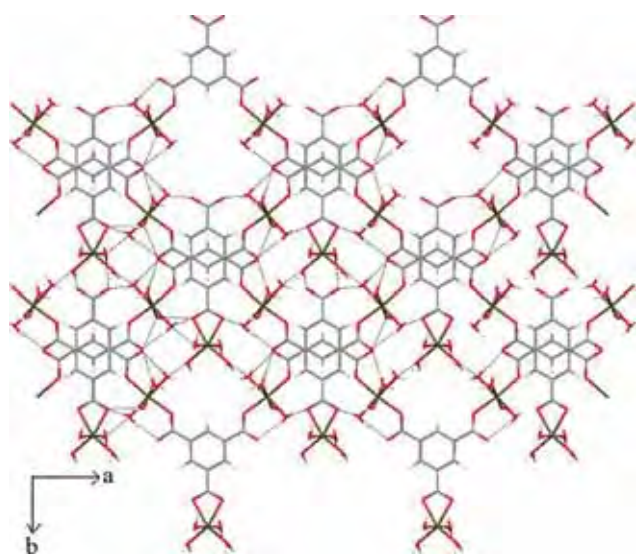


**Fig. 4** (a) A Packing diagram of **3** along *c*-axis showing the 3D supra-architecture build by the overlapping of infinite 1D zigzag chains of  $[\text{Fe}_3(\text{btc})(\text{Hbtc})(\text{OH})(\text{H}_2\text{O})_{11}]$  *via* strong hydrogen bonding.

### Thermogravimetric analysis

Thermogravimetric analyses (TGA) were performed on samples **1–4** to explore their thermal stabilities, Fig. 5. Complex **1** shows a plateau region ranging from 50–450 °C suggesting that there are no solvent molecules in the crystalline lattice, followed by a decrease in weight suggesting the decomposition of the complex to the

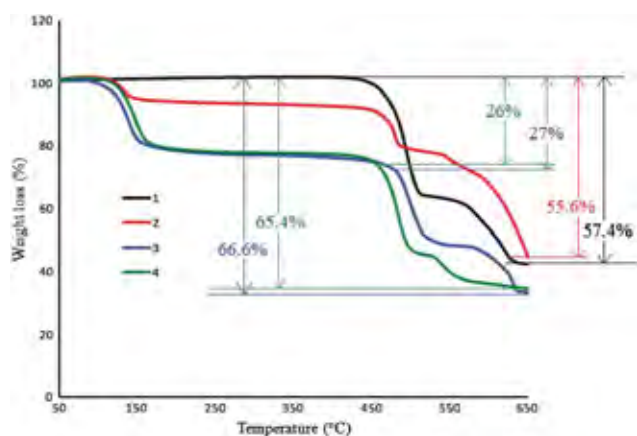


**Fig. 5** Thermogravimetric analysis of **1–4**.

respective oxide with a weight loss of 57.4% (calc. 53%). Complex **2** showed almost the same pattern as **1** except that an initial weight loss around 150 °C is due to impurities of compound **4** in the sample used. The weight loss above 450 °C to the oxide of 55.6% compares to a calc. value of 56.4%. Both complexes **3** & **4** show similar TGA curves to each other and undergo dehydration at around 100–150 °C, with respective weight losses of 27% and 26% which corresponds to the loss of all of the water molecules. The effect of dehydration is the collapse of the structure, as evidenced in the powder XRD of **3** & **4** before and after dehydration, shown in Fig. 6.

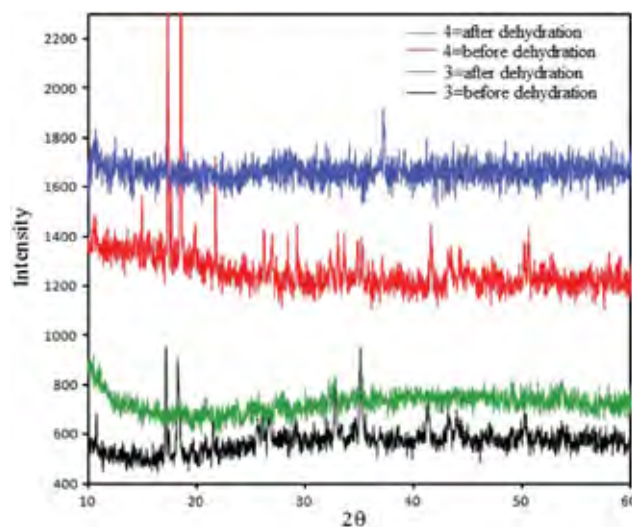


**Fig. 6** Powder XRD of hydrated and dehydrated samples of **3–4**.

When hydrated the powder XRD for **3** & **4** contain distinct peaks that disappear upon dehydration. The loss of crystallinity in the dehydrated **3** & **4** is a reflection of the role that water molecules play in the crystalline structure; the loss of water around 150 °C also leads to a distinct colour change in both **3** & **4**, with **4** going from pink in the fully hydrated as-crystallized form, to blue in the dehydrated form. This colour change is due to the change in the coordination sphere about the metal ions, in the case of cobalt shifting from an octahedral environment absorbing in the blue region of the spectrum to a tetrahedral geometry absorbing in the red.<sup>10a,b</sup> This is consistent with the reduced number of ligands available in the dehydrated amorphous metal–organic material. The anhydrous amorphous solid finally undergoes a sudden weight loss above 450 °C, indicative of the decomposition of the organic components of **3** & **4** into the respective metal oxides, with total weight losses of 66.6% and 65.4% (calc. 72.8% & 71.9%), respectively.

### Magnetic properties

The magnetic susceptibilities of **1**, **2** and **4** were measured in the temperature range of 2–300 K with an applied magnetic field of 0.1 T. The magnetic susceptibility data of **1** is shown in Fig. 7. At room temperature the  $\chi_M T$  value of 7.604 cm<sup>3</sup> K mol<sup>-1</sup> is comparable with the expected spin only value of 8.75 cm<sup>3</sup> K mol<sup>-1</sup> ( $S = 5/2$ ,  $g = 2.0$ ). Upon cooling from room temperature, the  $\chi_M T$  exhibits a continuous decrease until a minimum of 0.193 cm<sup>3</sup> K mol<sup>-1</sup> is reached at 2 K. This behaviour is indicative

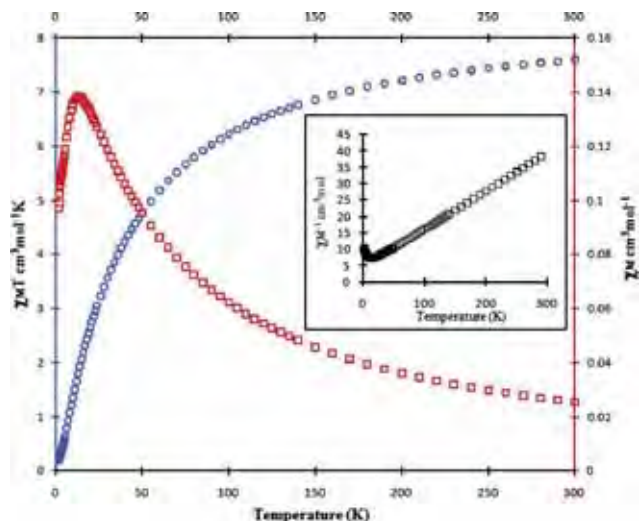


Fig. 7 Graph of field cooled magnetic susceptibility data of **1** at 0.1 T. Inset shows the plot of  $\chi_M^{-1}$  vs.  $T$  (K).

of antiferromagnetic coupling between the Mn(II) centres, further confirmed by fitting the  $\chi_M^{-1}$  vs.  $T$  plot to the Curie–Weiss Law ( $\chi_M = C/(T - \theta)$ ), resulting in  $\theta = -46.635$  K and  $C = 7.107$  cm<sup>3</sup> K mol<sup>-1</sup>.

According to the structural data, it is expected that the polymer **1** exhibits strong Mn(II)–Mn(II) magnetic exchange interactions *via* bridging fluoride ions within the 1D chain, as indicated by the high negative value of  $\theta = -46.635$  K. In addition, no 3D antiferromagnetic ordering was observed in this temperature range because the 1D fluoride bridged Mn(II) chains are interconnected by large btc bridges and are thus magnetically isolated, prohibiting the onset of long range magnetic ordering.<sup>11</sup> The magnetic properties of compound **2** in the form of  $\chi_M$  and  $\chi_M T$  vs.  $T$  are represented in Fig. 8. The room temperature value of  $\chi_M T$  (5.331 cm<sup>3</sup> K mol<sup>-1</sup>) is higher than the spin only value (4.125 cm<sup>3</sup> K mol<sup>-1</sup> considering  $g = 2.2$ ) for two Co(II) ions, due to the orbital contribution from octahedral Co(II) ions and/or minor impurities in the sample.<sup>12</sup> It

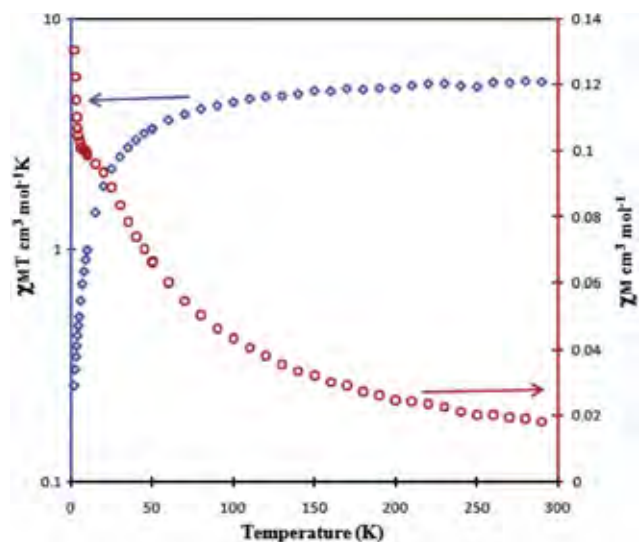


Fig. 8 Graph of field cooled magnetic susceptibility data of **2** at 0.1 T.

slowly decreases until 50 K and then rapidly upon further cooling, reaching a minimum value of 0.259 cm<sup>3</sup> K mol<sup>-1</sup> at 2 K. The fit of  $\chi_M^{-1}$  vs.  $T$  in the temperature range of 25–300 K gives a Weiss constant  $\theta = -49.179$  K and a Curie constant  $C = 6.261$  cm<sup>3</sup> K mol<sup>-1</sup>. The magnetic behaviour is interpreted as dominated by strong antiferromagnetic coupling interactions between the Co(II) ions within 1D fluoride bridged chain, as indicated by the high negative value of Weiss constant. Since, a bifurcation in the ZFC-FC curves or a rapid increase of  $\chi_M T$  value in  $\chi_M T$  vs.  $T$  plot were not observed, **2** showed neither bulk magnetic ordering or spin canting, again interpreted as being due to the long distance between the 1D chains. It must be noted however that an anomalous increase in the  $\chi_M$  value of **2** was observed, Fig. 8, which is believed to be due to a small quantity of the largely paramagnetic compound **4** as an impurity in the sample; this is easily rationalised as both of these compounds co-crystallised out of the same reaction mixture. The field dependent magnetization data of **1** and **2** shows that saturation magnetization is not reached even at the applied magnetic field of 9 and 7 T for **1** and **2** respectively (Figure S1†). Although MOFs with fluoride bridged metal ions have not been reported to date, literature reports suggest that magnetic interactions *via* fluoride ion bridges in simple inorganic complexes are relatively strong, for example, the complex [Co<sub>3</sub>F<sub>6</sub>(SO<sub>4</sub>)<sub>2</sub>] showed strong antiferromagnetic coupling between the cobalt ions with a Weiss constant value of  $\theta = -35.5$  K.<sup>7</sup>

The magnetic properties of compound **4** are represented in Fig. 9; the  $\chi_M$  curve increases when the compound is cooled until a maximum is reached at 2.307 at 2 K. The  $\chi_M T$  value of 9.405 cm<sup>3</sup> K mol<sup>-1</sup> (calculated per 3 Co<sup>II</sup> ions) at room temperature is also significantly higher than spin only value of 6.187 cm<sup>3</sup> K mol<sup>-1</sup> ( $g = 2.2$ ) due to spin orbit coupling. By plotting  $\chi_M^{-1}$  vs.  $T$  in the temperature range of 50–300 K, we obtained a Weiss constant value of  $\theta = -24.98$  K and a Curie constant of  $C = 9.38$  cm<sup>3</sup> K mol<sup>-1</sup>. This behaviour suggests moderate antiferromagnetic coupling interactions between the Co(II) ions widely separated from each other by organic linkers within the 1D zigzag chain, resulting in a largely paramagnetic material. The field dependent magnetization at 2 K suggests that saturation magnetization is

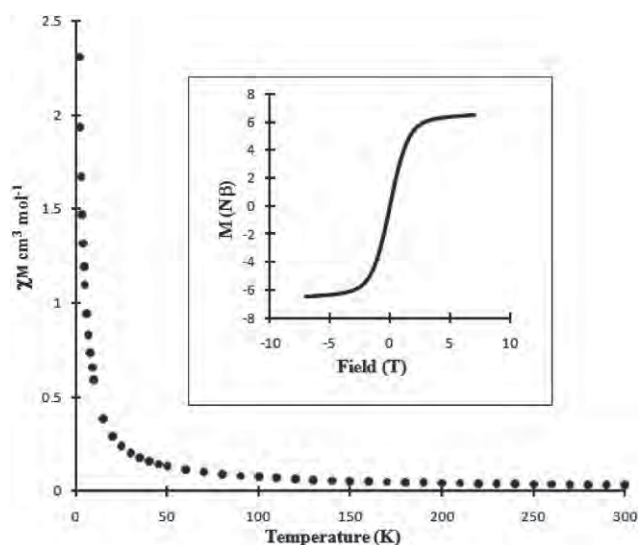


Fig. 9 The curve of  $\chi_M$  vs.  $T$  of **4** at 0.1 T (1 kOe) field. Inset showing the field dependent magnetization curve.



almost reached at the applied magnetic field of 7 T, Fig. 9 inset. The weak magnetic coupling interactions are consistent with the large distances between the metal centres. The minimum inter-chain and intra-chain Co(II)⋯Co(II) distances are 5.682 Å and 7.816 Å respectively. The magnetic data of **3** has not been collected because the structural data shows that the Fe(II) ions are far apart which can only give rise to weak magnetic interactions as in **4**.

## Conclusion

Two pairs of isostructural coordination polymers were hydrothermally synthesized. Compounds **1** and **2** are characterized by unique fluoride bridged 1D chains, whilst **3** and **4** are constructed via a complex hydrogen bonding network. Thermal analyses shows that the compounds **1** & **2** are thermally stable up to around 450 °C, whilst compounds **3** & **4** lost crystallinity upon dehydration at 150 °C. Magnetic data indicates that there are strong antiferromagnetic coupling interactions among metal atoms within the 1D fluoride chains in both compounds **1** and **2**, whilst only moderate antiferromagnetic interactions among Co<sup>II</sup> ions in compound **4**. The results show that fluoride bridged chains among coordination polymers can lead to interesting magnetic properties and that the incorporation of fluoride bridged chains of metals into 3D MOFs provides another route to controlled magnetic interactions as the inter-chain distance may be varied with the use of a range of organic linkers. This work also highlights the importance of the hydrothermal approach to the synthesis of complex supramolecular structures incorporating hydrogen bonding interactions.

## Acknowledgements

This work was supported by the Australian Research Council Discovery Project grant DP0880199. The authors acknowledge the Rene Macquart at the University of Sydney for his assistance with collecting magnetic data.

## Notes and references

- (a) R. Evans and W. B. Lin, *Acc. Chem. Res.*, 2002, **35**, 511; (b) B. Kesanli and W. B. Lin, *Coord. Chem. Rev.*, 2003, **246**, 305; (c) M. Yaghi, M. O'Keeffe, N. W. Ockwig, H. K. Chae, M. Eddaoudi and J. Kim, *Nature*, 2003, **423**, 705; (d) S. L. James, *Chem. Soc. Rev.*, 2003, **32**, 276; (e) S. Kitagawa, R. Kitaura and S. Noro, *Angew. Chem. Int. Ed.*, 2004, **116**, 2388; S. Kitagawa, R. Kitaura and S. Noro, *Angew. Chem. Int. Ed.*, 2004, **43**, 2334; (f) C. N. R. Rao, S. Natarajan and R. Vaidyanathan, *Angew. Chem. Int. Ed.*, 2004, **116**, 1490; C. N. R. Rao, S. Natarajan and R. Vaidyanathan, *Angew. Chem. Int. Ed.*, 2004, **43**, 1466; (g) J. L. C. Rowsell and O. M. Yaghi, *Microporous Mesoporous Mater.*, 2004, **73**, 3; (h) G. Férey, C. Mellot-Draznieks, C. Serre and F. Millange, *Acc. Chem. Res.*, 2005, **38**, 217; (i) D. Bradshaw, J. B. Claridge, E. J. Cussen, T. J. Prior and M. J. Rosseinsky, *Acc. Chem. Res.*, 2005, **38**, 273; (j) Y. Robin and K. M. Fromm, *Coord. Chem. Rev.*, 2006, **250**, 2127; (k) L. Arai, M. A. Nadeem, M. Bhadbhade and J. A. Stride, *Dalton Trans.*, 2010, **39**, 3372.
- (a) O. M. Yaghi, C. E. Davis, G. Li and H. Li, *J. Am. Chem. Soc.*, 1997, **119**, 2861; (b) S. S. Y. Chui, S. M. F. Lo, J. P. H. Charmant, A. G. Orpen and I. D. Williams, *Science*, 1999, **283**, 1148; (c) C. J. Kepert, T. J. Prior and M. J. Rosseinsky, *J. Am. Chem. Soc.*, 2000, **122**, 5158; (d) G. Férey, C. Serre, C. Mellot-Draznieks, F. Millange, S. Surble, J. Dutour and I. Margiolaki, *Angew. Chem.*, 2004, **116**, 6456; G. Férey, C. Serre, C. Mellot-Draznieks, F. Millange, S. Surble, J. Dutour and I. Margiolaki, *Angew. Chem.*, 2004, **43**, 6296; (e) D. Bradshaw, T. J. Prior, E. J. Cussen, J. B. Claridge and M. J. Rosseinsky, *J. Am. Chem. Soc.*, 2004, **126**, 6106; (f) Z. Q. Wang, V. C. Kravtsov and M. J. Zaworotko, *Angew. Chem. Int. Ed.*, 2005, **117**, 2937; V. C. Kravtsov and M. J. Zaworotko, *Angew. Chem. Int. Ed.*, 2005, **44**, 2877; (g) M. A. Nadeem, M. Bhadbhade, R. Bircher and J. A. Stride, *CrystEngComm*, 2010, **12**, 1391.
- (a) J. S. Miller and M. Drillon (ed.), *Magnetism: Molecules to Materials*, vol. 3, Wiley-VCH, Weinheim, 2002; (b) S. Konar, P. S. Mukherjee, E. Zangrando, F. Lloret and R. N. Chaudhuri, *Angew. Chem., Int. Ed.*, 2002, **41**, 1561; (c) E. W. Lee, Y. Kim and D.-Y. Jung, *Inorg. Chem.*, 2002, **41**, 501; (d) N. Guillou, S. Pastre, C. Livage and G. Férey, *Chem. Commun.*, 2002, 2358; (e) E. Coronado, J. R. Galan-Mascaros, C. J. Gomez-Garcia and V. Laikhin, *Nature*, 2000, **408**, 447.
- (a) E. Colacio, J. M. Domínguez-Vera, M. Ghazi, R. Kivekäs, M. Klinga and J. M. Moreno, *Eur. J. Inorg. Chem.*, 1999, 441; (b) P. King, R. Clerac, C. E. Anson, C. Coulon and A. K. Powell, *Inorg. Chem.*, 2003, **42**, 3492; (c) D. Schulz, T. Weyhermüller, K. Wieghardt, C. Butzlaff and A. X. Trautwein, *Inorg. Chim. Acta*, 1996, **246**, 387; (d) M. A. Nadeem, D. J. Craig, R. Bircher and J. A. Stride, *Dalton Trans.*, 2010, **39**, 4358.
- (a) R. Matsuda, R. Kitaura, S. Kitagawa, Y. Kubota, R. V. Belosludov, T. C. Kobayashi, H. Sakamoto, T. Chiba, M. Takata, Y. Kawazoe and Y. Mita, *Nature*, 2005, **436**, 238.
- N. Shin-ichiro, A. Tomoyuki and N. Takayoshi, *Cryst. Growth Des.*, 2007, **7**, 1205.
- J. N. Behera, G. Paul, A. Choudhury and C. N. R. Rao, *Chem. Commun.*, 2004, 456.
- O. Kahn, *Molecular Magnetism*; VCH: Weinheim, Germany, 1993.
- G. M. Sheldrick, SHELXS 97, *Program for the Solution of Crystal Structures*; University of Göttingen: Germany, 1997.
- (a) O. M. Yaghi, H. Li and T. L. Groy, *J. Am. Chem. Soc.*, 1996, **118**, 9096; (b) D. Cheng, M. A. Khan and R. P. Houser, *Cryst. Growth Des.*, 2004, **4**, 599; (c) A. Majumder, S. Shit, C. R. Choudhury, S. R. Batten, G. Pilet, D. Luneau, N. Daro, J.-P. Sutter, N. Chattopadhyay and S. Mitra, *Inorg. Chim. Acta*, 2005, **358**, 3855; (d) M. Riou-Cavellec, C. Albinet, J.-M. Grenèche and G. Férey, *J. Mater. Chem.*, 2001, **11**, 3166; (e) S. Liang, H. Wang, Z. Wang and J.-Y. Han, *Acta Crystallogr., Sect. E: Struct. Rep. Online*, 2006, **62**, m3014.
- D. Cave, J. M. Gascon, A. D. Bond, S. J. Teat and P. T. Wood, *Chem. Commun.*, 2002, 1050.
- (a) Y.-Z. Zheng, M.-L. Tong, W.-X. Zhang and X.-M. Chen, *Chem. Commun.*, 2006, 165; (b) Y.-Z. Zheng, M.-L. Tong, W.-X. Zhang and X.-M. Chen, *Angew. Chem., Int. Ed.*, 2006, **45**, 6310; (c) Y.-Z. Zheng, M.-L. Tong and X.-M. Chen, *J. Mol. Struct.*, 2006, **796**, 9; (d) M.-H. Zeng, W.-X. Zhang, X.-Z. Sun and X.-M. Chen, *Angew. Chem., Int. Ed.*, 2005, **44**, 3079; (e) X.-N. Chen, Y.-Z. Zheng, W.-X. Zhang and X.-M. Chen, *Chem. Commun.*, 2006, 3603.

## Supporting information:

### Four new coordination polymers constructed from benzene tricarboxylic acid: synthesis, crystal structure, thermal and magnetic properties

Muhammad Arif Nadeem,<sup>a</sup> Mohan Bhadbhade,<sup>b</sup> and John Arron Stride\*<sup>a,c</sup>

<sup>a</sup> School of Chemistry, University of New South Wales, Sydney, NSW 2052, Australia. Fax: +61 (02) 9385 6141; Tel: +61 (0)2 9385 4672; E-mail: j.stride@unsw.edu.au

<sup>b</sup> Analytical Centre, University of New South Wales, Sydney, NSW 2052, Australia.

<sup>c</sup> Bragg Institute, Australian Nuclear Science and Technology Organisation, PMB 1, Menai, NSW 2234, Australia.

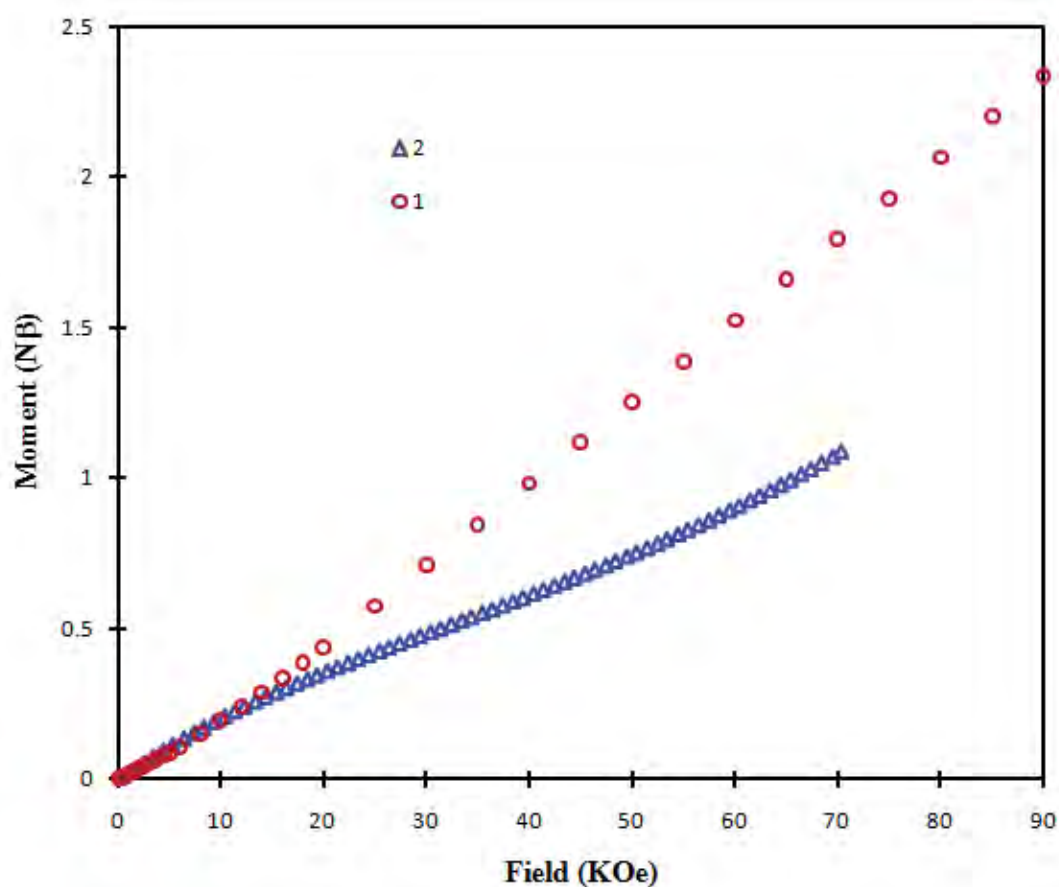


**Figure S1:** A graph of field dependent magnetization of **1** and **2**

**Table S1:** Selected bond lengths (Å) and bond angles (°) of **1** and **2**

Compound <b>1</b> <sup>a</sup>			
Mn1-F1	2.1490(7)	O1 <sup>i</sup> -Mn1-O3	94.43 (6)
Mn1-O2 <sup>ii</sup>	2.1519(14)	F1-Mn1-O3	143.53 (5)
Mn1-O3 <sup>iii</sup>	2.1597(14)	O2 <sup>ii</sup> -Mn1-O3	114.36 (5)
Mn1-O3	2.1932(14)	O3 <sup>iii</sup> -Mn1-O3	88.31 (5)
Mn1-F1 <sup>iv</sup>	2.3398 (10)	O1 <sup>i</sup> -Mn1-F1 <sup>iv</sup>	99.74 (6)
F1-Mn1 <sup>ix</sup>	2.1490 (7)	F1-Mn1-F1 <sup>iv</sup>	72.356 (15)
F1-Mn1 <sup>iii</sup>	2.3398 (10)	O2 <sup>ii</sup> -Mn1-F1 <sup>iv</sup>	170.21 (5)
F1-Mn1 <sup>iv</sup>	2.3398 (10)	O3 <sup>iii</sup> -Mn1-F1 <sup>iv</sup>	87.71 (5)
O1-Mn1 <sup>v</sup>	2.0454 (15)	O3-Mn1-F1 <sup>iv</sup>	73.45 (4)
O2-Mn1 <sup>vi</sup>	2.1519 (14)	Mn1 <sup>vii</sup> -O3-Mn1	152.12(7)
O3-Mn1 <sup>vii</sup>	2.1597 (14)	Mn1 <sup>ix</sup> -F1-Mn1	135.92 (8)
O1 <sup>i</sup> -Mn1-F1	103.44 (6)	Mn1 <sup>ix</sup> -F1-Mn1 <sup>iii</sup>	107.644 (15)
O1 <sup>i</sup> -Mn1-O2 <sup>ii</sup>	85.85 (6)	Mn1-F1-Mn1 <sup>iii</sup>	96.721 (16)
F1-Mn1-O2 <sup>ii</sup>	98.61 (4)	Mn1 <sup>ix</sup> -F1-Mn1 <sup>iv</sup>	96.721 (16)
O1 <sup>i</sup> -Mn1-O3 <sup>iii</sup>	172.52 (6)	Mn1-F1-Mn1 <sup>iv</sup>	107.64 (15)
F1-Mn1-O3 <sup>iii</sup>	78.06 (5)	Mn1 <sup>iii</sup> -F1-Mn1 <sup>iv</sup>	111.91 (7)
O2 <sup>ii</sup> -Mn1-O3 <sup>iii</sup>	86.68 (6)		
Compound <b>2</b> <sup>b</sup>			
Co1-O1 <sup>i</sup>	1.9631 (18)	O3-Co1-O3 <sup>iii</sup>	90.27 (6)
Co1-O3	2.0599 (17)	O2 <sup>ii</sup> -Co1-O3 <sup>iii</sup>	110.97 (7)
Co1-O2 <sup>ii</sup>	2.0799 (18)	F1-Co1-O3 <sup>iii</sup>	147.06 (6)
Co1-F1	2.1021(7)	O1 <sup>i</sup> -Co1-F1 <sup>iv</sup>	100.12 (7)
Co1-O3 <sup>iii</sup>	2.1082 (17)	O3-Co1-F1 <sup>iv</sup>	89.88 (6)
Co1-F1 <sup>iv</sup>	2.2171 (11)	O2 <sup>ii</sup> -Co1-F1 <sup>iv</sup>	172.16 (5)
O1-Co1 <sup>iv</sup>	1.9631 (18)	F1-Co1-F1 <sup>iv</sup>	73.484 (18)
O2-Co1 <sup>iii</sup>	2.0799 (18)	O3 <sup>iii</sup> -Co1-F1 <sup>iv</sup>	75.46 (5)
O3-Co1 <sup>ii</sup>	2.1082 (17)	Co1-O3-Co1 <sup>ii</sup>	152.12(7)
F1-Co1 <sup>vii</sup>	2.2171 (11)	Co1 <sup>vii</sup> -F1-Co1	139.64 (10)
F1-Co1 <sup>iv</sup>	2.2171 (11)	Co1 <sup>vii</sup> -F1-Co1 <sup>iv</sup>	95.361 (19)
O1 <sup>i</sup> -Co1-O3	169.19 (7)	Co1-F1-Co1 <sup>iv</sup>	106.516 (19)
O1 <sup>i</sup> -Co1-O2 <sup>ii</sup>	83.90 (7)	Co1 <sup>vii</sup> -F1-Co1 <sup>ii</sup>	106.516 (19)
O3-Co1-O2 <sup>ii</sup>	85.69 (7)	Co1-F1-Co1 <sup>ii</sup>	95.361(19)
O1 <sup>i</sup> -Co1-O3 <sup>iii</sup>	96.18 (7)	Co1 <sup>iv</sup> -F1-Co1 <sup>ii</sup>	113.62 (9)

<sup>a</sup> (i)  $x-1/2, -y+1/2, z-1/2$ ; (ii)  $x, y, z+1$ ; (iii)  $x, -y+1, z+1/2$ ; (iv)  $-x+1, -y+1, -z$ ; (v)  $x+1/2, -y+1/2, z+1/2$ ; (vi)  $x, y, z-1$ ; (vii)  $x, -y+1, z-1/2$ ; (viii)  $-x+2, y, -z+1/2$ ; (ix)  $-x+1, y, -z+1/2$ . <sup>b</sup> (i)  $x-1/2, y+1/2, z-1$ ; (ii)  $x, -y+2, z+1/2$ ; (iii)  $x, -y+2, z-1/2$ ; (iv)  $-x, -y+2, -z$ ; (v)  $-x+1, y, -z+3/2$ ; (vi)  $x+1/2, y-1/2, z+1$ ; (vii)  $-x, y, -z+1/2$ .

**Table S2.** Selected bond lengths (Å) and bond angles (°) of **3** and **4**

Compound <b>3</b> <sup>c</sup>			
Co1-O6W <sup>i</sup>	2.007 (4)	O6W-Co1-O5	92.39(17)
Co1-O6W	2.007 (4)	O5 <sup>i</sup> -Co1-O5	176.5 (2)
Co1-O5 <sup>i</sup>	2.123 (4)	O6W <sup>i</sup> -Co1-O3B <sup>i</sup>	98.31(18)
Co1-O5	2.123 (4)	O6W-Co1-O3B <sup>i</sup>	156.50 (17)
Co1-O3B	2.148 (4)	O5 <sup>i</sup> -Co1-O3B <sup>i</sup>	85.78 (15)
Co1-O3B <sup>i</sup>	2.148 (4)	O5-Co1-O3B <sup>i</sup>	97.27 (15)
Co1-C8B	2.510 (7)	O6W <sup>i</sup> -Co1-O3B	156.50 (17)
Co2-O1W	2.123 (4)	O6W-Co1-O3B	98.31 (18)
Co2-O2W	2.131 (4)	O5 <sup>i</sup> -Co1-O3B	97.27 (15)
Co2-O3W	2.087 (4)	O5-Co1-O3B	85.78 (15)
Co2-O4W	2.106 (4)	O3B-Co1-O3B <sup>i</sup>	61.3 (2)
O6W <sup>i</sup> -Co1-O6W	103.8 (3)	O1A-Co2-O1B	174.62 (16)
O6W <sup>i</sup> -Co1-O5 <sup>i</sup>	92.39 (17)	O1A-Co2-O3W	90.07 (14)
O6W-Co1-O5 <sup>i</sup>	85.43 (16)	O1B-Co2-O3W	87.14 (15)
O6W <sup>i</sup> -Co1-O5	85.43 (17)	O1A-Co2-O4W	90.43 (14)
O3W-Co2-O2W	87.39 (15)	O1B-Co2-O4W	92.64 (15)
O4W-Co2-O2W	89.15 (15)	O3W-Fe2-O4W	176.53 (16)
O1W-Co2-O2W	177.52 (16)	O1A-Fe2-O1W	85.63 (15)
O4W-Co2-O1W	93.32 (15)	O1B-Co2-O1W	89.78 (15)
O1A-Co2-O2W	94.42 (15)	O3W-Co2-O1W	90.14 (15)
O1B-Co2-O2W	90.05 (15)		
Compound <b>4</b> <sup>d</sup>			
Fe1-O6W <sup>i</sup>	2.034 (5)	O6W-Fe1-O5W	92.71(19)
Fe1-O6W	2.034 (5)	O5W <sup>i</sup> -Fe1-O5W	177.6 (3)
Fe1-O5W <sup>i</sup>	2.137 (5)	O6W <sup>i</sup> -Fe1-O3B <sup>i</sup>	154.71(19)
Fe1-O5W	2.137 (5)	O6W-Fe1-O3B <sup>i</sup>	97.44 (19)
Fe1-O3B <sup>i</sup>	2.203 (4)	O5W <sup>i</sup> -Fe1-O3B <sup>i</sup>	95.69 (18)
Fe2-O1B	2.076 (4)	O5W-Fe1-O3B <sup>i</sup>	86.37 (18)
Fe2-O1A	2.081 (4)	O6W <sup>i</sup> -Fe1-O3B	97.44 (19)
Fe2-O1W	2.117 (4)	O6W-Fe1-O3B	154.71 (19)
Fe2-O4W	2.138 (5)	O5W <sup>i</sup> -Fe1-O3B	86.37 (18)
Fe2-O2W	2.158 (5)	O5W-Fe1-O3B	95.69 (18)
Fe2-O3W	2.207 (5)	O3B <sup>i</sup> -Fe1-O3B	59.5 (2)
O4W-Fe2-O2W	92.76 (19)	O1B-Fe2-O1A	174.38 (18)
O1B-Fe2-O3W	91.51 (17)	O1B-Fe2-O1W	86.64 (17)
O1A-Fe2-O3W	92.41 (18)	O1A-Fe2-O1W	86.64 (16)
O1W-Fe2-O3W	86.03 (18)	O1B-Fe2-O4W	92.91 (17)
O4W-Fe2-O3W	90.06 (18)	O1A-Fe2-O4W	91.11 (17)
O2W-Fe2-O3W	177.13 (19)	O1W-Fe2-O4W	176.1 (2)
O6W <sup>i</sup> -Fe1-O6W	106.93 (3)	O1B-Fe2-O2W	88.91 (19)
O6W <sup>i</sup> -Fe1-O5W <sup>i</sup>	92.71 (19)	O1A-Fe2-O2W	86.98 (19)
O6W-Fe1-O5W <sup>i</sup>	85.88 (19)	O1W-Fe2-O2W	91.15 (18)
O6W <sup>i</sup> -Fe1-O5W	85.88 (19)		

<sup>c</sup> (i) -x, y, -z; (ii) -x+1, y, -z+1. <sup>d</sup> (i) -x, y, -z; (ii) -x+1, y, -z+1.

**A 2D cobalt based coordination polymer constructed from benzimidazole and acetate ion exhibiting spin-canted antiferromagnetism**

*Leo Arai, Muhammad Arif Nadeem, Mohan Bhadbhade and John Arron Stride*

**ACKNOWLEDGMENT OF CONTRIBUTION TO AUTHORSHIP**

The article is published in journal “*Dalton Transactions*”. J.A.S. conceived and managed the research project, L.A. synthesised the samples. M.A.N. and M.B. solved the crystal structure. M.A.N. collected, interpreted the magnetic data and wrote the manuscript. All authors discussed the results and commented on this manuscript.

# A 2D cobalt based coordination polymer constructed from benzimidazole and acetate ion exhibiting spin-canted antiferromagnetism†

Leo Arai,<sup>a</sup> Muhammad Arif Nadeem,<sup>a</sup> Mohan Bhadbhade<sup>b</sup> and John Arron Stride<sup>\*a,c</sup>

Received 25th November 2009, Accepted 10th February 2010

First published as an Advance Article on the web 23rd February 2010

DOI: 10.1039/b924818h

A coordination polymer, [Co<sup>II</sup>(bIM)(acetate)] (bIM = benzimidazole) was synthesized using a solvothermal method; the complex has a two dimensional non-interpenetrated network structure and exhibits a spin-canted antiferromagnetic behaviour at low temperature and a high coercive field.

Over the past two decades the bulk magnetic properties of hybrid organic–inorganic materials have been increasingly reported, primarily due to the fact that such materials are excellent candidates for the study of fundamental phenomena in magnetism, including spin canting, metamagnetism and low dimensional magnetism.<sup>1</sup> The development of low dimensional magnets (1D and 2D magnetic structures) have generated considerable interest in recent years and despite a great number of molecule-based magnetic materials having been reported to display spin canting effects,<sup>2</sup> the notion of effective design and synthesis of such materials, has received less attention.<sup>3</sup> When aiming to achieve such hybrid magnetic materials, the choice of appropriate bridging ligands is of primary importance; the ligands may behave as superexchange pathways, communicating magnetic information between metal ions, thus determining both the nature and strength of the magnetic interactions. As such, relatively short bridging ligands such as oxalate,<sup>4</sup> cyanide, dicyanamide,<sup>5</sup> azide,<sup>6</sup> triazole,<sup>7</sup> hydroxypicolinate<sup>8</sup> and pyridine-3,4-dicarboxylic acid<sup>9</sup> have been used for this purpose to date. It has been demonstrated however, that heterocyclic ligands having two donor nitrogens separated by a ring carbon (as in the imidazolate ion) can create a bridged geometry that leads to the systematic alternation in relative orientations of neighbouring chromophores, a situation that can produce significant spin canting and long range ferromagnetic ordering.<sup>10</sup> The imidazolate ion has been previously used in the synthesis of canted spin systems.<sup>11</sup> Inspired by the fact that the imidazolate ion has been used to build hybrid organic-inorganic frameworks showing interesting magnetic properties, we chose benzimidazole (bIM) in the preparation of a 2D hybrid material found to display spin canted long range magnetic ordering and a hysteresis loop having a high coercive field.

The complex [Co(bIM)(acetate)] (**1**) was synthesized by a solvothermal approach. A mixture of Co(CH<sub>3</sub>CO<sub>2</sub>)<sub>2</sub>·4H<sub>2</sub>O

(125 mg, 0.5 mmol), benzimidazole (bIM; 83 mg, 0.7 mmol), and *N,N*-dimethylacetamide (6 mL) was stirred for 30 min and sealed in 23 mL Teflon lined stainless steel autoclave, which was heated to 120 °C and held at that temperature for 6 days. After cooling to room temperature, thin purple crystals of **1** were recovered by filtration and washed with ethanol (yield: 84% based on Co). The purity of the bulk phase was also confirmed by PXRD, Figure S1,† indicating the presence of a small amount of impurity, estimated at around the 1–2% level. The impurity is not a simple oxide of cobalt or any other simple salt that may be expected to have a strong magnetic response due to a high density of moments. As such this phase is expected to have an insignificant contribution to the magnetic behaviours observed. Thermal analysis shows that complex **1** is stable up to 380 °C.

**1** crystallizes in a monoclinic system in the *P2<sub>1</sub>/c* space group.‡ The basic structural unit consists of a single crystallographic site of cobalt (Co1), one benzimidazole (bIM) and one acetate ion, Fig. 1. Each Co1 atom is in a tetrahedral coordination geometry and bridges two benzimidazole ligands by forming bonds with two nitrogen atoms (N1 and N3) of each ligand at a distance of 1.99 and 2.00 Å respectively, forming a linear zigzag chain along the *b*-axis. The benzene rings of parallel bIM ligand are π...π stacked along the *b*-axis with a face to face distance of 9.69 Å. This cobalt–bIM zigzag chain is very similar to the 1D Co–benzotriazole chain synthesised by Liu *et al.*<sup>12</sup> Along the chain, the nearest-neighbour Co–Co distance is 5.968 Å and the Co–Co–Co bond angle is 108.57°, which is also similar to previously reported Co–imidazoles.<sup>11a</sup> The two oxygen atoms (O1 and O2) of the acetate ion bind with two neighbouring cobalt atoms (Co...O1 1.99 Å; Co...O2 1.97 Å) in adjacent zigzag chains, to form a two dimensional sheet lying in the *bc*-plane. Each acetate ion separates two Co atoms at a distance of 4.42 Å along the *c*-axis and the Co...Co...Co bond angle is 169.12° along this direction,

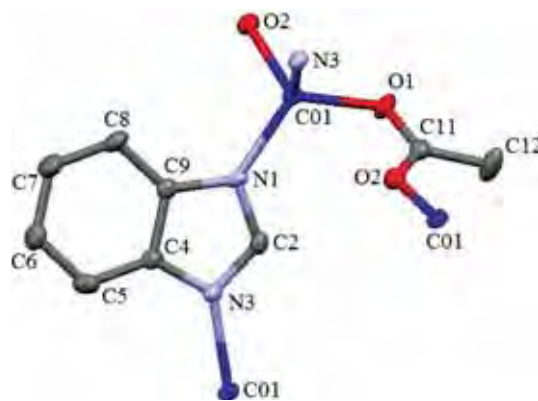


Fig. 1 Basic structural unit of **1**.

<sup>a</sup>School of Chemistry, University of New South Wales, Sydney, NSW, 2052, Australia. E-mail: j.stride@unsw.edu.au; Fax: +61 (02) 9385 6141; Tel: +61 (0)2 9385 4675

<sup>b</sup>Analytical Centre, University of New South Wales, Sydney, NSW, 2052, Australia

<sup>c</sup>Bragg Institute, Australian Nuclear Science and Technology Organisation, PMB 1, Menai, NSW, 2234, Australia

† Electronic supplementary information (ESI) available: Fig. S1–S4. CCDC reference number 754589. For ESI and crystallographic data in CIF or other electronic format see DOI: 10.1039/b924818h



which suggests a highly linear chain. These 2D sheets are then stacked on top of one another along the *a*-axis forming a 3D supramolecular network, Fig. 2. The formation of the 3D network can be largely attributed to the  $\pi$ - $\pi$  stacking interactions between the neighbouring bIM rings of the 2D sheets.

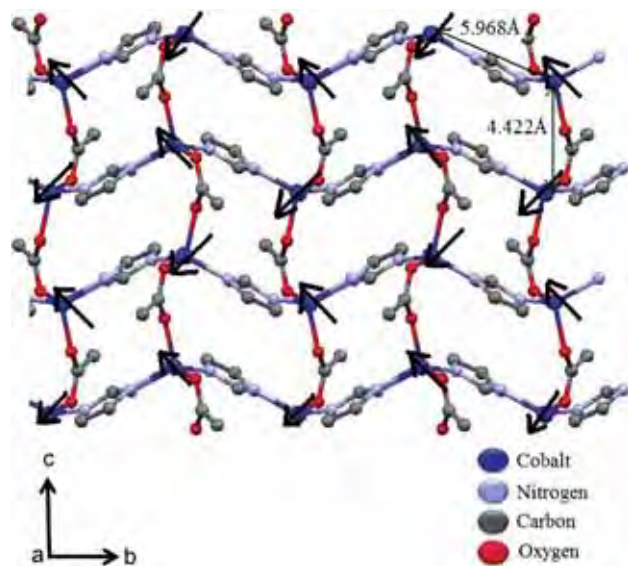


**Fig. 2** A packing diagram of **1** along the *a*-axis highlighting the 2D sheets of bIM ligands showing nature of magnetic exchange coupling in a canted antiferromagnetic behaviour. Benzene ring is omitted for clarity.

The magnetic properties of **1** are shown in Fig. 2. At room temperature, the value of  $\chi_M T$  is  $2.064 \text{ cm}^3 \text{ mol}^{-1} \text{ K}$  per  $\text{Co}^{\text{II}}$  atom, equal to the expected value with  $g = 2.10$ , for  $\text{Co}^{\text{II}}$  atoms.<sup>13</sup> Upon cooling,  $\chi_M T$  decreases continuously with decreasing temperature and reaches a minimum of  $0.911 \text{ cm}^3 \text{ mol}^{-1} \text{ K}$  at 15 K. On cooling further  $\chi_M T$  increases abruptly and reaches a maximum value of  $10.409 \text{ cm}^3 \text{ mol}^{-1} \text{ K}$  (Fig. 3b), suggesting that the magnetic behaviour at low temperature is canted-antiferromagnetic.<sup>14</sup> The  $\chi_M^{-1}$  vs  $T$  curve is shown as the inset of Fig. 3b. Above 15 K, the plot is linear and well fitted by Curie-Weiss law ( $\chi_M = C/(T - \theta)$ ), with  $C = 2.079 \text{ cm}^3 \text{ mol}^{-1} \text{ K}$ ,  $\theta = -24.139 \text{ K}$ . The value of the Weiss constant is larger than those of similar cobalt(II) imidazoles,<sup>11a</sup> indicating a dominant antiferromagnetic coupling between the  $\text{Co}^{\text{II}}$  ions. The field-cooled (FC), measured at 1000 Oe, and zero field-cooled (ZFC) magnetizations down to 2 K, show a bifurcation at 13 K. The FC  $\chi_M T$  values at different applied fields as a function of temperature show a spontaneous increase around 13 K, which is more pronounced at lower field strengths, Fig. 3c. The drop in  $\chi_M T$  value below 13 K may be due to magnetic field saturation effects.<sup>10</sup> A graph of  $\chi_M$  vs  $T$  in different applied dc fields clearly suggests the onset of spontaneous magnetization below 13 K and the susceptibility increases as the applied field decreases, corresponding to canted-antiferromagnetism, Figure S2.<sup>†</sup><sup>15</sup> The field dependence of magnetization of **1** at 2 K, Figure S3,<sup>†</sup> shows that the magnetization increases rapidly with increasing applied field at low external magnetic fields, then increases slowly at higher fields. However, complete saturation of magnetization is not reached, even at the highest applied field of 90 kOe, where the magnetization reaches a moment, ( $T = 2 \text{ K}$ ) of  $0.917 \text{ N}\beta$ , less than half the expected saturation value of  $3 \text{ N}\beta$  for a

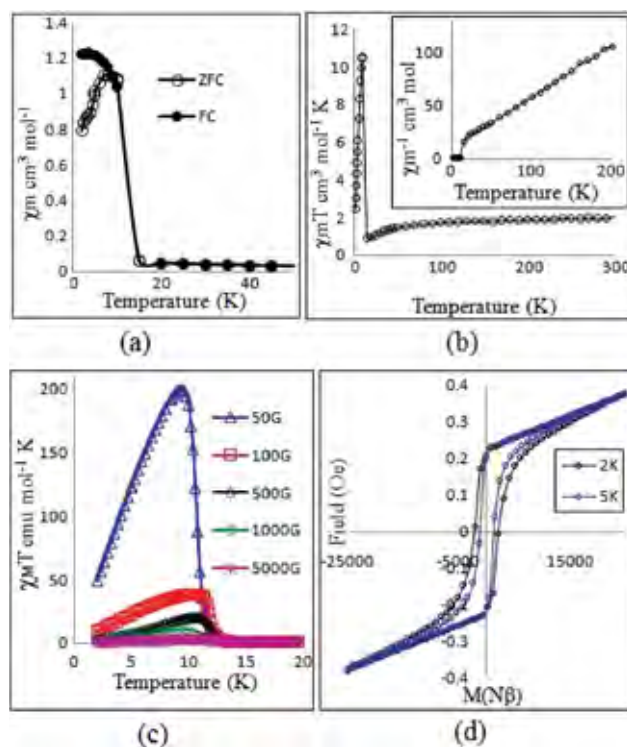


**Fig. 3** (a) Field cooled (FC) and zero-field (ZFC) plot of  $\chi_M$  vs.  $T$  at  $H = 1000 \text{ Oe}$ , (b) Plot of  $\chi_M T$  vs.  $T$  ( $H = 1000 \text{ Oe}$ ) (FC). Inset shows the  $\chi_M^{-1}$  vs.  $T$  plot, (c)  $\chi_M T$  vs.  $T$  at various fields, (d) Magnetic hysteresis loops at 2 and 5 K.

spin only  $\text{Co}^{\text{II}}$  ion. The absence of saturation at high fields confirms that the low temperature magnetic ground state is a canted-antiferromagnet.<sup>16</sup> The onset of ferromagnetic ordering at 13 K resulting from spin-canted antiferromagnetic coupling is further supported by cycling the applied field between +25 and -25 kOe at 2 and 5 K, which result in hysteresis loops, Fig. 3d. From these loops the coercive fields ( $H_c$ ) of 2089, 1490 Oe and remnant magnetizations ( $M_r$ ) of 0.2, 0.23  $\text{N}\beta$  are obtained at 2 and 5 K respectively. It is worthy to note that the hysteresis loop has a coercive field is much greater than previously reported canted-antiferromagnetic Co-imidazoles, making the material an inherently *harder* magnet.<sup>11a,17</sup> The angle of canting,  $\phi$ , is calculated as  $16.1^\circ$ .<sup>18</sup>

Taking into account the structural features of this compound, the single bridging imidazolate linkages produce a low symmetry  $\text{Co}^{\text{II}}\text{-L-Co}^{\text{II}}$  exchange pathway which should be responsible for spin-canting due to the antisymmetric interaction.<sup>17</sup> Strong magnetic exchange coupling is expected within the 2D sheets, however, the interactions between two sheets are expected to be small, as the minimum  $\text{Co} \cdots \text{Co}$  distance between two layers is  $8.838 \text{ \AA}$ . Considering the long distance between two 2D sheets, the existence of long range magnetic ordering in this low dimensional complex is remarkable.

In summary, the study of  $[\text{Co}(\text{bIM})(\text{acetate})]$  demonstrates that benzimidazole complexation leads to antiferromagnetic superexchange interactions between the cobalt(II) ions, however, in the low temperature region, the magnetic behaviour changes from antiferromagnetic to weak ferromagnetic ordering as a result of spin canting in the antiferromagnetic coupling regime. This work



leads to the prospect of using additional imidazole ligands, to further manipulate and tune the exchange interactions, with the Co<sup>II</sup> derivatives of particular interest.

## Notes and references

† Crystal data: C<sub>9</sub>H<sub>8</sub>CoN<sub>2</sub>O<sub>2</sub>,  $M_r = 235.10$ , Monoclinic, space group  $P2_1/c$ ,  $a = 10.7998(15)$ ,  $b = 9.6915(15)$ ,  $c = 8.8039(12)$  Å,  $\alpha = 90.00^\circ$ ,  $\beta = 98.168(7)^\circ$ ,  $\gamma = 90.00^\circ$ ,  $V = 912.1(2)$  Å<sup>3</sup>,  $T = 150(2)$  K,  $Z = 4$ ,  $\rho_c = 1.712$  g cm<sup>-3</sup>,  $\lambda = 0.7107$  Å, 5899 reflections collected, 1580 unique ( $R_{\text{int}} = 0.0672$ ),  $R(F) = 0.0427$  and  $wR_2 = 0.1037$  using 1176 reflections with  $I > 2\sigma(I)$ . Data was collected on a Bruker kappa APEXII CCD Area Detector instrument and the structure was solved by direct methods (SHELXS-97). All non-hydrogen atoms were refined with anisotropic thermal parameters. CCDC-754589.†

Elemental analysis. Anal. calcd. for C<sub>9</sub>H<sub>8</sub>CoN<sub>2</sub>O<sub>2</sub> ( $M_r = 235.10$ ): C, 45.93% N, 11.90% H, 3.40%. Found: C, 45.99% N, 11.94% 3.42%.

FT-IR data ( $\nu_{\text{max}}/\text{cm}^{-1}$ ): 1608w, 1538 s, 1456 s, 1297w, 1274 m, 1238 s, 1201w, 1184w, 1116w, 908 m, 755w, 744 s, 694m.

- 1 (a) R. L. Carlin, *Magnetochemistry*, Springer-Verlag, Berlin, 1986; (b) O. Kahn, *Molecular Magnetism*, VCH, Weinheim, 1993.
- 2 (a) P. Jensen, S. R. Batten, G. D. Fallon, B. Moubaraki, K. S. Murray and D. J. Price, *Chem. Commun.*, 1999, 177; (b) S. Martin, M. G. Barandika, L. Lezama, J. L. Pizarro, Z. E. Serna, J. I. Ruiz de Larramendi, M. I. Arriortua, T. Rojo and R. Cortés, *Inorg. Chem.*, 2001, **40**, 4109.
- 3 H.-P. Jia, W. Li, Z.-F. Ju and J. Zhang, *Chem. Commun.*, 2008, 371.
- 4 S. Decurtins, R. Pellaux, G. Antorrena and F. Palacio, *Coord. Chem. Rev.*, 1999, **190–192**, 841.
- 5 P. Jensen, D. J. Price, S. R. Batten, B. Moubaraki and K. S. Murray, *Chem.-Eur. J.*, 2000, **6**, 3186.
- 6 (a) J. Ribas, A. Escuer, M. Monfort, R. Vicente, R. Cortés, L. Lezama and T. Rojo, *Coord. Chem. Rev.*, 1999, **193–195**, 1027; (b) H. H. Ko, J. H. Lim, H. C. Kim and C. S. Hong, *Inorg. Chem.*, 2006, **45**, 8847; (c) F. A. Mautner, L. Ohrstrom and R. Vicente, *Inorg. Chem.*, 2009, **48**,

6280; (d) J. R. Li, Q. Yu, E. C. Sanudo, Y. Tao and X.-H. Bu, *Chem. Commun.*, 2007, 2602.

- 7 W. Ouellette, J. R. Galan-Mascaros, K. R. Dunbar and J. Zubieta, *Inorg. Chem.*, 2006, **45**, 1909.
- 8 M.-H. Zeng, W.-X. Zhang, X.-Z. Sun and X.-M. Chen, *Angew. Chem., Int. Ed.*, 2005, **44**, 3079.
- 9 Y. G. Huang, D. Q. Yuan, L. Pan, F.-L. Jiang, M.-Y. Wu, X.-D. Zhang, W. Wei, Q. Gao, J. Y. Lee, J. Li and M.-C. Hong, *Inorg. Chem.*, 2007, **46**, 9609.
- 10 (a) S. J. Retting, V. Sanchez, A. Storr, R. C. Thompson and J. Trotter, *J. Chem. Soc., Dalton Trans.*, 2000, 3931; (b) S. J. Rettig, A. Storr, D. A. Summers, R. C. Thompson and J. Trotter, *J. Am. Chem. Soc.*, 1997, **119**, 8675; (c) S. J. Rettig, A. Storr, D. A. Summers, R. C. Thompson and J. Trotter, *Can. J. Chem.*, 1999, **77**, 425.
- 11 (a) Y.-Q. Tian, C.-X. Cai, X.-M. Ren, C.-Y. Duan, Y. Xu, S. Gao and X.-Z. You, *Chem.-Eur. J.*, 2003, **9**, 5673; (b) S. J. Rettig, V. Sánchez, A. Storr, R. C. Thompson and J. Trotter, *Inorg. Chem.*, 1999, **38**, 5920.
- 12 G.-X. Liu, L.-F. Huang, X.-J. Kong, R.-Y. Huang and H. Xu, *Inorg. Chim. Acta*, 2009, **362**, 1755.
- 13 (a) S. O. H. Gutschke, D. J. Price, A. K. Powell and P. T. Wood, *Angew. Chem., Int. Ed.*, 2001, **40**, 1920; (b) D. Cave, J.-M. Gascon, A. D. Bond, S. J. Teat and P. T. Wood, *Chem. Commun.*, 2002, 1050; (c) S. M. Humphrey and P. T. Wood, *J. Am. Chem. Soc.*, 2004, **126**, 13236; (d) A. Rujiwatra, C. J. Kepert, J. B. Claridge, M. J. Rosseinsky, H. Kumagai and M. Kurmoo, *J. Am. Chem. Soc.*, 2001, **123**, 10584.
- 14 (a) M. Yang, J. Yu, L. Shi, P. Chen, G. Li, Y. Chen, R. Xu and S. Gao, *Chem. Mater.*, 2006, **18**, 476; (b) P. Mahata, D. Sen and S. Natarajan, *Chem. Commun.*, 2008, 1278.
- 15 X.-M. Zhang, Z.-M. Hao, W.-X. Zhang and X.-M. Chen, *Angew. Chem., Int. Ed.*, 2007, **46**, 3456.
- 16 (a) R. L. Carlin, *Magnetochemistry*, Springer-Verlag, Berlin, 1986; (b) F. Sanz, C. Parada, J. M. Rojo and C. Ruiz-Valero, *Chem. Mater.*, 2001, **13**, 1334; (c) T. Moriya, *Magnetism*, Vol. 1, G. T. Rado and H. Suhl, ed.; Academic Press, London, 1963, p 85.
- 17 Y.-Q. Tian, Z.-X. Chen, L.-H. Weng, H.-B. Guo, S. Gao and D. Y. Zhao, *Inorg. Chem.*, 2004, **43**, 4631.
- 18 Canting angle  $\phi = \tan^{-1}[M_s(T = 2\text{ K})/M_{\text{max}}]$  S. O. H. Gutschke, D. J. Price, A. K. Powell and P. T. Wood, *Angew. Chem., Int. Ed.*, 1999, **38**, 1088.

## Supporting Information

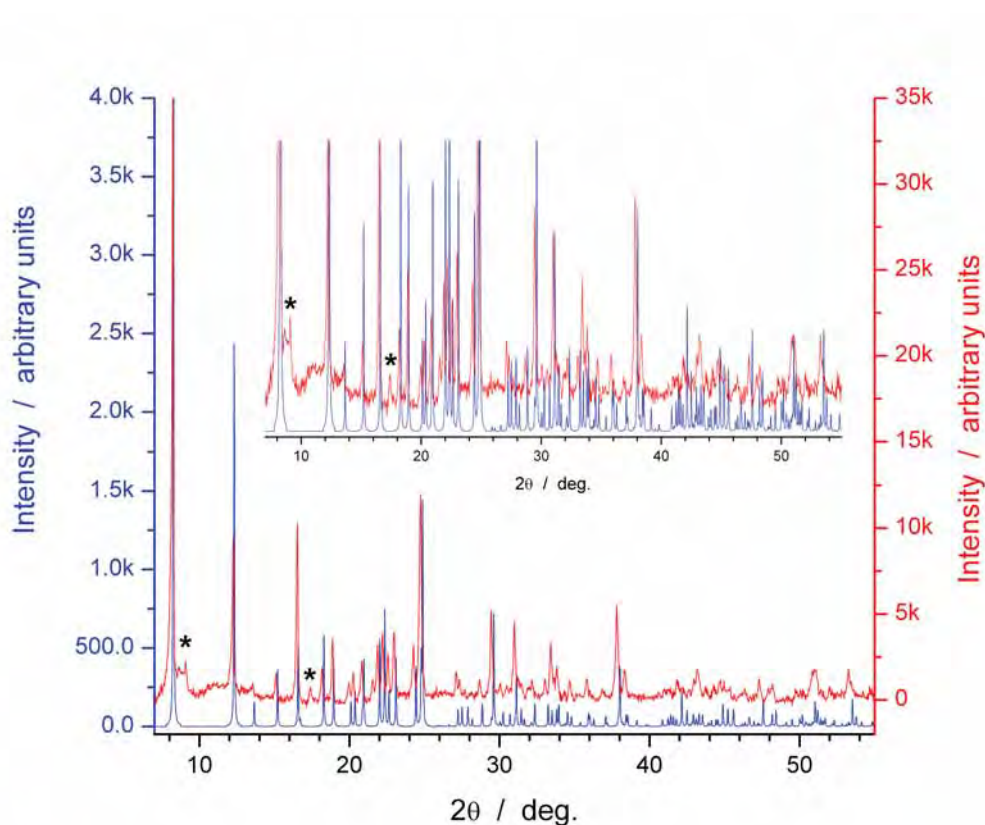
### A 2D Cobalt based coordination polymer constructed from benzimidazole and acetate ion exhibiting spin-canted antiferromagnetism

Leo Arai,<sup>a</sup> Muhammad Arif Nadeem,<sup>a</sup> Mohan Bhadbhade<sup>b</sup> and John Arron Stride\*<sup>a,c</sup>

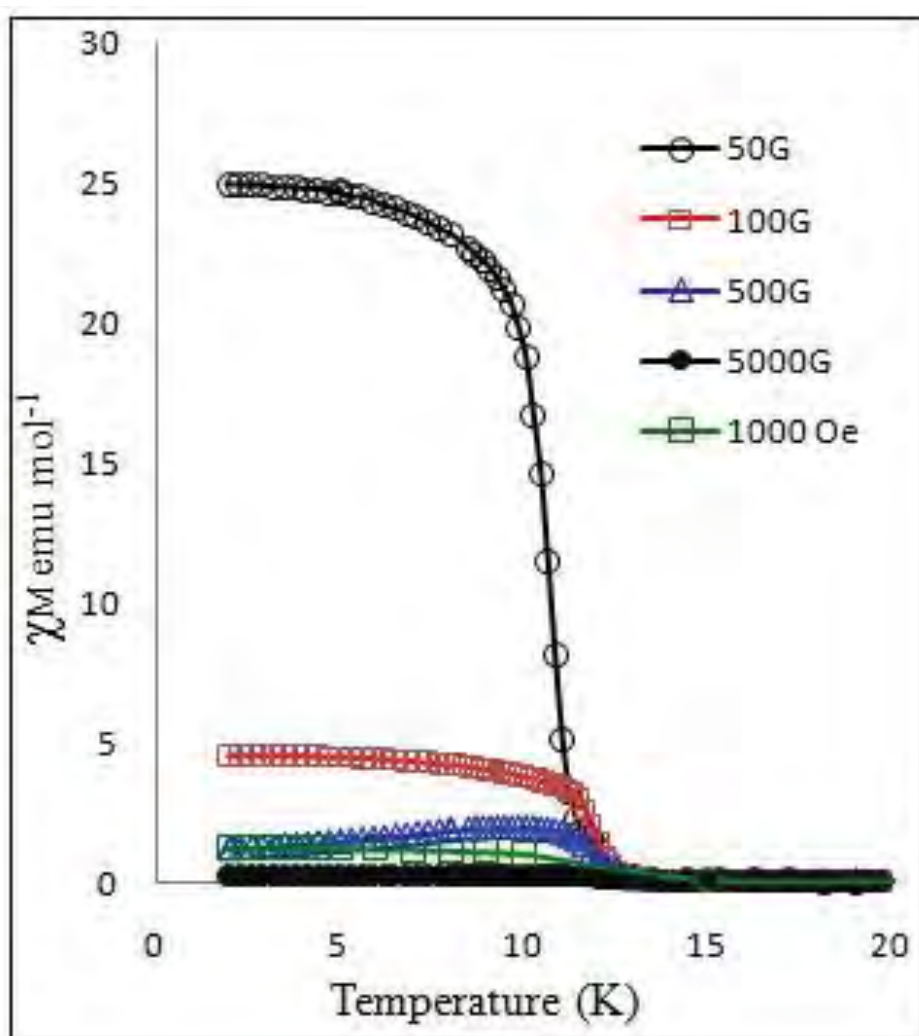
<sup>a</sup> School of Chemistry, University of New South Wales, Sydney, NSW 2052, Australia. Fax: +61 (02) 9385 6141; Tel: +61 (0)2 9385 4675; E-mail: j.stride@unsw.edu.au

<sup>b</sup> Analytical Centre, University of New South Wales, Sydney, NSW 2052, Australia.

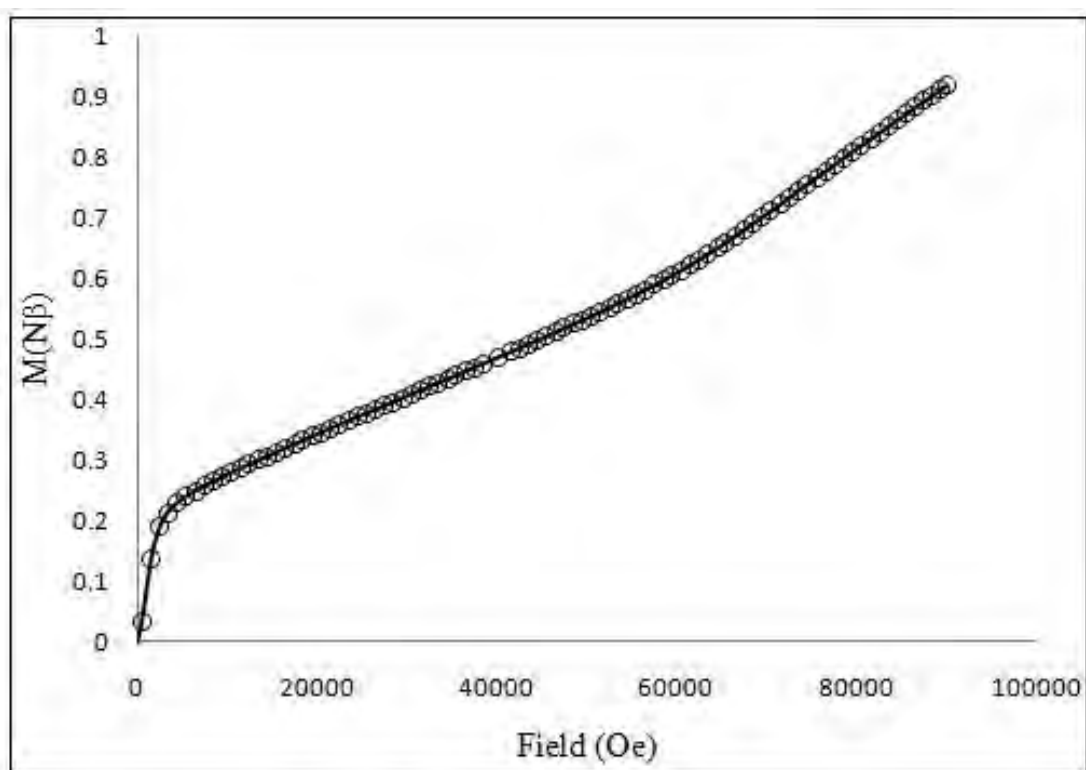
<sup>c</sup> Bragg Institute, Australian Nuclear Science and Technology Organisation, PMB 1, Menai, NSW 2234, Australia.



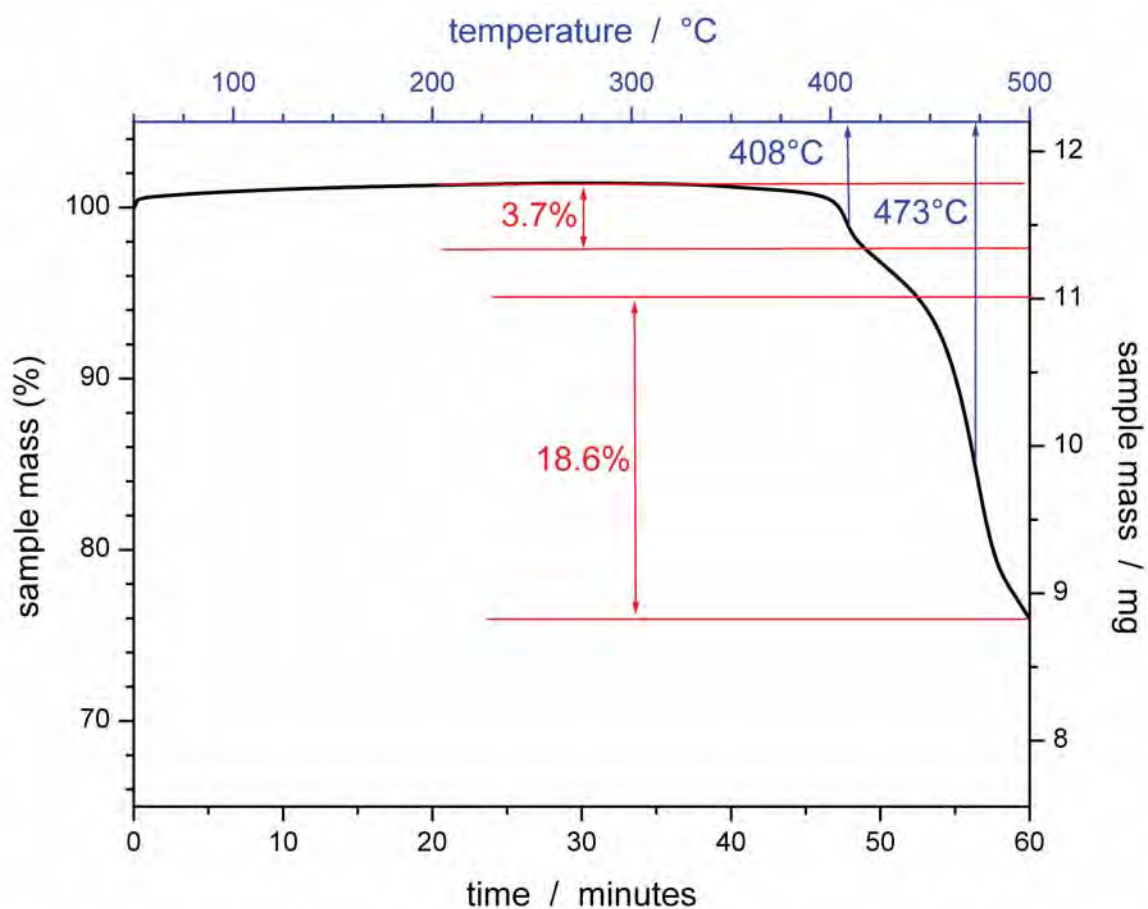
**S1.** Calculated and experimental powder XRD pattern of **1**. The highlighted peaks at 8° and 17.5° belong to a small amount of impurity present in the sample, estimated to ca. 1-2%.



S2.  $\chi_M$  vs.  $T$  plot at various fields



**S3.**  $M$  vs.  $H$  plot at  $T = 2$  K



**S4.** TGA curve of **1**: two regions of sample decomposition are observed, the first at 408°C which represents a partial degassing of the sample and the second at 473°C which is consistent with the evolution of one molecule of CO<sub>2</sub> per formula unit.

**Two iso-structural metal-organic frameworks having  
long-range magnetic ordering at 45 K**

*Muhammad Arif Nadeem, Mohan Bhadbhade and John Arron Stride*

**ACKNOWLEDGMENT OF CONTRIBUTION TO AUTHORSHIP**

The article is submitted in journal “*Chem. Eur. J.*” J.A.S. conceived and managed the research project, M.A.N. synthesised the samples. M.B. and M.A.N. solved the crystal structure. M.A.N. collected, interpreted the magnetic data and wrote the manuscript. All authors discussed the results and commented on this manuscript.



## Two iso-structural metal-organic frameworks having long-range magnetic ordering at 45 K

Muhammad Arif Nadeem,<sup>[a]</sup> Mohan Bhadbhade<sup>[b]</sup> and John Arron Stride\*<sup>[a, c]</sup>

**Abstract:** Two new isostructural coordination polymers, {[M<sup>III</sup>(pydc)<sub>3</sub>(μ<sub>3</sub>-O)].Cl, M = Mn (**1**), Co (**2**), pydc = pyridine-3,5-dicarboxylic acid} have been synthesised under hydrothermal conditions. These new compounds were characterised by single-crystal X-ray diffraction, elemental analysis, IR spectroscopy, thermo-gravimetric analysis and variable temperature magnetic susceptibility measurements. X-ray analysis reveals that both

compounds crystallise in the hexagonal space group *R*-3*c*, with the basic structure made up of μ<sub>3</sub>-O centered [M<sub>3</sub>(μ<sub>3</sub>-O)(CO<sub>2</sub>)<sub>6</sub>] trimetallic clusters. Thermal analysis shows that **1-2** are stable up to 500 °C. Variable temperature magnetic susceptibility measurements revealed that there are antiferromagnetic coupling interactions between the metal ions within the trimetallic units above 45 K. The neighbouring trimers then couple antiferromagnetically to show bulk

magnetic ordering below ca. 45 K. whilst, in compound **2** only, there is also an indication of magnetic phase transition from colinear antiferromagnetism to canted antiferromagnetism.

**Keywords:** molecular magnets • metal organic frameworks • long range magnetic ordering

### Introduction

Amongst the classes of new materials currently of widespread interest, metal-organic framework materials occupy a prominent position by virtue of potential applications in catalysis, as optical materials, membranes, and as sorption substrates.<sup>[1]</sup> In addition to the typical applications of these materials, attaining magnetic metal-organic frameworks (MMOFs) is of considerable interest because of their potential applications as magnetic sensors and data storage, in addition to those otherwise attributed to MOFs.<sup>[2]</sup> A common approach that has been employed is to connect paramagnetic

transition metal ions via short bridging ligands into multidimensional networks. The metal ions are the source of the magnetic moments, whilst the bridging ligands provide superexchange pathways between the magnetic centres. However, it remains difficult to predict *a priori* both the structure and magnetic behaviour due to the wide diversity of coordination geometries and the complex nature of magnetic interactions.<sup>[3]</sup> Magnets having controlled structural and physical properties are a very topical field; crystal-engineering plays an important role in this by determining the magnetic dimensionality.<sup>[4]</sup> Unfortunately, the complete design of structural topologies of MMOFs, that largely control the magnetic behaviour of these materials, is still a challenge. A particular interest in this context is the design of molecular systems combining magnetism and porosity.<sup>[5]</sup> Another challenge in this field is to increase the bulk magnetic ordering temperature. To date, most MMOFs show long range magnetic ordering only at very low temperatures. In order to realise the above mentioned targets, we selected a highly symmetrical (3,9)-connected topology that has been previously reported by Xian *et al.* This was achieved by selecting pyridine-3,5-dicarboxylic acid as an organic linker.<sup>[6]</sup> However, we have discovered that the incorporation of chloride ions into this topology drastically changes the magnetic properties of the material.

Herein, two novel isostructural 3D antiferromagnetic microporous MMOFs, {[M<sup>III</sup>(pydc)<sub>3</sub>(μ<sub>3</sub>-O)].Cl, M = Mn (**1**), Co (**2**), pydc = pyridine-3,5-dicarboxylic acid}, are reported as having a bulk magnetic ordering temperature of 45 K. To date, only a few microporous MMOFs are known to exhibit long range magnetic

[a] M. A. Nadeem, A/Prof. J. A. Stride\*  
School of Chemistry, University of New South Wales, Sydney, Australia  
Fax: (+61) (2)93856141  
E-mail: j.stride@unsw.edu.au

[b] M. Bhadbhade  
Analytical Centre, University of New South Wales, Sydney, NSW 2052, Australia.

[c] A/Prof. J. A. Stride  
Bragg Institute.  
Australian Nuclear Science and Technology Organisation  
PMB 1, Menai, NSW 2234, Australia.

Supporting information for this article is available on the WWW under <http://www.chemeurj.org/> or from the author.

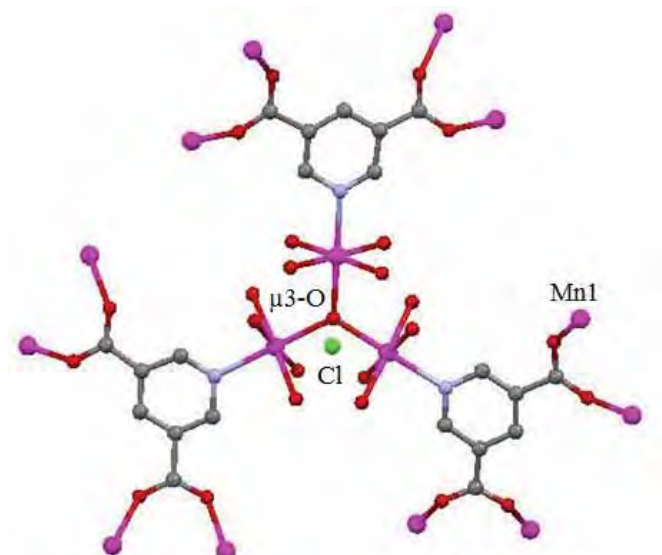
**Table 1.** Crystallographic data of **1-2**

	Compound 1	Compound 2
Empirical formula	C <sub>21</sub> H <sub>9</sub> Mn <sub>3</sub> N <sub>3</sub> O <sub>13</sub> Cl	C <sub>21</sub> H <sub>9</sub> Co <sub>3</sub> N <sub>3</sub> O <sub>13</sub> Cl
Formula weight	711.58	723.55
Temperature	150(2) K	150(2) K
Wavelength	0.71073 Å	0.71073 Å
Crystal system	Hexagonal	Hexagonal
Space group	<i>R</i> -3 <i>c</i>	<i>R</i> -3 <i>c</i>
<i>a</i> / Å	17.4418(11)	17.147(7)
<i>b</i> / Å	17.4418(11)	17.147(7)
<i>c</i> / Å	12.5327(15)	12.552(12)
$\alpha$	90°	90°
$\beta$	90°	90°
$\gamma$	120°	120°
Volume / Å <sup>3</sup>	3301.9 (5) (4)	3196.4(4)
<i>Z</i>	36	36
$\rho$ / Mg m <sup>-3</sup>	2.361	3.491
<i>S</i>	1.25	0.93
<i>F</i> (000)	3198	3270
Limiting indices	-11 ≤ <i>h</i> ≤ 20 -17 ≤ <i>k</i> ≤ 20 -14 ≤ <i>l</i> ≤ 13	-20 ≤ <i>h</i> ≤ 20 -19 ≤ <i>k</i> ≤ 20 -7 ≤ <i>l</i> ≤ 14
Reflections number	5059	4621
<i>R</i> <sub>int</sub>	0.040	0.066
$\Theta_{\max}$	25.0°	25.0°
<i>wR</i> ( <i>F</i> <sup>2</sup> )	0.136	0.128

ordering in this temperature range. In 2003, Kurmoo *et al.*, reported a cobalt based polymer having large cavities of 3.7 x 2.3 Å<sup>2</sup> showing magnetic ordering at 60.5 K.<sup>[7 a]</sup> Later in 2007, Kitagawa *et al.*, reported a 2D cyanide bridged bimetallic Mn<sup>II</sup>Cr<sup>III</sup> coordination polymer [Mn(NNdmenH)(H<sub>2</sub>O)][Cr(CN)<sub>6</sub>].H<sub>2</sub>O (NNdmen N,N-dimethylethylenediamine) having 1D channels of 0.8 x 1.6 Å<sup>2</sup> and exhibiting ferrimagnetic ordering at 35.2 K; upon dehydration this shifted to 60.4 K.<sup>7b</sup> Meanwhile in 2008, Zheng *et al.* also observed bulk magnetic ordering in a layered inorganic-organic hybrid material [Mn<sub>3</sub>(OH)<sub>2</sub>(chedc)<sub>2</sub>] (chedc, cyclohexene-1,2-dicarboxylic acid) at 42 K.<sup>7c</sup>

## Results and Discussion

### Crystal Structure

**Figure 1.** Basic structural unit of **1**

Single crystal X-ray analysis reveals that both **1** and **2** crystallize in the space group *R*-3*c*. Complex **1** is taken as an example to depict the structure in more detail. The basic structural unit consists of a  $\mu_3$ -O centered Mn<sub>3</sub>( $\mu_3$ -O)(CO<sub>2</sub>)<sub>6</sub> cluster, figure 1. Each Mn<sub>3</sub>(OH)(CO<sub>2</sub>)<sub>6</sub> cluster is connected to nine heterocyclic pyridine rings via six C-O bonds and three Mn-N bonds, whilst each pyridine ring is connected to three Mn<sub>3</sub>(OH)(CO<sub>2</sub>)<sub>6</sub> trimers via two C-O bonds and one Co-N bond. The  $\mu_3$ -O and three Mn atoms within the Mn<sub>3</sub>( $\mu_3$ -O)(CO<sub>2</sub>)<sub>6</sub> cluster are coplanar with a Mn-O-Mn angle of 120° and as such the three Mn atoms are separated at equal distances of 3.76 Å within a cluster, figure 2a. The trimers are alternately stacked in a staggered fashion (60° offset) at a distance of 6.63 Å along the *c*-axis with one chloride ion equidistant between neighbouring trimers. This gives the appearance of a one dimensional cylinder running along the *c*-axis, figure 2b. Within the *ab*-plane each trimer is separated by pydc ligands at a distance of 6.99 Å. In addition, all of the pyridine rings display  $\pi$ - $\pi$  stacking along the *c*-axis with a minimum face to face distance of 3.854 Å. The overall structure of **1** is a 3D (3,9)-connected framework in which pyridine rings and Mn<sub>3</sub>( $\mu_3$ -O)(CO<sub>2</sub>)<sub>6</sub> clusters act as three and nine-connected nodes, respectively. The packing diagram of **1** along the *c*-axis is shown in figure 2c. The single chloride ion between two Mn<sub>3</sub> clusters in the lattice plays a key role in providing the superexchange pathway between the magnetic centres, as the previously reported structure with a water molecule between two trimers did not show any magnetic ordering.<sup>6</sup> On the basis of charge balance, the oxidation state of the metal ions within the clusters is assigned as +3 and given the light colours of final products the possibility of mixed valency is ruled out. The structure also shows a microporous nature (see Figure S1 in the Supporting Information), however, the channels are too narrow (1.4 Å) to admit nitrogen molecules for the purpose of calculating the BET surface area.

### Thermogravimetric analysis

Thermal analyses of **1** and **2** were performed to explore the thermal stabilities. As depicted in the Figure S7 of the ESI, both the complexes are thermally very stable upto 500°C. With no solvent molecules trapped in the framework, there is a broad plateau region followed by sudden decrease in the weight, suggesting the onset of decomposition at a temperature of ca. 520 and 460 °C, with a total weight loss of ca. 37% and 50% for complexes **1** and **2** respectively.

This represents the total loss of the organic fragments in each, resulting in simple oxides.

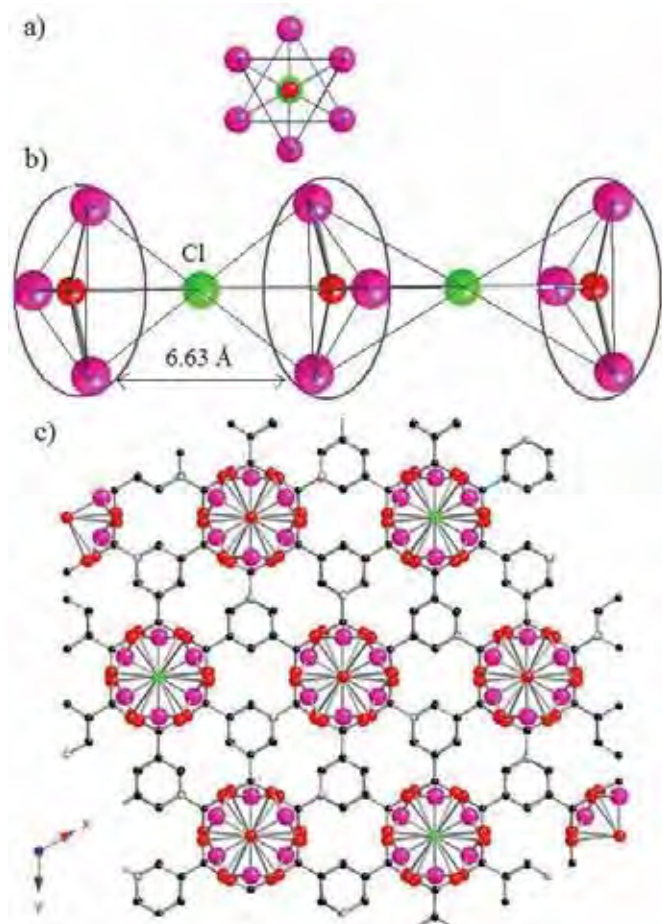


**Figure 2.** (a) The two trimer units are alternately stacked along the *c*-axis (b) alternative packing of trimers with chloride ions between them viewed perpendicular to the *c*-axis (c) View of 3-D framework on *ab*-plane

### Magnetic Properties

The dc magnetic susceptibility ( $\chi_M$ ) data of a polycrystalline sample of **1** is given in figure 3. The data shows that the plot of  $\chi_M T$  vs  $T$  at 1000 Oe, figure 3b, where  $T$  is the absolute temperature, decreases slowly with decreasing temperature. At 300 K the  $\chi_M T$  value is  $10.557 \text{ cm}^3 \text{ mol}^{-1} \text{ K}$  and decreases down to a local minimum value of  $7.221 \text{ cm}^3 \text{ mol}^{-1} \text{ K}$  at 45 K. Upon further cooling, the  $\chi_M T$  value rapidly increases, reaching a maximum of  $8.269 \text{ cm}^3 \text{ mol}^{-1} \text{ K}$  at 40 K and then decreasing to  $1.202 \text{ cm}^3 \text{ mol}^{-1} \text{ K}$  at 2 K, the lowest temperature measured. At room temperature, the value of  $\chi_M T$  is  $10.557 \text{ cm}^3 \text{ mol}^{-1} \text{ K}$  per three  $\text{Mn}^{\text{III}}$  atoms, equivalent to the expected value of  $10.595 \text{ cm}^3 \text{ mol}^{-1} \text{ K}$  with  $g = 2.17$ . The abrupt discontinuity in  $\chi_M T$  at 45 K is an indication of the on-set of long range magnetic ordering. The bulk magnetic ordering is also confirmed by plotting the  $\chi_M$  vs  $T$  for zero-field cooled (ZFC) and field-cooled (FC) experiments, where a bifurcation appears at 45 K, figure 3a. The fit of the  $\chi_M^{-1}$  vs  $T$  curve in the range of 50 - 300 K gives a Weiss constant  $\theta = -20.08 \text{ K}$  and a Curie constant  $C = 11.22 \text{ cm}^3 \text{ mol}^{-1} \text{ K}$ . The interpretation of this magnetic behavior is that of being dominated by long range antiferromagnetic ordering below 45 K, with antiferromagnetic coupling between Mn ions within the trimer above this temperature. The FC susceptibility in different applied dc fields also clearly shows the onset of spontaneous magnetization below 45 K, figure 3d. The field dependent magnetization at 2 K

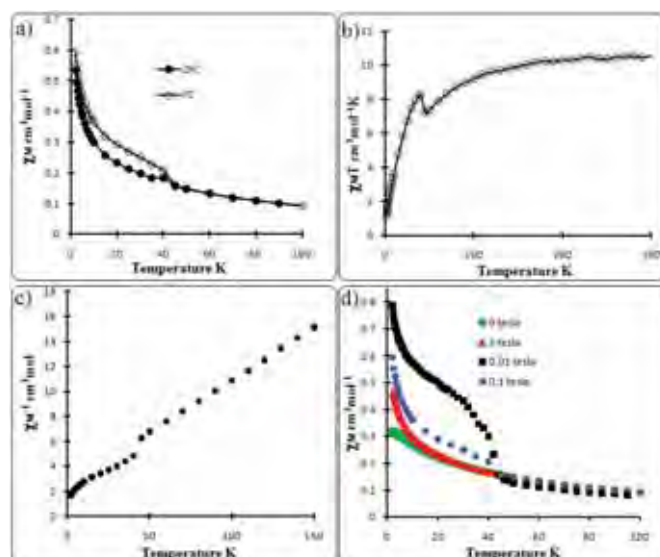


**Figure 3.** (a) Field cooled (FC) and zero-field (ZFC) plot of  $\chi_M$  vs.  $T$  at  $H = 1000 \text{ Oe}$ , (b) Plot of  $\chi_M T$  vs.  $T$  ( $H = 1000 \text{ Oe}$ ) (FC). (c) Plot of  $\chi_M^{-1}$  vs.  $T$  ( $H = 1000 \text{ Oe}$ ) (d)  $\chi_M$  vs.  $T$  at various fields

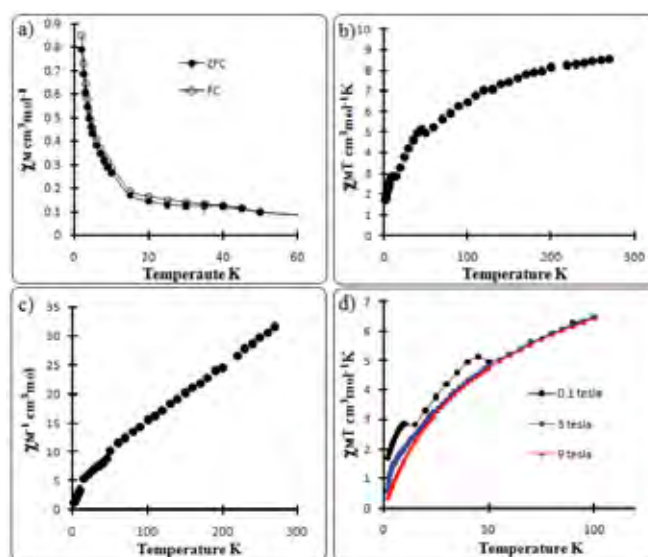


**Figure 4.** (a) Field cooled (FC) and zero-field (ZFC) plot of  $\chi_M$  vs.  $T$  at  $H = 1000 \text{ Oe}$ , (b) Plot of  $\chi_M T$  vs.  $T$  ( $H = 1000 \text{ Oe}$ ) (FC). (c) Plot of  $\chi_M^{-1}$  vs.  $T$  ( $H = 1000 \text{ Oe}$ ) (d)  $\chi_M T$  vs.  $T$  at various fields

suggests that saturation magnetization is not reached even at the highest field of 70 kOe (7 T) and a hysteresis loop was obtained with a coercive field of 109 Oe (see Figure S2 in the Supporting Information). The moiety of  $\mu_3\text{-O}$  centered  $\text{Mn}^{\text{III}}$  ion triangles is a common form and such materials have been reported previously as single molecule magnets (SMMs),<sup>[8]</sup> however in 3D extended systems, such examples are rare. It is worth noting that a bulk magnetic ordering of 45 K for **1** is rather high for Mn based molecular magnets, and exceeds the critical temperature of the purely inorganic mixed-valence material hausmannite ( $\text{Mn}_3\text{O}_4$ ), which has a ferrimagnetic Curie point at 41.9 K.<sup>[9]</sup> The magnetic susceptibility data of a polycrystalline sample of **2** in the range of 2 - 300 K under 1000 Oe applied field is given in figure 4. The data shows a similar form to compound **1**. The  $\chi_M T$  value at



300 K is 8.588 cm<sup>3</sup>mol<sup>-1</sup>K per Co<sub>3</sub> unit, which is slightly lower than the spin only value (9.00 cm<sup>3</sup>mol<sup>-1</sup> K) for three high spin Co<sup>III</sup> ions, probably due to spin quenching by orbital angular momentum contributions of the octahedral Co<sup>III</sup> ions.<sup>[10]</sup> Upon cooling,  $\chi_M T$  decreases to a value of 4.914 cm<sup>3</sup>mol<sup>-1</sup>K at 50 K and then suddenly increases to a value of 5.12 cm<sup>3</sup>mol<sup>-1</sup>K, again an indication of the onset of bulk magnetic ordering in this temperature range. Upon further cooling, the  $\chi_M T$  value again starts to decrease to a value of 2.849 cm<sup>3</sup>mol<sup>-1</sup>K at 15 K before once again increasing to a value of 2.860 cm<sup>3</sup>mol<sup>-1</sup>K at 10 K, most probably an indication of phase change from colinear antiferromagnetic to canted antiferromagnetic ordering. Subsequently  $\chi_M T$  decreases to a minimum value of 1.692 cm<sup>3</sup>mol<sup>-1</sup>K at 2 K, figure 4b. The long range magnetic ordering at around 40 K in **2** is also confirmed by the bifurcation of FC and ZFC curves, figure 4a. The fit of  $\chi_M^{-1}$  vs  $T$  in the range of 50 - 300 K gives a Weiss constant  $\theta = -26.241$  K and a Curie constant  $C = 9.057$  cm<sup>3</sup>mol<sup>-1</sup>K; the negative value of the Weiss constant suggests an antiferromagnetic nature of exchange coupling between metal centers. A graph of  $\chi_M$  vs  $T$  in different applied dc fields again clearly suggests the onset of spontaneous magnetization below 45 K, with the susceptibility increasing as the applied field decreases, corresponding to canted antiferromagnetism at 10 K, (see Figure S3 in the Supporting Information).<sup>[11]</sup> It is clear from figure 4d that spontaneous magnetization diminishes with increasing applied magnetic field. The field dependence of magnetization of **2** at 2 K (see Figure S4 in the Supporting Information), shows that the magnetization increases rapidly with increasing applied field at low external magnetic fields, as expected for a bulk magnet,<sup>[12]</sup> and then increases much more slowly at higher fields. However, complete saturation of magnetization was not reached even at the highest applied field of 70 kOe. A hysteresis loop was observed at 2 K with a coercive field of 80 Oe. The narrow hysteresis loops observed at 2 K with correspondingly small coercive fields, indicate a soft-magnetic behavior in both **1** and **2**.<sup>[13]</sup>

## Conclusion

In summary, two 3D isostructural MMOFs based on  $\mu_3$ -O centered metal clusters, have been synthesized offering a rare example of controlled bulk magnetic ordering at significantly higher temperatures than similar materials. Both MMOFs showed bulk magnetic ordering at around 45 K, whilst only compound **2** displayed a canting behavior at 10 K. These results demonstrate the concept of structural topology controlling the nature of magnetic ordering and opens the way for further work aimed at topological control of magnetism, particularly in light of incorporating spin centres of having a large spin anisotropies in order to increase both the transition temperature and the coercive fields in such materials.

## Experimental Section

### Materials and Physical Techniques

All reagents and solvents employed were commercially available and used as received without further purification. The syntheses of **1-4** were carried out in 23 mL Teflon-lined autoclaves under autogenous pressure. Elemental analyses were performed on a Carlo Erba Elemental Analyser EA 1108. The FT-IR spectra were measured with an AVATAR 320 spectrometer on KBr disks. Thermal analyses were carried out under nitrogen using a Mettler Toledo TGA/DSC 1, with the heating rate of 10°C min<sup>-1</sup>.

### Magnetometry

Variable temperature magnetic susceptibility and magnetization measurements were performed with a Quantum Design PPMS EverCool system equipped with a vibrating sample magnetometer and a 9 T magnet. Clean crystals were picked out manually, crushed and loaded in a plastic sample holder for data collection. The magnetic susceptibility measurements were performed for field-cooled and zero-field-cooled samples in magnetic fields of 0.1 T. Pascal's constants were used to estimate the diamagnetic corrections.<sup>[13]</sup> Magnetization data were collected in fields up to 9 T and in the temperature range between 2 and 300.0 K. Hysteresis loops were measured at 2 and 5 K with maximum fields of  $\pm 9.0$  T.

### Synthesis of [Mn<sub>3</sub>(pydc)<sub>3</sub>( $\mu_3$ -O)]·Cl (**1**) and [Co<sub>3</sub>(pydc)<sub>3</sub>( $\mu_3$ -O)]·Cl (**2**)

A mixture of 0.5 mmol of pyridine-3,5-dicarboxylic acid (0.0835 g) and 2 mmol of KOH (0.112 g) in 3 mL distilled water was stirred for 10 minutes followed by the addition of a solution of MnCl<sub>2</sub>·4H<sub>2</sub>O (0.1 g, 0.5 mmol) in 2 mL H<sub>2</sub>O, 0.5 g of KCl was then added to the stirred solution. The resulting solution was then sealed in a 23 mL Teflon-lined stainless steel autoclave and heated at 220°C for three days under autogenous pressure. The reaction vessel was then cooled to room temperature over 4 hours. Light pink rectangular crystals of **1** suitable for single crystal X-ray diffraction analysis were collected from the final reaction system by filtration and dried in air at ambient temperature (43.35% yield based on Mn). *Anal.* calcd: C, 35.41% H, 1.26 N, 5.90%. Found: C, 35.32% H, 1.34%, N, 5.76%. IR data ( $\nu_{\text{max}}$  / cm<sup>-1</sup>): 3471sbr, 1634s, 1587m, 1448w, 1429m, 1403m, 1375s, 1270w, 1121m, 1033m, 928w, 802w, 797s, 722m, 687s.

An identical procedure as that for **1** was followed to prepare **2**, except that equimolar CoCl<sub>2</sub>·6H<sub>2</sub>O was used in place of MnCl<sub>2</sub>·4H<sub>2</sub>O. For **2**, yield: 49.11% based on Co. *Anal.* calcd: C, 34.82% H, 1.24 N, 5.80%. Found: C, 34.70% H, 1.55%, N, 5.72%. IR data ( $\nu_{\text{max}}$  / cm<sup>-1</sup>): 3472sbr, 1632s, 1584m, 1448w, 1429m, 1403m, 1373s, 1270w, 1152m, 1032m, 921w, 805w, 767s, 718m, 680s. The IR spectra of **1** and **2** are fully identical.

### Crystallographic Analyses

Crystallographic data of **1** and **2** were collected at 150 K on a Bruker kappa APEXII-CCD area detector instrument with Mo K $\alpha$  monochromated radiation ( $\lambda = 0.71073$  Å) using the  $\omega$ - $\phi$  scan technique. An empirical absorption correction was applied. The structures were solved by direct methods and refined by full-matrix least squares against  $F^2$  using the SHELXS-97 and SHELXL-97 programs.<sup>[14]</sup> Anisotropic thermal parameters were assigned to all non-hydrogen atoms. The hydrogen atoms were set in calculated positions and refined as riding atoms with a common fixed isotropic thermal parameter. Analytical expressions of neutral atom scattering factors were employed, and anomalous dispersion corrections were incorporated. The crystallographic data for **1** and **2** are listed in Table 1. Selected bond angles and bond lengths are given in table S1 in the supplementary data. The crystallographic data has been deposited in the CCDC and can be obtained free of charge from The Cambridge Crystallographic Data Centre via [www.ccdc.cam.ac.uk/data\\_request/cif](http://www.ccdc.cam.ac.uk/data_request/cif) quoting: CCDC 780933 & 780934.

## Acknowledgements

This work was supported by the Australian Research Council Discovery Project grant DP0880199. The authors acknowledge Dr. Roland Bircher for helpful discussions when preparing the manuscript. The authors also would like to thank Dr. Rene Macquart at the University of Sydney for his assistance with collecting magnetic data.

- [1] a) H. L. Ngo, A. G. Hu, W. B. Lin, *J. Mol. Catal. A* **2004**, *215*, 177; b) C. Sanchez, B. Lebeau, F. Chaput, J. P. Boilet, *Adv. Mater.* **2003**, *15*, 1969; c) I. Honma, S. Nomura, H. Nakajima, *J. Membr. Sci.* **2001**, *185*, 83; d) A. C. Sudik, A. R. Millward, N. W. Ockwig, A. P. Cote, J. Kim, O. M. Yaghi, *J. Am. Chem. Soc.* **2005**, *127*, 7110; e) J. L. C. Rowsell, A. R. Millward, K. S. Park, O. M. Yaghi, *J. Am. Chem. Soc.* **2004**, *126*, 5666.
- [2] a) O. Kahn, J. Larionova, J. V. Yakhmi, *Chem. Eur. J.* **1999**, *5*, 3443; b) D. Maspocho, D. Ruiz-Molina, K. Wurst, N. Domingo, M. Cavallini, F. Biscarini, J. Tejada, C. Rovira, J. Veciana, *Nat. Mater.* **2003**, *2*, 190; c) M. A. Nadeem, D. J. Craig, R. Bircher, J. A. Stride, *Dalton Trans.* **2010**, *39*, 4358.
- [3] a) T. Kajiwar, A. Kamiyama, T. Ito, *Chem. Commun.* **2002**, 1256; b) J. R. Galán-Mascarós, K. R. Dunbar, *Angew. Chem., Int. Ed.* **2003**, *42*, 2289; c) D. Maspocho, D. Ruiz-Molina, J. Veciana, *J. Mater. Chem.* **2004**, *14*, 2713; d) R. D. Poulsen, A. Bentien, M. Chevalier, B. B. Iversen, *J. Am. Chem. Soc.* **2005**, *127*, 9156; e) L. Arai, M. A. Nadeem, M. Bhadbhade, J. A. Stride, *Dalton Trans.* **2010**, *39*, 3372.
- [4] a) P. Rabu, M. Drillon, *Adv. Eng. Mater.* **2003**, *5*, 189; b) V. Laget, C. Hornick, P. Rabu, M. Drillon, R. Ziessel, *Coord. Chem. Rev.* **1998**, *178*, 1533; c) E. Coronado, P. Day, *Chem. Rev.* **2004**, *104*, 5419.

- [5] a) A. Rujiwatra, C. J. Kepert, J. B. Claridge, M. J. Rosseinsky, H. Kumagai, M. Kurmoo, *J. Am. Chem. Soc.* **2001**, *123*, 10584; b) M. Kurmoo, H. Kumagai, S. M. Hughes, C. J. Kepert, *Inorg. Chem.* **2003**, *42*, 6709; c) Z. M. Wang, B. Zhang, M. Kurmoo, A. Green, H. Fujiwara, T. Otsuka, H. Kobayshi, *Inorg. Chem.* **2005**, *44* 1230; d) L. G. Beauvais, J. R. Long, *J. Am. Chem. Soc.* **2002**, *124*, 12096; e) J. L. Atwood, *Nat. Mater.* **2002**, *1*, 91.
- [6] X.-M. Zhang, Y.-Z. Zheng, C.-R. Li, W.-H. Zhang, X.-M. Chen, *Crys. Grow. Des.* **2007**, *7*, 980.
- [7] a) M. Kurmoo, H. Kumagai, S. M. Hughes, C. J. Kepert, *Inorg. Chem.* **2003**, *42*, 6709; b) W. Kaneko, M. Ohba, S. Kitagawa, *J. Am. Chem. Soc.* **2007**, *129*, 13706; c) Y.-Z. Zheng, X. Xue, S.-L. Zheng, M.-L. Tong, X.-M. Chen, *Adv. Mater.* **2008**, *20*, 1534.
- [8] (a) C. J. Milios, R. Inglis, A. Vinslava, R. Bagai, W. Wernsdorfer, S. Parsons, S. P. Perlepes, G. Christou, E. K. Brechin, *J. Am. Chem. Soc.* **2007**, *129*, 1250; b) R. Inglis, L. F. Jones, K. Mason, A. Collins, S. A. Moggach, S. Parsons, S. P. Perlepes, W. Wernsdorfer, E. K. Brechin, *Chem. Eur. J.* **2008**, *14*, 9117.
- [9] K. Dwight, N. Menyuk, *Phys. Rev.* **1960**, *119*, 1470.
- [10] a) Y.-Z. Zheng, M.-L. Tong, W.-X. Zhang, X.-M. Chen, *Chem. Commun.* **2006**, 165; b) Y.-Z. Zheng, M.-L. Tong, W.-X. Zhang, X.-M. Chen, *Angew. Chem., Int. Ed.* **2006**, *45*, 6310; c) Y.-Z. Zheng, M.-L. Tong, X.-M. Chen, *J. Mol. Struct.* **2006**, *796*, 9; d) M.-H. Zeng, W.-X. Zhang, X.-Z. Sun, X.-M. Chen, *Angew. Chem., Int. Ed.* **2005**, *44*, 3079; e) X.-N. Chen, Y.-Z. Zheng, W.-X. Zhang, X.-M. Chen, *Chem. Commun.* **2006**, 3603.
- [11] X.-M. Zhang, Z.-M. Hao, W.-X. Zhang, X.-M. Chen, *Angew. Chem., Int. Ed.* **2007**, *46*, 3456.
- [12] Y.-Z. Zheng, M.-L. Tong, W.-X. Zhang, X.-M. Chen, *Chem. Commun.* **2006**, 165.
- [13] O. Kahn, *Molecular Magnetism*; VCH: Weinheim, Germany, **1993**.
- [14] G. M. Sheldrick, *SHELXS 97*, Program for the Solution of Crystal Structures; University of Göttingen: Germany, **1997**.

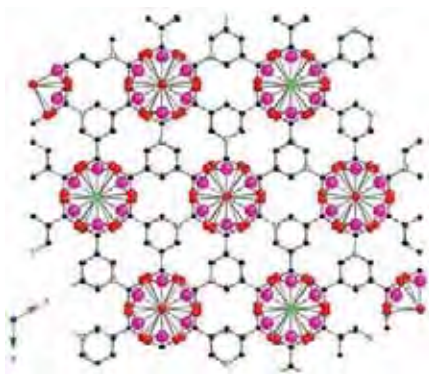
---

Received: ((will be filled in by the editorial staff))  
 Revised: ((will be filled in by the editorial staff))  
 Published online: ((will be filled in by the editorial staff))

## Molecular magnets

Muhammad A. Nadeem, M. Bhadbhade  
and John A. Stride\* \_\_\_\_\_ **Page –**  
**Page**

Two iso-structural metal-organic  
frameworks having long-range magnetic  
ordering at 45 K\*\*



Two 3D isostructural magnetic metal-organic frameworks (MMOFs) based on  $\mu_3$ -O centered trimetallic clusters, have been synthesized which offer a rare example of controlled bulk magnetic ordering at significantly higher temperatures (45 K) than other similar materials.



## Supporting Information

### Two iso-structural metal-organic frameworks having long-range magnetic ordering at 45 K

*Muhammad Arif Nadeem, Mohan Bhadbhade, Roland Bircher and John Arron Stride\**

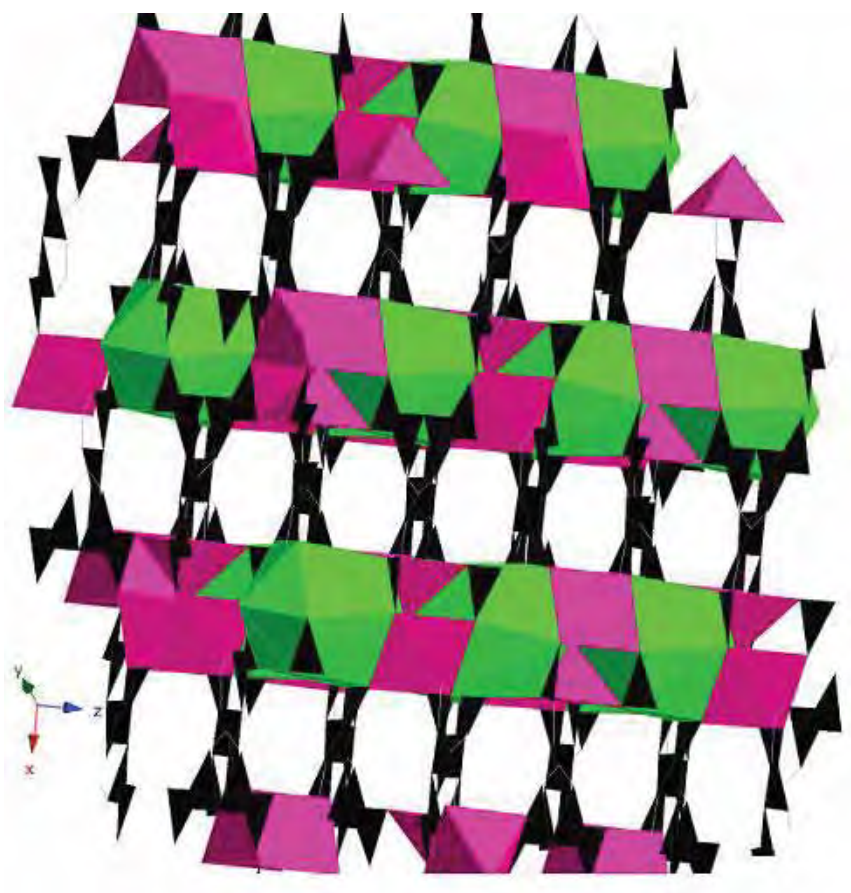


**Figure S1.** A view showing the microporous nature of the materials

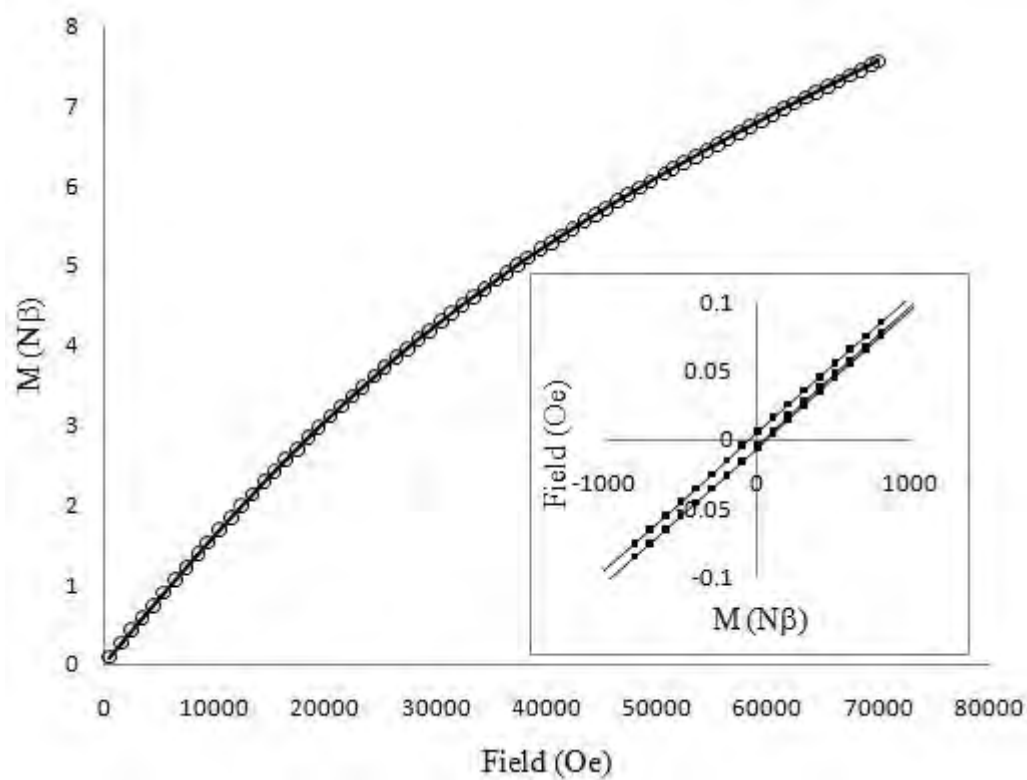


**Figure S2.** Moment vs. Field plot of Complex **1**, inset showing the hysteresis loop

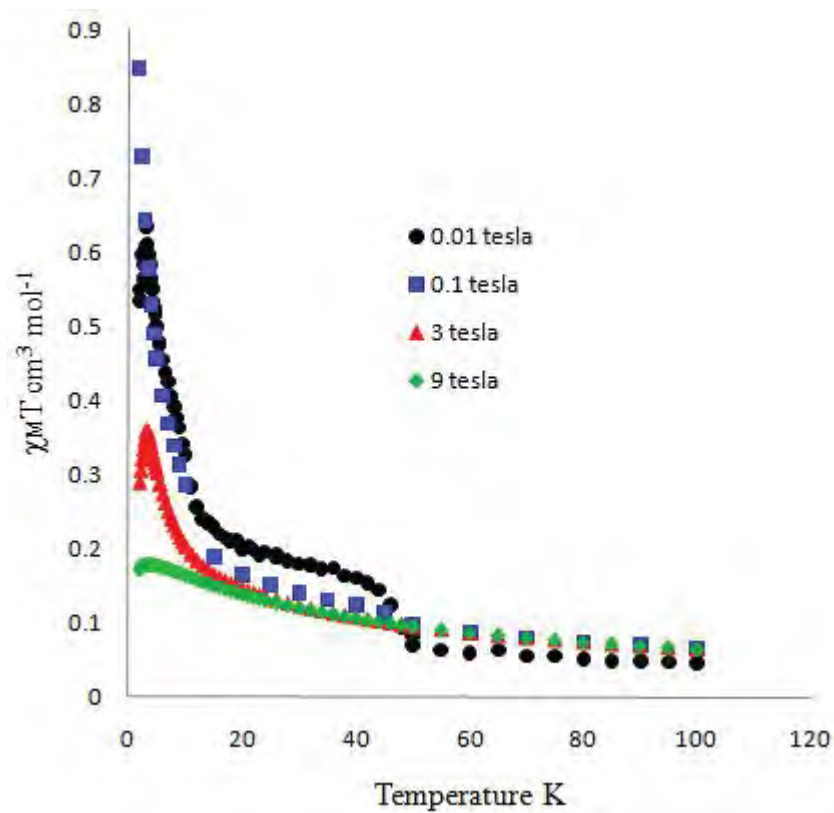


**Figure S3.**  $\chi_M$  vs.  $T$  plot of complex **2** at various fields

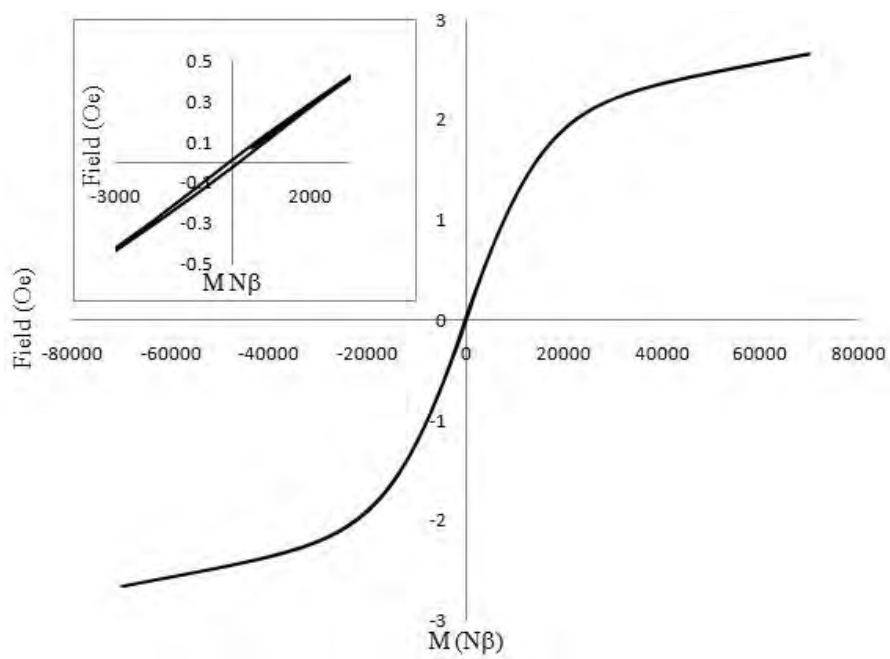


**Figure S4.** Moment vs. Field plot of Complex **2**, inset showing the hysteresis loop

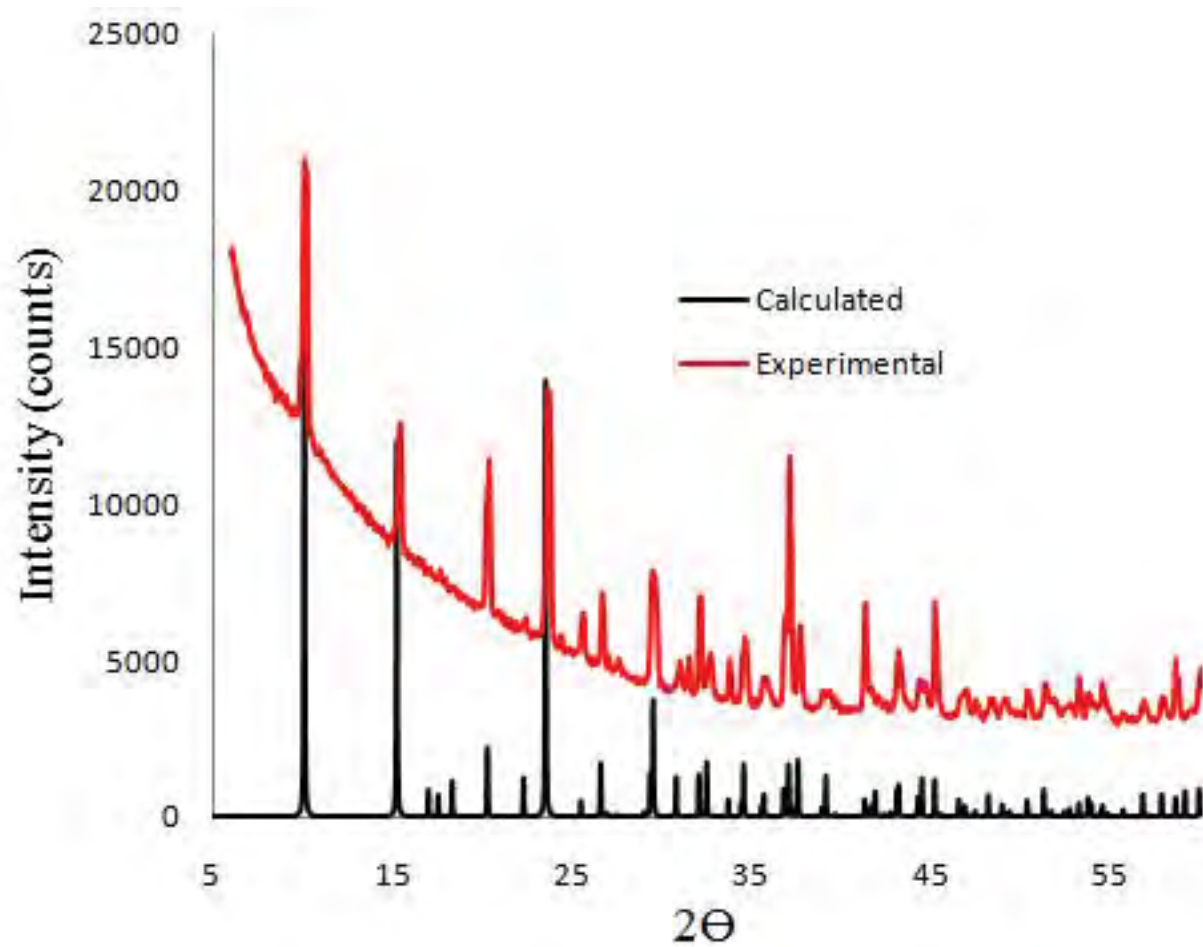


**Figure S5.** Comparison of calculated and experimental powder XRD pattern of complex **1**

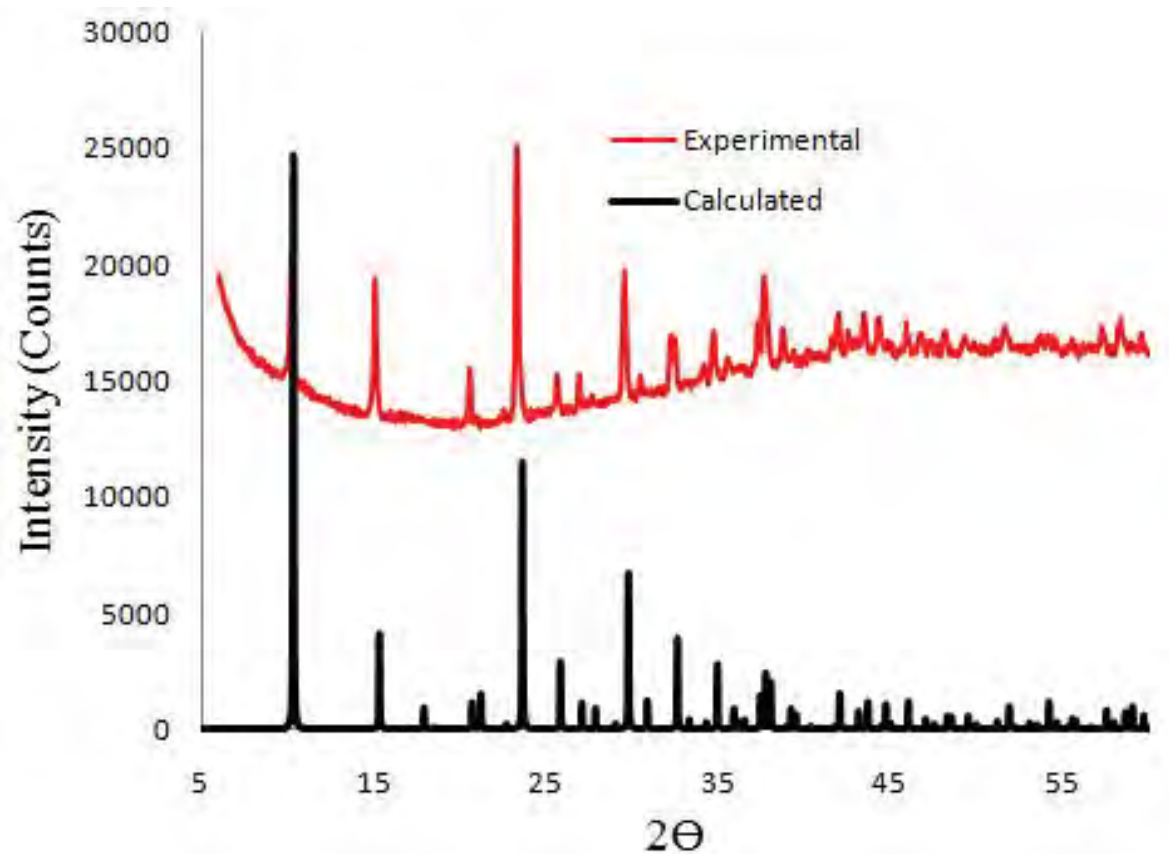


**Figure S6.** Comparison of calculated and experimental powder XRD pattern of complex 2



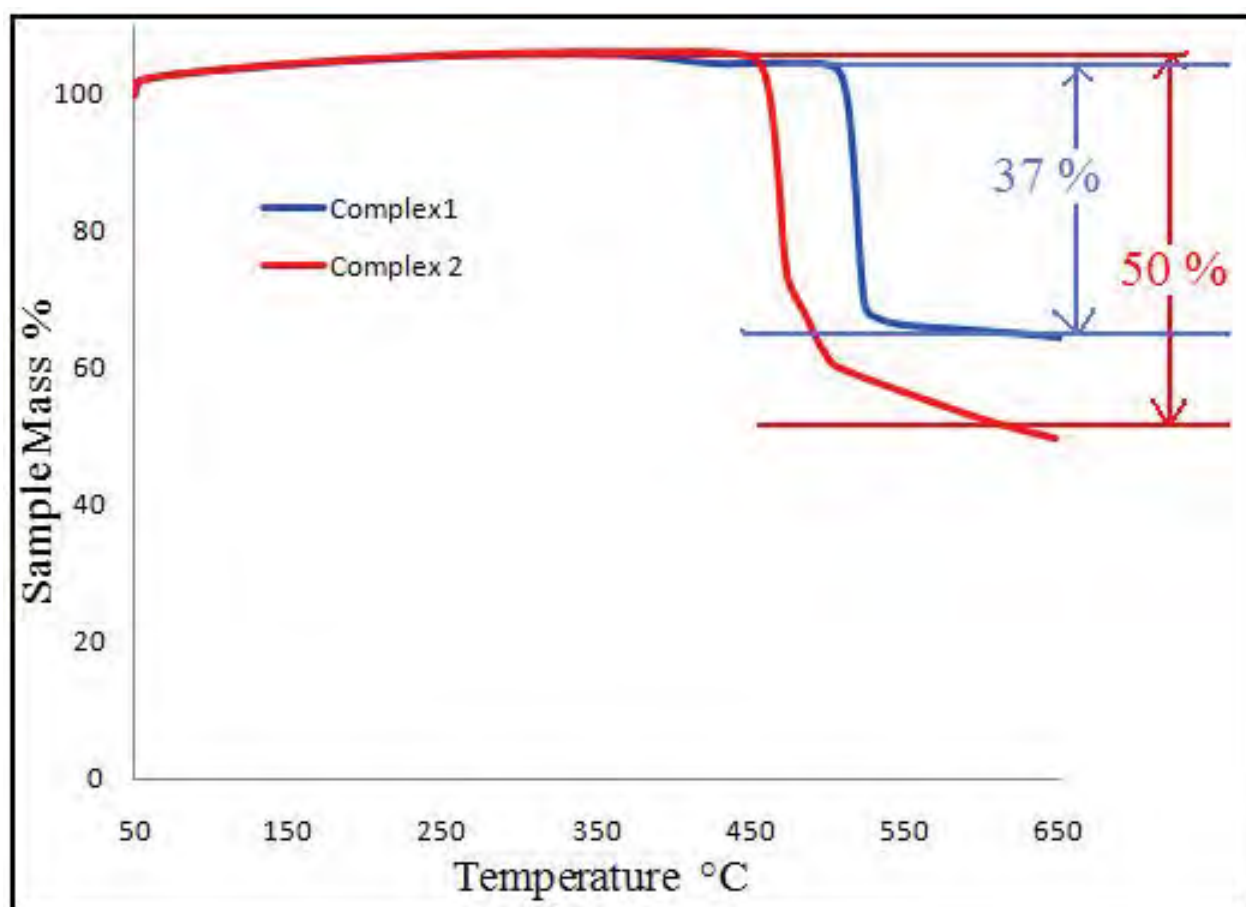


**Figure S7.** Thermogravimetric analysis of complex 1-2

**Table S1:** Selected bond lengths (Å) and bond angles (°) of **1** and **2**

Compound <b>1</b> <sup>a</sup>			
Mn1-O1 <sup>i</sup>	2.154 (2)	O1-Mn1-O1A	90.64 (6)
Mn1-O3 <sup>i</sup>	2.165 (2)	O3 <sup>i</sup> -Mn1-O1A	88.76 (6)
Mn1-O3	2.165 (2)	O3-Mn1-O1A	88.76 (6)
Mn1-O1A	2.1725 (6)	O1 <sup>i</sup> -Mn1-N1	89.36 (6)
Mn1-N1	2.264 (4)	O1-Mn1-N1	89.36 (6)
O1 <sup>i</sup> -Mn1-O1	178.73 (12)	O3 <sup>i</sup> -Mn1-N1	91.24 (6)
O1 <sup>i</sup> -Mn1-O3 <sup>i</sup>	90.03 (10)	O3-Mn1-N1	91.24 (6)
O1-Mn1-O3 <sup>i</sup>	90.00 (10)	O1A-Mn1-N1	180.0
O1 <sup>i</sup> -Mn1-O3	90.00 (10)	Mn1 <sup>iii</sup> -O1A-Mn1	120.0
O1-Mn1-O3	90.02 (10)	Mn1 <sup>iii</sup> -O1A-Mn1 <sup>iv</sup>	120.0
O3 <sup>i</sup> -Mn1-O3	177.52 (13)	Mn1-O1A-Mn1 <sup>iv</sup>	120.0
O1 <sup>i</sup> -Mn1-O1A	90.64 (6)		
Compound <b>2</b> <sup>b</sup>			
Co1-O1 <sup>i</sup>	2.099 (3)	O2-Co1-O3	92.55 (9)
Co1-O1	2.099 (3)	O1 <sup>i</sup> -Co1-O3 <sup>i</sup>	89.96 (14)
Co1-O2	2.1008 (8)	O1-Co1-O3 <sup>i</sup>	90.02 (15)
Co1-O3	2.101 (4)	O2-Co1-O3 <sup>i</sup>	92.55 (9)
Co1-O3 <sup>i</sup>	2.101 (4)	O3-Co1-O3 <sup>i</sup>	174.90 (18)
Co1-N1	2.160 (5)	O1 <sup>i</sup> -Co1-N1	89.77 (9)
O2-Co1 <sup>iii</sup>	2.1008 (8)	O1-Co1-N1	89.77 (9)
O2-Co1 <sup>iv</sup>	2.1008 (8)	O2-Co1-N1	180.000 (2)
O1-Co1-O2	90.23 (9)	O3-Co1-N1	87.45 (9)
O1 <sup>i</sup> -Co1-O3	90.02 (15)	O3 <sup>i</sup> -Co1-N1	87.45 (9)
O1-Co1-O3	89.96 (14)		

<sup>a</sup> (i)  $y-1/3, x+1/3, -z+11/6$ ; (ii)  $-x, -y+1, -z+2$ ; (iii)  $-x+y, -x+1, z$ ; (iv)  $-y+1, x-y+1, z$ .

<sup>b</sup> (i)  $-x+2, -x+y+1, -z+3/2$ ; (ii)  $-x+5/3, -y+4/3, -z+4/3$ ; (iii)  $-y+2, x-y+1, z$ ; (iv)  $-x+y+1, -x+2, z$ .

**A series of novel isostructural metal-organic  
frameworks constructed from mixed flexible ligands:  
Synthesis, crystal structure and physical properties**

*Maggie Chai Cin Ng, Muhammad Arif Nadeem and John Arron Stride*

**ACKNOWLEDGMENT OF CONTRIBUTION TO AUTHORSHIP**

The article is submitted in journal “*Inorganic Chemistry*”. J.A.S. conceived and managed the research project, M.A.N. and M.C.C.N. synthesised the samples. M.A.N. solved the crystal structure. M.A.N. and M.C.C.N. collected, interpreted the magnetic data and wrote the manuscript. All authors discussed the results and commented on this manuscript.

# **A series of novel isostructural metal-organic frameworks constructed from mixed flexible ligands: Synthesis, crystal structure and physical properties**

*Maggie Chai Cin Ng,<sup>†</sup> Muhammad Arif Nadeem,<sup>†</sup> and John Arron Stride<sup>\*†,‡</sup>*

<sup>†</sup> *School of Chemistry, University of New South Wales, Sydney, NSW 2052, Australia. Fax: +61 (02) 9385 6141; Tel: +61 (0)2 9385 4675; E-mail: j.stride@unsw.edu.au*

<sup>‡</sup> *Bragg Institute, Australian Nuclear Science and Technology Organisation, PMB 1, Menai, NSW 2234, Australia.*

Four new isostructural coordination polymers,  $[M(pda)(dpe)]_n$  where  $[M = Mn^{II}(1), Co^{II}(2), Ni^{II}(3) \text{ and } Cu^{II}(4)]$  have been synthesised based upon the flexible ligand 1,4-phenylene diacetic acid ( $H_2pda$ ) and auxiliary ligand 1,2-di-(4-pyridyl)-ethane ( $dpe$ ) under hydrothermal conditions. These new compounds were characterised by single-crystal X-ray diffraction, elemental analysis, IR spectroscopy, thermo-gravimetric analysis and variable temperature magnetic susceptibility measurements. X-ray analysis reveals that all 4 compounds crystallise in the monoclinic space group  $P2_1/n$ , with the basic structure made up of dimers of metals linked with  $pda$  ligands to form a chain. Each chain is then linked by the  $dpe$  ligand. Thermal analysis shows that **1-2** are stable up to 310°C whilst **3** showed the highest stability at 375°C among all of the isostructural compounds. Variable temperature magnetic susceptibility measurements revealed that there are antiferromagnetic coupling interactions between the metal ions within the dimers of compounds **1-3**. These dimers then couple

ferromagnetically along the chains in **1** and **2**, each chain then couples antiferromagnetically to neighbouring chains. Compounds **1-2** also show bulk magnetic ordering at ca. 45 and 55 K, respectively. However, in **3**, there is no indication of magnetic ordering phenomena in the temperature range from 300 – 2.5 K. The thermal and magnetic data of **4** were not collected as a result of insufficient sample quantity.

## Introduction

The considerable attention garnered by porous coordination polymers or metal organic frameworks (MOFs) as they are commonly known, is attributed to their porosity, tunability and potential utilisation in a wide variety of applications.<sup>1</sup> The ability of MOFs to outperform porous carbon in the sequestration of carbon dioxide,<sup>2</sup> holding the highest recorded Langmuir surface area to date of 10400 m<sup>2</sup>/g<sup>3</sup> and to exceed targets set out by the DOE for H<sub>2</sub> storage by weight percent,<sup>4</sup> proves the versatility and utility of these materials. The wide diversity in the binding modes of carboxylate groups has made ligands containing carboxylate groups some of the most widely used, in forming rigid MOFs upon polymeric coordination to metal centres, or small metallic clusters. The rigidity of MOFs has been intrinsically linked to their stability in the absence of guest molecules located within the pores and as such, has been a characteristic much sought after over the past decade or so.<sup>5</sup> However, only recently has there been a pronounced shift to incorporate more flexibility into MOFs.<sup>6</sup> According to Zeng *et al.*, flexible ligands may result in the connection of metal ions in different directions, depending upon the freedom of rotation and the twist angles of the flexible skeletons. This character of flexible ligands may lead to interesting MOFs with unique properties such as breathing or bellows-like behaviours, magnetism and adaptive recognition properties,<sup>7</sup> all features that have drawn us to the synthesis of MOFs incorporating flexible ligands. Nevertheless with the introduction of flexibility, the stability of these materials upon guest desorption must also be considered; a fine balance between highly flexible ligands and stable MOFs is not trivial to achieve. In addition, over the past two decades, many researchers have been interested in the bulk magnetic properties of hybrid organic-inorganic materials. Such materials are excellent candidates for the study of fundamental magnetism phenomena, such as spin canting, metamagnetism and three dimensional magnetism.<sup>8</sup> To achieve such magnetic entities, the reasonable choice of proper bridging ligands is of ultimate importance because they can communicate magnetic couplings between metal ions, determining both the nature and strength of the magnetic interactions.<sup>9</sup>

In light of above mentioned facts, we decided to use the combination of flexible organic ligands to form 3D MOFs, with the view that flexible ligands not only can give rise to a variety of structures but also adopt various pathways to communicate the magnetic information between metal ions.

In this present study, we carried out the hydrothermal synthesis of four novel MOFs  $[\text{Mn}(\text{pda})(\text{dpe})]_n$  **1**,  $[\text{Co}(\text{pda})(\text{dpe})]_n$  **2**,  $[\text{Ni}(\text{pda})(\text{dpe})]_n$  **3** and  $[\text{Cu}(\text{pda})(\text{dpe})]_n$  **4**, controlling the conditions to synthesize these four isostructural and stable MOFs using the flexible ligand 1,4-phenylene diacetic acid ( $\text{H}_2\text{pda}$ ) with the auxiliary ligand 1,2-di-(4-pyridyl)-ethane (dpe), also we were able to incorporate the aforementioned desired characteristics into the MOFs.

## **Experimental Section**

### **Materials and Physical Techniques**

All reagents and solvents employed were commercially available and used as received without further purification. The syntheses of **1-4** were carried out in 23 mL Teflon-lined autoclaves under autogenous pressure. Elemental analyses were performed on a Carlo Erba Elemental Analyser EA 1108. The FT-IR spectra were measured with an AVATAR 320 spectrometer on KBr disks. Thermal analyses were carried out under nitrogen using a Mettler Toledo TGA/DSC 1, with the heating rate of  $10^\circ\text{C min}^{-1}$ .

### **Magnetometry**

Variable temperature magnetic susceptibility and magnetization measurements were performed with a Quantum Design PPMS EverCool system equipped with a vibrating sample magnetometer and a 9 T magnet. Clean crystals were picked out manually, crushed and loaded in a plastic sample holder for data collection. The magnetic susceptibility measurements were performed for field-cooled and zero-field-cooled samples in magnetic fields of 0.1 T. Pascal's constants were used to estimate the diamagnetic corrections.<sup>10</sup> Magnetization data were collected in fields up to 9 T and in the temperature range between 2.5 and 300.0 K. Hysteresis loops were measured at 2.5 and 5 K with maximum fields of  $\pm 9.0$  T.



**Synthesis of [Mn(pda)(dpe)]<sub>n</sub> (1), [Co(pda)(dpe)]<sub>n</sub> (2), [Ni(pda)(dpe)]<sub>n</sub> (3) and [Cu(pda)(dpe)]<sub>n</sub> (4)**

1 mmol of 1,4-H<sub>2</sub>pda (0.194 g) was stirred in a 6 mL solution of KOH (3 mmol, 0.168 g) for 10 minutes, followed by the dropwise addition of a solution of MnCl<sub>2</sub>·4H<sub>2</sub>O (0.197 g, 1 mmol) in 4 mL H<sub>2</sub>O. The resulting solution was stirred for about 15 minutes at room temperature, sealed in a 23-mL Teflon-lined stainless steel autoclave and heated at 170°C for three days under autogenous pressure. The reaction system was subsequently cooled to room temperature over 6 hours. Light pink crystals of **1** suitable for single crystal X-ray diffraction analysis were collected from the final reaction mixture by filtration and dried in air at ambient temperature. Yield: 23.5% based on Mn. *Anal.* Calcd.: C, 61.26% H, 5.14% Found: C, 60.31% H, 4.69%. IR data ( $\nu_{\max}$  / cm<sup>-1</sup>): 3405mbr, 3057s, 3032m, 2939s, 2915s, 1571s, 1566, 1514m, 1428s, 1324m, 1287m, 1222s, 1167m, 1070m, 1014s, 944m, 930w, 829s, 813m, 744s, 722m, 648m, 630m, 588m, 546s, 492w, 456m.

An identical procedure as that for **1** was followed to prepare **2**, except that MnCl<sub>2</sub>·4H<sub>2</sub>O was replaced by CoCl<sub>2</sub>·6H<sub>2</sub>O (0.207 g, 1 mmol). Red crystals of **2** were obtained. Yield: 47% based on Co. *Anal.* calcd: C, 60.69.% H, 5.09% Found: C, 58.80 % H, 4.50 %. IR data ( $\nu_{\max}$  / cm<sup>-1</sup>): 3435wbr, 3062m, 2937s, 2917s, 1611s, 1567m, 1421s, 1399m, 1288m, 1220s, 1166m, 1070m, 1018s, 944m, 930w, 830s, 814m, 744s, 721m, 647m, 631m, 590m, 548s, 492w.

An identical procedure as that for **1** was followed to prepare **3**, except that MnCl<sub>2</sub>·4H<sub>2</sub>O was replaced by NiCl<sub>2</sub>·6H<sub>2</sub>O (0.237 g, 1 mmol). Light green crystals of **3** were obtained. Yield: 54% based on Ni. *Anal.* calcd: C, 60.72% H, 5.10% Found: C, 60.69 % H, 4.69 %. IR data ( $\nu_{\max}$  / cm<sup>-1</sup>): 3417wbr, 3065m, 2940s, 2917s, 1629s, 1567m, 1550m, 1421s, 1393m, 1286m, 1220s, 1165m, 1071m, 1023s, 944m, 930w, 831s, 815m, 743s, 721m, 647m, 631m, 591m, 546s, 466w.

An identical procedure as that for **1** was followed to prepare **4**, except that MnCl<sub>2</sub>·4H<sub>2</sub>O was replaced by Cu(NO<sub>3</sub>)<sub>2</sub>·2.5H<sub>2</sub>O (0.241 g, 1 mmol). Only few green crystals of **4** were obtained. Yield: <1% based on Cu. IR data ( $\nu_{\max}$  / cm<sup>-1</sup>): 3419wbr, 3051m, 2939s, 1609s, 1567m, 1551m, 1422s, 1396m, 1286w, 1221m, 1166w, 1071w, 1015m, 944m, 830s, 743m, 721m, 647m, 631w, 546s.

Powder XRD pattern of complexes **2** and **3** is shown in figures S2 and S3 of supplementary information.

## Crystallographic Analyses

Crystallographic data of **1-4** were collected at 150 K on a Bruker kappa APEXII-CCD area detector instrument with Mo K $\alpha$  monochromated radiation ( $\lambda = 0.71073$  Å) using the  $\omega$ - $\phi$  scan technique. An empirical absorption correction was applied. The structures were solved by direct methods and refined by full-matrix least squares against  $F^2$  using the SHELXS-97 and SHELXL-97 programs.<sup>11</sup> Anisotropic thermal parameters were assigned to all non-hydrogen atoms. The hydrogen atoms were set in calculated positions and refined as riding atoms with a common fixed isotropic thermal parameter. Analytical expressions of neutral atom scattering factors were employed, and anomalous dispersion corrections were incorporated. The crystallographic data for **1-4** are listed in Table 1. Selected bond angles and bond lengths are given in table S1 and S2 in the supplementary data. The crystallographic data has been deposited in the CCDC and can be obtained free of charge from The Cambridge Crystallographic Data Centre *via* [www.ccdc.cam.ac.uk/data\\_request/cif](http://www.ccdc.cam.ac.uk/data_request/cif) quoting: CCDC 796333 - 796336.

## Crystal Structure

The X-ray structure analysis revealed that **1-4** are isostructural, crystallising in a monoclinic system in the  $P2_1/n$  space group; complex **3** is taken here as an example to depict the structure in detail, which. Analysis of the single crystal X-ray diffraction data identifies only one crystallographically unique Ni<sup>II</sup> ion lying in an octahedral geometry. The basic structural unit of compound **3** (figure 1) highlights the differing binding modes of the carboxylate terminated pda ligands. The equatorial plane is occupied by 4 oxygen atoms, two of which (O3 and O4) belongs to two different pda ligands and make bonds with Ni1 at distance of 2.0225(15) and 2.0228(16) Å, respectively. The other two oxygen atoms (O1 and O2) belong to the same carboxylic group of a third pda ligand bound to Ni1 at respective distances of 2.1720(15) and 2.1527(16) Å. The axial positions are occupied by two nitrogen atoms (N1 and N2) of two different dpe ligands, having Ni-N bond lengths of 2.0799(17) and 2.0768(17) Å, to complete a distorted octahedral geometry. By twisting, the two flexible arms of the pda ligand can coordinate with Ni1 atoms in different fashions, two oxygen atoms of a carboxylic group of one arm are coordinated to two different Ni1 atoms, forming a dimer having a Ni-Ni distance of 4.219 Å, whilst the two oxygen atoms of other arm are connected with a single Ni1 atom of a neighbouring dimer; the dimers are thus separated by 8.050 Å. In addition, each dimer is linked to another dimer via nitrogen atoms of the dpe ligand at a

distance of 13.375 Å, forming 1D linear chains. All the benzene rings of pda and dpe ligands are alternately  $\pi$ - $\pi$  stacked with face-to-face distances of 13.375 and 4.198 Å. The flexibility of both the organic ligands allows the layers to interpenetrate to form 3D architectures (packing diagrams along *b* and *c*- axes are shown in figures 2 and 3 respectively).

### Thermogravimetric analysis

Thermogravimetric analyses were performed on samples **1-3** to explore their thermal stabilities (see figure S1 of supplementary informations). Complexes **1** and **2** show similar thermal stabilities with a plateau region from 50-310 °C suggesting that there are no solvent molecules in the crystalline lattice. A slight loss of mass (<5%) starting at 200°C for complex **1** is attributed to the loss of excess 1,4-phenylene diacetic acid. The decomposition of complexes **1** and **2** to their respective oxides is indicated by the weight loss of 63.51% (Calc: 83.55% assuming MnO as residue) and 65.56 % (Calc: 82.78% assuming CoO as residue) respectively. Complex **3** shows the highest thermal stability of the three iso-structural complexes with a plateau region extending from 50 to 375 °C, followed by a decrease in weight, indicative of decomposition of the complex, with a weight loss of 67.71% (Calc: 82.83% assuming NiO as residue). Due to the very low yield, the thermal analysis of complex **4** has not performed.

### Magnetic Properties

The temperature dependence of the magnetic susceptibilities of **1-3** were measured in the temperature range of 2.5-300 K, with an applied magnetic field of 0.1 T. The magnetic susceptibility data of **1** is shown in figure 4. The reciprocal susceptibility *versus* temperature plot obeys the Curie-Weiss law, with  $C = 4.2493(117) \text{ cm}^3 \text{ K mol}^{-1}$  and  $\theta = -3.842(3) \text{ K}$ . At room temperature the  $\chi_M T$  value of  $4.195 \text{ cm}^3 \text{ K mol}^{-1}$  is comparable with the expected spin only value of  $4.375 \text{ cm}^3 \text{ K mol}^{-1}$  for a single  $\text{Mn}^{\text{II}}$  ion ( $S = 5/2$ ,  $g = 2.0$ ), consistent with **1** being paramagnetic at room temperature. As the temperature was decreased,  $\chi_M T$  decreased slightly to  $3.821 \text{ cm}^3 \text{ K mol}^{-1}$  at 49 K, indicative of slight antiferromagnetic coupling interactions between the  $\text{Mn}^{\text{II}}$  ions within the dimers. Upon further cooling  $\chi_M T$  then increases to a maximum value of  $4.966 \text{ cm}^3 \text{ K mol}^{-1}$  at around 38 K and additional cooling

brings about a gradual decrease, until finally reaching a minimum value of  $0.903 \text{ cm}^3 \text{ K mol}^{-1}$  at 3 K (figure 4b). Therefore at low temperatures, it can be seen that there is an onset of long-range ferromagnetic ordering between the dimers of  $\text{Mn}^{\text{II}}$  ions along the chain, which is consistent with the bifurcation at 40 K of the direct-current zero-field-cooled (ZFC) and field-cooled (FC) susceptibilities. At 25 K a slight bump in the  $\chi_M T$  values is indicative of a change in the magnetic response, going from a ferromagnetic to an antiferromagnetic behaviour. Spontaneous magnetization is confirmed by plotting the FC  $\chi_M T$  values at different applied fields as a function of temperature, which shows a spontaneous increase around 45 K and is more pronounced at lower field strengths (figure 4d). The bulk magnetic ordering is also confirmed by plotting FC and ZFC curve against temperature, where a bifurcation of ZFC-FC the curves provides a clear indication of long-range magnetic ordering (LRMO). The field dependent magnetization at 2.5 K suggests that saturation magnetization is not reached even at the highest applied magnetic field of 9 T (figure S4 of supporting information). The magnetization reaches a saturation moment,  $M_s$  ( $T = 2.5 \text{ K}$ ) of  $4.40 \text{ N}\beta$ , slightly less than the expected maximum value of  $5 \text{ N}\beta$ , whilst the hysteresis loop measured at 5 K is consistent with soft magnetic behaviour in **1** (figure 4c), having a remanent magnetization of  $0.02 \text{ N}\beta$  and a coercive field of ca.  $300 \text{ Oe}$ .<sup>12</sup>

The dc-magnetic susceptibility ( $\chi_M$ ) data of a polycrystalline sample of **2** is given in figure 5. At room temperature, the value of  $\chi_M T$  is  $2.868 \text{ cm}^3 \text{ mol}^{-1} \text{ K}$  is comparable with the expected spin only value for a single  $\text{Co}^{\text{II}}$  ion ( $g = 2.4$ ), indicating paramagnetism at room temperature. Upon cooling,  $\chi_M T$  decreases slowly with decreasing temperature and reaches a value of  $2.610 \text{ cm}^3 \text{ mol}^{-1} \text{ K}$  at 65 K. The  $\chi_M^{-1}$  vs  $T$  plot above 65 K is linear and well fitted by Curie-Weiss law ( $\chi_M = C/(T - \theta)$ ), with  $C = 2.876(4) \text{ cm}^3 \text{ mol}^{-1} \text{ K}$ ,  $\theta = -3.2597(16)$ ; the value of the Weiss constant is indicating a moderate antiferromagnetic coupling between the  $\text{Co}^{\text{II}}$  ions within the dimers. On cooling further  $\chi_M T$  increases abruptly and reaches a maximum value of  $3.083 \text{ cm}^3 \text{ mol}^{-1} \text{ K}$  at 55 K, which again indicates ferromagnetic interactions between the dimers. On further cooling  $\chi_M T$  once again steadily decreases to  $2.21 \text{ cm}^3 \text{ K mol}^{-1}$  at 18 K before again increasing to  $2.82 \text{ cm}^3 \text{ K mol}^{-1}$  at 10 K.  $\chi_M T$  then decreases down dramatically to a minimum of  $1.32 \text{ cm}^3 \text{ K mol}^{-1}$  at about 3 K. The abrupt changes in the  $\chi_M T$  at ca. 65 and 10 K are attributed to the onset of LRMO and a magnetic phase change from collinear antiferromagnetic to canted antiferromagnetism at 10 K. The LRMO in compound **2** is also confirmed by the bifurcation of FC and ZFC curves, figure 5a. The FC  $\chi_M T$  values at

different applied fields as a function of temperature show a spontaneous increase around 65 and 10 K, which are more pronounced at lower field strengths (figure 5d). The decrease in the value of  $\chi_M T$  below 10 K may be a result of magnetic field saturation effects.<sup>10</sup> The presence of bulk ordering in **2** is further supported by cycling the applied field between  $\pm 25$  kOe at 2.5 and 5 K, resulting in hysteresis loops (figure 5c), in which the coercive field ( $H_c$ ) of 390 Oe and remanent magnetizations ( $M_r$ ) of 0.0225 N $\beta$  are obtained at 2.5 K, highlighting the soft magnetic behaviour of **2**, consistent with **1**. The field dependent magnetization at 2.5 K suggests that saturation magnetization is not reached even at the highest applied magnetic field of 9 T (figure S4 of supporting information), where the magnetization reaches a saturation moment,  $M_s$  ( $T = 2.5$  K) of 2.30 N $\beta$ , less than the expected maximum value of 3.6 N $\beta$ . This observation supports the canted antiferromagnetic behaviour of **2** at low temperature. Recently we have reported the magnetic interactions between similar dimeric systems linked together via rigid ligands such as 4,4'-dipyridyl, where we have seen that coupling interactions between the dimers are not strong enough to give rise to LRMO phenomena.<sup>13</sup> This study allows us to conclude that the use of flexible ligands not only changes the structural topology but also plays an important role in changing the magnetic exchange pathways between the metal centers in the structure.

The magnetic properties of compound **3** are shown in figure 6. The  $\chi_M T$  value of 1.276 cm<sup>3</sup> K mol<sup>-1</sup> (calculated per high-spin d<sup>8</sup> Ni<sup>II</sup> ions) at room temperature is slightly higher than the spin only value of 1.21 cm<sup>3</sup> K mol<sup>-1</sup> ( $g = 2.2$ ) due to spin orbit coupling. Upon cooling the sample,  $\chi_M T$  decreases slowly with decreasing temperature until 100 K, which upon further cooling starts decreasing gradually before reaching a minimum value of 0.0949 cm<sup>3</sup> K mol<sup>-1</sup> at 3 K. By plotting  $\chi_M^{-1}$  vs.  $T$  in the temperature range of 100 - 300 K, we obtained a Weiss constant value of  $\theta = -22.359(5)$  K and a Curie constant of  $C = 1.3927(8)$  cm<sup>3</sup> K mol<sup>-1</sup>. This behaviour suggests antiferromagnetic coupling interactions between the Ni<sup>II</sup> ions, as indicated by the negative value of the Weiss constant. There was no discernable difference between the ZFC and FC curves for **3**, indicating the absence of LRMO. It was surprising for us that **3** did not show any LRMO phenomena given that **3** is isostructural to **1** and **2**. However, apart from the structural topologies, the magnetic nature is basically dependent on the metal centers and their interactions within the structure. Even for isostructural frameworks, dissimilar magnetic phenomena often arise from different local anisotropy of the metal centers.<sup>14</sup> Several isomorphous systems having varying magnetic behaviours have been reported before.<sup>14,15</sup> Recently, Sun *et al.*, reported three isostructural metal-organic frameworks with a

10-connected net based topology, but their magnetic properties were significantly different from each other.<sup>16</sup>

As the yield of the reaction forming **4** was very low, the magnetic data of this compound was not collected as a result of insufficient sample.

## Conclusions

Four new isostructural coordination polymers,  $[M(pda)(dpe)]_n$  where  $M = Mn(II), Co(II), Ni(II)$  or  $Cu(II)$  were hydrothermally synthesised. Compounds **1** and **2** display similar thermal properties and at low temperatures exhibit strong magnetic coupling interactions amongst metal ions which results in bulk magnetic ordering phenomena at ca. 45 and 55 K respectively. Compound **3** shows a higher degree of thermal stability, however, no bulk ordering has been observed even at temperatures as low as 2.5 K. The work shows that flexibility introduced by the pda ligand can be used to enhance and create new coordination polymers and exciting magnetic properties. This work also highlights our ability to control on isostructural syntheses of MOFs, which is rather difficult using flexible ligand systems.

## Acknowledgements

This work was supported by the Australian Research Council Discovery Project grant DP0880199. The authors acknowledge Dr. Hank De Bruyn at the University of Sydney for his assistance with collecting magnetic data and Dr. Mohan Bhadbhade of the Mark Wainwright Analytical Centre, UNSW, for his assistance with X-ray single crystallography.



**Table 1** Crystallographic data and structure refinement results for **1-4**

	<b>1</b>	<b>2</b>	<b>3</b>	<b>4</b>
Empirical formula	C <sub>22</sub> H <sub>20</sub> MnN <sub>2</sub> O <sub>4</sub>	C <sub>22</sub> H <sub>20</sub> CoN <sub>2</sub> O <sub>4</sub>	C <sub>22</sub> H <sub>20</sub> NiN <sub>2</sub> O <sub>4</sub>	C <sub>22</sub> H <sub>20</sub> CuN <sub>2</sub> O <sub>4</sub>
Formula weight	431.34	435.33	435.11	439.94
Temperature	150(2) K	150(2) K	150(2) K	150(2) K
Crystal system	Monoclinic	Monoclinic	Monoclinic	Monoclinic
Space group	<i>P</i> 2 <sub>1</sub> / <i>n</i>	<i>P</i> 2 <sub>1</sub> / <i>n</i>	<i>P</i> 2 <sub>1</sub> / <i>n</i>	<i>P</i> 2 <sub>1</sub> / <i>n</i>
<i>a</i> / Å	10.0972(9)	10.0823(6)	10.0663(14)	10.0566(5)
<i>b</i> / Å	14.3407(13)	14.3189(9)	14.3408(19)	14.3526(5)
<i>c</i> / Å	13.7469(10)	13.4931(6)	13.3748(15)	13.3587(5)
$\alpha$	90°	90°	90°	90°
$\beta$	102.892(3)	102.971(2)	102.744(6)	102.742(2)
$\gamma$	90°	90°	90°	90°
Volume / Å <sup>3</sup>	1940.4(3)	1898.26(18)	1883.2(4)	1880.69(13)
<i>Z</i>	4	4	4	4
$\rho$ / Mg m <sup>-3</sup>	1.477	1.523	1.535	1.554
<i>S</i>	1.06	1.36	1.03	1.13
<i>F</i> (000)	892	900	904	908
Limiting indices	-12 ≤ <i>h</i> ≤ 11 -17 ≤ <i>k</i> ≤ 15 -10 ≤ <i>l</i> ≤ 16	-11 ≤ <i>h</i> ≤ 11 -17 ≤ <i>k</i> ≤ 17 -15 ≤ <i>l</i> ≤ 16	-11 ≤ <i>h</i> ≤ 10 -12 ≤ <i>k</i> ≤ 17 -14 ≤ <i>l</i> ≤ 15	-9 ≤ <i>h</i> ≤ 11 -16 ≤ <i>k</i> ≤ 17 -15 ≤ <i>l</i> ≤ 15
Reflections number	3390	3328	3301	3283
<i>R</i> <sub>int</sub>	0.055	0.085	0.061	0.046
θ <sub>max</sub>	25.0°	25.0°	25.0°	25.0°
<i>wR</i> ( <i>F</i> <sup>2</sup> )	0.078	0.062	0.072	0.117

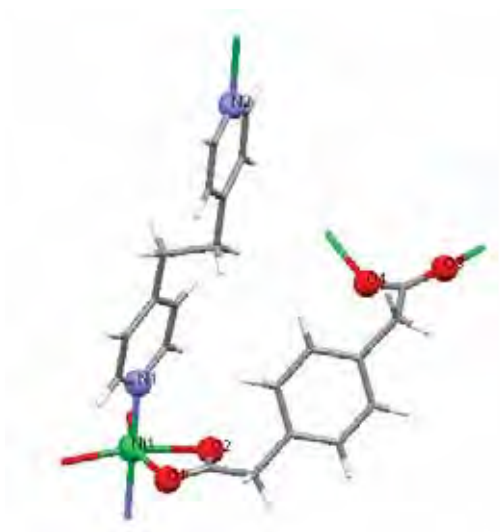


**Figure 1.** The basic structural unit of **3** showing flexibility of two pda and dpe ligands.

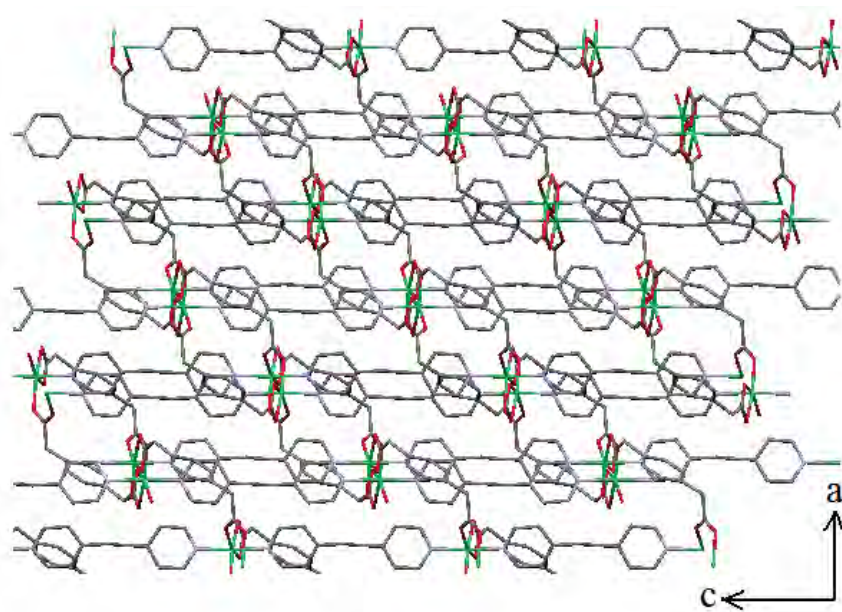


**Figure 2. (a)** A packing diagram of complex **3** in the *ac*-plane, showing connections between dimers via dpe ligands to form 1D chains along the *c*-axis, whilst two arms of interpenetrated pda ligands point towards same side to linking the dimers in the other direction.

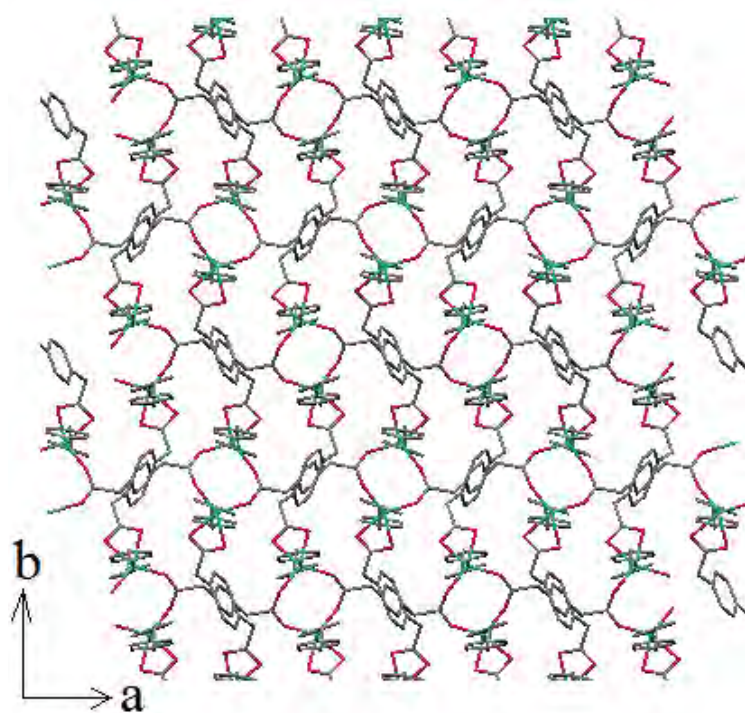


**Figure 3.** A packing diagram of complex **3** in the *ab*-plane, showing different binding modes of two arms of pda ligand to form the 3D architecture.

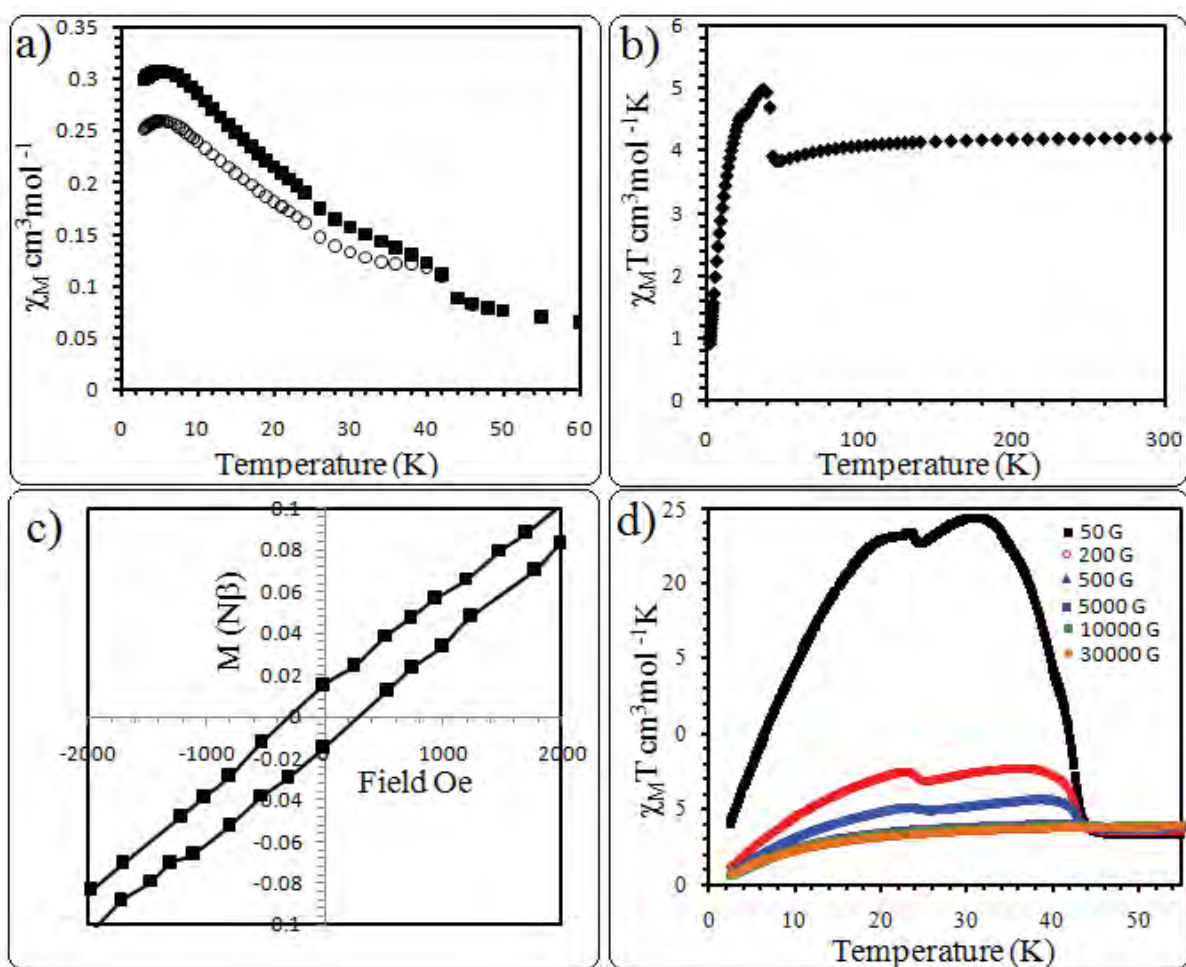


**Figure 4.** Magnetic data of **1**, (a) Field cooled (FC) and zero-field (ZFC) plot of  $\chi_M$  vs.  $T$  at  $H = 1000$  Oe, (b) Plot of  $\chi_M T$  vs.  $T$  ( $H = 1000$  Oe) (FC), (c) Magnetic hysteresis loops at 5 K, (d) Plot of  $\chi_M T$  vs.  $T$  at different applied fields.

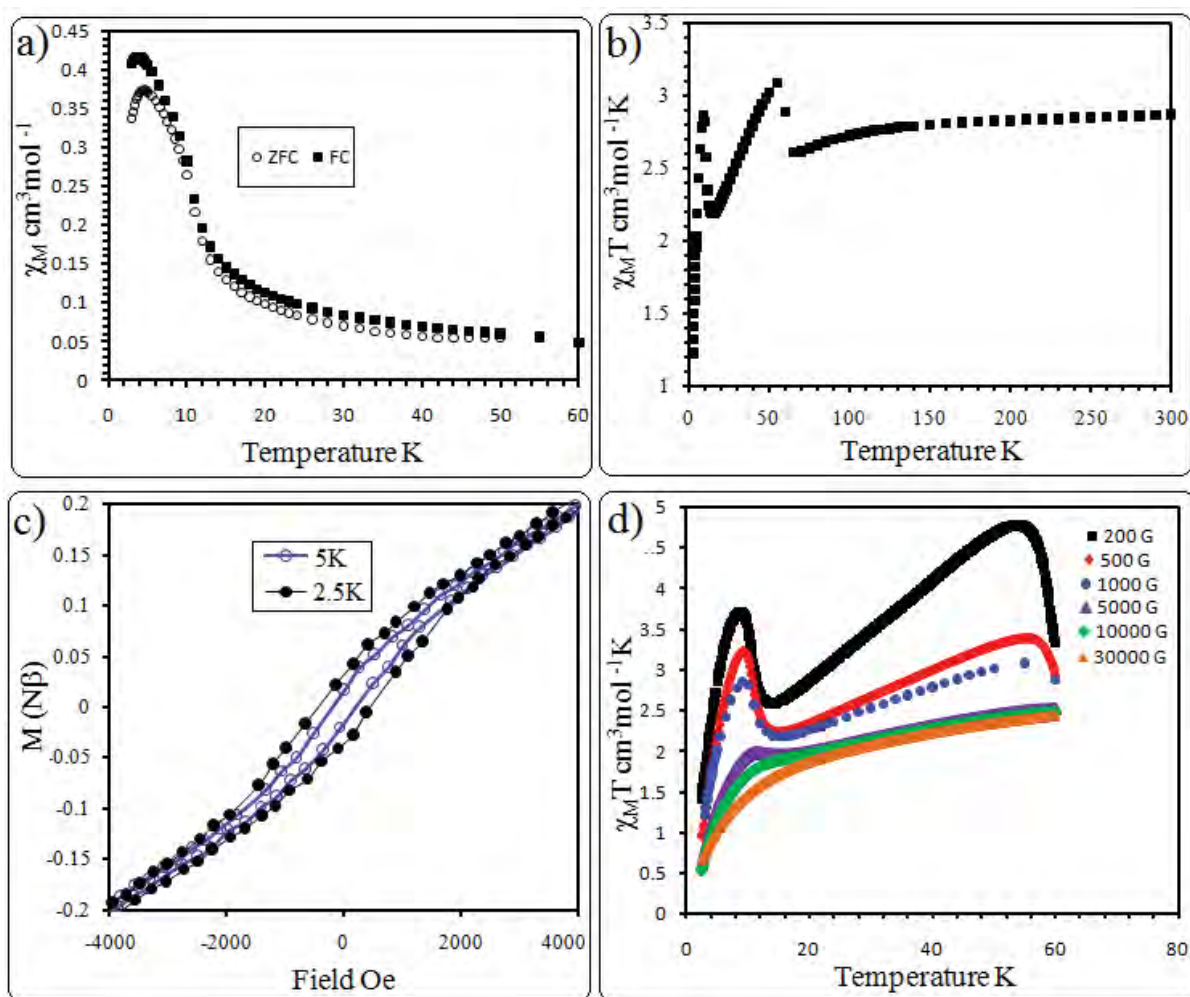


**Figure 5.** Magnetic data of **2**, (a) Field cooled (FC) and zero-field (ZFC) plot of  $\chi_M$  vs.  $T$  at  $H = 1000$  Oe, (b) Plot of  $\chi_M T$  vs.  $T$  ( $H = 1000$  Oe) (FC), (c) Magnetic hysteresis loops at 2.5 K 5 K (black) and 5 K (blue). (d) Plot of  $\chi_M T$  vs.  $T$  at different applied fields.



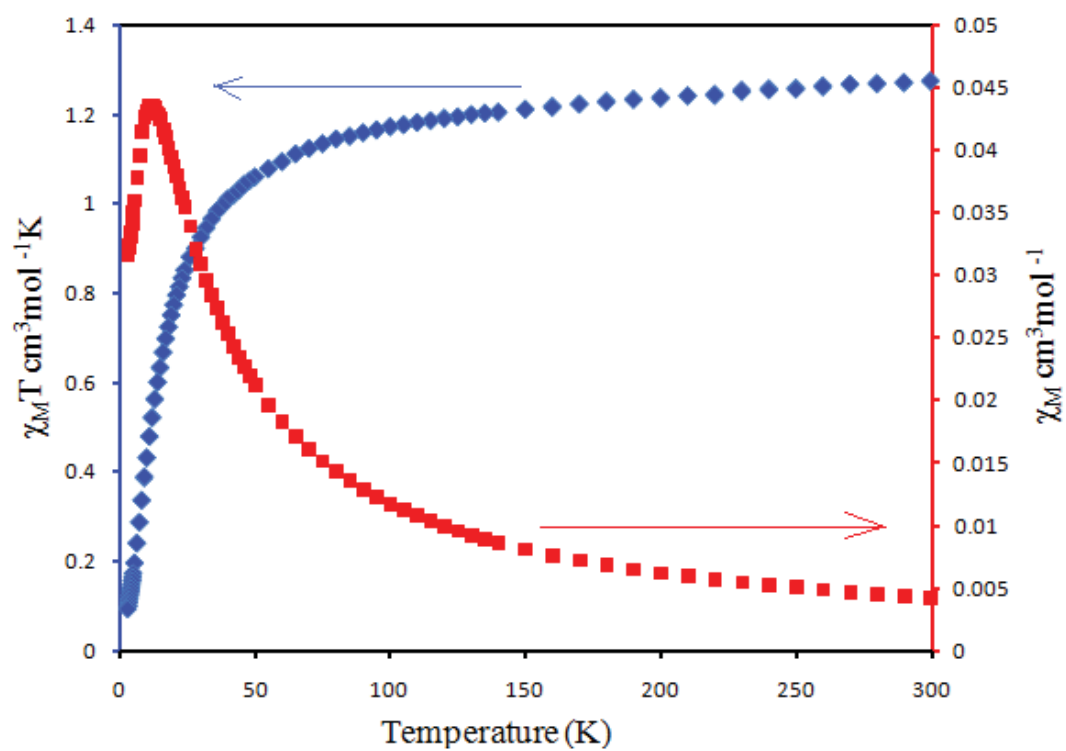


**Figure 6.** Magnetic data of **3**, a plot of  $\chi_M$  and  $\chi_M T$  vs.  $T$  ( $H = 1000$  Oe).

## References

- <sup>1</sup> (a) Evans, R.; Lin, W. B. *Acc. Chem. Res.* **2002**, *35*, 511-522. (b) Kesanli, B.; Lin, W. B. *Coord. Chem. Rev.* **2003**, *246*, 305-326. (c) Yaghi, M.; O'Keeffe, M.; Ockwig, N. W.; Chae, H. K.; Eddaoudi, M.; Kim, J. *Nature*, **2003**, *423*, 705-714. (d) James, S. L. *Chem. Soc. Rev.* **2003**, *32*, 276-288. (e) Kitagawa, S.; Kitaura, R.; Noro, S. *Angew. Chem. Int. Ed.* **2004**, *116*, 2388-2430. (f) Rao, C. N. R.; Natarajan, S.; Vaidhyanathan, R. *Angew. Chem. Int. Ed.* **2004**, *116*, 1490-1521. (g) Rowsell, J. L. C.; Yaghi, O. M. *Micropor. Mesopor. Mat.* **2004**, *73*, 3-14. (h) Ferey, G.; Mellot-Draznieks, C.; Serre, C.; Millange, F. *Acc. Chem. Res.* **2005**, *38*, 217-225. (i) Bradshaw, D.; Claridge, J. B.; Cussen, E. J.; Prior, T. J.; Rosseinsky, M. J. *Acc. Chem. Res.* **2005**, *38*, 273-282. (j) Robin, Y.; Fromm, K. M. *Coord. Chem. Rev.* **2006**, *250*, 2127-2157. (k) Nadeem, M. A.; Bhadbhade, M.; Bircher, R.; Stride, J. A. *CrysEngComm.* **2010**, *12*, 1391-1393.
- <sup>2</sup> Morris, W.; Leung, B.; Furukawa, H.; Yaghi, O. K.; He, N.; Hayashi, H.; Houndonougbo, Y.; Asta, M.; Laird, B. B.; Yaghi, O. M. *J. Am. Chem. Soc.*, **2010**, *132*, 11006-11008
- <sup>3</sup> Furukawa, H.; Ko, N.; Go, Y. B.; Aratani, N.; Choi, S. B.; Choi, E.; Yazaydin, A. O.; Snurr, R. Q.; O'Keeffe, M.; Kim, J.; Yaghi, O. M. *Science*, **2010**, *239*, 424-428.
- <sup>4</sup> Leslie, J. M.; Mircea, D.; Long, J. R. *Chem. Soc. Rev.* **2009**, *38*, 1294-1314.
- <sup>5</sup> (a) Luo, J. H.; Xu, H. W.; Liu, Y.; Zhao, Y. S. *J. Am. Chem. Soc.* **2008**, *130*, 9626-9627. (b) Eddaoudi, M.; Li, H. L.; Yaghi, O. M. *J. Am. Chem. Soc.* **2000**, *122*, 1391-1397. (c) Walton, K. S.; Millward, A. R.; Dubbeldam, D.; Frost, H.; Low, J. J.; Yaghi, O. M. *J. Am. Chem. Soc.* **2008**, *130*, 406-407. (d) Horcajada, P.; Serre, C.; Ferey, G. *J. Am. Chem. Soc.* **2008**, *130*, 6774-6780. (e) Volkringer, C.; Loiseau, T.; Guillou, N.; Ferey, G. *Sol. Sta. Sci.* **2009**, *11*, 1507-1512.
- <sup>6</sup> Yang, J.; Zhu, D.; Zhang, H.; Xu, Y.; Shen, L.; Wang, X.; Yuan, R. Z. *Anorg. Allg. Chem.* **2010**, *636*, 1129-1132.
- <sup>7</sup> (a) Su, C. Y.; Cai, Y. P.; Chen, C. L.; Smith, M. D.; Kaim, W.; Zur Loye, H. C. *J. Am. Chem. Soc.* **2003**, *125*, 8595-8613. (b) Dobrzanska, L.; Lloyd, G. O.; Raubenheimer, H. G.; Barbour, L. J. *J. Am. Chem. Soc.* **2005**, *127*, 13134-13135. (c) Chatterjee, B.; Noveron, J. C.; Resendiz, M. J. E.; Liu, J.; Yamamoto, T.; Parker, D.; Cinke, M.; Nguyen, C. V.; Ariff, A. M.; Stang, P. J. *J. Am. Chem. Soc.* **2004**, *126*, 10645-10656.
- <sup>8</sup> (a) Carlin, R. L. *Magnetochemistry*, Springer-Verlag, Berlin, **1986**
- <sup>9</sup> (a) Arai, L.; Nadeem, M. A.; Bhadbhade, M.; Stride, J. A. *Dalton Trans.*, **2010**, *39*, 3372-3374, (b) Nadeem, M. A.; Craig, D. J.; Bircher, R.; Stride, J. A. *Dalton Trans.* **2010**, *39*,

---

4358-X. (c) Nadeem, M. A.; Bhadbhade, M.; Stride, J. A. *Dalton Trans.* **2010**, 39, 9860-9865.

<sup>10</sup> Kahn, O. *Molecular Magnetism*; VCH: Weinheim, Germany, **1993**.

<sup>11</sup> Sheldrick, G. M. SHELXS 97, Program for the Solution of Crystal Structures; University of Göttingen: Germany, **1997**.

<sup>12</sup> Zheng, Y.-Z.; Tong, M.-L.; Zhang, W.-X.; Chen, X.-M. *Chem. Commun.* **2006**, 165-167.

<sup>13</sup> Nadeem, M. A.; Bhadbhade, M.; Bircher, R.; Stride, J. A. *Cryst. Growth Des.* **2010**, 10, 4060-4067.

<sup>14</sup> Li, J. R.; Yu, Q.; Tao, Y.; Bu, X. H.; Ribas, J.; Batten, S. R. *Chem. Commun.* **2007**, 2290-2292.

<sup>15</sup> Wang, Z.; Zhang, B.; Inoue, K.; Fujiwara, H.; Otsuka, T.; Kobayashi, H.; Kurmoo, M. *Inorg. Chem.* **2007**, 46, 437-445.

<sup>16</sup> Su, Z.; Song, Y.; Bai, Z.-S.; Fan, J.; Liu, G.-X.; Sun, W.-Y. *CrystEngComm*, **2010**, 12, 4339-4346.

## Supplementary information

### **A series of novel isostructural metal-organic frameworks constructed from mixed flexible ligands: Synthesis, crystal structure and physical properties**

*Maggie Chai Cin Ng,<sup>†</sup> Muhammad Arif Nadeem,<sup>†</sup> and John Arron Stride<sup>\*†,‡</sup>*

<sup>†</sup> *School of Chemistry, University of New South Wales, Sydney, NSW 2052, Australia. Fax: +61 (02) 9385 6141; Tel: +61 (0)2 9385 4675; E-mail: j.stride@unsw.edu.au*

<sup>‡</sup> *Bragg Institute, Australian Nuclear Science and Technology Organisation, PMB 1, Menai, NSW 2234, Australia.*

**Table S1:** Selected bond lengths (Å) and bond angles (°) of **1** and **2**

Compound <b>1</b> <sup>a</sup>			
Mn1-O3 <sup>i</sup>	2.0991 (13)	O4 <sup>ii</sup> -Mn1-O1	92.18 (5)
Mn1-O4 <sup>ii</sup>	2.1166 (13)	N2 <sup>iii</sup> -Mn1-O1	95.36 (5)
Mn1-N2 <sup>iii</sup>	2.2535 (15)	O3 <sup>i</sup> -Mn1-N1	91.92 (5)
Mn1-N2 <sup>iii</sup>	2.2665 (14)	O4 <sup>ii</sup> -Mn1-N1	92.09 (5)
Mn1-N1	2.2711 (15)	N2 <sup>iii</sup> -Mn1-N1	176.47 (6)
Mn1-O2	2.2958 (13)	O1-Mn1-N1	84.84 (5)
O3 <sup>i</sup> -Mn1-O4 <sup>ii</sup>	117.48 (6)	O3 <sup>i</sup> -Mn1-O2	92.50 (5)
O3 <sup>i</sup> -Mn1-N2 <sup>iii</sup>	86.16 (5)	O4 <sup>ii</sup> -Mn1-O2	149.84 (5)
O4 <sup>ii</sup> -Mn1-N2 <sup>iii</sup>	91.43 (5)	N2 <sup>iii</sup> -Mn1-O2	94.02 (5)
O3 <sup>i</sup> -Mn1-O1	150.28 (5)	O1-Mn1-O2	57.79 (5)
		O1-Mn1-O2	83.09 (5)
Compound <b>2</b> <sup>b</sup>			
O3-Co1 <sup>i</sup>	2.0166 (15)	O4 <sup>iv</sup> -Co1-N1	92.63 (7)
Co1-O3 <sup>iii</sup>	2.0166 (15)	N2 <sup>v</sup> -Co1-N1	176.48 (7)
Co1-O4 <sup>iv</sup>	2.0322 (16)	O3 <sup>iii</sup> -Co1-O1	152.86 (6)
Co1-N2 <sup>v</sup>	2.1366 (18)	O4 <sup>iv</sup> -Co1-O1	92.65 (6)
Co1-N1	2.1419 (18)	N2 <sup>v</sup> -Co1-O1	92.79 (6)
Co1-O1	2.1916 (14)	N1-Co1-O1	86.08 (6)
Co1-O2	2.2105 (15)	O3 <sup>iii</sup> -Co1-O2	92.93 (6)
O3 <sup>iii</sup> -Co1-O4 <sup>iv</sup>	114.48 (6)	O4 <sup>iv</sup> -Co1-O2	152.55 (6)
O3 <sup>iii</sup> -Co1-N2 <sup>v</sup>	86.24 (6)	N2 <sup>v</sup> -Co1-O2	92.69 (6)
O4 <sup>iv</sup> -Co1-N2 <sup>v</sup>	90.75 (7)	N1-Co1-O2	83.86 (6)
O3 <sup>iii</sup> -Co1-N1	93.24 (6)	O1-Co1-O2	59.99 (6)

<sup>a</sup> (i)  $x-1/2, -y+1/2, z-1/2$ ; (ii)  $-x+3/2, y-1/2, -z+1/2$ ; (iii)  $x, y, z-1$ ; (iv)  $x+1/2, -y+1/2, z+1/2$ ; (v)  $-x+3/2, y+1/2, -z+1/2$ ; (vi)  $x, y, z+1$ . <sup>b</sup>(i)  $x-1/2, -y+3/2, z-1/2$ ; (ii)  $x, y, z-1$ ; (iii)  $x+1/2, -y+3/2, z+1/2$ ; (iv)  $-x-1/2, y+1/2, -z+3/2$ ; (v)  $x, y, z+1$ ; (vi)  $-x-1/2, y-1/2, -z+3/2$ .

**Table S2:** Selected bond lengths (Å) and bond angles (°) of **3** and **4**

Compound <b>3</b> <sup>c</sup>			
Ni1-O3 <sup>i</sup>	2.0225 (15)	N2 <sup>iii</sup> -Ni1-N1	176.59 (7)
Ni1-O4 <sup>ii</sup>	2.0228 (16)	O3 <sup>i</sup> -Ni1-O2	94.04 (6)
Ni1-N2 <sup>iii</sup>	2.0768 (17)	O4 <sup>ii</sup> -Ni1-O2	155.06 (6)
Ni1-N1	2.0799 (17)	N2 <sup>iii</sup> -Ni1-O2	93.00 (6)
Ni1-O2	2.1527 (16)	N1-Ni1-O2	86.08 (6)
Ni1-O1	2.1720 (15)	O3 <sup>i</sup> -Ni1-O1	155.24 (6)
O3 <sup>i</sup> -Ni1-O4 <sup>ii</sup>	110.86 (6)	O4 <sup>ii</sup> -Ni1-O1	93.89 (6)
O3 <sup>i</sup> -Ni1-N2 <sup>iii</sup>	90.35 (6)	N2 <sup>iii</sup> -Ni1-O1	92.01 (6)
O4 <sup>ii</sup> -Ni1-N2 <sup>iii</sup>	85.85 (7)	N1-Ni1-O1	84.67 (6)
O3 <sup>i</sup> -Ni1-N1	93.00 (6)	O2-Ni1-O1	61.22 (6)
O4 <sup>ii</sup> -Ni1-N1	93.59 (7)		
Compound <b>4</b> <sup>d</sup>			
Cu1-O2 <sup>i</sup>	2.018 (2)	N1 <sup>ii</sup> -Cu1-N2	176.70 (9)
Cu1-O1	2.023 (2)	O2 <sup>i</sup> -Cu1-O3 <sup>iii</sup>	94.39 (8)
Cu1-N1 <sup>ii</sup>	2.074 (2)	O1-Cu1—O3 <sup>iii</sup>	154.83 (8)
Cu1-N2	2.080 (2)	N1 <sup>ii</sup> -Cu1-O3 <sup>iii</sup>	92.98 (9)
Cu1-O3 <sup>iii</sup>	2.157 (2)	N2-Cu1-O3 <sup>iii</sup>	86.18 (9)
Cu1-O4 <sup>iii</sup>	2.175 (2)	O2 <sup>i</sup> -Cu1-O4 <sup>iii</sup>	155.34 (8)
O2 <sup>i</sup> -Cu1-O1	110.76 (9)	O1-Cu1-O4 <sup>iii</sup>	93.90 (8)
O2 <sup>i</sup> -Cu1-N1 <sup>ii</sup>	90.32 (9)	N1 <sup>ii</sup> -Cu1-O4 <sup>iii</sup>	91.95 (9)
O1-Cu1-N1 <sup>ii</sup>	85.89 (9)	N2-Cu1-O4 <sup>iii</sup>	84.84 (9)
O2 <sup>i</sup> -Cu1-N2	92.93 (9)	O3 <sup>iii</sup> -Cu1-O4 <sup>iii</sup>	60.98 (8)
O1-Cu1-N2	93.50 (9)		

<sup>c</sup>(i)  $-x-1/2, y+1/2, -z+3/2$ ; (ii)  $x+1/2, -y+3/2, z+1/2$ ; (iii)  $x, y, z+1$ ; (iv)  $-x-1/2, y-1/2, -z+3/2$ ; (v)  $-x-1/2, -y+3/2, z-1/2$ ; (vi)  $x, y, z-1$ . <sup>d</sup>(i)  $-x, -y+2, -z+2$ ; (ii)  $x, y, z+1$ ; (iii)  $-x-1/2, -y+3/2, z-1/2$ ; (iv)  $x+1/2, -y+3/2, z+1/2$ ; (v)  $x, y, z-1$ .



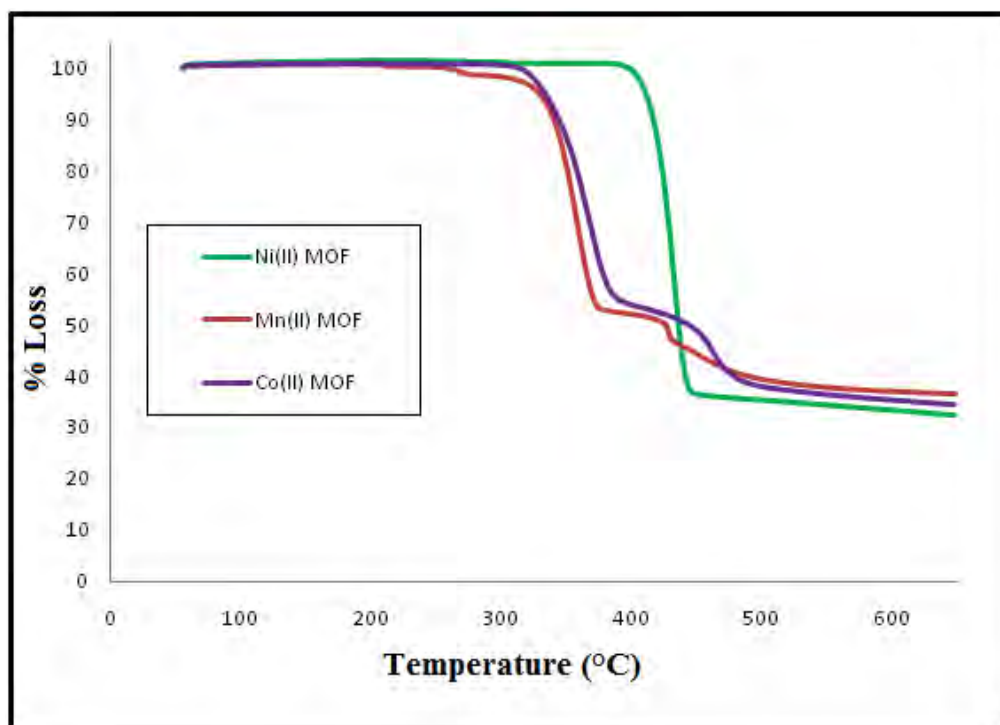


**Figure S1.** Thermogravimetric curves of **1-3**

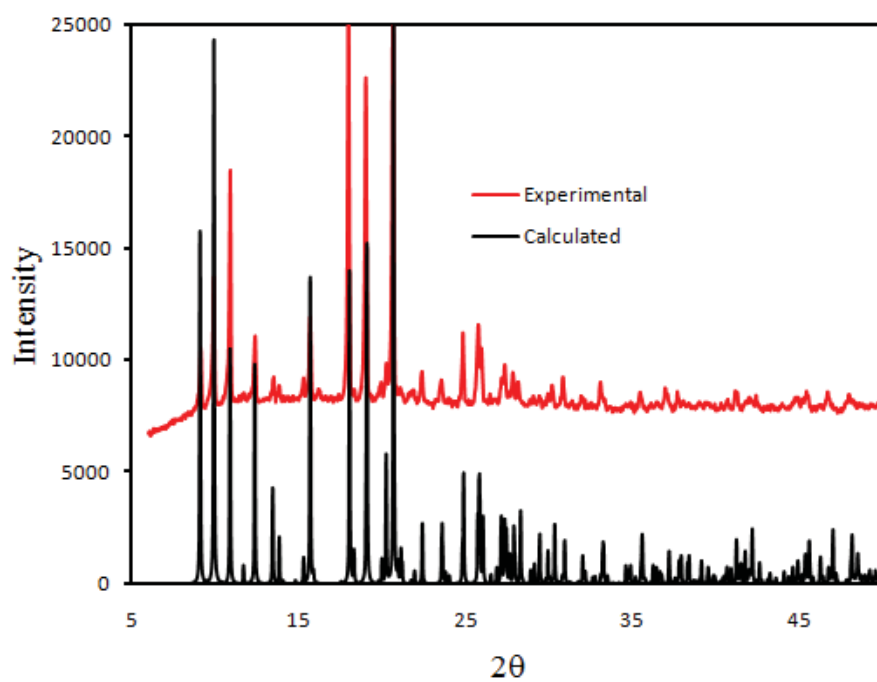


**Figure S2.** A comparison of calculated powder XRD pattern of **2** with simulated form single crystal data

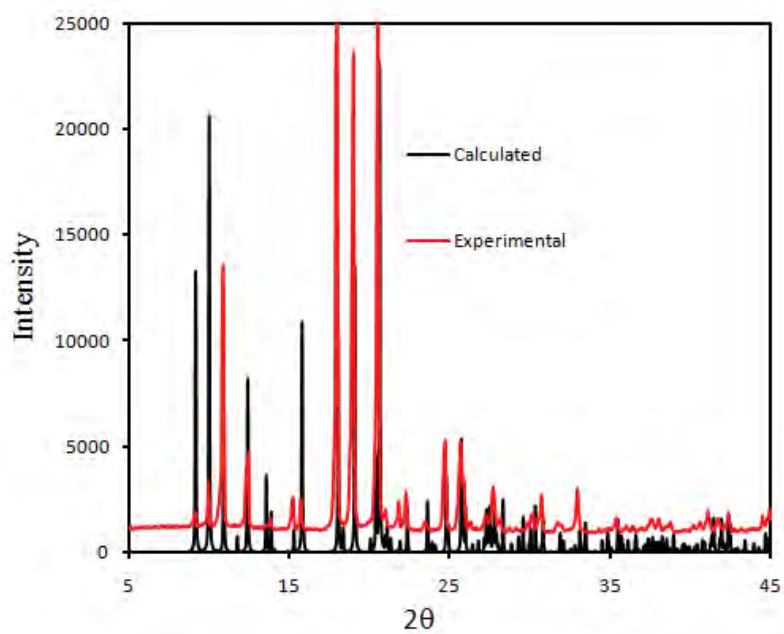


**Figure S3.** A comparison of calculated powder XRD pattern of **3** with simulated form single crystal data

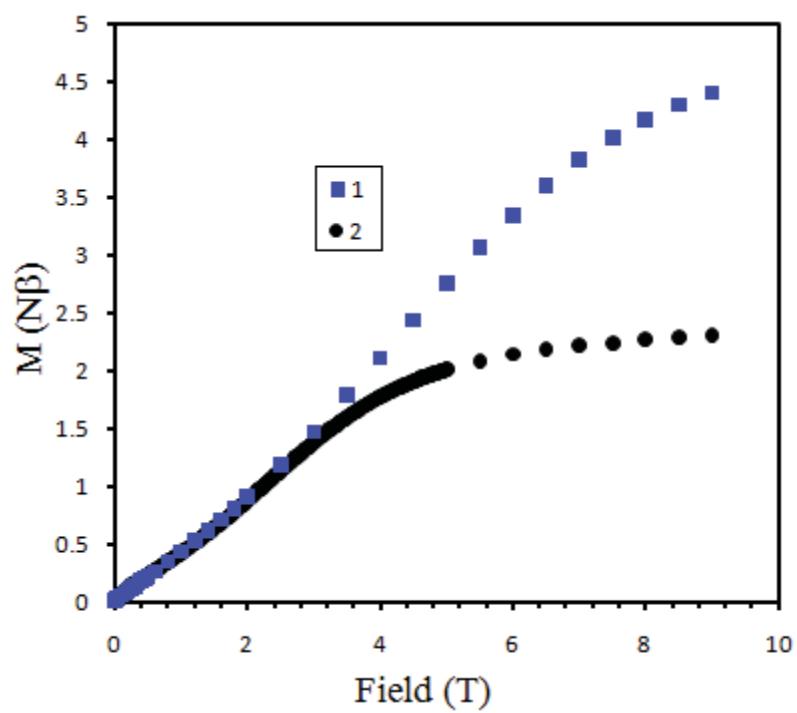


**Figure S4.** A graph of moment vs field for **1-2** showing that saturation magnetisation at 9 T.

## **Magnetic phase transition in an unprecedented Ni<sub>4</sub>O<sub>4</sub>- cubane based 3D metal-organic framework.**

*Muhammad Arif Nadeem, Maggie Chai Cin Ng and John Arron Stride*

### **ACKNOWLEDGMENT OF CONTRIBUTION TO AUTHORSHIP**

The article is submitted in journal “*Angew. Chem., Int. Ed.*” J.A.S. conceived and managed the research project, M.A.N. and M.C.C.N. synthesised the samples. M.A.N. solved the crystal structure. M.A.N. and M.C.C.N. collected, interpreted the magnetic data and wrote the manuscript. All authors discussed the results and commented on this manuscript.

# Magnetic phase transition in an unprecedented Ni<sub>4</sub>O<sub>4</sub>-cubane based 3D metal-organic framework.

Muhammad Arif Nadeem,<sup>†</sup> Maggie Chai Cin Ng,<sup>†</sup> and John Arron Stride<sup>\*,†,‡</sup>

Interest in molecular-based magnetic materials has greatly increased over the last decade with the recognition that such materials can help in the understanding of magneto-structural correlations and the fundamental phenomena of magnetism; some may even lead to potential applications.<sup>[1]</sup> In addition to the nature of the metal centers, the bulk magnetic properties mainly depend on the bridging modes and geometries of the bridging ligands. Due to the fact that the structural factors governing the exchange coupling between paramagnetic centers are complex and elusive, the pursuit of designed polynuclear complexes and extended networks with predictable magnetic properties remains a challenge. Magnetic phenomena such as ferromagnetic, ferrimagnetic, and antiferromagnetic long-range ordering at low temperatures have been observed for many transition-metal complexes.<sup>[2]</sup> In contrast, only a few magnetically ordered complexes exhibit magnetic phase transitions (MPTs) such as metamagnetic phase transitions<sup>[2b,c]</sup>. In most cases of porous extended systems displaying bulk ordering phenomena, MPTs are associated with solvation/desolvation.<sup>[3]</sup> Meanwhile, slow magnetic relaxation in molecular clusters is considered as one of the most important achievements of molecular magnetism of the last few years.<sup>[4]</sup>

Although few examples of single molecule magnet (SMM) based 3D networks have been reported,<sup>[5]</sup> a MPT coupled to slow relaxation has not been reported, to date; particularly the coexistence of spin canting and slow relaxation phenomena at the same temperature. Despite the fact that Ni<sup>II</sup> is known to display large single ion anisotropy,<sup>[6]</sup> to date only a handful of Ni<sup>II</sup> complexes have been reported as showing spin canting behaviour.<sup>[7]</sup> Recently, Cheng *et al.* reported a 3D nickel-organic framework which exhibited canted antiferromagnetism at 5.0 K whilst below this temperature slow relaxation was also observed.<sup>[8]</sup> We herein report the first example of Ni<sup>II</sup>-cubane based three dimensional (3D) network [Ni<sub>12</sub>(pdaa)(OH)<sub>2</sub>(H<sub>2</sub>O)]<sub>n</sub>, (pdaa = 1,4-phenylene diacetic acid), **1**, exhibiting a MPT from antiferromagnetic (AF) to canted antiferromagnetic (CAF) which is possibly associated with a slow

relaxation behaviour below 2.8 K.

Compound **1** was hydrothermally synthesized and crystallizes in the tetragonal space group *I*4<sub>1</sub>/*a* (*Z* = 16). Analysis of the single crystal X-ray diffraction data indicates the presence of one dimensional (1D) linear chains of Ni<sup>II</sup> atoms running perpendicular to each other held together via pdaa organic ligands (figure 1a). Each chain consists of two types of Ni<sup>II</sup> centers (Ni1 and Ni2) having the same coordination environment, but with slightly different bond distances and angles, and separated at a distance of 3.057 Å. Each Ni<sup>II</sup> atom in the chain is coordinated by four oxygen atoms belonging to four different pdaa ligands and two oxygen atoms of two different -OH (O6W) ions (the Ni-O bond lengths are in the range of 1.977(2) - 2.172(3) Å and the O-Ni-O angles are in the range of 80.20(10) - 179.999.56(1)°) to form a distorted octahedral geometry. The characteristic feature of **1** is that linear 1D Ni<sup>II</sup> chains are bridged via distorted Ni<sub>4</sub>O<sub>4</sub>-cubane units (figure 1b). Each Ni<sub>4</sub>O<sub>4</sub>-cubane unit adopts *S*<sub>4</sub> symmetry and consists of one type of nickel centre (Ni3) which is connected with three different oxygen atoms (μ<sub>3</sub>-O) of bridging -OH groups of the Ni<sub>4</sub>O<sub>4</sub>-cubane, one oxygen atom (O6W) which bridges the Ni3 atom with the 1D linear chains, one oxygen atom (O7) of a pdaa ligand and one water molecule (O4), to form a distorted octahedral geometry (the Ni3-O bond lengths are in the range of 2.003(2) - 2.125(3) Å and the O-Ni3-O angles are in the range of 81.84(11) - 179.9991(1)°).

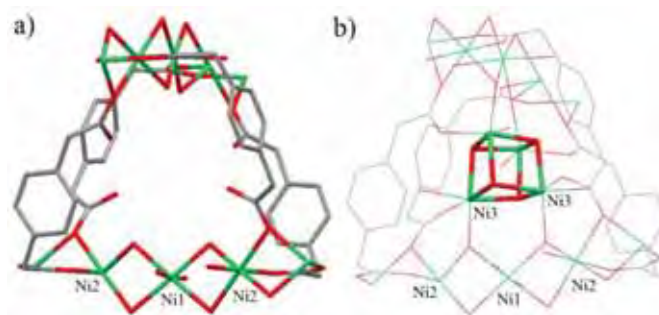


**Figure 1.** (a) A view showing pdaa ligand linked the two neighbouring 1D chains running perpendicular to each other (Ni<sub>4</sub>O<sub>4</sub> cubane is omitted for clarity), (b) two 1D chains are also bridged via Ni<sub>4</sub>O<sub>4</sub> cubane.

In Ni<sub>4</sub>O<sub>4</sub>-cubane, four Ni-Ni distances are equal to 3.069 Å with the remaining two Ni-Ni distances of 3.072 Å, both less than the mean literature value of 3.11 Å calculated by Isele *et al.*<sup>[9]</sup> The six faces of the cubane are not all equivalent, with the four side faces (parallel to the *c* axis) having Ni-O-Ni bridging angles in the range of 81.83° - 97.75°, whereas the top and bottom faces (perpendicular to the *c* axis) have Ni-O-Ni angles 94.94°. Each Ni3 atom of the Ni<sub>4</sub>O<sub>4</sub>-cubane is linked to Ni1 and Ni2 centres of the 1D linear chains via -OH groups above and below the Ni<sub>4</sub>O<sub>4</sub>-cubane at a distance of 3.644 Å and 3.407 Å respectively. The single crystallographic unique pdaa separates the two linear chains via two different carboxylate groups at a distance of 8.776 Å. Two oxygen atoms (O1 and O2) of one carboxylate coordinates with the two

[\*] M. A. Nadeem, M. C. C. Ng, A/Prof. J. A. Stride.  
School of Chemistry  
University of New South Wales  
Sydney, NSW 2052, Australia  
Fax: (+61) (2)93856141  
E-mail: j.stride@unsw.edu.au

A/Prof. J. A. Stride  
Bragg Institute.  
Australian Nuclear Science and Technology Organisation  
PMB 1, Menai, NSW 2234, Australia.

[\*\*] The authors would like to thank Prof. Oliver Waldmann and Drs. Richard Mole and Roland Bircher for helpful discussions when preparing the manuscript.

Supporting information for this article is available on the WWW under <http://www.angewandte.org> or from the author.



different Ni atoms (Ni1 and Ni2) in a syn-syn  $\eta^1:\eta^1:\mu_2$  chelating mode, whilst one oxygen atom (O7) of the second carboxylate group is coordinated with a  $\text{Ni}^{\text{II}}$  centre of the  $\text{Ni}_4\text{O}_4$ -cubane unit and a second oxygen atom (O5) bridges the two  $\text{Ni}^{\text{II}}$  centers of neighbouring linear chains. The two flexible arms of the pdaa ligand are directed towards the same side and twist perpendicular to each other to coordinate with the metal centres of the 1D linear chains, bridged via  $\text{Ni}_4\text{O}_4$ -cubanes, to form a 3D network (figure 2).

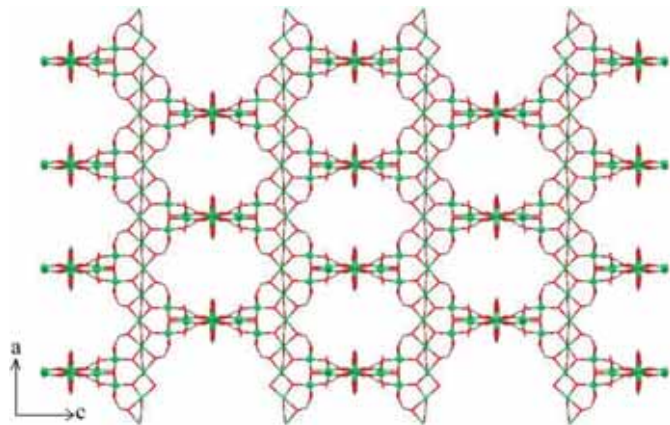


**Figure 2.** A packing diagram of **1** showing 1D chains are separated via  $\text{Ni}_4\text{O}_4$  cubane, running perpendicular to each along the direction of the *a* and *b* axes direction (pdaa ligand is partially omitted for clarity).

The dc magnetic susceptibility ( $\chi_M$ ) data of a polycrystalline sample of **1** is given in figure 3. At room temperature, the value of  $\chi_M T$  is  $2.71 \text{ cm}^3 \text{mol}^{-1} \text{K}$  per two  $\text{Ni}^{\text{II}}$  atoms, equivalent to the expected value of  $2.65 \text{ cm}^3 \text{mol}^{-1} \text{K}$  with  $g = 2.30$ , for two  $\text{Ni}^{\text{II}}$  atoms.<sup>[10]</sup> Upon cooling,  $\chi_M T$  increases gradually with decreasing temperature and reaches a maximum of  $9.92 \text{ cm}^3 \text{mol}^{-1} \text{K}$  at 21 K. The  $\chi_M^{-1}$  vs  $T$  curve is shown as the inset of figure 3b. Above 20 K, the plot is linear and well fitted by Curie-Weiss law ( $\chi_M = C/(T - \theta)$ ), with  $C = 2.6 \text{ cm}^3 \text{mol}^{-1} \text{K}$ ,  $\theta = 8.4$ . The value of the Weiss constant indicates a moderate ferromagnetic coupling between the  $\text{Ni}^{\text{II}}$  ions.

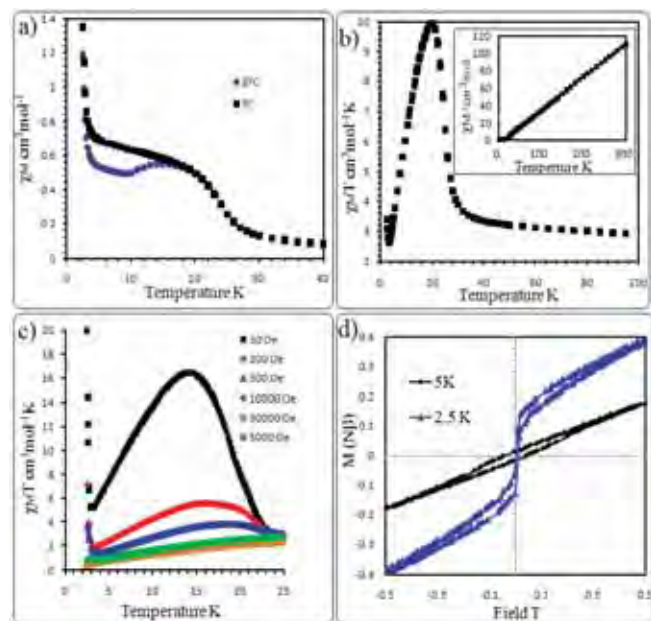


**Figure 3.** (a) Field cooled (FC) and zero-field (ZFC) plot of  $\chi_M$  vs.  $T$  at  $H = 1000 \text{ Oe}$ , (b) Plot of  $\chi_M T$  vs.  $T$  ( $H = 1000 \text{ Oe}$ ) (FC), inset shows plot of  $\chi_M^{-1}$  vs.  $T$  (c)  $\chi_M T$  vs.  $T$  at various fields (d) Magnetic hysteresis loops at 2.5 K (blue) and 5 K (black).

On cooling further  $\chi_M T$  starts to decrease and reaches a minimum value of  $2.739 \text{ cm}^3 \text{mol}^{-1} \text{K}$  at 3.7 K, which upon further cooling increases abruptly to reach a value of  $3.389 \text{ cm}^3 \text{mol}^{-1} \text{K}$  at the lowest possible measurement temperature of 2.5 K (figure 3b). The field-cooled (FC), 1000 Oe, and zero field-cooled (ZFC) magnetization data down to 2.5 K, show a bifurcation at 21 K (figure 3a), which is an indication of the onset of long range magnetic ordering. The FC susceptibility in different applied dc fields also clearly shows the onset of spontaneous magnetization below 21 K, as indicated by the field dependent moment against temperature (figure 3c). The magnetic behaviour is interpreted as the onset of antiferromagnetic coupling between neighbouring 1D ferromagnetic chains below 21 K, which gives rise to a bulk long-range magnetic ordering. The existence of a spontaneous magnetization is also confirmed by magnetic hysteresis measurements at 5 K in which a coercive field of  $H_C = 474 \text{ Oe}$  and a remanent magnetization of  $M_R = 0.085 \text{ N}\mu\beta$  were observed (figure 3d). The FC  $\chi_M T$  values at different applied fields as a function of temperature also shows an abrupt increase at 2.5 K, which is more pronounced at lower field (50 Oe) strengths and reaches a maximum value of  $19.89 \text{ cm}^3 \text{mol}^{-1} \text{K}$  (figure 3c), suggesting that the magnetic behaviour at low temperature is that of a canted-antiferromagnet.<sup>[11, 12]</sup>

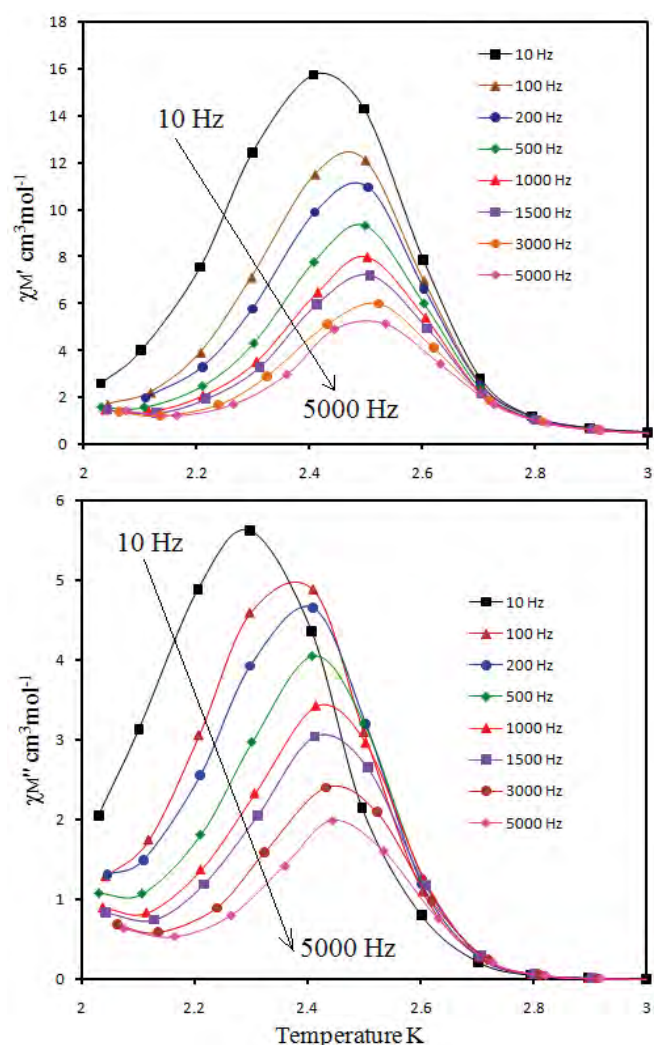


**Figure 4.** Temperature and frequency dependence of the real ( $\chi_M'$ ) and imaginary ( $\chi_M''$ ) parts of the ac susceptibility for **1**. The solid lines are guide for the eyes.

The field dependent magnetization at 2.5 K suggests that saturation magnetization is not reached even at the highest applied magnetic field of 9 T (figure S2 of supporting information), where

the magnetization reaches a saturation moment,  $M_s$  ( $T = 2.5$  K) of  $2.37$  N $\beta$ , half the expected maximum value of  $4.6$  N $\beta$ . The absence of saturation at high fields confirms that the low temperature magnetic ground state is a canted-antiferromagnet.<sup>[13]</sup> By using the formula [Canting angle  $\varphi = \sin^{-1} M_{rem}/M_{max}$ ], we determine a canting angle  $\varphi = 2.9^\circ$ . To further investigate the properties at low temperature, we have performed ac susceptibility measurements. Alternating current (ac) susceptibility was measured on polycrystalline samples of **1** under  $3$  Oe oscillating field and zero dc field as a function of temperature and frequency. Figure 4 shows the temperature dependence of the ac susceptibility for **1**. The frequency and temperature dependent  $\chi_M T$  components exhibits small and sharp peaks at  $21$  K and  $2.8$  K respectively, which is a clear indication of bulk magnetic ordering at  $21$  K and a phase transition from AF to CAF phenomena at ca.  $2.8$  K (figure S1 of supplementary information). The MPT is also confirmed by the different shapes of the hysteresis curves at  $5$  K and  $2.5$  K (figure 3d). The temperature at the peak of  $\chi_M'$  increases and the peak height decreases with increasing frequency, implying a slow relaxation process. The shift in temperature of maxima in  $\chi_M'$  and  $\chi_M''$  with the frequency are reminiscent of single-molecule magnet (SMM) or spin glass behaviour.<sup>[16]</sup> The intensity of the ac response is significantly frequency dependent, however, only very small but non-negligible shift in peaks with respect to temperature can be seen (figure 4).

Taking into account the structural features of this compound, the ferromagnetic 1D chains are separated at a distance of  $8.776$  Å via a pdaa ligands which can only give rise to weak interactions between the chains, it is expected that the 1D chains are magnetically coupled with each other via the  $Ni_4O_4$ -cubane units which results in bulk magnetic ordering below  $21$  K. However, below  $2.8$  K the  $Ni_4O_4$ -cubanes act as independent SMMs which results in an overall MPT from AF to CAF at this temperature (figure 5). The SMM behaviour of  $Ni_4O_4$ -cubane is also supported by the peculiar butterfly hysteresis loop measurements with no remanent magnetization at  $2.5$  K whilst having a normal hysteresis loop at  $5$  K (figure 3d).<sup>[17]</sup> It is also of note that whilst  $Ni_4O_4$ -cubanes are well known SMMs,<sup>[14,15]</sup> however to date no  $Ni_4O_4$ -cubane based 3D network has been reported showing both SMM and classical bulk magnetic behaviour.

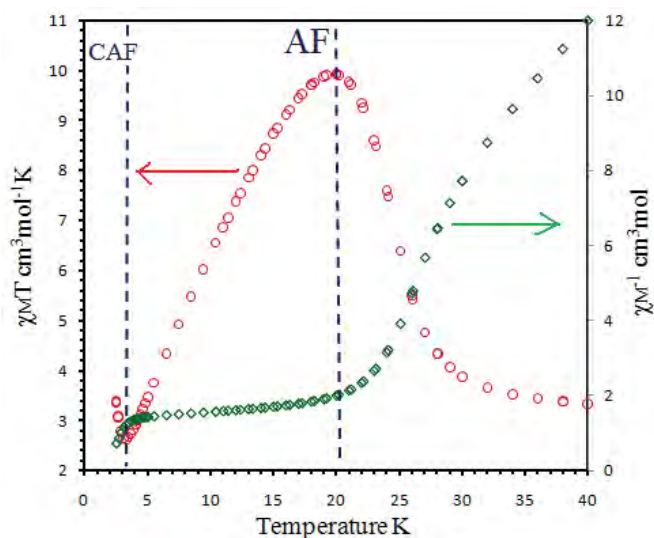


**Figure 5.** Magnetic dc susceptibility data showing the various magnetic phase changes at low temperature for **1**

In conclusion, a new 3D MOF based on 1D  $Ni^{II}$  linear chains connected via  $Ni_4O_4$ -cubanes, has been synthesized, offering a rare example of a magnetic material, which shows MPTs possibly coupled with a slow relaxation phenomena. **1** showed antiferromagnetic ordering at  $21$  K and a magnetic phase transition from AF to CAF at  $2.8$  K. These results demonstrate the concept of magnetic connections between 1D layers via  $Ni_4O_4$ -cubanes to tune

the overall properties of magnetic materials and open the way for further work in search of new nano-magnets.

## Experimental Section

Elemental Analyses were performed on a Carlo Erba Elemental Analyser EA 1108. The FT-IR spectra were recorded from KBr pellets in range  $400 - 4000$   $cm^{-1}$  on a AVATAR 320 spectrometer. Thermal gravimetric analyses were performed under nitrogen using a Mettler Toledo TGA/DSC 1 at a heating rate of  $10^\circ C\ min^{-1}$ . PXRD data were recorded on a Philips X'Pert Multipurpose X-ray Diffractometer ( $Cu_{K\alpha}$ ,  $\lambda = 1.54056$  Å). The magnetic measurements were carried out with Quantum Design PPMS EverCool instrument. Powder XRD experiment was carried out to check the purity of bulk samples (see figure S3 in the Supporting Information). Thermal Analysis was performed to explore the thermal stability. As depicted in the Figure S4 of ESI, **1** is thermally stable up to  $380^\circ C$ . The initial weight loss (ca. 5%) starting at  $150^\circ C$  is due to loss of one water molecule coordinated with  $Ni3$  ion (Calc weight 5.06%) in the framework. After that there is a plateau region followed by sudden decrease in the weight, suggesting the onset of decomposition temperature of ca.  $380$  with a total weight loss of 55.26% (Calcd = 57.98%), resulting in simple oxides (NiO). Suitable single crystals of **1** ( $0.13 \times 0.10 \times 0.05$  mm<sup>3</sup>) was used in the intensity data collection using a Bruker SMART APEX CCD diffractometer at  $150(2)$  K ( $\lambda = 0.71073$  Å). The structures were solved by direct methods and refined by full-matrix least squares against  $F^2$  using the SHELXS-97 and SHELXL-97 programs.<sup>[18]</sup> Anisotropic thermal parameters were assigned to all non-hydrogen atoms. The hydrogen atoms were set in calculated positions and refined as riding atoms with a common fixed isotropic thermal parameter. Analytical expressions of neutral atom scattering factors were employed, and anomalous dispersion corrections were incorporated.

**Synthesis of 1:** A mixture of  $0.5$  mmol of 1,4-phenylene diacetic acid ( $0.097$  g) and  $2$  mmol of KOH ( $0.112$  g) in  $6$  mL distilled water was stirred for  $10$  minutes followed by addition of a solution of  $NiCl_2 \cdot 6H_2O$  ( $0.237$  g,  $1$  mmol) in  $4$  mL  $H_2O$ . The resulting solution was then sealed in a  $23$  mL Teflon-lined stainless steel autoclave and heated at  $170^\circ C$  for three days under autogenous pressure. The reaction vessel was then cooled to room temperature over  $4$  hours. Green diamond like crystals of **1** suitable for single crystal X-ray diffraction analysis were collected from the final reaction system by filtration and dried in air at ambient temperature (42% yield based on Ni). Anal. calcd: C, 33.7% H, 1.7%. Found: C, 33.4% H, 3.31%. IR data ( $\lambda_{max}/cm^{-1}$ ): 3677s, 3589s, 3570s, 3355s, 3045w, 3032w, 2968m, 2922m, 2907m, 1623s, 1560sd, 1435s, 1389s, 1277m, 1201w, 1139m, 940s, 810s, 737s

Crystal data for **1**.  $C_{10}H_6Ni_2O_7$ ,  $M_r = 355.57$ , tetragonal, space group  $I4_1/a$ ,  $a = 12.1839$  (6) Å,  $b = 12.1839$  (6) Å,  $c = 33.0206$  (18) Å,  $V = 4901.8$  (4) Å<sup>3</sup>,  $T = 150(2)$  K,  $Z = 16$ ,  $\rho_{calcd} = 1.927$  gcm<sup>-3</sup>,  $\lambda = 0.7107$  Å, 8548 reflections collected, 1812 unique ( $R_{int} = 0.037$ ),  $R[F^2 > 2\sigma(F^2)] = 0.031$  and  $wR(F^2) = 0.086$ ,  $S = 1.05$ .

Received: ((will be filled in by the editorial staff))

Published online on ((will be filled in by the editorial staff))

**Keywords:** Bulk magnetic ordering • Magnetic phase transition • Cubane-based polymer • Spin canting

- 
- [1] a) O. Kahn, *Acc. Chem. Res.* **2000**, *33*, 647; b) J. S. Miller, J. L. Manson, *Acc. Chem. Res.* **2001**, *34*, 563; c) M. Sakamoto, K. Manseki, H. Okawa, *Coord. Chem. Rev.* **2001**, *219-221*, 379; d) C. Benelli, D. Gatteschi, *Chem. Rev.* **2002**, *102*, 2369; e) I. Ciofini, C. A. Daul, *Coord. Chem. Rev.* **2003**, *238-239*, 187; f) A. L. Barra, A. Caneschi, A. Cornia, F. Fabrizi de Biani, D. Gatteschi, C. Sangregorio, R. Sessoli, L. Sorace, *J. Am. Chem. Soc.* **1999**, *121*, 5302; g) D. Gatteschi, R. Sessoli, *Angew. Chem. Int. Ed.* **2003**, *42*, 268; h) R. H. Laye, E. J. L. McInnes, *Eur. J. Inorg. Chem.* **2004**, 2811; i) N. T. Madhu, J.-K. Tang, I. J. Hewitt, R. Clérac, W. Wernsdorfer, J. van Slageren, C. E. Anson, A. K. Powell, *Polyhedron* **2005**, *24*, 2864.
- [2] a) E. Coronado, F. Palacio, J. Veciana, *Angew. Chem.* **2003**, *115*, 2674; b) C. Janiak, *Dalton Trans.* **2003**, 2781; c) P. Day, A. E. Underhill, *Philos. Trans. R. Soc. London Ser. A* **1999**, *357*, 2849.
- [3] a) J. Milon, M. C. Daniel, A. Kaiba, P. Guionneau, S. Brandés, J. P. Sutter, *J. Am. Chem. Soc.* **2007**, *129*, 13872; b) W. Kaneko, M. Ohba, S. Kitagawa, *J. Am. Chem. Soc.* **2007**, *129*, 13706; c) Z. M. Wang, B. Zhang, H. Fujiwara, H. Kobayashi, M. Kurmoo, *Chem. Commun.* **2004**, 416; d) J. A. R. Navarro, E. Barea, A. Rodríguez-Diéguez, J. M. Salas, C. O. Ania, J. B. Parra, N. Masciocchi, S. Galli, A. Sironi, *J. Am. Chem. Soc.* **2008**, *130*, 3978; e) D. Maspoch, D. Ruiz-Molina, K. Wurst, N. Domingo, M. Cavallini, F. Biscarini, J. Tejada, C. Rovira, J. Veciana, *Nat. Mater.* **2003**, *2*, 190.
- [4] a) D. Gatteschi, R. Sessoli, *Angew. Chem., Int. Ed.* **2003**, *42*, 268; b) R. Sessoli, H. L. Tsai, A. R. Schake, S. Y. Wang, J. B. Vincent, K. Folting, D. Gatteschi, G. Christou, D. N. Hendrickson, *J. Am. Chem. Soc.* **1993**, *115*, 1804; d) R. Sessoli, D. Gatteschi, A. Caneschi, M. A. Novak, *Nature*, **1993**, *365*, 141.
- [5] a) J. Yoo, W. Wernsdorfer, E.-C. Yang, M. Nakano, A. L. Rheingold, D. N. Hendrickson, *Inorg. Chem.* **2005**, *44*, 3377; b) H. Miyasaka, K. Nakata, L. Lecren, C. Coulon, Y. Nakazawa, T. Fujisaki, K. Sugiura, M. Yamashita, R. Clérac, *J. Am. Chem. Soc.* **2006**, *128*, 3770; c) H. Miyasaka, K. Nakata, K. Sugiura, M. Yamashita, R. Clérac, *Angew. Chem., Int. Ed.* **2004**, *43*, 707.
- [6] a) G. Rogez, J. N. Rebilly, A. L. Barra, L. Sorace, G. Blondin, N. Kirchner, M. Duran, J. Van Slageren, S. Parsons, L. Ricard, A. Marvilliers, T. Mallah, *Angew. Chem., Int. Ed.* **2005**, *44*, 2; b) J. Krzystek, J. H. Park, M. W. Meisel, M. A. Hitchman, H. Stratemeier, L. C. Brunel, J. Telser, *Inorg. Chem.* **2002**, *41*, 4478.
- [7] a) X.-T. Liu, X.-Y. Wang, W.-X. Zhang, P. Cui, S. Gao, *Adv. Mater.* **2006**, *18*, 2852; b) D.-K. Cao, Y.-Z. Li, L.-M. Zheng, *Inorg. Chem.* **2007**, *46*, 7571.
- [8] F.-P. Huang, J.-L. Tian, D.-D. Li, G.-J. Chen, W. Gu, S.-P. Yan, X. Liu, D.-Z. Liao, P. Cheng, *Inorg. Chem.* **2010**, *49*, 2525.
- [9] K. Isele, F. Gigon, A. F. Williams, G. Bernardinelli, P. Franz, S. Decurtins, *Dalton Trans.* **2007**, 332.
- [10] A. Ferguson, J. Lawrence, A. Parkin, J. Sanchez-Benitez, K. V. Kamenev, E. K. Brechin, W. Wernsdorfer, S. Hill, M. Murrie, *Dalton Trans.* **2008**, 6409.
- [11] a) M. Yang, J. Yu, L. Shi, P. Chen, G. Li, Y. Chen, R. Xu, S. Gao, *Chem. Mater.* **2006**, *18*, 476; b) P. Mahata, D. Sen, S. Natarajan, *Chem. Commun.* **2008**, 1278.
- [12] L. Arai, M. A. Nadeem, M. Bhabhade, J. A. Stride, *Dalton Trans.* **2010**, 39, 3372.
- [13] a) R. L. Carlin, *Magnetochemistry*, Springer-Verlag, Berlin, **1986**; b) F. Sanz, C. Parada, J. M. Rojo, C. Ruiz-Valero, *Chem. Mater.* **2001**, *13*, 1334.
- [14] S. O. H. Gutschke, D. J. Price, A. K. Powell, P. T. Wood, *Angew. Chem., Int. Ed.* **1999**, *38*, 1088.
- [15] Q.-P. Lin, J. Zhang, X.-Y. Cao, Y.-G. Yao, Z.-J. Li, L. Zhang, Z.-F. Zhou, *CrystEngComm* **2010**, *12*, 2938.
- [16] D. Li, L. Zheng, Y. Zhang, J. Huang, S. Gao, W. Tang, *Inorg. Chem.* **2003**, *42*, 6123.
- [17] a) S.-D. Jiang, B.-W. Wang, G. Su, Z.-M., Wang, S. Gao, *Angew. Chem. Int. Ed.* **2010**, *49*, 7448; b) R. Schenker, M. N. Leuenberger, G. Chaboussant, H. U. Gudel, D. Loss, *Chem. Phys. Lett.* **2002**, *358*, 413.
- [18] G. M. Sheldrick, *SHELXS 97*, Program for the Solution of Crystal Structures; University of Göttingen:Germany, **1997**.
-



## Entry for the Table of Contents (Please choose one layout)

Layout 2:

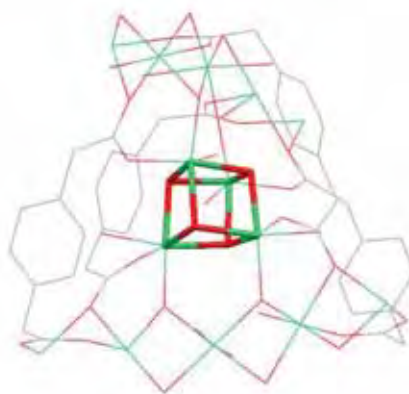
### Magnetic Phase Transitions

M. A. Nadeem, M. C. C. Ng, A/Prof. J. A. Stride

Page – Page

Magnetic phase transition in an unprecedented  $\text{Ni}_4\text{O}_4$ -cubane based 3D metal-organic framework

An unprecedented architecture  $\{[\text{Ni}^{\text{II}}_2(\text{pdaa})(\text{OH})_2(\text{H}_2\text{O})]_n\}$  (pdaa = 1,4-phenylene diacetic acid)}, comprising of 1D linear chains of  $\text{Ni}^{\text{II}}$  ions cross linked together via  $\text{Ni}_4\text{O}_4$ -cubanes, was synthesized using a hydrothermal method; the complex exhibited a long range antiferromagnetic ordering at ca. 21 K and a magnetic phase transition from antiferromagnetism to canted antiferromagnetism below 2.8 K which is possibly associated with slow relaxation behaviour.



## Supporting Information

### **Magnetic phase transition in an unprecedented Ni<sub>4</sub>O<sub>4</sub>-cubane based 3D metal-organic framework**

*Muhammad Arif Nadeem,<sup>†</sup> Maggie Chai Cin Ng,<sup>†</sup> and John Arron Stride<sup>\*†,‡</sup>*

<sup>†</sup> *School of Chemistry, University of New South Wales, Sydney, NSW 2052, Australia. Fax:*

*+61 (02) 9385 6141; Tel: +61 (0)2 9385 4675; E-mail: j.stride@unsw.edu.au*

<sup>‡</sup> *Bragg Institute, Australian Nuclear Science and Technology Organisation, PMB 1, Menai, NSW 2234, Australia.*

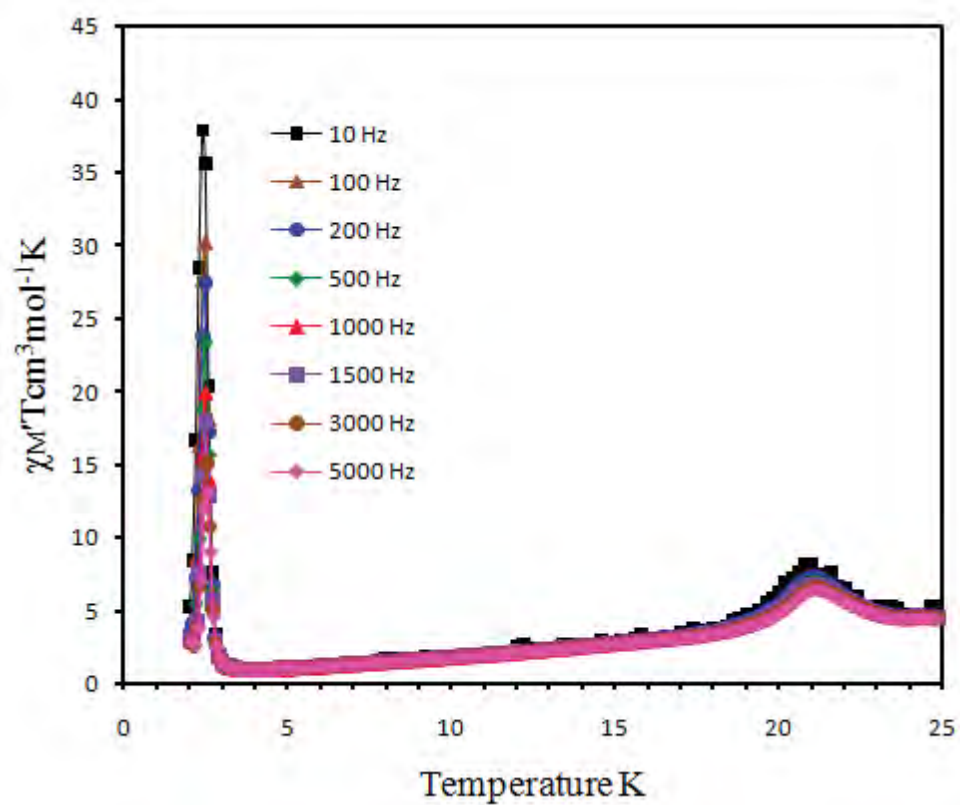


**Figure S1:** Temperature and frequency dependence of  $\chi_M' T$  parts of the ac susceptibility for **1**



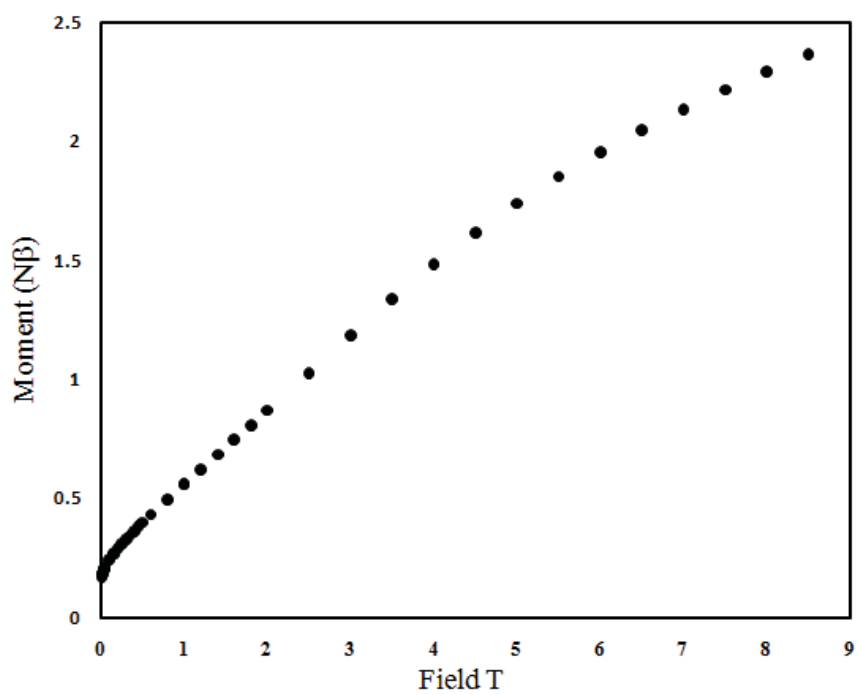


**Figure S2:** A graph of field dependent magnetization of **1**

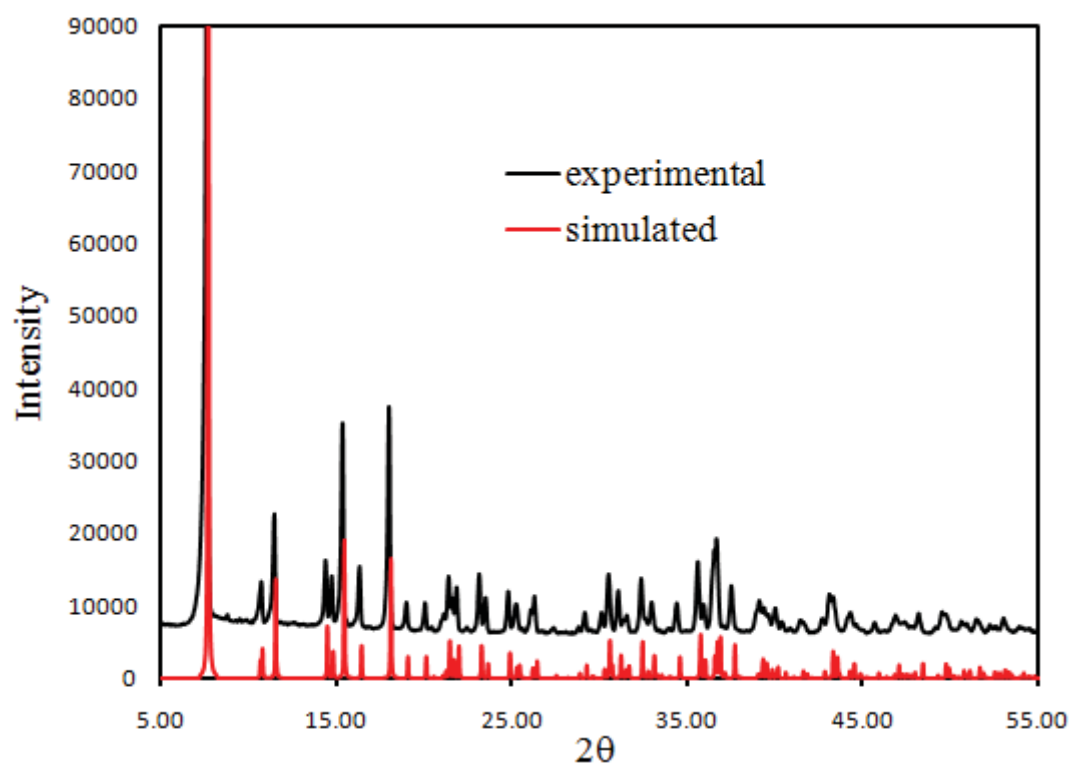


**Figure S3:** Comparison of powder XRD of calculated (red) with experimental (black) pattern of **1**

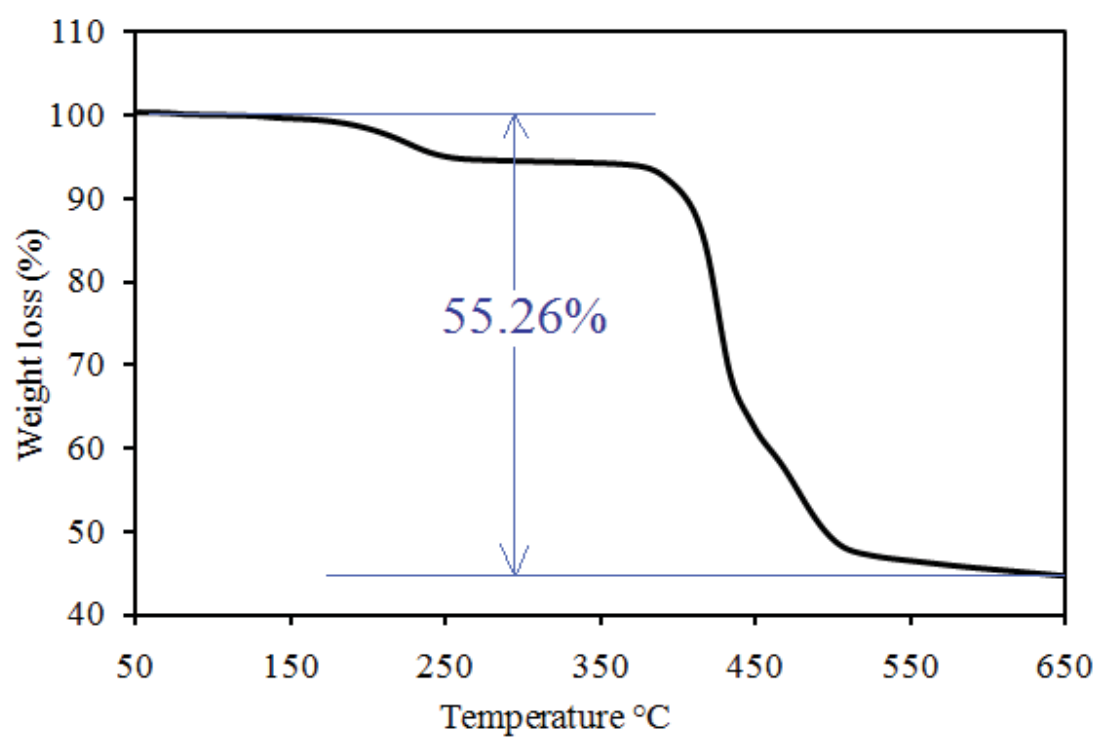


**Figure S4:** Thermogravimetric analytical curve of **1**

**A flexible copper based microporous metal–organic framework displaying selective adsorption of hydrogen over nitrogen**

*Muhammad Arif Nadeem, Aaron W. Thornton, Matthew R. Hill and John Arron Stride*

**ACKNOWLEDGMENT OF CONTRIBUTION TO AUTHORSHIP**

The article is published in journal “*Dalton Transactions*” and has been selected as *Dalton Transactions* Hot Article. J.A.S. conceived and managed the research project, M.A.N. synthesised the samples, solved the crystal structure, collected and interpreted the characterization data. A.W.T. had done mathematic calculations and simulations. M.R.H. collected and interpreted the gas loading data. All authors discussed the results and commented on this manuscript.

Cite this: *Dalton Trans.*, 2011, **40**, 3398

www.rsc.org/dalton

PAPER

## A flexible copper based microporous metal–organic framework displaying selective adsorption of hydrogen over nitrogen†

Muhammad Arif Nadeem,<sup>a</sup> Aaron W. Thornton,<sup>b</sup> Matthew R. Hill<sup>b,c</sup> and John Arron Stride<sup>\*a,d</sup>

Received 4th November 2010, Accepted 10th February 2011

DOI: 10.1039/c0dt01531h

A microporous metal–organic framework [Cu<sub>3</sub>(ipO)<sub>2</sub>(pyz)<sub>2</sub>]<sub>n</sub>, (ipO = 2-hydroxyisophthalic acid, pyz = pyrazine) was synthesized *via* an *in situ* ligand transformation reaction. The microporous framework displays helical arrays of ipO ligands holding the Cu atoms in 2D sheets, whilst the coordination of pyz molecules acts to arrange these sheets into a microporous 3D structure. Remarkable selective sorption behaviour (>5) for H<sub>2</sub> over N<sub>2</sub> is observed and explained with molecular dynamics simulations.

Metal–organic frameworks (MOFs) are novel porous crystalline materials consisting of metal ions or clusters interconnected by a variety of organic linkers and have attracted great attention because of their potential applications in gas separation,<sup>1</sup> gas storage,<sup>2</sup> ion exchange,<sup>3</sup> catalysis,<sup>4</sup> magnetism,<sup>5</sup> and others. In addition to the above mentioned promising applications, their unique properties, such as their highly diversified structures, large range of pore sizes, very high surface areas, and even specific adsorption affinities, make MOFs excellent candidates for use in the construction of molecular sieve membranes of superior performance.<sup>6</sup> The preparation of MOF membranes for gas separation is rapidly becoming a major research focus. Unlike traditional porous zeolite materials whose pores are confined by tetrahedral oxide skeletons and are thus difficult to tune, the pores within MOFs can be systematically adjusted by the judicious choice of metal-containing secondary building units and/or bridging organic linkers.<sup>7</sup> This superior feature is very important for developing novel microporous materials with selective sorption behaviours or molecular sieving attributes.<sup>8</sup> Despite their importance, MOFs showing selective gas adsorption behaviours are currently not so common. In particular, MOFs that can selectively absorb H<sub>2</sub> over N<sub>2</sub> are very important because they have the potential to be applied in the separation of H<sub>2</sub> enrichment from the N<sub>2</sub>–H<sub>2</sub> exhaust in ammonia synthesis. To the best of our knowledge, preferential adsorption of H<sub>2</sub> over N<sub>2</sub> by a coordination solid Mn(HCO<sub>2</sub>)<sub>2</sub>, was first reported by

Dybtsev *et al.*, in 2004.<sup>9</sup> In 2007, Chen *et al.*, reported a zinc based interpenetrated microporous MOF for selective adsorption of H<sub>2</sub> over N<sub>2</sub>.<sup>10</sup> In addition, a number of attempts have been made to prepare supported-MOF membranes.<sup>11</sup> Recently, supported MOFs were reported as molecular sieve membranes for high hydrogen selectivity over nitrogen.<sup>12</sup> However, progress is very limited and there is a need to focus on developing materials better tuned for this process. Further control may be obtained by utilizing short bridging ligands to target small pores,<sup>13</sup> also flexibility in the structure may help in allowing the gas molecules to enter through the pores. We expect that introduction of short carboxylates and bidentate pillar linkers will lead to the formation of 3D frameworks having small pores suited to the selective uptake of small molecules like hydrogen. Herein, we report the discovery of preferential adsorption of H<sub>2</sub> over N<sub>2</sub> in just such a copper based microporous 3D metal–organic framework, [Cu<sub>3</sub>(ipO)<sub>2</sub>(pyz)<sub>2</sub>]<sub>n</sub> (**1**).

**1** was synthesized by the *in situ* ligand transformation in a hydrothermal approach. A mixture of Cu(NO<sub>3</sub>)<sub>2</sub>·2.5H<sub>2</sub>O (242 mg, 1 mmol), 1,2,3-benzene tricarboxylic acid (H<sub>3</sub>btc; 123 mg, 0.5 mmol), pyrazine (pyz, 40 mg, 0.5 mmol), KOH (112 mg, 2 mmol) and H<sub>2</sub>O (10 mL) was stirred for 10 min and sealed in a 23 mL Teflon lined stainless steel autoclave, which was heated to 220 °C and held at that temperature for 3 days. After cooling to room temperature, green hexagonal plates of **1** were recovered by filtration, washed, dried and picked out manually for further analysis. (yield: 32% based on Cu). The complex has previously been reported and our structural data is in close accord with Zheng *et al.* in 2009.<sup>14</sup>

The microporous framework **1** consists of two crystallographically different types of copper centers (Cu1 and Cu2). The Cu1 centre is in a distorted square pyramidal geometry and is bridged to another Cu1 atom *via* the central oxygen atom of the hydroxyl group of the ipO ligand, to form a dimer. Each Cu2 is in a distorted octahedral geometry, coordinated with the four oxygen atoms from two ipO ligands in the equatorial plane and with two nitrogen atoms of pyz at the axial positions. The compound displays helical arrays of ipO ligands, which hold the Cu atoms in 2D sheets, whilst

<sup>a</sup>School of Chemistry, University of New South Wales, Sydney, NSW 2052, Australia. E-mail: j.stride@unsw.edu.au; Fax: +61 (0)2 9385 6141; Tel: +61 (0)2 9385 4675

<sup>b</sup>CSIRO Materials Science and Engineering, Private Bag 33, Clayton South MDC, Victoria, Australia 3169

<sup>c</sup>School of Chemistry, University of Melbourne, Parkville, Victoria, Australia 3020

<sup>d</sup>Bragg Institute, Australian Nuclear Science and Technology Organisation, PMB 1, Menai, NSW 2234, Australia

† Electronic supplementary information (ESI) available. See DOI: 10.1039/c0dt01531h

the coordination of pyz molecules acts to arrange these sheets into a microporous 3D structure, Fig. 1. The phase purity of the bulk sample was independently confirmed by powder X-ray diffraction (PXRD), Fig S1.†

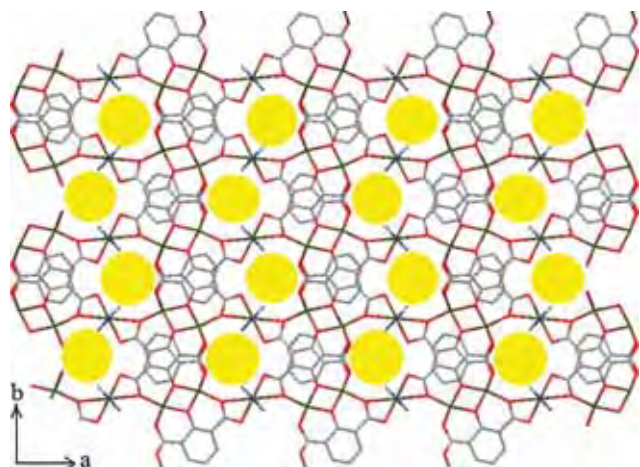


**Fig. 1** A view of the microporous framework **1** showing pores along the *c*-axis.

The microporous framework **1** shows remarkable preferential adsorption of  $H_2$  over  $N_2$ . Given the lower adsorption enthalpies typically associated with hydrogen in comparison to nitrogen, this is all the more exceptional. Molecular dynamics simulations indicate that **1** has a flexible structure that is able to accommodate  $H_2$  15.8% of the time, but  $N_2$  only on a sporadic basis <1.5% of the time.

The structure of the microporous framework **1** reveals a topology that includes small, microporous channels aligned to the *c*-axis (Fig. 1). Blue and grey channels in Fig. 4 indicate the accessible surface areas available within the structure. These channels are too small to include solvent from the synthesis, which were absent during both crystallographic investigations and thermal analysis (Fig. S3†). Gas adsorption was conducted on the material at 77 K with  $H_2$  and  $N_2$  adsorbents. The gas adsorption/desorption data is given in Table S1 of the ESI.†

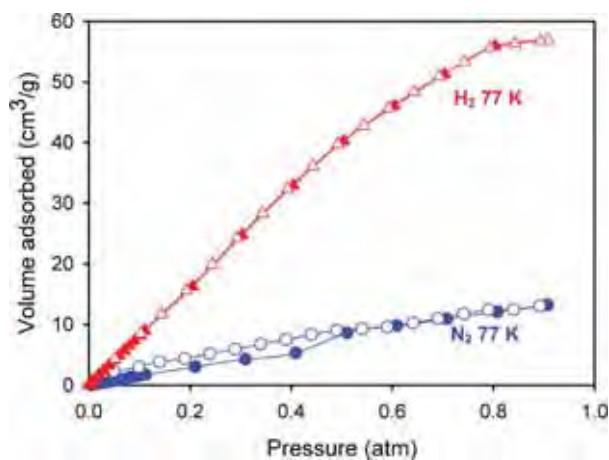


**Fig. 2** Plot of  $N_2$  and  $H_2$  adsorption/desorption isotherms at 77 K.

The selectivity for this adsorption process was calculated by fitting the Toth isotherm model<sup>15</sup> to each adsorption branch, as

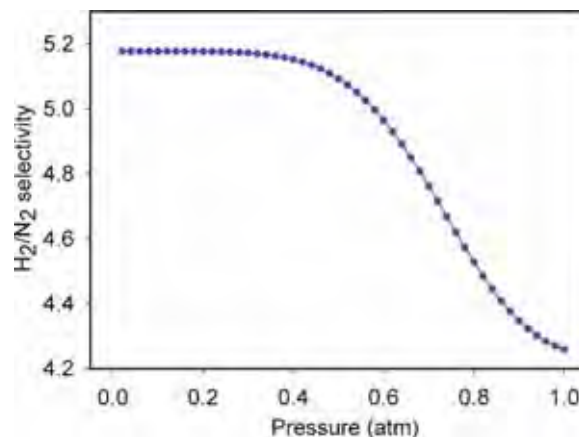


**Fig. 3**  $H_2/N_2$  selectivity as a function of pressure. In order to match equivalent pressures, raw data has been fitted to the Toth isotherm model.

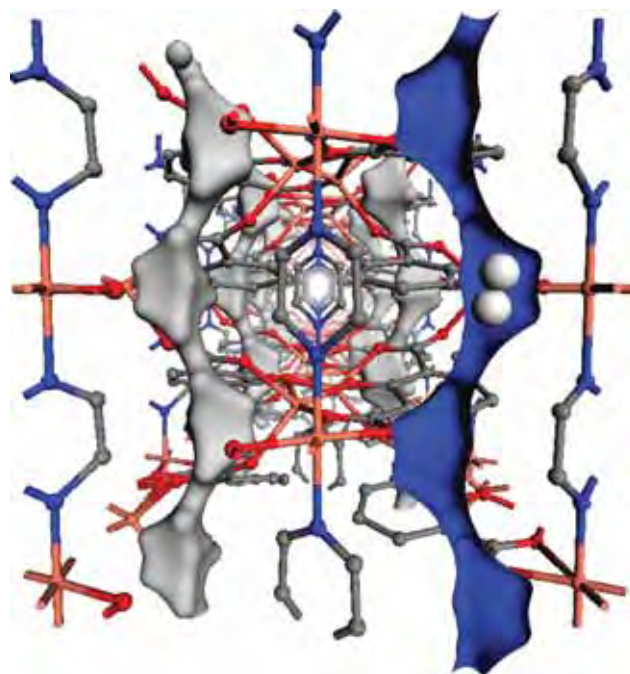


**Fig. 4** Perspective view down the *a*-axis of microporous framework **1**. Blue and grey channels indicate the accessible surface areas available within the structure.

shown in Fig. 3. At low pressures  $H_2$  adsorbs in preference to  $N_2$  at a selectivity of greater than 5, a value which decays at higher partial pressures. The nitrogen isotherm does not exhibit the type I behaviour expected of a microporous material, and shows very low adsorption levels. Whilst the measurement was performed at the longest possible equilibration times, there may be large timescale diffusion effects that inhibit the adsorption curve. These effects are likely due to the flexibility observed within the structure (*vide infra*), and there may also be a small contribution from surface adsorption. Nevertheless, the uptake is extremely low; the material is essentially non-porous to nitrogen. Analysis with other gaseous probes at higher temperatures did not reveal sufficient uptake for a reliable interpretation.

Further investigations were undertaken to determine the cause of the remarkable preferential adsorption of  $H_2$  over  $N_2$ . The



accessible free volume has been outlined in Fig. 4 for a probe radius of 1 Å, using a commercial package, Materials Studio.<sup>16</sup>

The narrow pore channels oriented in 1-dimension are likely to be responsible for the limited storage capacity of small molecules over larger molecules, for example H<sub>2</sub> over N<sub>2</sub>. As shown in Fig. 5, the pore size distribution, calculated geometrically with the open source package RASPA 1.0,<sup>17</sup> indicates a channel size of 1.75 Å in diameter. Though this is smaller than the estimated kinetic diameter of hydrogen (2.89 Å, assuming single spherical entity),<sup>18</sup> by considering structural flexibility the axially orientated gas molecules and the known axial acceptance diameter for H<sub>2</sub> into a pore of 2.27 Å and N<sub>2</sub> 2.92 Å,<sup>19</sup> it is reasonable that these channels are capable of gas storage. Molecular dynamics of the unit-cell has been performed with Materials Studio using the Universal Forcefield<sup>20</sup> and a microcanonical (NVE) ensemble over 1000 ps simulation time. Other simulation details include use of the Forcite module after an initial geometry optimization with an energy tolerance of  $2 \times 10^{-5}$  kcal mol<sup>-1</sup>. Molecular dynamics was then performed in a NVT ensemble with a time step of 0.5 fs. Total simulation time was 2.1 ps with  $2 \times 10^5$  equilibration steps and  $4 \times 10^6$  simulation steps. The temperature was held constant at 77 K using a Nose–Hoover thermostat.

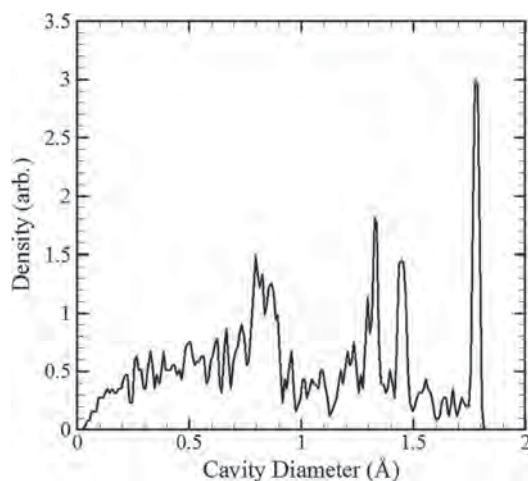


Fig. 5 Calculated cavity diameter distribution within the microporous framework 1 using RASPA 1.0.<sup>17</sup>

During the course of the simulation of **1**, an average measure of pore size fluctuation was determined, resulting in a standard deviation of 0.51 Å about the mean pore size of 1.75 Å. This means that the pore channel will expand to a size larger than 2.27 Å about 15.8% of the time and 2.92 Å < 1.5% of the time and as such, the structural flexibility of **1** is enough to allow hydrogen to penetrate the crystal at a higher rate than nitrogen. Additionally, the measured uptake at 0.9 atm. translates to 3 hydrogen molecules and 0.6 nitrogen molecules per unit cell, respectively. A video file demonstrating this flexibility is included with the ESI.†

In conclusion, we have reported a microporous framework, [Cu<sub>3</sub>(ipO)<sub>2</sub>(pyz)<sub>2</sub>]<sub>n</sub> (**1**), that exhibits a remarkable preferential adsorption for H<sub>2</sub> over N<sub>2</sub>, with selectivity above 5 at sub-ambient pressures. This result has important implications for the isolation of H<sub>2</sub> from N<sub>2</sub> in ammonia synthesis waste streams, where energy expensive pressure-swing adsorption is typically required,

and N<sub>2</sub> is the typical adsorbent. The microporous framework **1** delivers the opportunity to conduct this separation in low H<sub>2</sub> streams by preferentially adsorbing it, and without the need for energy-expensive pressurisation. Molecular dynamics simulations revealed that although the channels of **1** are too small for inclusion of hydrogen, the structure is flexible, and adopts more open topologies that account for the preferential adsorption. Such flexibility was also observed in the hysteretic nitrogen adsorption isotherm.

Thermo-gravimetric analyses were performed under nitrogen using a Mettler Toledo TGA/DSC 1 at a heating rate of 10 °C min<sup>-1</sup>. PXRD data were recorded on a Philips X'Pert Multipurpose X-ray Diffractometer (CuKα, λ = 1.54056 Å). Gas adsorption experiments were performed on a Micromeritics ASAP 2420 equipped with a micropore pressure transducer. Data points were regarded to be measured after less than 2% variance in pressure was recorded over 1200 s intervals (typical conditions: 5 s intervals with 5% variance).

## Notes and references

- (a) S. Ma, X.-S. Wang, D. Yuan and H.-C. Zhou, *Angew. Chem., Int. Ed.*, 2008, **47**, 4130; (b) S. Ma, D. Yuan, X.-S. Wang and H.-C. Zhou, *Inorg. Chem.*, 2009, **48**, 2072; (c) S. Ma, D. Sun, X.-S. Wang and H.-C. Zhou, *Angew. Chem., Int. Ed.*, 2007, **46**, 2458; (d) J.-R. Li, Y. Tao, Q. Yu, X.-H. Bu, H. Sakamoto and S. Kitagawa, *Chem.-Eur. J.*, 2008, **14**, 2771; (e) S. Ma, X.-S. Wang, E. S. Manis, C. D. Collier and H.-C. Zhou, *Inorg. Chem.*, 2007, **46**, 3432; (f) Y. E. Cheon and M. P. Suh, *Chem. Commun.*, 2009, 2296; (g) S. Ma, X.-S. Wang, C. D. Collier, E. S. Manis and H.-C. Zhou, *Inorg. Chem.*, 2007, **46**, 8499; (h) M. Dinca and J. R. Long, *J. Am. Chem. Soc.*, 2005, **127**, 9376; (i) P. L. Llewellyn, S. Bourrelly, C. Serre, Y. Filinchuk and G. Férey, *Angew. Chem., Int. Ed.*, 2006, **45**, 7751.
- (a) M. Dinca and J. R. Long, *Angew. Chem., Int. Ed.*, 2008, **47**, 6766; (b) A. G. Wong-Fillard, A. J. Matzger and O. M. Yaghi, *J. Am. Chem. Soc.*, 2006, **128**, 3494; (c) H. J. Park and M. P. Suh, *Chem.-Eur. J.*, 2008, **14**, 8812; (d) Y.-G. Lee, H. R. Moon, Y. E. Cheon and M. P. Suh, *Angew. Chem., Int. Ed.*, 2008, **47**, 7741; (e) A. W. Thornton, K. M. Nairn, J. M. Hill, A. J. Hill and M. R. Hill, *J. Am. Chem. Soc.*, 2009, **131**, 10662; (f) A. W. Thornton, K. M. Nairn, D. Buso, M. R. Hill and M. R. Hill, *S. Horike, A. Dailly and J. R. Long, J. Am. Chem. Soc.*, 2009, **131**, 15120.
- (a) K. S. Min and M. P. Suh, *J. Am. Chem. Soc.*, 2000, **122**, 6834; (b) H. J. Choi and M. P. Suh, *Inorg. Chem.*, 2003, **42**, 1151; (c) F. Nouar, J. Eckert, J. F. Eubank, P. Forster and M. Eddaoudi, *J. Am. Chem. Soc.*, 2009, **131**, 2864; (d) S. Yang, X. Lin, A. J. Blake, K. M. Thomas, P. Hubberstey, N. R. Champness and M. Schröder, *Chem. Commun.*, 2008, 6108; (e) M. Dinca and J. R. Long, *J. Am. Chem. Soc.*, 2007, **129**, 11172.
- (a) J. Y. Lee, O. K. Farha, J. Roberts, K. A. Scheidt, S. T. Nguyen and J. T. Hupp, *Chem. Soc. Rev.*, 2009, **38**, 1450.
- (a) M. A. Nadeem, D. Craig, R. Bircher and J. A. Stride, *Dalton Trans.*, 2010, **39**, 4358; (b) L. Arai, M. A. Nadeem, M. Bhadrabade and J. A. Stride, *Dalton Trans.*, 2010, **39**, 3372; (c) M. Kurmoo, *Chem. Soc. Rev.*, 2009, **38**, 1353.
- (a) J.-R. Li, R. J. Kuppler and H.-C. Zhou, *Chem. Soc. Rev.*, 2009, **38**, 1477; (b) D. Zacher, O. Shekhah, C. Woll and R. A. Fischer, *Chem. Soc. Rev.*, 2009, **38**, 1418.
- (a) M. Eddaoudi, D. B. Moler, H. Li, B. Chen, T. M. Reineke, M. O'Keeffe and O. M. Yaghi, *Acc. Chem. Res.*, 2001, **34**, 319; (b) S. Kitagawa, R. Kitaura and S. Noro, *Angew. Chem., Int. Ed.*, 2004, **43**, 2334; (c) C. Janiak, *Dalton Trans.*, 2003, 2781; (d) B. Kesanli and W. Lin, *Coord. Chem. Rev.*, 2003, **246**, 305; (e) G. Férey, C. Mellot-Draznieks, C. Serre and F. Millange, *Acc. Chem. Res.*, 2005, **38**, 217; (f) D. Bradshaw, J. B. Claridge, E. J. Cussen, T. J. Prior and M. J. Rosseinsky, *Acc. Chem. Res.*, 2005, **38**, 273; (g) W. B. Lin, *J. Solid State Chem.*, 2005, **178**, 2486; (h) J. L. C. Rowsell and O. M. Yaghi, *Angew. Chem., Int. Ed.*, 2005, **44**, 4670.

- 8 (a) R. Kitaura, K. Seki, G. Akiyama and S. Kitagawa, *Angew. Chem., Int. Ed.*, 2003, **42**, 428; (b) L. Pan, K. M. Adams, H. E. Hernandez, X. Wang, C. Zheng, Y. Hattori and K. Kaneko, *J. Am. Chem. Soc.*, 2003, **125**, 3062; (c) T. K. Maji, K. Uemura, H.-C. Chang, R. Matsuda and S. Kitagawa, *Angew. Chem., Int. Ed.*, 2004, **43**, 3269; (d) S. Bourrelly, P. L. Llewellyn, C. Serre, F. Millange, T. Loiseau and G. Férey, *J. Am. Chem. Soc.*, 2005, **127**, 13519; (e) R. Matsuda, R. Kitaura, S. Kitagawa, Y. Kubota, R. V. Belosludov, R. C. Kobayashi, H. Sakamoto, T. Chiba, M. Takata, Y. Kawazoe and Y. Mita, *Nature*, 2005, **436**, 238; (f) D. G. Samsonenko, H. Kim, Y. Sun, G.-H. Kim, H.-S. Lee and K. Kim, *Chem.-Asian J.*, 2007, **1**, 484; (g) J. A. R. Navarro, E. Barea, J. M. Salas, N. Masciocchi, S. Galli, A. Sironi, C. O. Ania and J. B. Parra, *Inorg. Chem.*, 2006, **45**, 2397; (h) L. Pan, D. H. Olson, L. R. Ciemnomolonski, R. Heddy and J. Li, *Angew. Chem., Int. Ed.*, 2006, **45**, 616; (i) T. J. Taylor, V. I. Bakhmutov and F. P. Gabbaï, *Angew. Chem., Int. Ed.*, 2006, **45**, 7030; (j) T. K. Maji, R. Matsuda and S. Kitagawa, *Nat. Mater.*, 2007, **6**, 142; (k) S. M. Humphrey, J.-S. Chang, S. H. Jhung, J. W. Yoon and P. T. Wood, *Angew. Chem., Int. Ed.*, 2007, **47**, 272.
- 9 D. N. Dybtsev, H. Chun, S. H. Yoon, D. Kim and K. Kim, *J. Am. Chem. Soc.*, 2004, **126**, 32.
- 10 B. Chen, S. Ma, E. J. Hurtado, E. B. Lobkovsky and H.-C. Zhou, *Inorg. Chem.*, 2007, **46**, 8490.
- 11 (a) M. Arnold, P. Kortunov, D. J. Jones, Y. Nedellec, J. Karger and J. Caro, *Eur. J. Inorg. Chem.*, 2007, 60; (b) Y. Yoo and H. K. Jeong, *Chem. Commun.*, 2008, 2441; (c) J. Gascon, S. Aguado and F. Kapteijn, *Microporous Mesoporous Mater.*, 2008, **113**, 132; (d) Y. Liu, Z. Ng, E. A. Khan, H. K. Jeong, C. Ching and Z. P. Lai, *Microporous Mesoporous Mater.*, 2009, **118**, 296; (e) Y. Yoo, Z.-P. Lai and H. K. Jeong, *Microporous Mesoporous Mater.*, 2009, **123**, 100.
- 12 (a) Y.-S. Li, F.-Y. Liang, H. Bux, A. Feldhoff, W.-S. Yang and J. Caro, *Angew. Chem., Int. Ed.*, 2010, **49**, 548; (b) H. Guo, G. Zhu, I. J. Hewitt and S. Qiu, *J. Am. Chem. Soc.*, 2009, **131**, 1646.
- 13 B. Chen, S. Ma, F. Zapata, F. R. Fronczek, E. B. Lobkovsky and H.-C. Zhou, *Inorg. Chem.*, 2007, **46**, 1233.
- 14 Y.-Z. Zheng, Y.-B. Zhang, M.-L. Tong, W. Xue and X.-M. Chen, *Dalton Trans.*, 2009, 1396.
- 15 D. D. Do, *Adsorption Analysis: Equilibria and Kinetics*, Imperial College Press, London, 1998.
- 16 Materials Studio v5.0 Accelrys, Inc. San Diego, CA, USA, 2009.
- 17 (a) D. Dubbeldam, S. Calero, D. E. Ellis, R. Q. Snurr, *RASPA 1.0*, Northwestern University: Evanston, 2008; (b) L. D. Gelb and K. E. Gubbins, *Langmuir*, 1999, **15**, 305.
- 18 D. W. Breck, *Zeolite Molecular Sieves: Structure, Chemistry, and Use.*, John Wiley & Sons: New York, 1973.
- 19 A. W. Thornton, T. Hilder, A. J. Hill and J. M. Hill, *J. Membr. Sci.*, 2009, **336**, 101.
- 20 A. K. Rappe, C. J. Casewit, K. S. Colwell, W. A. Goddard and W. M. Skiff, *J. Am. Chem. Soc.*, 1992, **114**, 10024.

## Supporting information:

### A flexible copper based microporous metal-organic framework displaying selective adsorption of hydrogen over nitrogen

Muhammad Arif Nadeem,<sup>a</sup> Aaron W. Thornton<sup>b</sup>, Matthew R. Hill<sup>b,c</sup> and John Arron Stride<sup>\*a,d</sup>

<sup>a</sup> School of Chemistry, University of New South Wales, Sydney, NSW 2052, Australia. Fax: +61 (02) 9385 6141; Tel: +61 (0)2 9385 4675; E-mail: j.stride@unsw.edu.au

<sup>b</sup> CSIRO Materials Science and Engineering, Private Bag 33, Clayton South MDC, Victoria, Australia 3169.

<sup>c</sup> School of Chemistry, University of Melbourne, Parkville Victoria, Australia 3020.

<sup>d</sup> Bragg Institute, Australian Nuclear Science and Technology Organisation, PMB 1, Menai, NSW 2234, Australia.

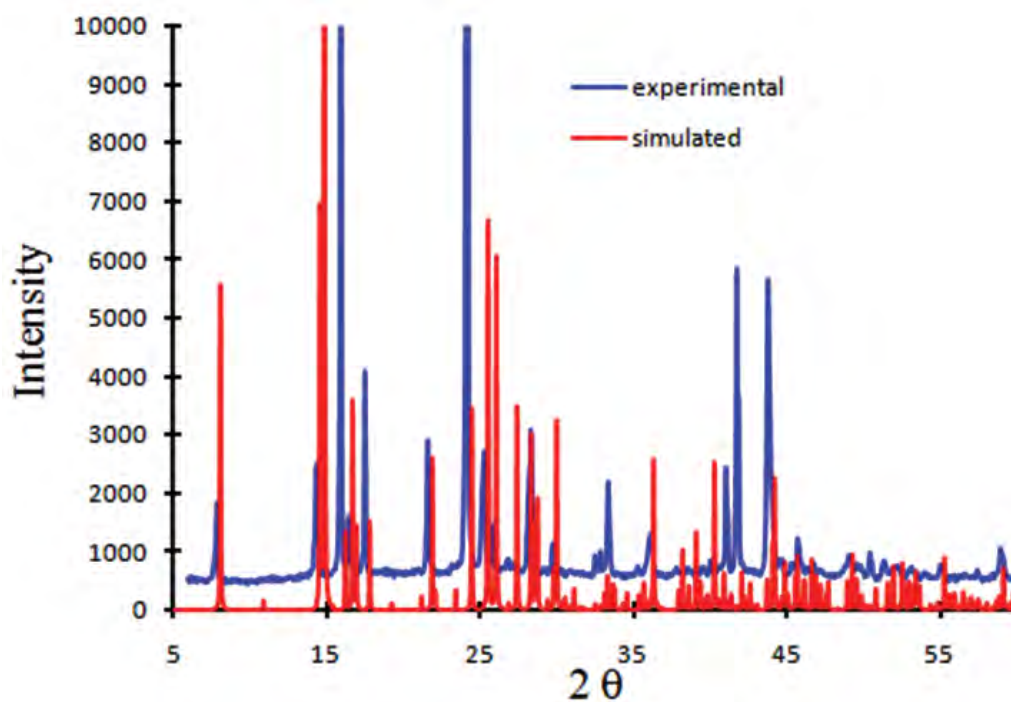


**Figure S1.** Powder diffraction of microporous framework **1** indicating a phase pure material

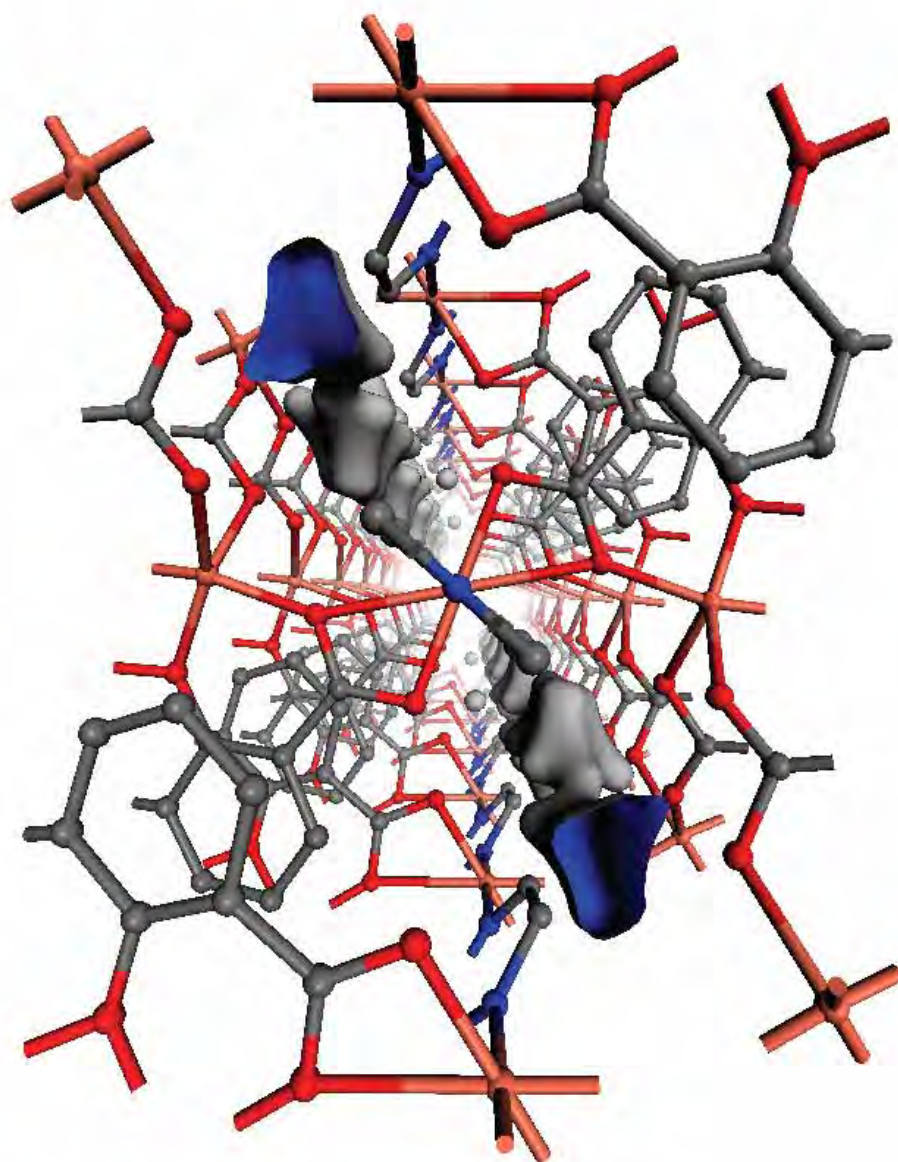


**Figure S2.** Perspective view down the  $c$ -axis of microporous framework **1**. Blue and grey channels indicate the accessible surface areas available within the structure.

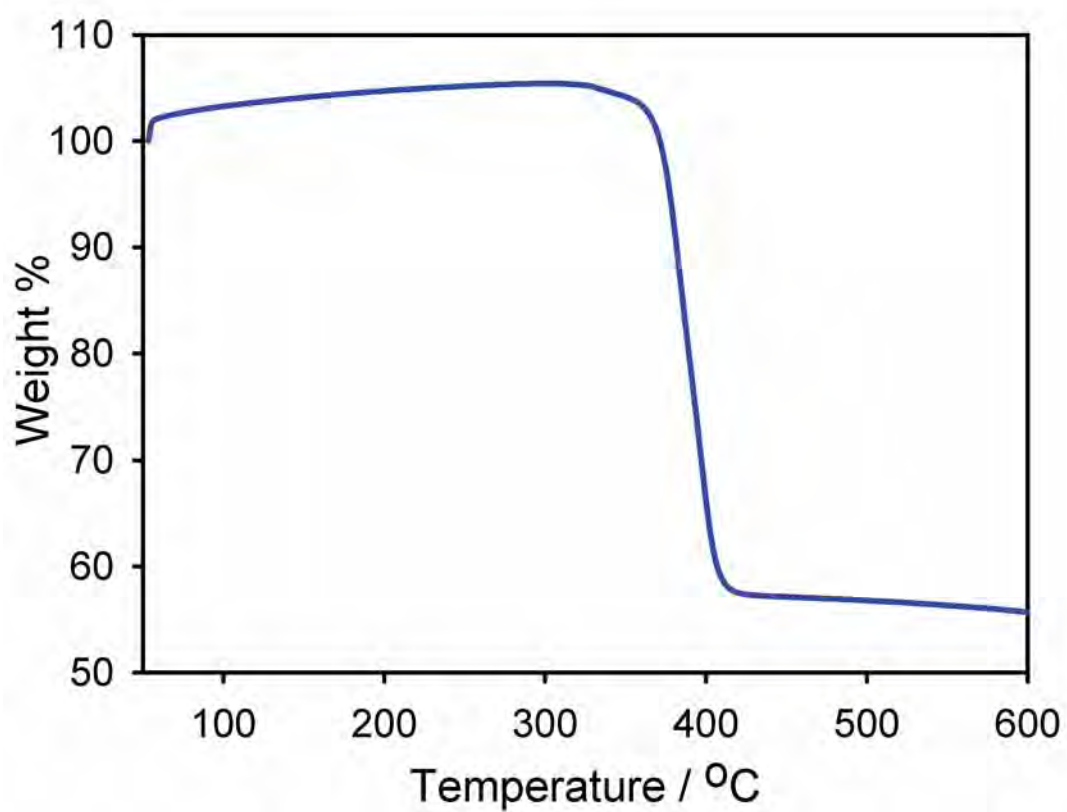


**Figure S3.** Thermogravimetric analysis of microporous framework **1**. The trace confirms the small size of the porous channels due to the absence of solvent-related weight loss at low temperature.



**Table S1.** Gas Adsorption/Desorption data

Nitrogen			Hydrogen	
Pressure (atm)	Volume adsorbed (cm <sup>3</sup> /g)		Pressure (atm)	Volume adsorbed (cm <sup>3</sup> /g)
5.24E-03	0.0082		5.13E-03	0.5326
6.26E-03	0.0261		6.14E-03	0.6176
7.27E-03	0.0544		7.15E-03	0.7027
8.29E-03	0.0743		8.16E-03	0.7879
9.31E-03	0.0939		1.90E-02	1.5951
2.16E-02	0.2793		2.06E-02	1.7168
3.16E-02	0.4414		3.01E-02	2.4504
4.17E-02	0.5871		4.00E-02	3.2889
5.16E-02	0.744		5.00E-02	4.1056
6.16E-02	0.8895		6.00E-02	4.9048
7.17E-02	1.0346		7.00E-02	5.7063
8.15E-02	1.3033		8.00E-02	6.5161
9.16E-02	1.4668		8.99E-02	7.334
1.02E-01	1.6203		1.00E-01	8.1487
1.12E-01	1.7707		1.10E-01	8.9616
2.10E-01	3.04		2.04E-01	16.2894
3.09E-01	4.2711		3.03E-01	24.7704
4.09E-01	5.3401		4.04E-01	32.9198
5.10E-01	8.6118		5.04E-01	40.2432
6.09E-01	9.8354		6.04E-01	46.0071
7.08E-01	10.9189		7.03E-01	51.3171
8.08E-01	12.0877		8.03E-01	55.9595
9.07E-01	13.254		9.08E-01	56.914
8.92E-01	13.0627		8.93E-01	56.7856
8.40E-01	12.4526		8.43E-01	56.3384
7.90E-01	12.4158		7.93E-01	55.604
7.41E-01	11.7725		7.43E-01	53.2994
6.90E-01	10.9869		6.93E-01	50.9534
6.41E-01	10.2674		6.43E-01	48.3219
5.90E-01	9.5922		5.93E-01	45.642
5.40E-01	9.3006		5.43E-01	42.7549
4.90E-01	9.0335		4.93E-01	39.7365
4.40E-01	8.3556		4.43E-01	36.0749
3.90E-01	7.5052		3.93E-01	32.3737
3.40E-01	6.7489		3.43E-01	28.3031
2.90E-01	5.9274		2.93E-01	24.2036
2.39E-01	5.1874		2.43E-01	19.8797
1.89E-01	4.3865		1.93E-01	15.6195
1.39E-01	3.8492		1.43E-01	11.7154
9.86E-02	3.0314		1.02E-01	8.485
4.90E-02	2.2821		5.18E-02	4.3521
2.06E-02	0.2755			



# Summary

The main aim of this project was to arrive at a better understanding of solvothermally prepared metal-organic frameworks by investigating their structural, magnetic and gas adsorption properties. Mainly this thesis is concerned with the study of magnetic network materials of varying dimensionality, with a view to elucidating the nature of the magnetic exchange interactions as a function of the topological connectivity.

Metal-organic hybrid materials, consisting of paramagnetic metal ions incorporated into coordination polymers to form extended structures, are currently of great interest in the field of molecular magnetism and materials chemistry, due to their fascinating structural diversities and potential applications as functional materials. Bridging ligands have been shown to transmit magnetic interactions via superexchange interactions in addition to simply acting to bind the of metal centers into specific coordination geometries. In this respect, we chose paramagnetic metal ions and bridging organic ligands to synthesize a range of metal-organic frameworks (MOFs). These have been fully characterized with a range of techniques including single crystal analysis, powder XRD, IR, TGA and elemental analysis. Following complete characterization, samples were subjected to magnetic and gas adsorption studies.

In the beginning of this project, it was decided to use simple carboxylate containing ligands such as benzene tricarboxylic acid (btc) for synthetic purposes, with benzene 1,2,3-tricarboxylic acid (1,2,3- $\text{H}_3\text{btc}$ ) one such ligand. MOFs are of interest not only for their potential applications, but also for the intriguing variety of architectures and topologies that they display, which led us to attempting to produce higher dimensional pillared-layer architectures through molecular recognition. A combination of a linear bridging ligands, 4,4'-bipyridyl (bpy) and  $\text{H}_3\text{btc}$  was selected to fabricate mixed-ligand network structures incorporating different metal ions. We were able to isolate an unusual topological framework **1** containing an intriguing unit cell with five geometrically distinct metal ions. In fact **1** contains three distinct coordination polymers within a crystalline structure: a 2D polymer consisting of Cu-dimers and Cu-chains  $[\text{Cu}_3(\text{Hbtc})(\text{btc})(\text{bpy})_2]_n$  (A), and two structurally identical, but crystallographically different, 1D linear chains, B and C, comprising  $[\text{Cu}(\text{bpy})(\text{H}_2\text{O})]_n$  units. In total, complex **1** was formulated as  $[(\text{A})(\text{B})(\text{C}).2\text{H}_2\text{O}.\text{OH}]$ . This result highlights the remarkable potential for complex hierarchical structures achievable courtesy of intermolecular interactions of lattice water molecules, coupled to guest-host interactions, within metal-organic networks and polymers.

As the project progressed, it was found that 1,2,3-H<sub>3</sub>btc can undergo synthetic transformation under specific hydrothermal conditions. It had been previously reported that *in situ*. transformation of 1,2,3-H<sub>3</sub>btc depends on the pH of the reaction system, however we decided to systematically study the hydrothermal reactions of 1,2,3-benzene tricarboxylic acid (1,2,3-btcH<sub>3</sub>) and linear bridging ligands 4,4'-dipyridyl (bpy) and pyrazine (pyz) with metal (Co<sup>II</sup>, Ni<sup>II</sup>, Cu<sup>II</sup>) salts, under different reaction conditions. The aim of this was to both directly study the affect of additional reaction conditions on the *in situ*. ligand transformation of 1,2,3-btcH<sub>3</sub> into isophthalic acid (ip = 1,3 benzene dicarboxylic acid) and to use this approach to arrive at pillared-layer structures of interest due the systematic modulation of the magnetic properties that this allows simply by varying the *length* of the pillars. The ligand transformation reaction was found to be highly dependent on reaction temperature and only to occur at higher temperatures (220°C); four isomorphous compounds [M<sub>2</sub>(ip)<sub>2</sub>(L)<sub>2</sub>]<sub>n</sub> (M = Co<sup>II</sup>, Ni<sup>II</sup>; ip = isophthalate; L = 4,4'-dipyridyl and pyrazine) were synthesized at 220°C (Chapter 3). Magnetic studies of this series revealed that ferromagnetic interactions exist within the M(II) dimers, with much weaker interdimer interactions in all of the compounds. No magnetic ordering was observed in the measured temperature range available to us (down to 2 K). The effect of reaction conditions leading to ligand decarboxylation reactions illustrates the importance of the various factors that may affect the final product in these relatively high-energy reaction pathways.

The research was then further extended into the preparation of new multifunctional MOFs, with particular focus on the ligand 1,3,5-H<sub>3</sub>btc as the three carboxylate groups located equally about the aromatic ring provide great structural flexibility being able to adopt multiple coordination modes, influencing the topology and magnetic properties of the final product. In Chapter 4, the synthesis, structure and magnetic properties of the new 3D compound [Na{Mn<sub>3</sub>(Hbtc)<sub>2</sub>(btc)}.5H<sub>2</sub>O]<sub>n</sub> (**2**) are detailed; this material consists of infinite zigzag chains [Mn2-Mn1-Mn2]<sub>n</sub>, linked by btc to form 2D layers. In this way each Hbtc ligand bridges 2D sheets to form a three-dimensional structure. Compound **2** exhibits dominant antiferromagnetic interactions within the chain, however the inter-chain interactions were found to be too weak to give rise to bulk magnetic ordering.

It was concluded that the distance and pathway between the metal centers is crucial in determining the strength of magnetic coupling interactions. Given that fluoride-bridged metal complexes are well known to have interesting magnetic properties and that previously no coordination polymers had been reported constructed from fluoride

bridged metal chains, we attempted to incorporate fluoride ions within 3D frameworks. Chapter 5 highlights the synthesis of isostructural MOFs  $\{[M_2(btc)(F)]_n, Mn^{II}, Co^{II}\}_n$  having unique fluoride ion bridged chains. Magnetic data indicates that there are strong antiferromagnetic coupling interactions between the metal atoms within the 1D fluoride chains, in both compounds. This work shows that fluoride bridged chains within coordination polymers can lead to interesting magnetic properties and that the incorporation of fluoride bridged chains of metals into 3D MOFs provides another route to controlling the magnetic interactions, with the inter-chain distance varied by virtue of a range of organic linkers.

This thesis has a particular emphasis on developing materials displaying bulk magnetic ordering. However, none of the materials mentioned above show bulk ordering, leading us to a change in the length and flexibility of ligand systems used.

Inspired by the fact that the imidazolate ion has been used to build hybrid organic-inorganic frameworks showing interesting magnetic properties, we then decided to use benzimidazole (bIM) in the preparation of a 2D hybrid material  $[Co(bIM)(acetate)]_n$ . Chapter 6 demonstrates that benzimidazole complexation led to antiferromagnetic superexchange interactions between the cobalt(II) ions, however, in the low temperature region, the magnetic behaviour changed from antiferromagnetic to weak ferromagnetic ordering as a result of spin canting in the antiferromagnetic coupling regime below 13 K. This leads to the prospect of using additional imidazole ligands, to further manipulate and tune the exchange interactions, with the  $Co^{II}$  derivatives of particular interest.

Although many MOFs with bulk magnetic ordering have been reported, it still remains a challenge to both increase the bulk magnetic ordering temperature and control the structural and physical properties of MOFs. Chapter 7 illustrates a method of controlling the magnetic properties by designing the topology of the 3D network specifically for magnetic ordering. We show that two isostructural polymers  $\{[M^{III}_3(pydc)_3(\mu_3-O)] \cdot Cl, M = Mn^{III}, Co^{III}\}$ , which were synthesized hydrothermally in the presence of excess chloride ions, offered a rare example of controlled bulk magnetic ordering at significantly higher temperatures than found in similar materials. Replacement of chloride ion with water molecule in these compounds was found to significantly change the magnetic properties; a previously reported structure, described as having water molecules in the lattice, did not show any magnetic ordering. Both MOFs showed bulk magnetic ordering at around 45 K, whilst only the cobalt based

compound displayed any canting behaviour, and then only below 10 K. These results demonstrate the concept of structural topology controlling the nature of magnetic ordering, opening the way for further work aimed at topological control of magnetism. This may be particularly relevant in light of incorporating spin centres of having large spin anisotropies in order to increase both the transition temperature and the coercive fields in such materials.

Chapter 8 introduces the concept of flexibility into the ligand systems in the synthesis of MOFs, allowing us to tune and improve the magnetic properties of materials. The flexible ligands increase the variety of binding and connectivity modes, which can then affect the magnetic properties. A series of isostructural MOFs  $[M(\text{pda})(\text{dpe})]_n$  where  $M = \text{Mn}^{\text{II}}, \text{Co}^{\text{II}}, \text{Ni}^{\text{II}}$  or  $\text{Cu}^{\text{II}}$ , ( $\text{pda} = 1,4\text{-phenylene diacetic acid}$ ,  $\text{dpe} = \text{di-(4-pyridyl)-ethane}$ ) have been synthesized by using a combination of flexible ligands.  $\text{Mn}^{\text{II}}$  and  $\text{Co}^{\text{II}}$  based polymers displayed similar thermal properties and at low temperatures exhibited strong magnetic coupling interactions, resulting in bulk magnetic ordering phenomena at ca. 45 and 55 K respectively. This work gave us an insight into role of flexibility offered by  $\text{pda}$  ligand to enhance and create new coordination polymers with interesting magnetic properties.

As a continuation of our work in the use of the flexible ligand ( $\text{pda}$ ), we also have discovered a  $\text{Ni}^{\text{II}}$ -cubane based three dimensional (3D) network  $[\text{Ni}_2^{\text{II}}(\text{pda})(\text{OH})_2(\text{H}_2\text{O})]_n$ , consisting of linear 1D  $\text{Ni}^{\text{II}}$  chains, connected via  $\text{Ni}_4\text{O}_4$ -cubanes (Chapter 9). It was synthesized hydrothermally which is also the first example of a cubane based polymer. The findings indicated that antiferromagnetic interactions with a magnetic phase transition from AF to CAF occurring at 21 K and 2.8 K respectively. These results demonstrates the concept of magnetic connectivity between 1D layers via  $\text{Ni}_4\text{O}_4$ -cubanes which modulate the overall magnetic properties with an obvious bridging of nano-magnets to magnetic networks.

MOFs that can selectively absorb  $\text{H}_2$  over  $\text{N}_2$  are very important as they have the potential to be applied in the separation of  $\text{H}_2$  enrichment from the  $\text{N}_2\text{-H}_2$  exhaust in ammonia synthesis. During this work it was possible to synthesize a microporous framework,  $[\text{Cu}_3(\text{ipO})_2(\text{pyz})_2]_n$ , that exhibits a remarkable preferential adsorption for  $\text{H}_2$  over  $\text{N}_2$ , with selectivity in excess of 5 at sub-ambient pressures (Chapter 10). This result has important implications for the isolation of  $\text{H}_2$  from  $\text{N}_2$  in ammonia synthesis waste streams, where energy expensive pressure-swing adsorption is typically required, and  $\text{N}_2$  is the typical adsorbent. The microporous framework delivers the opportunity to

conduct this separation in low partial-pressure  $H_2$  streams by preferential adsorption, without the need for energy-expensive pressurisation.

In a nutshell, given the range of synthesized magnetic coordination polymers, along with some microporous materials for gas separation applications, the significance of the body of work is obvious. It is assumed that this thesis may provide a platform to the greater understanding of magneto-structural correlations in MOFs, in addition to having gas selectivity and some intriguing architectures. Finally, the author hopes that this work will be continued on and that this thesis will be the source of inspiration for future work.



---

# Appendix

Roland Bircher  
Rua Alves Guimarães 856, apto 14  
CEP 05410-001  
Pinheiros – São Paulo - SP  
Brasil

São Paulo, 12.01.2011

+55 11 8760 5502  
roland.bircher@sherwin.com.br

Faculty of Science  
The University of New South Wales  
Sydney  
Australia

### **Permission Letter**

Dear Sir or Madam,

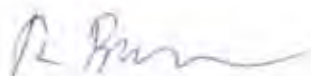
Please take note of my agreement to include the following three scientific publications, of which I have been one of the co-authors, in the Doctoral Thesis of Muhammad Arif Nadeem.

Muhammad A. Nadeem, Mohan Bhadbhade, Roland Bircher and John A. Stride, *Cryst Eng Comm*, 2010, 12, 1391

Muhammad A. Nadeem, Donald J. Craig, Roland Bircher and John A. Stride, *Dalton Trans*, 2010, 39, 4358

Muhammad A. Nadeem, Mohan Bhadbhade, Roland Bircher and John A. Stride, *Cryst Growth Des* 2010, 10, 4060

Yours sincerely,



Roland Bircher

28/2/11

Dr Matthew Hill  
CSIRO Materials Science and Engineering  
Private bag 33 Clayton South MDC  
VIC 3169  
Matthew.hill@csiro.au

Faculty of Science  
The University of New South Wales  
Sydney  
Australia

### Permission Letter

Dear Sir or Madam,

Please take note of my agreement to include the following scientific publication, of which I have been one of the co-authors, in the Doctoral Thesis of Muhammad Arif Nadeem.

Muhammad Arif Nadeem, Aaron W. Thornton, Matthew R. Hill and John Arron Stride,  
*Dalton Trans.*, 2011, **40**, 3398–3401

Sincerely



Dr Matthew Hill

28/2/11

Dr Aaron Thornton  
CSIRO Materials Science and Engineering  
Private bag 33 Clayton South MDC  
VIC 3169  
Aaron.thornton@csiro.au

Faculty of Science  
The University of New South Wales  
Sydney  
Australia

### Permission Letter

Please take note of my agreement to include the following scientific publication, of which I have been one of the co-authors, in the Doctoral Thesis of Muhammad Arif Nadeem.

Muhammad Arif Nadeem, Aaron W. Thornton, Matthew R. Hill and John Arron Stride,  
*Dalton Trans.*, 2011, **40**, 3398–3401

Sincerely



Dr Aaron Thornton



UNSW  
THE UNIVERSITY OF NEW SOUTH WALES

# Analytical Centre

31/03/11

UNSW Analytical Centre  
Chemical Sciences Building (F10)  
University of NSW  
Sydney 2052 Australia

**Dr. Mohan M. Bhadbhade**  
**Scientific Officer (Crystallography)**  
**Conjoint Lecturer (School of Chemistry)**  
University of New South Wales  
Sydney NSW 2052  
Australia

Tel +61-2-9385 9898 Fax +61-2-9385 4663  
[m.bhadbhade@unsw.edu.au](mailto:m.bhadbhade@unsw.edu.au)

## Permission Letter

Dear Sir or Madam,

Please take note of my agreement to include the following scientific publications, of which I have been one of the co-authors, in the Doctoral Thesis of Muhammad Arif Nadeem.

- 1) Muhammad A. Nadeem, M. Bhadbhade and John A. Stride, *Dalt. Trans.*, 2010, 39, 9860-9865
- 2) Muhammad A. Nadeem, M. Bhadbhade, R. Bircher and John A. Stride, *Cryst. Growth Des.* 2010, 10, 4060-4067
- 3) Muhammad A. Nadeem, M. Bhadbhade, R. Bircher and John A. Stride, *CrystEngCommun.*, 2010, 12, 1391-1393
- 4) Leo Arai, Muhammad A. Nadeem, M. Bhadbhade and John A. Stride, *Dalt. Trans.*, 2010, 39, 3372-3374
- 5) Maggie Ng, Muhammad A. Nadeem, M. Bhadbhade and John A. Stride, A series of isostructural metal organic frameworks constructed from flexible ligand system, synthesis, crystal structure and magnetic properties, *Inorg. Chem.*, 2010, manuscript submitted.
- 6) Muhammad A. Nadeem, M. Bhadbhade and John A. Stride, Two iso-structural metal-organic frameworks having long-range magnetic ordering at 45 K, *Chem. Eur. J.*, 2011, manuscript submitted.

[MOHAN M. BHADBHADE]



Thank you for your request for permission to include \_\_\_\_\_ paper s or portions of text from \_\_\_\_\_ paper s in your thesis. Permission is now automatically granted please pay special attention to the implications paragraph below. The copyright Subcommittee of the Joint Board Council Committees on Publications approved the following

copyright permission for published and submitted material from theses and dissertations

A S extends blanket permission to students to include in their theses and dissertations their own articles, or portions thereof, that have been published in A S journals or submitted to A S journals for publication, provided that the A S copyright credit line is noted on the appropriate page s .

Publishing implications of electronic publication of theses and dissertation material

Students and their mentors should be aware that posting of theses and dissertation material on the Web prior to submission of material from that thesis or dissertation to an A S journal may affect publication in that journal. Whether Web posting is considered prior publication may be evaluated on a case-by-case basis by the journal s editor. If an A S journal editor considers Web posting to be prior publication , the paper will not be accepted for publication in that journal. If you intend to submit your unpublished paper to A S for publication, check with the appropriate editor prior to posting your manuscript electronically.

If your paper has \_\_\_\_\_ yet been published by A S, we have no objection to your including the text or portions of the text in your thesis dissertation in \_\_\_\_\_ please note, however, that electronic distribution or Web posting of the unpublished paper as part of your thesis in electronic formats might jeopardize publication of your paper by A S. Please print the following credit line on the first page of your article Reproduced or Reproduced in part with permission from J RNA NAM , in press or submitted for publication . Unpublished work copyright \_\_\_\_\_ RR NT AR American Chemical Society. Include appropriate information.

If your paper has already been published by A S and you want to include the text or portions of the text in your thesis dissertation in \_\_\_\_\_, please print the A S copyright credit line on the first page of your article Reproduced or Reproduced in part with permission from \_\_\_\_\_ R R N ITATI N. copyright \_\_\_\_\_ AR American Chemical Society. Include appropriate information.

If you plan to submit your thesis to \_\_\_\_\_ MI or to another dissertation distributor, you should not include the unpublished A S paper in your thesis if the thesis will be disseminated electronically, until A S has published your paper. After publication of the paper by A S, you may release the entire thesis \_\_\_\_\_ for electronic dissemination through the distributor A S s copyright credit line should be printed on the first page of the A S paper.

The inclusion of your A S unpublished or published manuscript is permitted in your thesis in print and microfilm formats. If A S has published your paper you may include the manuscript in your thesis on an intranet that is not publicly available. Your A S article cannot be posted electronically on a publicly available medium i.e. one that is not password protected , such as but not limited to, electronic archives, Internet, library server, etc. The only material from your paper that can be posted on a public electronic medium is the article abstract, figures, and tables, and you may link to the article s DOI or post the article s author-directed URL link provided by A S. This paragraph does not pertain to the dissertation distributor paragraph above.

Questions call 1 202 8 2-43 8 43 . Send e-mail to [copyright@acs.org](mailto:copyright@acs.org) or fax to 1 202- \_\_\_\_\_ -8112. 10 10 03, 01 1 04, 0 0 0



**“End of documents”**